

SPATIAL AND ENERGETIC ASPECTS OF ELECTRON ENERGY DEPOSITION

By

CHARLES HERBERT JACKMAN

A DISSERTATION PRESENTED TO THE GRADUATE COUNCIL OF  
THE UNIVERSITY OF FLORIDA  
IN PARTIAL FULFILLMENT OF THE REQUIREMENTS FOR THE  
DEGREE OF DOCTOR OF PHILOSOPHY

UNIVERSITY OF FLORIDA

1978

## ACKNOWLEDGEMENTS

Dr. A.E.S. Green has helped the author a great deal in his efforts to complete this work. The author sincerely appreciates this guidance. He also wishes to thank Dr. R.H. Garvey and Dr. R.A. Hedinger for their helpful discussion about the dissertation. David Doda, David Killian, E. Whit Ludington, George Shercuse, and Ken Cross were instrumental in providing assistance with computer problems and other dissertation-related work.

Woody Richardson, Marjorie Niblack, and Wesley Bolch were extremely helpful in drafting the figures. The final manuscript was then typed and refined by Adele Koehler. The author is grateful to Adele for her prompt and professional assistance.

The author wishes to thank Joseph Pollack for aiding in editorial matters concerning the dissertation. A thorough reading and criticism of the dissertation by the author's committee (including Dr. A.E.S. Green, Dr. L.R. Peterson, Dr. T.L. Bailey, Dr. S.T. Gottesman, and Dr. G.R. Lebo), Dr. W.L. Chameides, and Dr. A.G. Smith was extremely helpful.

The author is especially grateful to his parents, Rev. and Mrs. H.W. Jackman, and to his sister, Kathi Jouvenat, for their encouragement and support throughout graduate school.

The author gratefully acknowledges financial support from the Department of Physics and Astronomy and the Graduate School of the University of Florida and from NASA grant number NGL-10-005-008.

## TABLE OF CONTENTS

	<u>Page</u>
ACKNOWLEDGEMENTS. . . . .	ii
ABSTRACT. . . . .	vi
CHAPTER	
I INTRODUCTION . . . . .	1
II A SHORT REVIEW OF ENERGY DEPOSITION TECHNIQUES . . . . .	5
A. Energy Deposition Techniques . . . . .	5
B. Monte Carlo Energy Deposition Techniques . . . . .	14
III ELASTIC AND INELASTIC DIFFERENTIAL AND TOTAL CROSS SECTIONS FOR N <sub>2</sub> . . . . .	18
A. Elastic Differential and Total Cross Sections for N <sub>2</sub> .	18
B. Inelastic Differential and Total Cross Sections for N <sub>2</sub> . . . . .	36
C. Total Cross Section (Elastic Plus Inelastic) . . . . .	45
IV THE MONTE CARLO METHOD OF ENERGY DEPOSITION BY ELECTRONS IN MOLECULAR NITROGEN. . . . .	47
A. Brief Discussion of the Monte Carlo Calculation. . . . .	48
B. Computer Programs and Machinery Used in the Monte Carlo Calculation. . . . .	51
C. Detailed Discussion of the Monte Carlo Electron Energy Degradation Technique . . . . .	52
1. First Random Number, R <sub>1</sub> . . . . .	53
2. Second and Third Random Numbers, R <sub>2</sub> and R <sub>3</sub> . . . . .	57
3. Fourth Random Number, R <sub>4</sub> . . . . .	61
4. Fifth Random Number, R <sub>5</sub> . . . . .	61

	<u>Page</u>
5. Sixth Random Number, $R_6$ . . . . .	67
6. Multiple Elastic Scattering Distribution Used Below 30 eV. . . . .	67
7. Value of the Cutoff Energy, 2 eV . . . . .	74
D. Statistical Error in the Monte Carlo Calculation . . .	75
V MONTE CARLO INTENSITY PLOTS AND COMPARISON WITH EXPERIMENT	77
A. Excitation of the $N_2^+ B^2\Sigma_u^+$ State. . . . .	77
B. Range of Electrons . . . . .	80
C. Previous Experimental and Theoretical Work on the 3914 Å Emission of $N_2^+$ . . . . .	81
D. Range Results and Longitudinal Intensity Plots from the Monte Carlo Calculation. . . . .	84
E. Intensity Plots in the Radial Direction. . . . .	87
VI SENSITIVITY STUDY OF THE ELECTRON ENERGY DEGRADATION . . .	98
A. Effects of Ionization Differential Cross Section on the Intensity Distributions. . . . .	99
B. Influence of Inelastic Differential Cross Sections on the Intensity Distributions . . . . .	104
C. Comparison of Different Elastic Phase Functions on the Electron- $N_2$ Collision Profile. . . . .	104
D. Influence of Different Elastic Phase Functions on the Intensity Profiles . . . . .	112
E. Effects of the Total Elastic Cross Section on the Electron Energy Degradation. . . . .	121
VII MONTE CARLO ENERGY LOSS PLOTS AND YIELD SPECTRA. . . . .	125
A. Energy Loss of Electrons in $N_2$ . . . . .	125
B. Spatial Yield Spectra for Electrons Impinging on $N_2$ . .	130
1. Three Variable Spatial Yield Spectra . . . . .	132
2. Four Variable Spatial Yield Spectra. . . . .	143
VIII CONCLUSIONS. . . . .	152

	<u>Page</u>
APPENDIX	
A    MONTE CARLO PROGRAM. . . . .	155
B    GETDAT PROGRAM . . . . .	200
REFERENCES. . . . .	220
BIOGRAPHICAL SKETCH . . . . .	227

Abstract of Dissertation Presented to the Graduate Council  
of the University of Florida in Partial Fulfillment of the Requirements  
for the Degree of Doctor of Philosophy

SPATIAL AND ENERGETIC ASPECTS OF ELECTRON ENERGY DEPOSITION

By

Charles Herbert Jackman

August, 1978

Chairman: A.E.S. Green  
Major Department: Physics and Astronomy

The spatial and energetic aspects of the electron energy degradation into molecular nitrogen gas have been studied by a Monte Carlo method. Perpendicularly monoenergetic incident electrons with energies from 0.1 through 5.0 KeV were injected into the  $N_2$  gas. This Monte Carlo degradation scheme employed previously developed  $N_2$  cross sections with new phenomenological differential elastic and doubly differential ionization cross sections. All these agree quite well with experimental work and are consistent with the higher energy theoretical total cross section fall-off with energy.

Information has been generated concerning the following topics:

- 1) range values and  $3914 \text{ \AA}$  intensity profiles for the longitudinal and radial directions which can be easily compared with experimental work;
- 2) a sensitivity study characterizing the influence of the input cross sections on the spatial energy deposition of the electrons;
- 3) the rate of energy loss by the electrons as they interact with the  $N_2$  gas; and
- 4) spatial yield spectra for incident electron energies in the range from 0.1 to 5.0 KeV (evaluated between 2 eV and the incident energy) which are analytically characterized for future work on atmospheric problems dealing with incident energetic electrons.

## CHAPTER I

### INTRODUCTION

Calculating the spatial and energetic aspects of the energy deposition of intermediate energy electrons (with incident energies from 100 to 5000 eV) in the earth's atmosphere is a difficult, yet intriguing, problem. These intermediate energy electrons (hereafter called IEEs) include the highest energy photoelectrons, a large bulk of the auroral electrons, and many secondary electrons produced by solar protons and cosmic rays.

These electrons lose most of their energy through ionization events, electronic excitations, vibrational excitations, and rotational excitations. Elastic collisions reduce the electron energy slightly, but mainly these interactions influence the direction of motion of the electron.

The atmosphere is dominated by the presence of molecular nitrogen up to a height of about 150 kilometers. Even above this altitude (at least up to 300 km),  $N_2$  continues to play a substantial role in the atmospheric processes. For this reason the study of the influence of impinging electrons on molecular nitrogen is the major thrust of this paper.

One aspect of this study is the formulation of a complete cross section (differential and total) set for IEEs impacting on  $N_2$ . The very difficult problem of modeling the interactions of the impinging IEEs in

the upper atmosphere is then reduced in complexity. Since  $N_2$  interacts with electrons similar to the way that other atmospheric gases interact with electrons, it follows that differential and total cross section sets for these gases could be assembled in a like manner.

Another aspect of this work is a sensitivity comparison among several of the influences on the electron energy deposition. The spatial energy degradation is vitally linked to the elastic phase function used. Since there are data available on the elastic differential cross sections of  $N_2$  as well as the energy degradation resulting from electron impact on  $N_2$ , a comparison illustrating the effects of a variation of the elastic phase function is quite useful. Other influences on the spatial energy deposition, including ionization and excitation differential cross sections and the total elastic cross sections, are also considered in this work.

In order to deal with these spatial and energetic aspects of electron energy degradation, a Monte Carlo (which may be abbreviated MC) calculation is used. The MC technique, depending on how it is used, can be the most accurate energy deposition approach. Use of this MC method at various incident energies helps in the assemblage of the best cross section set for  $N_2$  and provides the easiest way of comparing some of the influences on the spatial energy deposition.

The details of this undertaking are discussed in Chapters II through VIII. A paragraph summary of each chapter is given below.

The second chapter presents a brief review of some of the standard electron energy deposition methods. The continuous slowing down approximation, discrete energy bin, Fokker-Planck equation, two-stream equation of transfer, and the multi-stream equation of transfer are all included

in section II.A. The MC method which was used in this study along with three other MC approaches are briefly described in section II.B.

This MC approach requires knowledge of differential and total cross sections. The third chapter discusses the cross sections that were used for  $N_2$ . Section III.A includes the elastic differential and total cross sections. The inelastic differential and total cross sections are next discussed in section III.B. Section III.C, then, considers the total (inelastic plus elastic) cross section of  $N_2$ .

In Chapter IV, the MC calculational procedure is considered. A brief discussion of the approach is given in section IV.A. The computer programs and machinery used in this work are discussed in section IV.B with the programs listed in appendices A and B. A detailed discussion of the MC electron energy degradation technique is presented in section IV.C. Finally, the statistical error resulting from the Monte Carlo calculation is given in section IV.D.

The MC three-dimensional intensity plots with comparison to experiment are given in Chapter V. The excitation of the  $N_2^+ B^2 \Sigma_u^+$  state is discussed in section V.A with the concept of range being defined in section V.B. Previous experimental and theoretical work on the 3914 Å emission from  $N_2^+$  is considered in section V.C and section V.D presents some range results and intensity plots in the longitudinal direction from this MC calculation. Section V.E, then, concludes the chapter with a comparison between the MC intensity plots in the radial direction and the experimental data.

The main concern of Chapter VI is a sensitivity study. The effects of the ionization differential cross section on the intensity distributions are considered in section VI.A. Section VI.B, then, discusses the

influence of inelastic differential cross sections on the intensity distribution. A comparison of different elastic phase functions on the electron-N<sub>2</sub> collision profile (no energy loss) is given in section VI.C. Next, the influence of different elastic phase functions on the electron energy deposition is presented in section VI.D. Finally, section VI.E considers the influence of the total elastic cross section on the electron energy deposition.

The energy loss plots and yield spectra from the MC calculations are given in Chapter VII. Section VII.A presents the energy loss plots and section VII.B includes a discussion of the yield spectra.

Chapter VIII concludes this paper with a summary of this work and its impact on the spatial and energetic aspects of the electron energy deposition problem.

## CHAPTER II

### A SHORT REVIEW OF ENERGY DEPOSITION TECHNIQUES

Several standard energy deposition techniques will be discussed in this chapter. In the first section, II.A, several general ways for treating the degradation of the energy of charged particles will be reviewed briefly. The second section, II.B, includes a brief sketch of four Monte Carlo energy deposition schemes: The MC approach applied in this work and three other MC techniques.

#### A. Energy Deposition Techniques

Since the turn of the century, researchers have been studying the energy degradation of rapidly moving particles in a medium. Initial work in this area was carried out by Roentgen, Becquerel, Thompson, Bragg, Rutherford, Bohr, and other founders of modern physics.

These pioneers in the energy degradation process were mainly concerned with the medium affecting the particle. In order to solve this complex energy degradation problem, most of the early workers used a local energy deposition approximation. Even today many degradation problems can be solved fairly accurately with this local approximation.

One of the earliest local energy deposition methods is that of the continuous slowing down approximation (hereafter called CSDA) first used by Niels Bohr (1913, 1915). Bethe (1930) expanded on this work and used an approximate theoretical treatment (valid at high energies) to describe the slowing down of particles in a medium.

This work of Bethe (1930) required knowledge of the stopping power,  $-\frac{dE}{dx}$  (the rate at which energy E is lost from the impinging particles incident along the x axis). This stopping power is given by

$$-\frac{dE}{dx} = n \sum_i^{\rightarrow} W_i \sigma_i(E) \quad (2.1)$$

(see Dalgarno, 1962, p. 624) where the summation  $\sum_i^{\rightarrow}$  includes integration over the continuum (thus allowing for energy loss through ionization),  $W_i$  is the energy loss for the ith state, and  $\sigma_i(E)$  is the cross section for excitation to the ith state at energy E. Knowledge of the stopping power then leads to information about the mean distance traveled by the particle (referred to as the range). This range R(E) of a particle of energy E is simply given by

$$R(E) = \int_0^E \frac{dE}{(-\frac{dE}{dx})} \quad (2.2)$$

Atmospheric researchers are more interested in the effects that the particles have on the medium rather than the medium affecting the particles. These effects could include both spectral emissions by the constituents and heating of the atmosphere.

Green and Barth (1965) were the first workers to adapt a variation of the CSDA to the problems in aeronomy. In this approach the total energy loss function  $L(E) = -(\frac{1}{n}) \frac{dE}{dx}$  is determined by

$$L(E) = \sum_k W_k \sigma_k(E) + \sum_j I_j \sigma_{I_j}(E) + \sum_j \int_0^{(E - I_j)/2} \frac{d\sigma_{I_j}(E, T)}{dT} dT \quad (2.3)$$

where  $W_k$  is the threshold for excitation to the kth state,  $\sigma_k(E)$  is the cross section for excitation to the kth state at energy E,  $I_j$  is the threshold for ionization and excitation to the jth state, and  $\frac{d\sigma_{I_j}(E, T)}{dT}$

is the secondary differential ionization cross section for the creation of a secondary electron of energy,  $T$ , from a primary electron of energy  $E$ . The loss function with detailed atomic cross sections (hereafter called DACSs) was used to make reasonable estimates of the ultraviolet emissions resulting from an aurora event. In this approach, the excitations  $J_k(E)$  of the  $k$ th state resulting from an electron of energy  $E$  were simply represented as

$$J_k(E) = \int_{W_k}^E \frac{\sigma_k(E')}{L(E')} dE' \quad (2.4)$$

Green and Dutta (1967) built on this work and used the Born-Bethe approximations, the Massey-Mohr-Bethe surface, the Bethe sum rule, and a "distorted" oscillator strength to lay the groundwork for extension of the DACS approach to other gases. Jusick, Watson, Peterson, and Green (1967), Stolarski, DuLock, Watson, and Green (1967), and Watson, DuLock, Stolarski, and Green (1967) applied this approach to helium, molecular nitrogen, and molecular oxygen, respectively.

Stolarski and Green (1967) used this CSDA to calculate auroral intensities with these DACSs and Green and Barth (1967) applied this method to the problem of photoelectrons exciting the dayglow. Other atmospheric physicists (namely, Kamiyami, 1967; and Rees, Stewart, and Walker, 1969) started around this same time and also employed a CSDA type approach to that problem of energetic electrons depositing their energy in the atmosphere.

The oldest discrete energy apportionment method is that of Fowler (1922-23) which is directly related to the Spencer and Fano (1954) approach (see Inokuti, Douthat, and Rau, 1975). The Fowler equation is

solved by building on the lower-energy solutions to obtain the higher energy solutions. The Spencer-Fano method introduces the electron at the highest energy and solves the equation at successively lower energies. An approach similar to the Spencer-Fano method was developed by Peterson (1969) and is called the discrete energy bin (hereafter called the DEB) method.

Peterson (1969) pointed out certain differences between the CSDA and the DEB results. In particular, he noted that the DEB method tends to predict higher populations of some excited states than does the CSDA.

In the modification of the DEB method by Jura (1971), Dalgarno and Lejeune (1971), and Cravens, Victor, and Dalgarno (1975), the equilibrium flux or degradation spectrum  $f(E, E_0)$  (for incident energy  $E_0$  and electron energy  $E$  and in units of  $\# \text{ cm}^{-2} \text{ sec}^{-1} \text{ eV}^{-1}$ ) of Spencer and Fano (1954) is obtained directly. Douthat (1975), in an effort to make the degradation spectra suitable for applications, proposed an approximate method of "scaling." Unfortunately, this method is quite cumbersome and not very accurate. This impelled Garvey, Porter, and Green (1977) to seek an analytic representation of the degradation spectra and, despite its complex nature, they found an analytic expression to represent this spectra for  $\text{H}_2$ .

The concept of the "yield spectra"  $U(E, E_0)$  was first initiated through a modified DEB approach given in Green, Jackman, and Garvey (1977) in an effort to find a quantity with simpler properties than the degradation spectra. By utilizing the product

$$U(E, E_0) = \sigma_T(E) f(E, E_0)$$

where  $\sigma_T(E)$  is the total inelastic cross section for an electron of energy  $E$ , one defines a quantity  $U(E, E_0)$  which not only has a simpler

shape than  $f(E, E_0)$  but also has approximately the same magnitude for all substances. This yield spectrum can also be represented analytically. It effectively embodies the non-spatial information of the degradation process.

Jackman, Garvey, and Green (1977a), using this modified DEB, elaborated on the differences between the DEB method and the CSDA. The more accurate modified DEB method was found to produce consistently more ions per energy loss while at the same time producing less excitations of some of the low lying states when compared with the CSDA. The CSDA, although inexpensive to use, appears to be ill-suited for calculations requiring an absolute accuracy better than about 20%. Since auroral and dayglow intensities are rarely measured to better than this accuracy, the CSDA has been adequate for most purposes of concern in aeronomy. However, with future improved measurements it should be purposeful to utilize more accurate deposition techniques.

Several recent spatial electron energy deposition studies have been concerned with the spatial aspects of auroral electron energy deposition. Walt, MacDonald, and Francis (1967) employed the Fokker-Planck diffusion equation to give a detailed description of kilovolt auroral electrons. The Fokker-Planck equation, as given in the Strickland, Book, Coffey, and Fedder (1976) paper, is written

$$\begin{aligned} \mu \frac{\partial \phi(z, E, \mu)}{n(z) \sigma(E) \partial z} = \frac{Q(E)}{2\sigma(E)} \frac{\partial}{\partial \mu} [(1 - \mu^2) \frac{\partial \phi(z, E, \mu)}{\partial \mu}] \\ + \frac{1}{\sigma(E)} \frac{\partial}{\partial E} [L(E) \phi(z, E, \mu)] \end{aligned} \quad (2.5)$$

where  $\phi(z, E, \mu)$  is the flux (in units of  $\text{cm}^{-2} \text{sec}^{-1} \text{eV}^{-1} \text{sr}^{-1}$ ),  $z$  is the distance into the medium along the  $z$  axis,  $E$  is the electron energy,

and  $\mu$  is the cosine of the pitch angle associated with the direction of motion of the electron. The symbols  $n$ ,  $\sigma$ ,  $Q$ , and  $L$  are the number density of the scatterers, the total cross section (both elastic and inelastic), the momentum transfer cross section, and the loss function, respectively.

The momentum transfer cross section, given in terms of the differential elastic cross section,  $\frac{d\sigma(E)}{d\Omega}$ , is written as

$$Q(E) = \int_0^{2\pi} \int_0^{\pi} \frac{d\sigma(E)}{d\Omega} (1 - \cos\theta) \sin\theta d\theta d\phi \quad (2.6)$$

This Fokker-Planck equation may be thought of as a CSDA approach to the spatial energy degradation problem. Its solution, therefore, is only accurate in the higher energy regime.

Banks, Chappell, and Nagy (1974) were able to calculate the emission as a function of altitude for a model aurora using the Fokker-Planck equation for electrons with energy  $E > 500$  eV along with a two-stream equation of transfer for electrons with energy  $E \leq 500$  eV. The two-stream equation of transfer solves the transport of electrons in terms of the hemispherical fluxes of two electron streams  $\phi^+(E, z)$ , the electron flux upward along  $z$ , and  $\phi^-(E, z)$ , the electron flux downward along  $z$ . The steady state continuity equations for  $\phi^+$  and  $\phi^-$  can then be written as

$$\begin{aligned} \frac{d\phi^+}{dz} = & \frac{-1}{\langle \cos\theta \rangle} \sum_k n_k [\sigma_a^k + p_e^k \sigma_e^k] \phi^+ \\ & + \frac{1}{\langle \cos\theta \rangle} \sum_k n_k p_e^k \sigma_e^k \phi^- + \frac{q}{2\langle \cos\theta \rangle} + \frac{q^+}{\langle \cos\theta \rangle} \end{aligned} \quad (2.7)$$

and

$$\begin{aligned}
 -\frac{d\phi^-}{dz} = & -\frac{1}{\langle \cos\theta \rangle} \sum_k n_k [\sigma_a^k + p_e^k \sigma_e^k] \phi^- \\
 & + \frac{1}{\langle \cos\theta \rangle} \sum_k n_k p_e^k \sigma_e^k \phi^+ + \frac{q}{2\langle \cos\theta \rangle} + \frac{q^-}{\langle \cos\theta \rangle}
 \end{aligned} \tag{2.8}$$

where

$$\sigma_a^k = \sum_i \sigma_{ai}^k \tag{2.9}$$

$$\begin{aligned}
 q^+(E, z) = & \sum_k n_k(z) \sum_{\substack{j \\ E' > E}} \{ p_{aj}^k(E') \sigma_{aj}^k(E' \rightarrow E) \phi^-(E, z) \\
 & + [1 - p_{aj}^k(E')] \sigma_{aj}^k(E' \rightarrow E) \phi^+(E', z) \}
 \end{aligned} \tag{2.10}$$

$$\begin{aligned}
 q^-(E, z) = & \sum_k n_k(z) \sum_{\substack{j \\ E' > E}} \{ p_{aj}^k(E') \sigma_{aj}^k(E' \rightarrow E) \phi^+(E', z) \\
 & + [1 - p_{aj}^k(E')] \sigma_{aj}^k(E' \rightarrow E) \phi^-(E', z) \}
 \end{aligned} \tag{2.11}$$

and  $z$  is the distance along a magnetic field line (positive outward);  $n_k(z)$  is the  $k$ th neutral species number density;  $p_e^k(E)$  is the electron backscatter probability for elastic collisions with the  $k$ th neutral species;  $\sigma_e^k(E)$  is the electron total scattering cross section for the  $k$ th neutral species;  $q(E, z)$  is the electron production rate in the range  $E$  to  $E+dE$  due to ionization processes (both electron ionization and photoionization);  $q^\pm$  is the electron production in the range  $E$  to  $E+dE$  due to cascading from higher-energy electrons undergoing inelastic collisions;  $p_{aj}^k$  is the electron backscatter probability for collisions with the  $k$ th neutral species resulting in the  $j$ th inelastic process; and  $\sigma_{aj}^k$  is the inelastic cross section for the  $j$ th excitation of the  $k$ th neutral species.

This approach combined these two methods of electron energy deposition in order to find a reasonable solution to the very difficult auroral energy deposition problem. The Fokker-Planck method is accurate only at large incident energies; therefore, it should only be used at energies above 500 eV. The two-stream equation of transfer approach, on the other hand, is more accurate at energies below 500 eV. This combination then provided a very reasonable solution to the auroral electron spatial deposition problem for a reasonable amount of calculation.

The Fokker-Planck equation and the two-stream equation of transfer may both be derived from the Boltzmann equation or the general equation of transfer. This general equation of transfer, in one of its simpler forms, is written as (from Strickland et al., 1976)

$$\mu \frac{d\phi(z, E, \mu)}{dz} = -n(z)\sigma(E)\phi(z, E, \mu) + n(z)\sigma(E) \int R(\mu', \mu, E', E)\phi(z, E', \mu')dE'd\mu' \quad (2.12)$$

(assuming a steady state condition and no external fields) where

$$R(\mu', \mu, E', E) = \frac{\sum_j \sigma_j(\mu', \mu, E', E)}{\sigma(E)} \quad (2.13)$$

with the sum over all processes. The symbols  $\mu$  and  $\mu'$  are the cosines of the pitch angles  $\theta$  and  $\theta'$  which are associated with the directions  $\vec{n}$  and  $\vec{n}'$  given in Figure 2.1.

The first term on the right hand side of Eq. (2.12) represents the scattering out of  $\mu$ . The  $R(\mu', \mu, E', E)$  in the second term is the probability ( $eV^{-1}(2\pi sr)^{-1}$ ) that a collision of an electron of energy  $E'$  and direction  $\mu'$  with some particle will result in an electron of energy  $E$

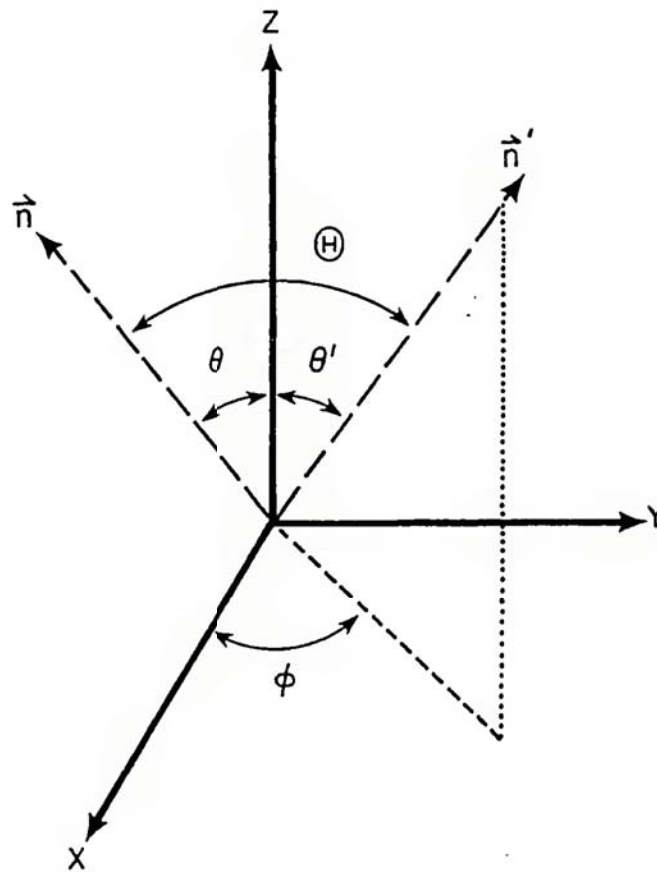


Figure 2.1 The directions denoted by  $\vec{n}'$  and  $\vec{n}$  are the incident and scattered directions of the electron, respectively.

and direction  $\mu$ . The integral in Eq. (2.12) is over all possible energies  $E'$  and directions of motion  $\mu'$ .

Strickland et al. (1976) studied the auroral electron scattering and energy loss with a multiangle equation of transfer. Their approach is one of the most accurate yet applied to auroral electrons. This multiangle method of solution is more realistic than the two-stream approach and it is computationally more difficult as well.

The methods discussed above are the "state of the art" approaches (excluding the Monte Carlo methods which are discussed in section II.B) to the IEEs degrading in the atmosphere. Other approaches used by Jasperse (1976, 1977) and Mantas (1975) are mainly concerned with photoelectrons and will not be discussed here.

The Monte Carlo approach can rival any of these electron energy deposition methods in accuracy when used in the proper manner. This stochastic technique for solving the deposition problem will be considered next in section II.B.

### B. Monte Carlo Energy Deposition Techniques

Another method of solving the spatial energy deposition problem is the use of the Monte Carlo approach. The MC technique, which is used in this paper, is a stochastic method of degrading an energetic electron. The approach can be one of the most exact methods of electron energy deposition. Briefly, one electron is taken at a time and allowed to degrade in energy collision by collision. This deposition attempts to mimic the randomness of the actual degradation process that occurs in nature.

Many MC schemes have been applied in all areas of physics. Some are more exact and more detailed than others. Since virtually all the MC methods are run on the computer, the most exact approaches cost the most computer time and money. The precision of the technique must be balanced against a finite computer budget.

Three approaches using the MC deposition scheme, that have been applied to electrons impinging on the atmosphere, are discussed below. Brinkmann and Trajmar (1970) applied experimental differential electron impact energy loss data in a MC computation for electrons of 100 eV energy. Because of the large amount of input cross sections in numerical form, only electrons of 100 eV incident energy were degraded with this method.

In the lower electron energy regime (below 25 eV), Cicerone and Bowhill (1970, 1971) used a MC technique to simulate photoelectron diffusion through the atmosphere. This method, which included both elastic and inelastic processes, predicted escape fluxes from the atmosphere.

Berger, Seltzer, and Maeda (1970, 1974) (hereafter called BSM) worked with high energy electrons (with energies from 2 KeV to 2 MeV). They employed a MC approach that has two variations which are pointed out below. They treat inelastic collisions in a continuous slowing down manner. The energy deposited by the electrons along their path is assumed to be equal to the mean loss given by the loss function,  $L(E)$ , from Rohrlich and Carlson (1954).

The angular deflection resulting from elastic collisions has been evaluated by two separate methods in BSM. One approach employed the multiple scattering distribution of Goudsmit and Saunderson (1940) applied to the screened Rutherford cross section given in BSM. The

other approach involved a sampling of each elastic collision. Application of the BSM technique to a constant density medium and no magnetic field gave good agreement with laboratory experiments (Grün, 1957; and Cohn and Caledonia, 1970).

In this study, a MC method was needed that could be applied to IEEs. The basic equation of transfer is solved with the use of the MC approach. This equation can be rewritten as

$$\begin{aligned}
 \mu \frac{dU(\mu, z, E, E_0)}{\sigma_T(E) dz} = & -n(z)U(\mu, z, E, E_0) \\
 & + n(z) \int_E^{E+\Delta E} \int_{-1}^1 p_e(\mu', \mu, E', E) U(\mu', z, E', E_0) d\mu' dE' \\
 & + n(z) \sum_i \int_{2E+I_i}^{E_0} \int_{-1}^1 p_{IOHi}(\mu', \mu, E', E) U(\mu', z, E', E_0) d\mu' dE' \\
 & + n(z) \sum_j \int_{W_j}^{E_0} p_{aj}(\mu', \mu, E', E) U(\mu', z, E', E_0) d\mu' dE' \quad (2.14)
 \end{aligned}$$

No external fields are included here and a steady state is assumed. The  $U(\mu, z, E, E_0)$  is the "yield spectra" (in  $\text{eV}^{-1} \text{sec}^{-1} \text{sr}^{-1}$ ) and it is assumed that there is only one neutral scattering species. In this equation  $\sigma_T(E)$  is the total cross section (elastic + inelastic) for the species,

$$\Delta E_{\text{Elas}} = 2E(1 - \cos\theta) \frac{M_{\text{electron}}}{M_{\text{neutral species}}} \quad (2.15)$$

is the energy loss during an elastic collision,  $p_e(\mu', \mu, E', E)$  is the probability during an elastic collision with a neutral specie that an electron with energy  $E'$  and direction  $\mu'$  will result in an electron of

energy  $E$  and direction  $\mu$ ,  $p_{IONi}(\mu',\mu, E',E)$  is the probability during an ionization collision with a neutral species that an incident electron with energy  $E'$  and direction  $\mu'$  will result in a secondary electron of energy  $E$  and direction  $\mu$ , and  $p_{aj}(\mu',\mu,E',E)$  is the probability during an inelastic collision (excitation or ionization) with a neutral specie that an incident electron with energy  $E'$  and direction  $\mu'$  will result in the incident electron being scattered into direction  $\mu$  with energy  $E$ .

Some techniques from each of the other three MC methods were included in this work. Some new approximations and assumptions were made, however, to enhance the accuracy of the computations as well as simplify some of the calculations. These assumptions are discussed in detail in Chapter IV.

In this MC work the information is stored in a collision by collision manner on a magnetic tape. Once all the case histories are generated, then, the tape is scanned and any correlations of interest may be determined. The choice of altitude and energy intervals is specified only during the scanning of the tape. This method allows for greater flexibility in minimizing the statistical uncertainties of the results, while, at the same time retaining good spatial or energy resolution (Porter and Green, 1975).

All the degradation methods mentioned in this chapter require cross sections as input. The cross sections used in this MC work are, therefore, discussed in the next chapter.

## CHAPTER III

### ELASTIC AND INELASTIC DIFFERENTIAL AND TOTAL CROSS SECTIONS FOR N<sub>2</sub>

In this chapter differential and total cross sections for electron impact on N<sub>2</sub> will be discussed. Section III.A reviews the elastic cross sections of N<sub>2</sub> and discusses three models for representation of these properties. In section III.B the inelastic cross sections of N<sub>2</sub> are presented with their relationship to theory and experiment. Section III.C, then, concludes this chapter with a discussion of the total (elastic plus inelastic) cross section for N<sub>2</sub>. Any energy degradation technique requires knowledge of these cross sections for a complete evaluation of the energy loss by electrons in a gas.

#### A. Elastic Differential and Total Cross Sections for N<sub>2</sub>

One of the most common differential elastic cross section forms is the screened Rutherford cross section which can be expressed in the form

$$\frac{d\sigma}{d\Omega} = \left[ \frac{z^2 e^4}{p^2 v^2 (1 - \cos\theta + 2\eta)^2} \right] K_{rel}(\theta) \quad (3.1)$$

where  $K_{rel}(\theta)$  is the spin-relativistic correction factor.

The familiar Rutherford cross section (unscreened case) which can be derived from classical scattering theory is given by

$$\frac{d\sigma}{d\Omega} = \frac{z^2 e^4}{p^2 v^2 (1 - \cos\theta)^2} \quad (3.2)$$

where

$$\sin^2 \frac{\theta}{2} = 1 - \cos\theta$$

Here, an electron is elastically scattered by a nucleus of charge  $Z$  using the Coulomb potential

$$V(r) = \frac{Ze^2}{r} \tag{3.3}$$

with  $r$  being the distance between the two particles.

Treating scattering in a quantum mechanical approach with the use of the Born approximation and a potential of the form

$$V(r) = \frac{Ze^2}{r} e^{-\gamma r} \tag{3.4}$$

where  $\gamma$  is a positive but small quantity approaching 0, Eq. (3.2) can again be derived. The Born approximation, using the potential in Eq. (3.4), is only valid in certain angle and energy regimes (Mott and Massey, 1965, pp. 24 and 466). At sufficiently high angles and low energies, the Born approximation fails. The range of validity varies for different substances and for  $N_2$  the Born approximation is probably not accurate at all angles for energies less than 100 eV and at large angles for energies less than 500 eV.

Equation (3.2) does, however, go to infinity when  $\theta$  approaches  $0^\circ$ . This differential cross section also leads to an infinite value in the total elastic cross section. Both of these results are unreasonable for elastic scattering of electrons by atoms and molecules. The most popular way of correcting this unreal behavior is to add a screening parameter  $\eta$ . Equation (3.1) portrays this resulting form.

Equation (3.1) has a maximum at  $\theta = 0^\circ$  and a minimum at  $\theta = 180^\circ$ . At energies below 200 eV, experimental results indicate a minimum in the elastic differential cross sections at about  $90^\circ$  with a strong forward scattering peak at  $\theta = 0^\circ$  and a secondary backward scattering peak at  $\theta = 180^\circ$ .

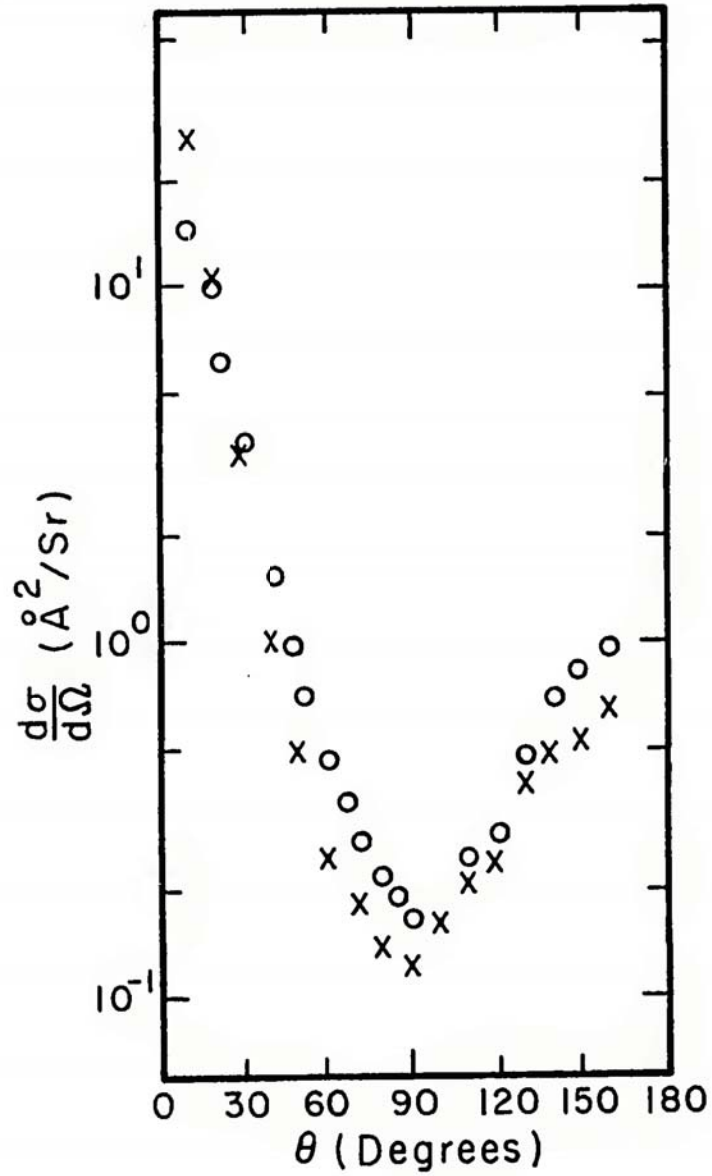
In Figure 3.1 experimental data for energies at  $E = 30$  and  $70$  eV are presented. These data are taken from Shyn, Stolarski, and Carignan (1972) with the small circles denoting  $30$  eV points and the crosses denoting the  $70$  eV data.

Later on in this section the screened Rutherford cross section and another analytic model of the differential elastic cross section are compared with experimental data. Before discussing the differential cross section in more detail, first, consider the total elastic cross section.

Several experiments have been performed deriving the total elastic cross sections for  $N_2$ . There have also been several theoretical studies on the  $N_2$  elastic total cross sections. Two recent reviews of the data available on this subject are Kieffer (1971) and Wedde (1976).

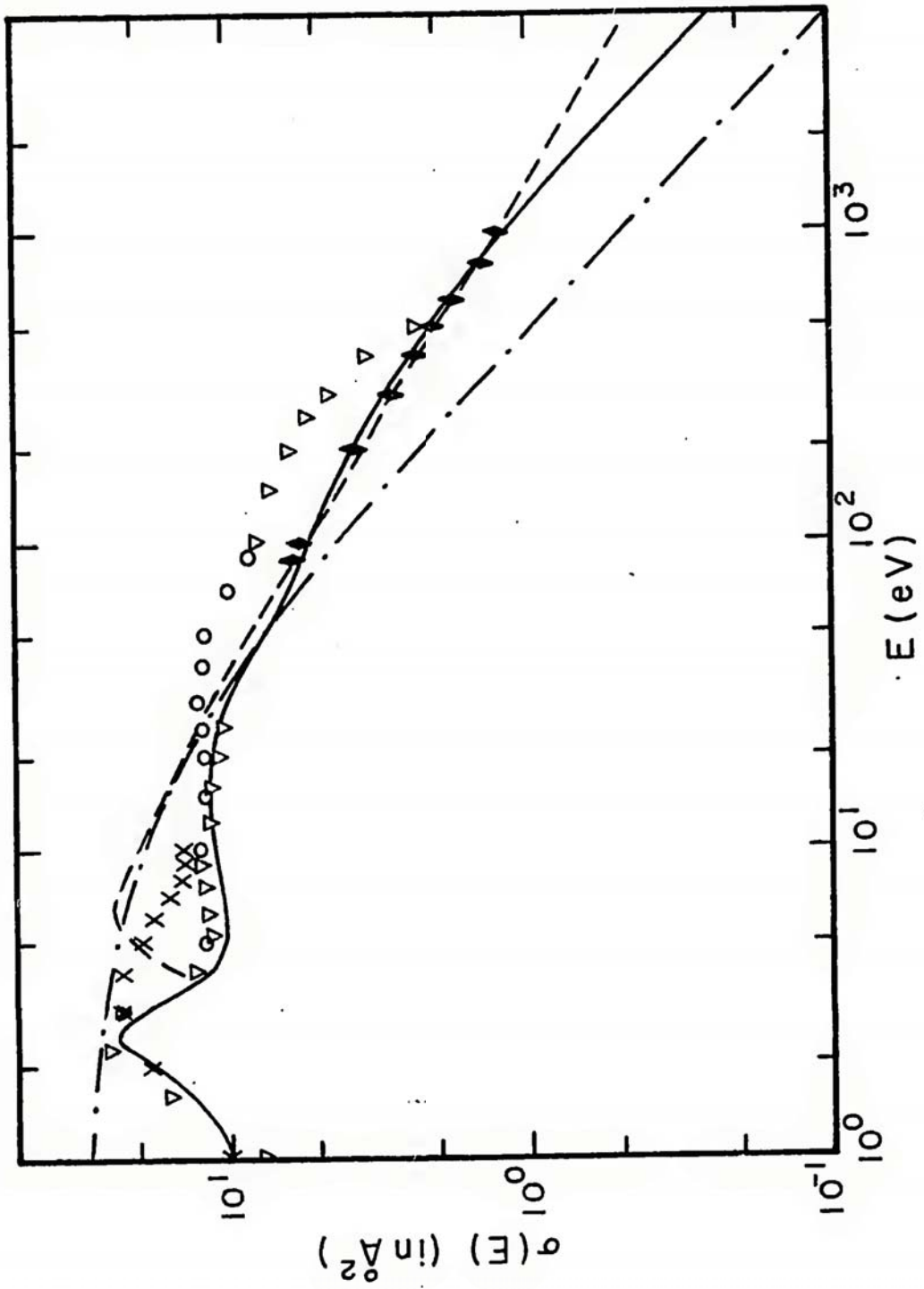
A plot of all this data would obscure the analytic total cross sections specifically considered in this work. Consequently, only data from Sawada, Ganas, and Green (1974) (theoretical), Shyn, Stolarski, and Carignan (1972) (experimental), and Herrmann, Jost, and Kessler (1976) (experimental) are plotted in Figure 3.2. The sets of data overlap to a degree such that the disagreement in absolute magnitude of the total cross sections is readily apparent.

In view of this disagreement, no experimental or theoretical data are assumed to be absolutely correct and some average of this data is



× Figure 3.1  $\text{N}_2$  experimental electron impact elastic cross section data from Shyn, Stolarski, and Carignan (1972). o's denote data from  $E = 30$  eV and the x's denote data from  $E = 70$  eV.

Figure 3.2 N<sub>2</sub> electron impact total elastic cross section data from Sawada, Ganas, and Green (1974), x; Shyn, Stolarski, and Carignan (1972), o; Herrmann, Jost, and Kessler (1976), ◆; and Banks, Chappell, and Nagy (1974), ∇. Equation (3.6) is represented by the dash-dot line, Eq. (3.8) by the dashed line, and Eq. (3.9) by the solid line.



desirable. An analytic function representing the total elastic cross section is most easily used in a computer program. Consider now an analytic form derived from the differential screened Rutherford cross section.

Knowledge of the differential cross section implies knowledge of the total elastic cross section as they are simply related by

$$\sigma(E) = \int_0^{2\pi} \int_0^{\pi} \frac{d\sigma}{d\Omega} \sin\theta d\theta d\phi \quad (3.5)$$

where  $\phi$  is the azimuthal angle. Substituting Eq. (3.1) into Eq. (3.5), the total elastic cross section,  $\sigma_R(E)$ , resulting from the screened Rutherford cross section is very simply given as

$$\sigma_R(E) = \frac{Z^2}{E^2} \frac{51.8}{\eta(1+\eta)} \pi \quad (3.6)$$

If  $E$  is given in eV then  $\sigma_R(E)$  is in units of  $10^{-16} \text{ cm}^2$ . The screening parameter

$$\eta = \eta_c \frac{1.70 \times 10^{-5} Z^{2/3}}{\tau(\tau + 2)} \quad (3.7)$$

according to the Moliere (1947, 1948) theory. Berger, Seltzer, and Maeda (1970) assumed that  $\eta_c$  was a constant value and decided on  $\eta_c = 1$  as its best value. The  $\tau$  in Eq. (3.7) is the electron energy in units of the electron rest energy so that  $\tau = E/mc^2$ . In the energy regime of interest ( $E \leq 5 \text{ KeV}$ ),  $\tau \ll 2$ , and  $Z = 7$ . Noting these observations, Eq. (3.7) can be rewritten as  $\eta \approx \frac{16}{E}$ .

The total cross section from Eq. (3.6) is plotted in Figure 3.2 as the dash-dot line. A noticeable difference is evident between this model and the experimental values at practically all energies.

Using the form

$$\sigma(E) = \frac{q_0 F [1 - (\frac{W}{E})^\alpha]^\beta}{E^c W} \quad (3.8)$$

implemented first by Green and Barth (1965), where  $q_0 = 651.3 \text{ \AA}^2 \text{ eV}^2$ , the total elastic cross section for  $N_2$  was characterized fairly well in the range from 30 to 1000 eV using the parameters  $\alpha = 1$ ,  $\beta = 0.6$ ,  $c = 0.64$ ,  $F = 0.43$ , and  $W = 2.66$ . The  $E^{-0.64}$  dependence of Eq. (3.8) at the larger energies is similar to that seen by Wedde and Strand (1974) for  $N_2$ . This form does not represent the data as well below 30 eV and, in fact, is not defined below an energy of 2.66 eV.

Porter and Jump (1978) have used a more complex total elastic cross section form which is written as

$$\sigma(E) = T \left\{ \frac{E^X}{\eta(\eta + 1)[V^{2+X} + E^{2+X}]} + \frac{F_1 G_1^2}{(E - E_1)^2 + G_1^2} + \frac{F_2 G_2^2}{(E - E_2)^2 + G_2^2} \right\} \quad (3.9)$$

Here,  $\eta = \frac{U}{E}$

and for $N_2$ :	$T = 2.5 \times 10^{-6} \text{ cm}^2$	$F_1 = 7.33$
	$U = 1.95 \times 10^{-3} \text{ eV}$	$E_1 = 2.47 \text{ eV}$
	$V = 150 \text{ eV}$	$G_2 = 24.3 \text{ eV}$
	$X = -0.770$	$F_2 = 2.71$
	$G_1 = 0.544 \text{ eV}$	$E_2 = 15.5 \text{ eV}$

In the large energy limit, the total cross section falls off as  $1/E$ , similar to the screened Rutherford cross section. This form does contain two other terms (the second and third terms) which were introduced

phenomenologically to describe the low energy shape and Feshbach resonances.

If either Eq. (3.8) or (3.9) is used as the total elastic cross section, the differential elastic cross section must be normalized such that:

$$\int_0^{2\pi} \int_0^{\pi} P(\theta, E) \sin\theta d\theta d\phi = 1 \quad (3.10)$$

where  $P(\theta, E)$  is the phase function and the differential cross section can be written as

$$\frac{d\sigma}{d\Omega} = \sigma(E) P(\theta, E) \quad (3.11)$$

With this in mind consider now three separate phase function forms. The first phase function form is very similar to the screened Rutherford cross section and it is written here as

$$P_{M1}(\theta, E) = \frac{-1}{2\pi[(2 + a(E))^{-1} - a(E)^{-1}][1 - \cos\theta + a(E)]^2} \quad (3.12)$$

This is known as model 1. The parameter "a" acts in a similar manner to the " $2\eta$ " term in the denominator of the screened Rutherford cross section form and is written

$$a(E) = a_1 \left( \frac{E}{1 \text{ eV}} \right)^{a_2}$$

The second phase function form (model 2) includes the forward scattering term of Eq. (3.12) along with a backscattering term and is given as

$$P_{M2}(\theta, E) = \frac{-f(E)}{2\pi[(2 + a(E))^{-1} - a(E)^{-1}][1 - \cos\theta + a(E)]^2} - \frac{(1 - f(E))}{2\pi[(2 + c(E))^{-1} - c(E)^{-1}][1 + \cos\theta + c(E)]^2} \quad (3.13)$$

where

$$f(E) = \frac{(E/f_1)^{f_2}}{(E/f_1)^{f_2} + f_3}$$

$$a(E) = a_1 \left(\frac{E}{1 \text{ eV}}\right)^{a_2}$$

and

$$c(E) = c_1 \left[1 - \left(\frac{c_2}{E}\right)^{c_3}\right]$$

Irvine (1965) was one of the first researchers in scattering problems to use a phase function containing forward and backward scattering terms. He applied a sum of two Henyey-Greenstein functions to the problem of photon scattering by large particles. Porter and Jump (1978) also have used a sum of two terms (one for forward scatter and one for backward scatter). They fitted experimental data at several separate energies with their form. Use of their differential cross section form in a deposition calculation probably would require the use of spline functions or other interpolative techniques.

The third phase function (model 3) is now considered. At small angles the differential cross section shows a near exponential-like fall off. This behavior has been pointed out by several experimenters (see, for example, Shyn, Carignan, and Stolarski, 1972; and Herrmann, Jost, and Kessler, 1976). It was this experimental observation that led to

model 3 which is written as

$$\begin{aligned}
 P_{M3}(\theta, E) = & \frac{f_1(E)[1 - b^2(E)]e^{-\theta/b(E)}}{2\pi b^2(E)[1 + e^{-\pi/b(E)}]} \\
 & - \frac{f_2(E)}{2\pi[(2 + a)^{-1} - a^{-1}][1 - \cos\theta + a]^2} \\
 & - \frac{[1 - f_1(E) - f_2(E)]}{2\pi[(2 + c(E))^{-1} - c(E)^{-1}][1 + \cos\theta + c(E)]^2} \quad (3.14)
 \end{aligned}$$

where

$$f_1(E) = \frac{(E/f_{11})^{f_{12}}}{[(E/f_{11})^{f_{12}} + f_{13}]}$$

$$f_2'(E) = \frac{(E/f_{21})^{f_{22}}}{[(E/f_{21})^{f_{22}} + f_{23}]}$$

$$f_2(E) = 1 - f_1(E) \quad \text{for } E > 200 \text{ eV}$$

$$f_2(E) = f_2'(E)[1 - f_1(E)] \quad \text{for } E \leq 200 \text{ eV}$$

$$b(E) = b_1 \left( \frac{E}{1 \text{ eV}} \right)^{b_2}$$

$$c(E) = c_1 \left[ 1 - \left( \frac{c_2}{E} \right)^{c_3} \right]$$

The parameters used for the rest of this study in Eq. (3.14) are

$$\begin{array}{ll}
 f_{11} = 100 \text{ eV} & a = 0.11 \\
 f_{12} = 0.84 & b_1 = 0.43 \\
 f_{13} = 1.92 & b_2 = -0.29
 \end{array}$$

$$\begin{array}{ll} f_{21} = 10 \text{ eV} & c_1 = 1.27 \\ f_{22} = 0.51 & c_2 = 12 \text{ eV} \\ f_{23} = 0.87 & c_3 = 0.27 \end{array}$$

This form is more complex than the other phase function models but it does describe the experimental differential cross section data the most realistically. It includes an exponential term for the near exponential-like forward scattering as well as a backward scattering term for electron energies below 200 eV.

Comparisons of the screened Rutherford and model 3 cross sections are given in Figures 3.3 and 3.4 at the two energies of 30 eV and 1000 eV. Both forms are normalized to the total elastic cross section form of Eq. (3.9). This modified screened Rutherford cross section vastly underestimates the forward scattering from  $\theta = 0^\circ$  to  $30^\circ$ , overestimates the scattering in the range from  $\theta = 30^\circ$  to  $120^\circ$ , and underestimates the scattering at the larger angles with  $\theta = 120^\circ$  to  $180^\circ$ . Model 3 does a fairly reasonable job of representing the differential cross section data at both of these representative energies and the other energies as well.

Although there is not a large amount of energy loss during an elastic collision, there is some. Using classical considerations (see Green and Wyatt, 1965), the energy loss is approximately given by Eq. (2.15). For molecular nitrogen and  $\theta = 90^\circ$ , the energy loss is about  $8 \times 10^{-5} E$ .

The MC approach, being a stochastic process, uses the concept of probability for scattering within a given angle interval. In order to compare phase functions, the probability for backscatter may be compared.

Figure 3.3  $N_2$  electron impact elastic differential cross sections.  
(a and b) The screened Rutherford (dashed line) and the model 3  
(solid line) are compared with the experimental data of  
Shyn et al. (1972), x, and Herrman et al. (1976), o, at  
the energies of 30 eV (Figure 3.3a) and 1000 eV (Figure  
3.3b).

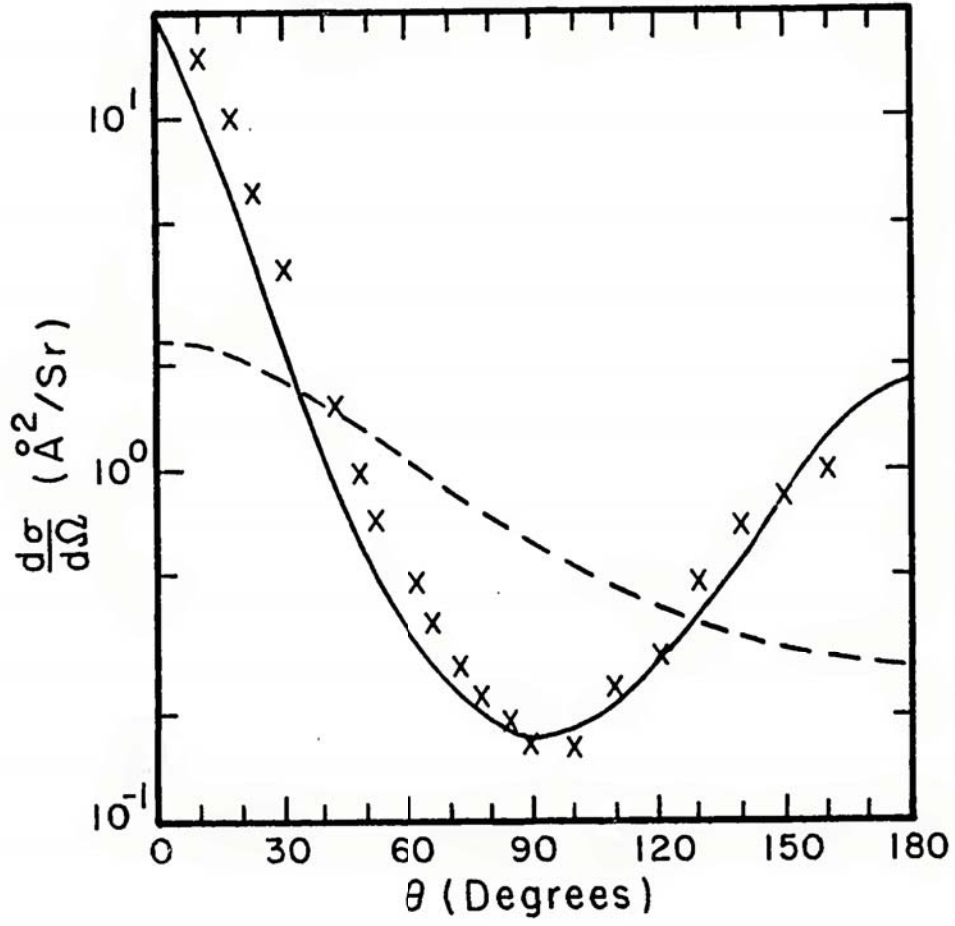


Figure 3.3a

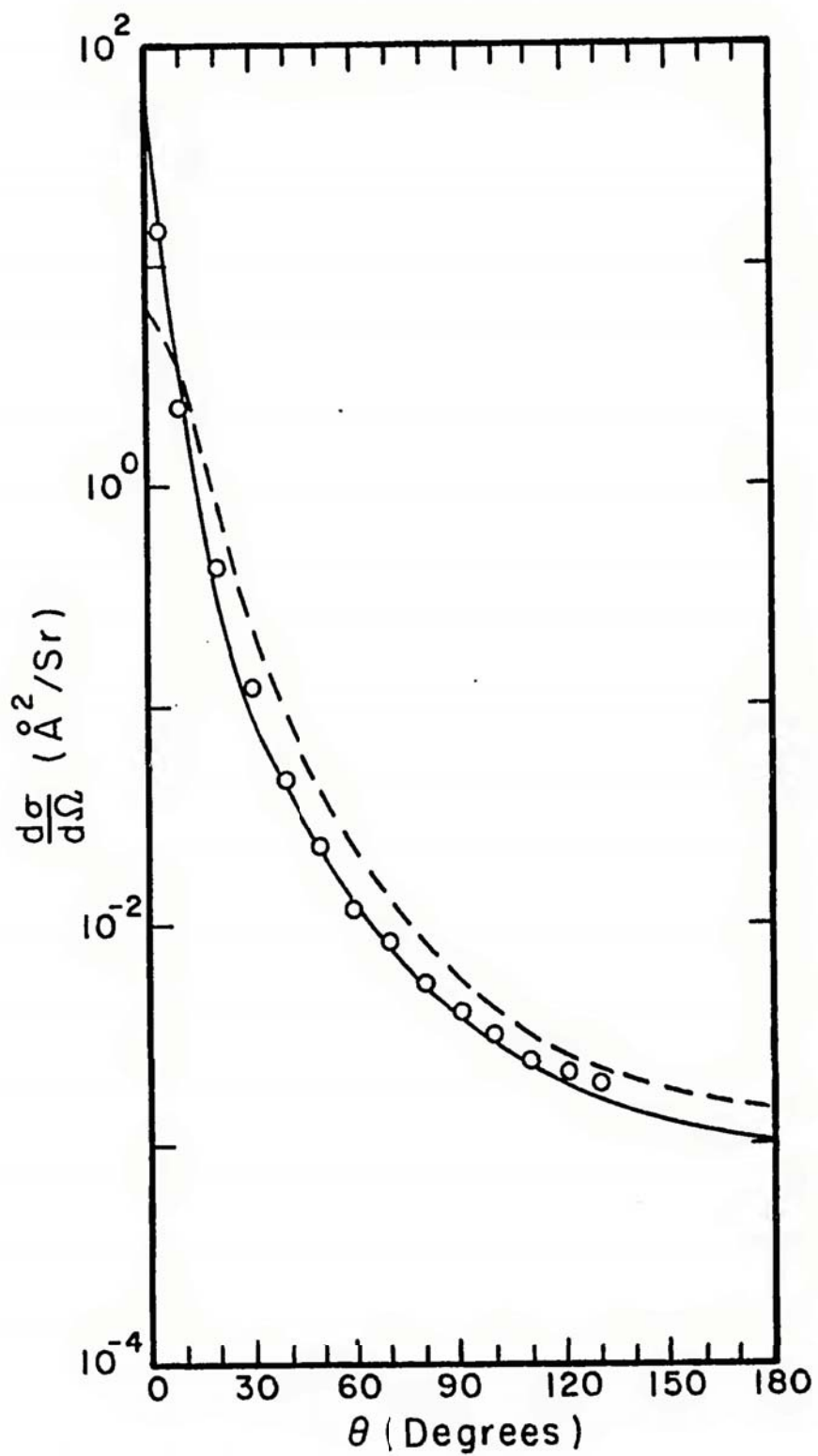


Figure 3.3b

Figure 3.4 N<sub>2</sub> electron impact elastic differential cross sections (a and b) between 0° and 20°. The screened Rutherford (dashed line) and the model 3 (solid line) are compared with the experimental data of Shyn et al. (1972), x (the ø's denote extrapolated points), and Herrmann et al. (1976), o, at the energies of 30 eV (Figure 3.3a) and 1000 eV (Figure 3.3b).

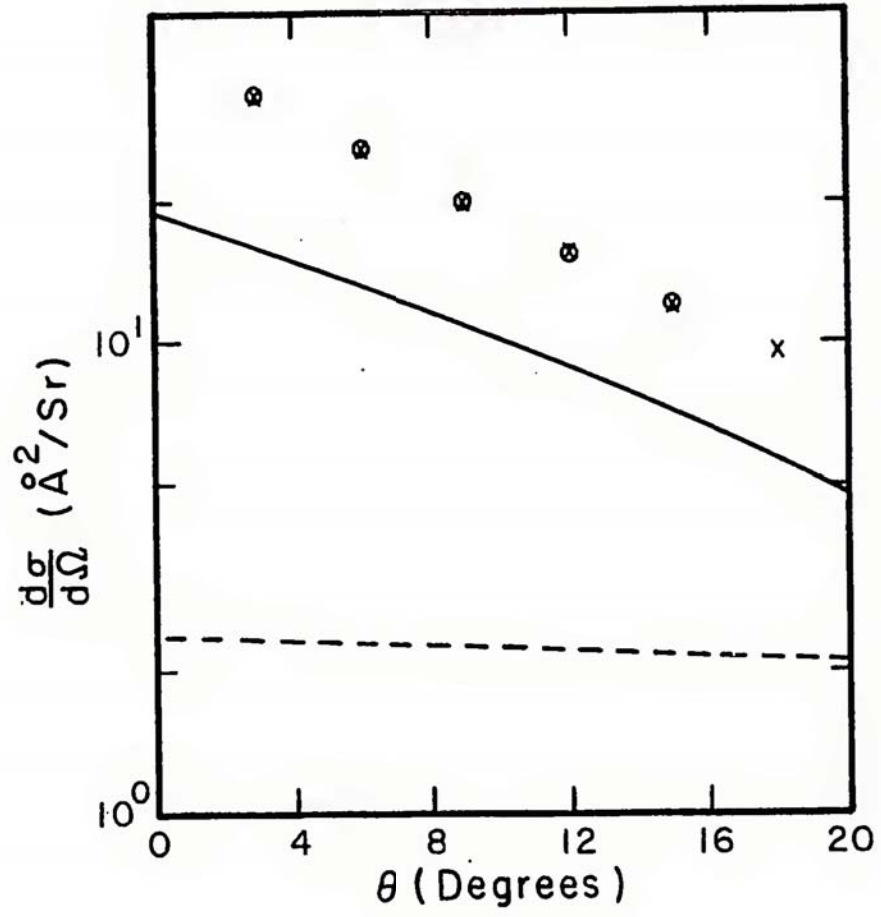


Figure 3.4a

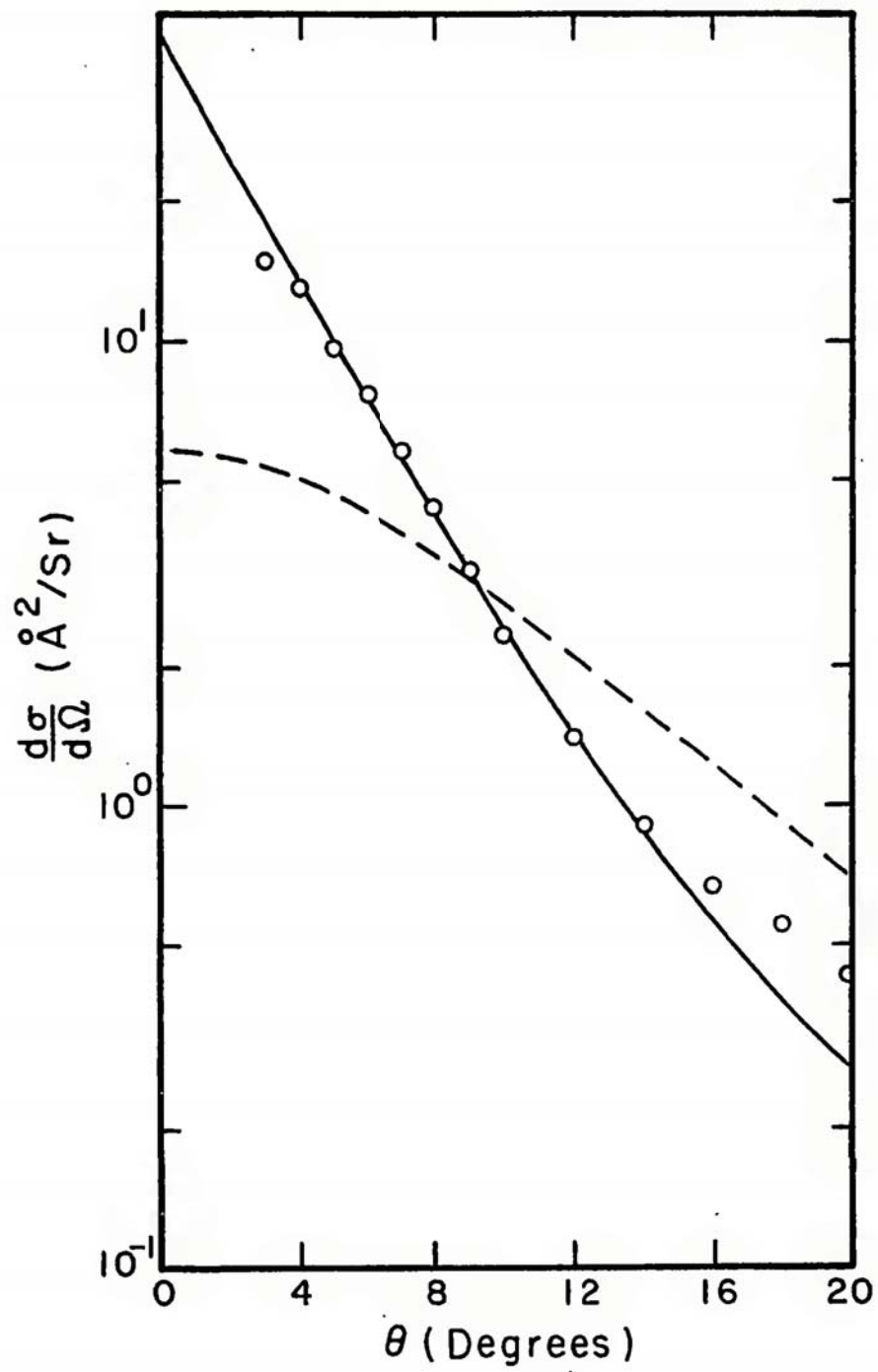


Figure 3.4b

This probability,  $P_B(E)$ , is simply calculated with

$$P_B(E) = \frac{\int_0^{2\pi} \int_{\pi/2}^{\pi} \frac{d\sigma}{d\Omega} \sin\theta d\theta d\phi}{\int_0^{2\pi} \int_0^{\pi} \frac{d\sigma}{d\Omega} \sin\theta d\theta d\phi} \quad (3.15)$$

In Figure 3.5,  $P_B(E)$  from the screened Rutherford and model 3 are compared with other theoretical (Wedde and Strand, 1974) and experimental (Shyn et al., 1972) values. Model 3 does have a tendency to estimate less backscatter than the screened Rutherford at the larger energies. (The  $P_B(E)$  curves for model 3 and the screened Rutherford do tend to converge at 5 KeV however.) The dominant exponential-like forward scattering is the reason behind this behavior. The discontinuity observed at 200 eV in model 3 values results from the lack of the backscatter characteristic above this energy.

The elastic scattering collisions influence mostly the direction of travel of the electrons. There is some energy loss during an elastic collision (as pointed out above), but this loss is not important for electrons with energies above 2 eV colliding only with  $N_2$  particles.

Inelastic collisions, on the other hand, result in a fairly substantial energy loss with some scattering. Consider now the differential and total cross sections for these inelastic events.

### B. Inelastic Differential and Total Cross Sections for $N_2$

Inelastic collisions are divided into two types: 1) electron excitation and 2) electron ionization. In the excitation process the electron is excited to a higher state which may either be an optically

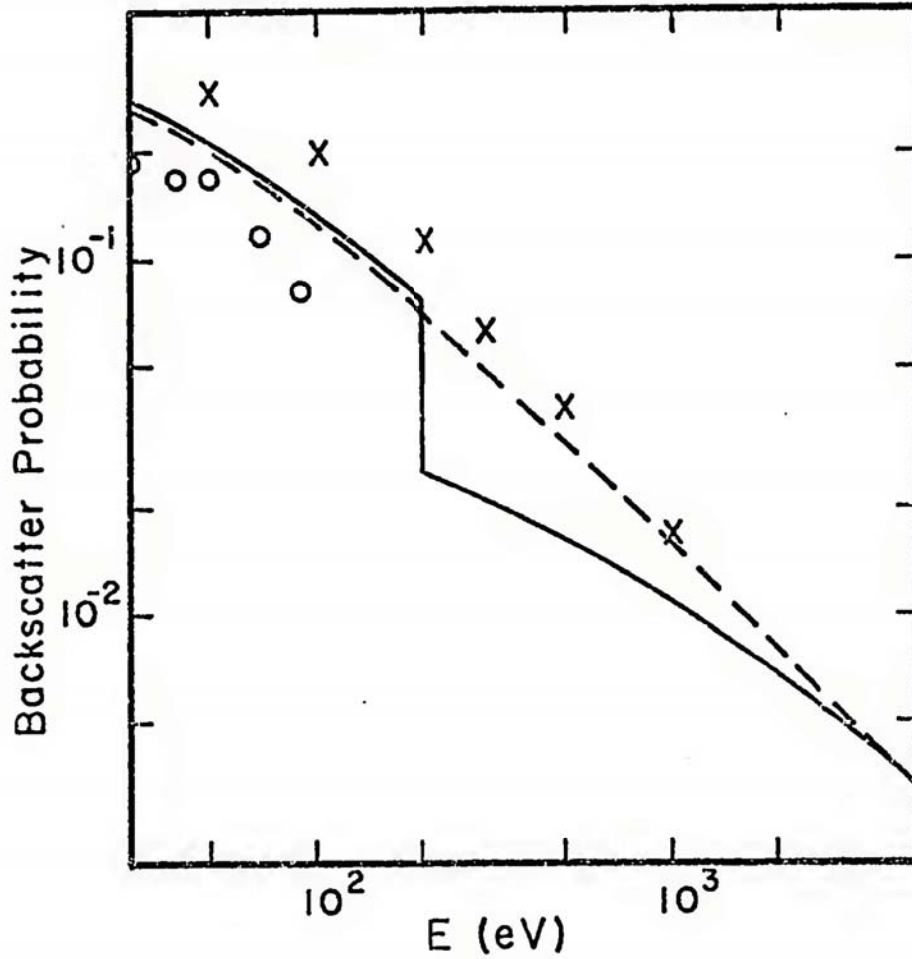


Figure 3.5 Backscatter probabilities for the screened Rutherford (dashed line) and the model 3 (solid line) are compared with Wedde and Strand (1974), x; and Shyn et al. (1972), o.

allowed or an optically forbidden transition. This transition for many molecules leads to a repulsive state which can dissociate the molecule. In  $N_2$ , dissociation of the molecule in this manner is virtually non-existent because  $N_2$  is a very stable homonuclear molecule in which both the singlet and triplet states are found to be strongly bound. As a consequence of this, the main process for dissociation is through pre-dissociation of stable electronic terms by repulsive states that are themselves strongly optically forbidden in direct excitation.

Porter, Jackman, and Green (1976) (hereafter called PJG) compiled branching ratios for dissociation of  $N_2$  using several experimental and theoretical papers (see, for example, Winters, 1966; Rapp, Englander-Golden, and Briglia, 1965; Polak, Slovetskii, and Sokolov, 1972; and Mumma and Zipf, 1971). In PJG the efficiencies for the production of atomic nitrogen from proton impact were determined.

This study does not include a calculation of the atomic nitrogen production; however, the PJG branching ratios with the yield spectra, discussed in section VII.B, can be applied to calculate this atomic yield. The excitation events, not resulting in the dissociation of the  $N_2$  molecule, are either electronic or vibrational transitions. Cross sections for these transitions are taken from both PJG and Jackman, Garvey, and Green (hereafter called JGG) (1977b).

In the ionization event an electron is stripped from the molecule and given some kinetic energy. The ionization cross section is a substantial portion of the total inelastic cross section above 50 eV (compare Figures 3.6 and 5.1) and the total amount of energy loss is always  $\geq$  the lowest ionization threshold (which is 15.58 eV for  $N_2$ ). Subsequently, most of the energy loss of the electrons (for energies

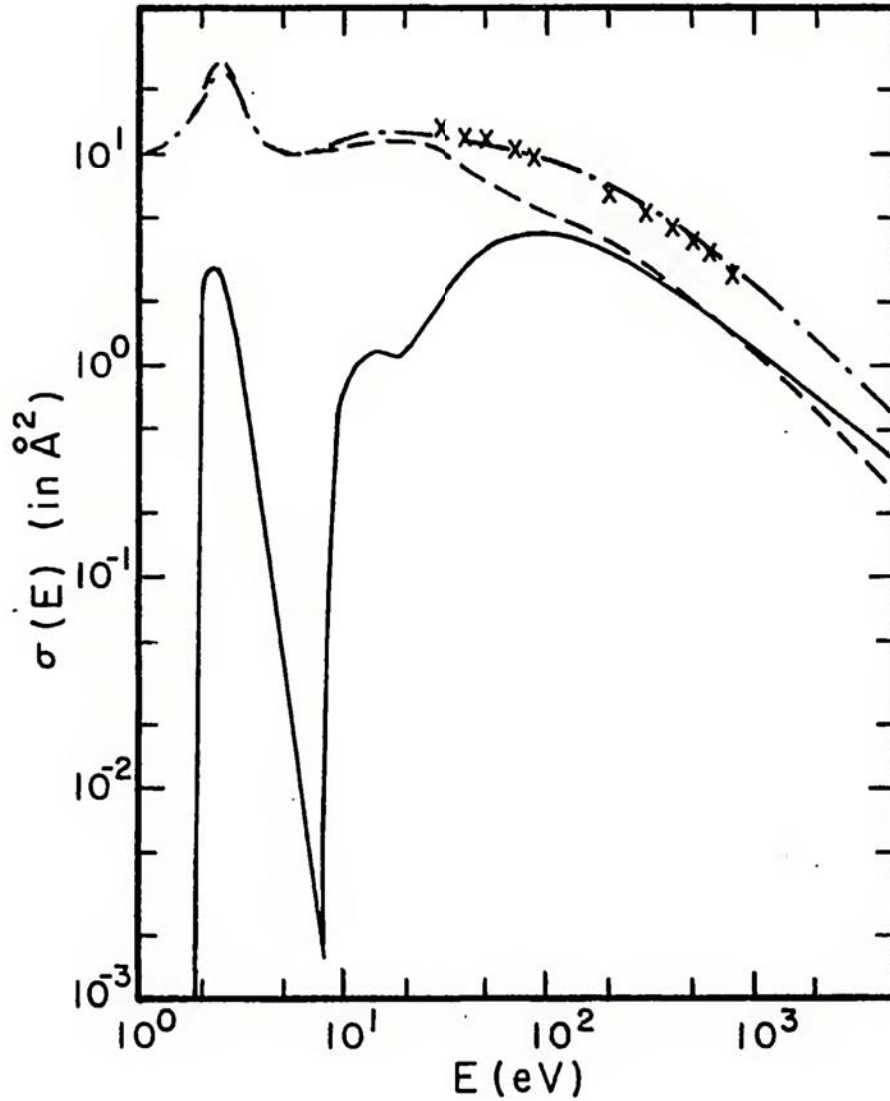


Figure 3.6 N<sub>2</sub> electron impact cross sections. The total inelastic, Eq. (3.16) (solid line), total elastic, Eq. (3.9) (dashed line), total inelastic plus elastic, Eq. (3.16) plus Eq. (3.9) (dash-dot line), and the experimental inelastic plus elastic values (Blaauw et al., 1977), x, are presented here.

> 50 eV) is from the ionization collisions. These ionization cross sections were also taken from PJG and JGG. The total inelastic cross section found by summing these inelastic cross sections was fit with the function

$$\sigma_{TI}(E) = \frac{q_0 F [1 - (\frac{W}{E})^\alpha]^\beta \ln(\frac{4EC}{W} + e)}{WE} \quad (3.16)$$

This form has the characteristic Born-Bethe  $\ln E/E$  fall off behavior at the large energies. The parameters  $\alpha = 1$ ,  $\beta = 4.81$ ,  $C = 0.36$ ,  $F = 4.52$ , and  $W = 11$  were found with the use of a nonlinear least square fitting program which fit Eq. (3.16) to the sum of all the inelastic cross sections. From 30 eV up to 5 KeV this form was used for the total inelastic cross section.

Below 30 eV much structure in the total inelastic cross section is evident. At these low energies, the total inelastic cross section can be read numerically into the MC program. This total inelastic cross section is illustrated by the solid line in Figure 3.6.

Consider now the scattering of the two electrons involved in an electron impact ionization collision. In reality, only the incident electron is scattered. The other electron is simply stripped from the molecule and given kinetic energy in a certain direction of travel. Experiments are unable to distinguish between the incident electron and the electron stripped from the molecule. In this paper, the ionization event is assumed to cause scattering of both electrons. The scattering angle of either is then measured with respect to the incident electron's path.

After the collision event the electron with the higher energy is designated the primary electron and the electron with the lower energy

is called the secondary electron. There should be a correlation between the primary and secondary scattering, but this mutual influence is difficult to quantify. The impinging electron ionizes a many body particle, a molecule of nitrogen, thus momentum and energy can be conserved without all the momentum and energy shared by the two resulting electrons. Only recently has work been done on triply differential cross sections for  $N_2$  and this interaction was measured only at one energy  $E = 100$  eV (see Jung, Schubert, Paul, and Ehrhardt, 1975). More experimental and theoretical work needs to be done in this area before any generalization can be made concerning the correlation between the primary and secondary scattering.

The primary and secondary scattering will thus be treated separately in this work. In dealing with the scattering of the primary electron after an ionization collision, a differential ionization cross section form based on the Massey-Mohr-Bethe surface of hydrogen, is used. The form (with  $a_0$ , the Bohr radius, and  $R_e$ , the Rydberg energy) is

$$\frac{d\sigma}{dTd\Omega} = \frac{4a_0^2 R_e}{Wx} \left(1 - \frac{W}{E}\right)^{1/2} F(x) \quad (3.17)$$

where  $x = (Ka_0)^2$  is the momentum transfer,  $W$  is the energy loss in the collision process which is equal to the ionization potential,  $I$ , plus the kinetic energy of the secondary,  $T$ , and  $F(x)$  is a complex function given in PJG.

Equation (3.17) is very highly forward peaked for small energy losses but becomes less forward peaked as the energy loss becomes significant when compared with the incident energy,  $E$ .

The secondary electron is also scattered in the ionization event. Probably the most comprehensive work that exists on secondary doubly

differential cross sections is that of Opal, Beaty, and Peterson (1972). (More recent data by DuBois and Rudd (1978) agrees with their work.) This data indicates a preferred angle range in the scattering process (usually between 45° and 90°) at all primary and secondary energies. A Breit-Wigner form has been chosen to represent the data. Here,

$$\frac{d\sigma}{dTd\Omega} = \frac{S(E,T)C^2}{[C^2 + B(\cos\theta - \cos\theta_0)^2]N_f} \quad (3.18)$$

where

$$B(E) = 0.0448 + \left(\frac{E}{72900 \text{ eV}}\right)^{0.91}$$

$$C(T) = \frac{36.6 \text{ eV}}{(T + 183 \text{ eV})}$$

$$\theta_0(E) = 0.873 + \frac{\theta_A(E)}{(T + \theta_B(E))}$$

$$\theta_A(E) = 20 \text{ eV} + 0.042 E$$

$$\theta_B(E) = 28 \text{ eV} + 0.066 E$$

$$N_f = \frac{-2\pi C}{\sqrt{B}} \left\{ \tan^{-1} \left[ \frac{-\sqrt{B} (1 + \cos\theta_0)}{C} \right] - \tan^{-1} \left[ \frac{\sqrt{B} (1 - \cos\theta_0)}{C} \right] \right\}$$

and

$$S(E,T) = \frac{d\sigma}{dT} = A(E)\Gamma^2(E)/[(T - T_0(E))^2 + \Gamma^2(E)] \quad (3.19)$$

is from Green and Sawada (1972) with

$$A(E) = \sigma_0 \frac{5.30}{E} \ln \left[ \frac{E}{1.74 \text{ eV}} \right]$$

$$T_0(E) = 4.71 \text{ eV} - \frac{1000 \text{ (eV)}^2}{(E + 31.2 \text{ eV})}$$

$$\Gamma(E) = 13.8 \text{ eV } E/(E + 15.6 \text{ eV})$$

$$\sigma_0 = 1 \times 10^{-16} \text{ cm}^2$$

Equation (3.18) may seem highly complicated; however, integration over the solid angle is given very simply as Eq. (3.19) which is the singly differential ionization cross section. The total ionization cross section is then

$$\sigma_{\text{ION}}(E) = \int_0^{T_M} \frac{d\sigma}{dT} dT \quad (3.20)$$

with

$$T_M = \frac{1}{2} (E - I)$$

so that

$$\sigma_{\text{ION}}(E) = A\Gamma\{\tan^{-1}[(T_M - T_0)/\Gamma] + \tan^{-1}(T_0/\Gamma)\} \quad (3.21)$$

The fit to Opal, Beaty, and Peterson's (1972) data is given in Figure 3.7 at several primary and secondary energies. The x's represent the experimental data and the solid line represents the analytic expression, Eq. (3.18).

Other inelastic processes include the simple excitation events. The scattering of the incident electron due to the excitation of a particular state has been studied by Silverman and Lassetre (1965), and more recently by Cartwright, Chutjian, Trajmar, and Williams (1977) and Chutjian, Cartwright, and Trajmar (1977).

In order to account for this scattering, the Silverman and Lassetre (1965) generalized oscillator strength data for the 12.85 eV peak (corresponding to the optically allowed  $b^1\pi_u$  state) were fit with the use of a phase function similar to model 1. The very sharply forward scattering

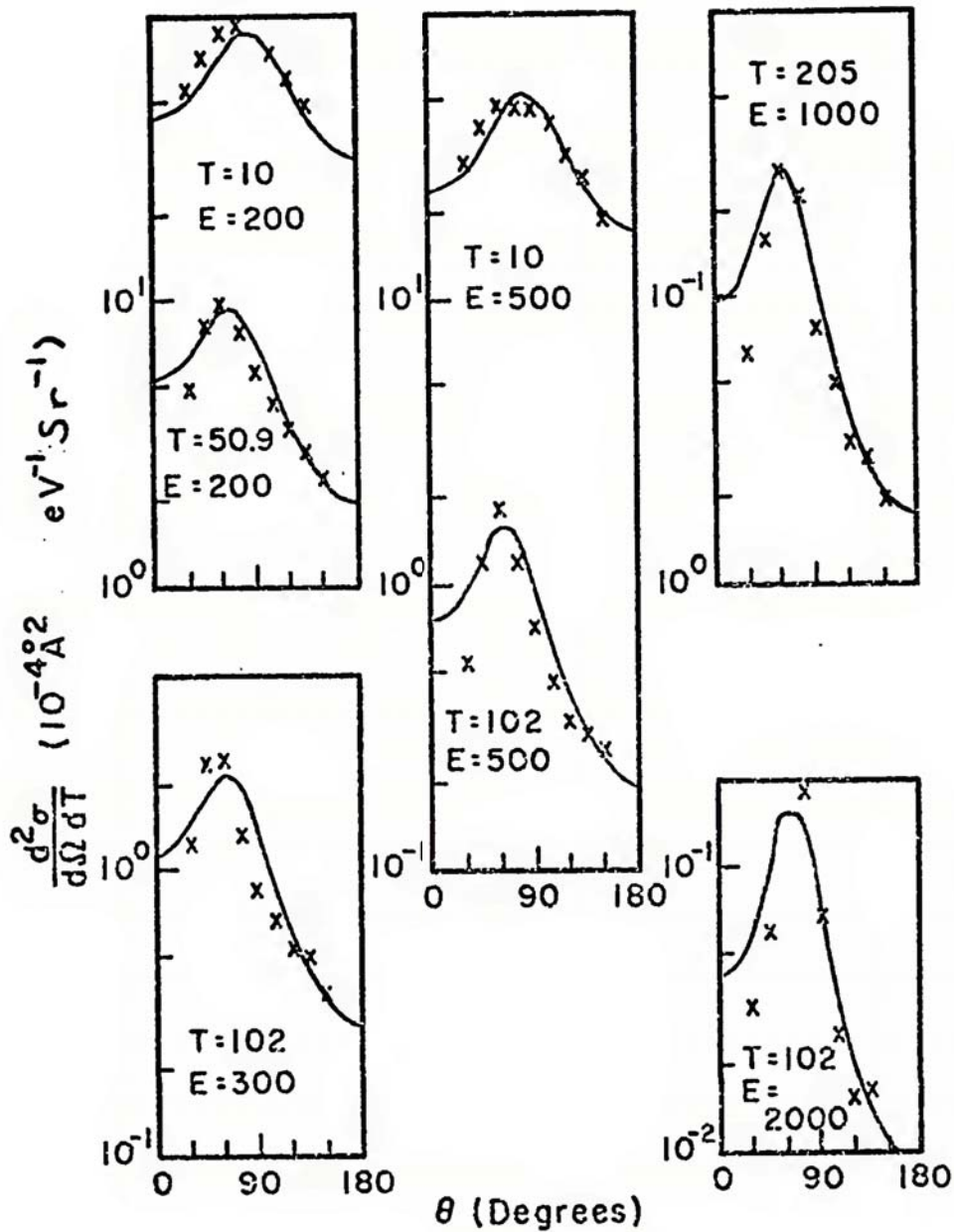


Figure 3.7  $N_2$  experimental ionization doubly differential cross sections from Opal, Beatty, and Peterson (1972) are represented by x's. The solid line (—) denotes the cross section resulting from the use of Eq. (3.18). The incident electron energy is denoted by E (eV) and the secondary electron energy is denoted by T (eV).

peak indicated in these data was used in a MC calculation. The electron scattering which results using this inelastic scattering approximation in a computation was so small as to be virtually undetectable.

Cartwright et al. (1977) and Chutjian et al. (1977) have studied a more comprehensive list of states and have observed significant electron scattering (especially due to the optically forbidden states) in the range from 10 eV to 60 eV. Characterizing this data in some way appears to be a rather endless task.

Dealing with this type of inelastic scattering is thus still a problem. Above 100 eV the optically allowed excitations are the most important; thus it is safe to conclude that the inelastic scattering events will not affect the energy degradation process. Below 100 eV, as a first approximation, it is assumed in this work that the inelastic excitation events scatter as much as the elastic events. This is probably a reasonable approximation to the very complex inelastic excitation scattering. In section VI.B the effects of this assumption are discussed.

### C. Total Cross Section (Elastic Plus Inelastic)

Elastic and inelastic processes have been considered in sections III.A and III.B. Another aspect of the cross sections is the total (elastic plus inelastic) cross section.

Blaauw, de Heer, Wagenaar, and Barends (1977) have recently published experimental data on the total cross section values of  $N_2$ . These experimental values are compared with the cross section values from this work in Figure 3.6.

Throughout the energy range the cross sections used in this study compare favorably with those of Blaauw et al. (1977). For an easy reference, the total inelastic and total elastic cross sections are also given in Figure 3.6 as separate curves.

All the major influences on the IEE energy loss and scattering have been accounted for in this chapter. The next chapter presents the MC energy deposition scheme which employs these cross sections.

CHAPTER IV  
THE MONTE CARLO METHOD OF ENERGY DEPOSITION BY ELECTRONS  
IN MOLECULAR NITROGEN

A Monte Carlo calculation is used here for energy degradation by energetic electrons in  $N_2$ . This stochastic process is probably the most accurate method for obtaining the energy loss of particles in a medium. The generalizations about electron impact on  $N_2$  that are made through the use of this technique can be applied in other energy deposition approaches to electrons impinging on the atmosphere. (This is true even though the magnetic field is neglected in these MC calculations. The three dimensional yield spectrum  $U(E,z,E_0)$  [see Chapter VII] is most useful for applications to the atmosphere and changes in the magnetic field will not affect the yield spectra greatly below altitudes of about 300 km where the gas density is fairly high [see Berger, Seltzer, and Maeda, 1970 and 1974].)

Building on the MC work done in this paper, more exact models of auroral electrons and photoelectrons can be established. In the first section, IV.A, a brief discussion of the MC calculation outlines the general procedure involved in the degradation process. The computer program and machinery used are briefly described in section IV.B. Section IV.C relates in detail the various aspects of the calculation. Finally, section IV.D discusses the statistical error that arises from the use of the MC calculation.

### A. Brief Discussion of the Monte Carlo Calculation

In Figure 4.1 a short version of the MC calculation is presented. Briefly, each electron is degraded in a collision by collision manner down to 30 eV. Below 30 eV the electrons are degraded with the use of a multiple scattering distribution. This multiple scattering approach characterizes the resultant coordinates of the electron which goes through several elastic collisions between each inelastic collision.

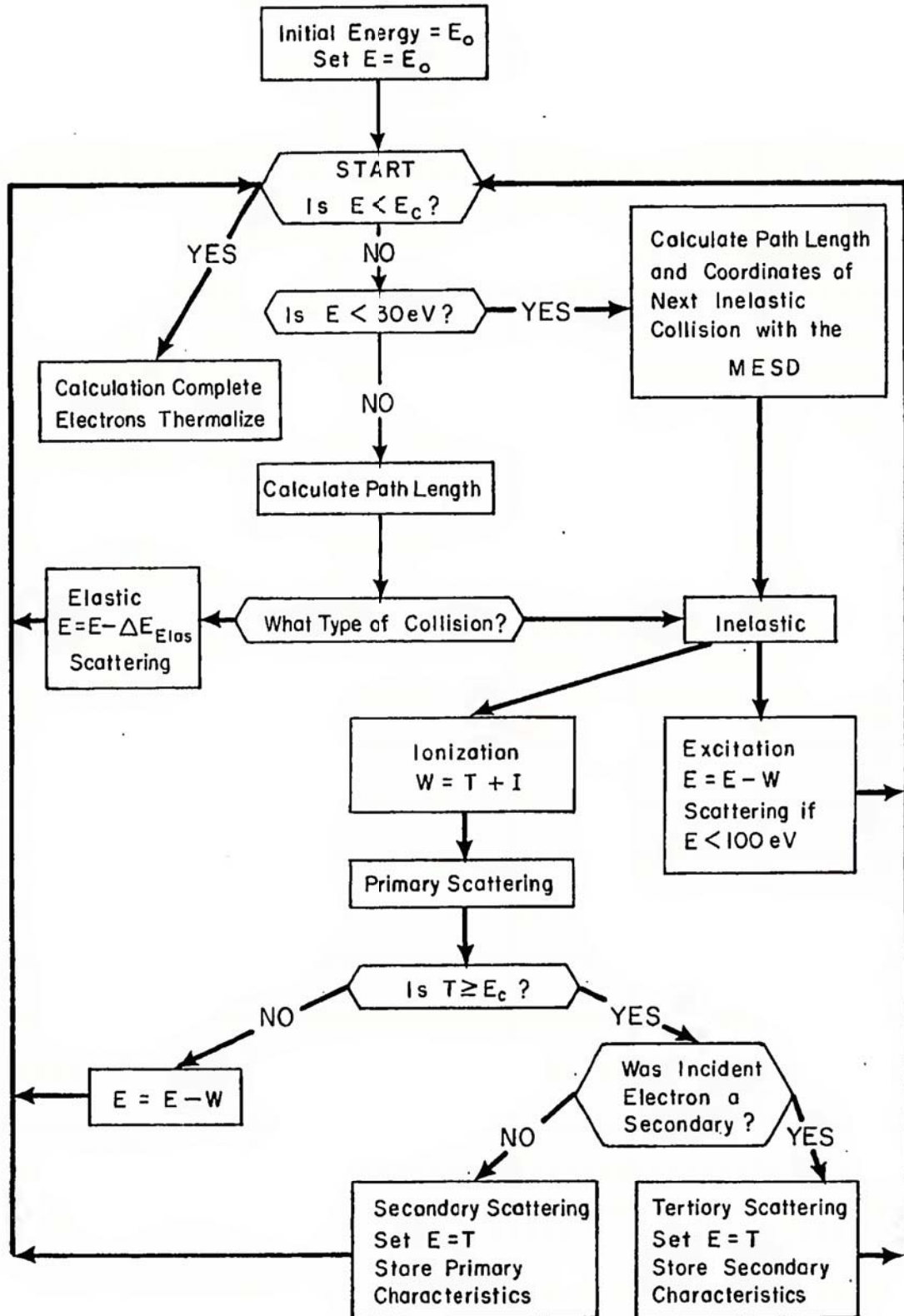
The incident electron has an energy  $E_0$ . To begin with, the running total of the electron energy,  $E$ , is set equal to  $E_0$ . At the position START, this energy  $E$  is checked against a cutoff energy,  $E_c$ . If the  $E$  is more than  $E_c$ , then, first the distance traveled by the electron to the collision is calculated.

Second, the type of collision which occurs is determined. If a collision is elastic then the electron is scattered with the use of a phase function, the appropriate energy  $\Delta E_{Elastic}$  is lost, and the electron goes back up to the START of the degradation process. Whether a collision is inelastic it is determined if the collision is an ionization event or an excitation event. In the excitation process, scattering occurs if the energy  $E$  is less than 100 eV,  $E$  is reduced by the threshold,  $W$ , for excitation of this state, and the electron goes back up to the START of the degradation process.

Ionization collisions are the most complex occurrences to compute. The energy loss,  $W$ , by the incident electron is equal to the kinetic energy,  $T$ , of the secondary electron produced plus the ionization threshold,  $I$ . The primary electron is then scattered and reduced in energy by  $W$ . If the secondary electron has a kinetic energy greater than  $E_c$ , then,

Figure 4.1 Flowchart of the Monte Carlo degradation of an incident electron of energy  $E_0$ .

### MONTE CARLO CALCULATION



it is scattered and sent back to the START to be degraded further. In the meantime, the primary electron's properties are stored.

If a secondary produces a tertiary electron with a kinetic energy greater than  $E_c$ , then that tertiary is completely degraded before any further degradation of the secondary is considered. Like the primary, the secondary electron's properties are stored in the meantime. No other generations were included in this study as their contribution would be, at most, a couple of tenths of a percent of the incident electron's energy.

After the tertiary is entirely degraded below  $E_c$ , then the secondary is again sent back to the START to be degraded further. The secondary is next entirely degraded below  $E_c$ , and, finally, the primary is again sent back to the START to be further degraded. This whole process may then again repeat itself.

#### B. Computer Programs and Machinery Used in the Monte Carlo Calculation

In the previous section a brief discussion was given of the electron energy degradation process. A brief discussion will be given below about the MC computer codes and the computing machinery used. The MC computer program employed in this work evolved from an original MC code written by R.T. Brinkmann (see applications in Brinkmann and Trajmar, 1970). This program was revised for use in Heaps and Green (1974), Kutcher and Green (1976), and Riewe and Green (1978). The author has further modified this MC technique for energetic electron impact into  $N_2$  to be used in the energy range from 2 eV to 5 KeV.

This MC technique was applied to several incident electron energies. The vast majority of the MC program runs used the Amdahl 470/175 computer at the Northeast Regional Data Center at the University of Florida. There were, however, several MC runs using the PDP 11/34 of the Aeronomy group of the University of Florida.

It should be noted here that running the same program on both machines at the same energy,  $E_0 = 1 \text{ KeV}$ , showed a factor of 240 difference in the execution time. Thus a program that takes four hours on the PDP 11/34 will take one minute on the Amdahl 470/175. This time advantage plus the ability to store each collision of the electrons on magnetic tape does make the Amdahl 470/175 a more desirable "number-crunching" machine. The PDP 11/34 is only able to produce intensity plots in the longitudinal direction. This mini-computer is thus mainly useful in deriving a range (to be described in the next chapter).

Two programs were used in deriving the MC results. The first program (listed in Appendix A), the modified version of Brinkmann's code, degraded the electrons in energy from their initial  $E_0$  down to the  $E_c$  and recorded each collision and its properties on the tape. The second program (listed in Appendix B) coalesces the data from the tape into an array of ordered output. This output contains information for three dimensional intensity plots, energy loss plots, and yield spectra.

### C. Detailed Discussion of the Monte Carlo Electron Energy Degradation Technique

Now, a more detailed discussion is given for the MC method of degrading an electron's energy. An electron will start off with an energy of  $E_0$  and coordinates  $x_0, y_0, z_0, \theta_0,$  and  $\phi_0$ . The symbols  $x, y,$

and  $z$  are the Cartesian coordinates of the electron. The polar angle  $\theta$  is measured with respect to the  $z$ -axis and the  $\phi$  denotes the azimuthal angle measured with respect to the  $x$ -axis (see Figure 4.2). In this approach, the initial coordinates  $x_0, y_0, z_0, \theta_0,$  and  $\phi_0$  were all set equal to zero. The coordinates  $x_b, y_b, z_b, \theta_b,$  and  $\phi_b$  of the electron before starting on its journey to a collision are, therefore, initially established as  $x_b = x_0, y_b = y_0, z_b = z_0, \theta_b = \theta_0,$  and  $\phi_b = \phi_0$ .

The MC approach relies on the random number,  $R$ , between 0.0 and 1.0 to aid in the deposition calculation. For each collision several  $R$ 's are needed and for each  $R$  a new property of the collision is gained. In order to explain this MC approach, an accounting of the random numbers and their subsequent usefulness is now made. The multiple elastic scattering distribution used below 30 eV and the lowest energy cutoff 2 eV are also described.

### 1. First Random Number, $R_1$

The first random number,  $R_1$ , is used to find the path,  $P_T$ , traveled by the electron before it collides with a molecule of  $N_2$ . Calculation of  $P_T$  proceeds in the following manner. The mean free path,  $\lambda$ , is defined as

$$\lambda = \frac{1}{n\sigma_T(E)} \quad (4.1)$$

where  $n$  is the density of  $N_2$  molecules in  $\#/cm^3$  and  $\sigma_T(E)$  is the total (inelastic plus elastic) cross section of  $N_2$  in units of  $cm^2$  at an energy  $E$ . The densities used at the various initial input energies are given in Table 4.1.

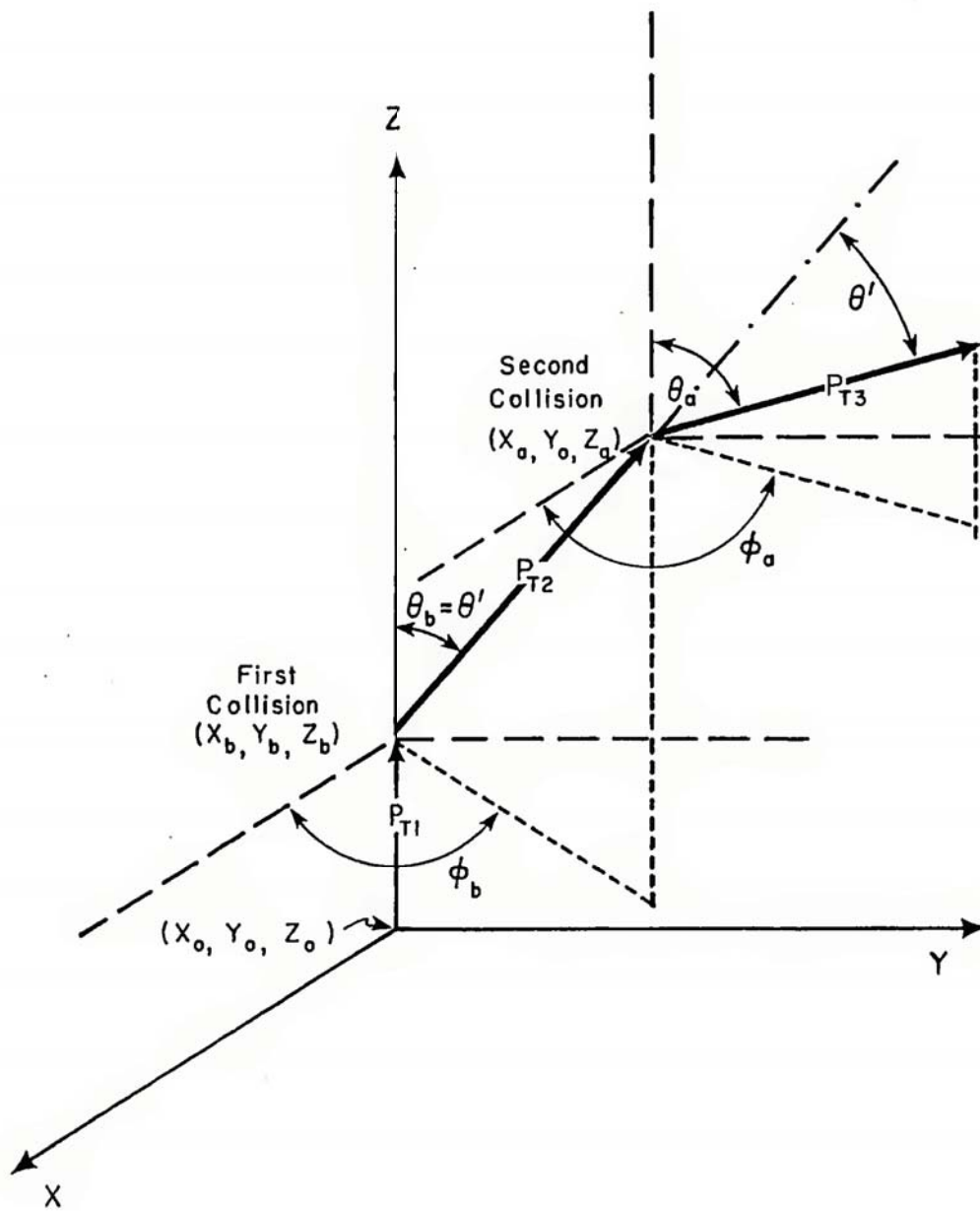


Figure 4.2 Schematic representation of the coordinates and directions of motion of the electron in its travel between collisions with the  $N_2$  molecules.

Table 4.1 The energy E is presented in the first column with the number density n, used in the MC calculation, being given in the second column. (8.0 E+ 14 means  $8.0 \times 10^{14}$ )

E (KeV)	n (#/cm <sup>3</sup> )
0.1	8.0 E+14
0.3	2.0 E+15
1.0	8.2 E+15
2.0	2.8 E+16
5.0	1.2 E+17

All electrons are forced to be degraded in a 30 cm long cylinder; thus an increase in the density is required for an increase in the energy. There are 10 cm allowed in the negative z direction and 20 cm allowed in the positive z direction. The x and y axes extend to infinity. Some electrons actually escape from the cylinder, but the energy lost due to these electrons is only a few tenths of a per cent of the incident electron energy. The path length  $P_T$  is then given as

$$P_T = -\lambda \ln(R_1) \quad (4.2)$$

using the relation that

$$R_1 = e^{-P_T/\lambda} \quad (4.3)$$

Figure 4.2 represents a schematic of the electron traveling and colliding with three  $N_2$  molecules. The  $P_{T1}$ ,  $P_{T2}$ , and  $P_{T3}$  are the path lengths traveled by the electron between the initial coordinates and the first collision, the first and second collisions, and the second and third collisions, respectively.

The  $x_a$ ,  $y_a$ , and  $z_a$  coordinates at this collision can now be found from  $P_T$ ,  $x_b$ ,  $y_b$ ,  $z_b$ ,  $\theta_b$ , and  $\phi_b$  using

$$x_a = x_b + P_T \sin\theta_b \cos\phi_b \quad (4.4)$$

$$y_a = y_b + P_T \sin\theta_b \sin\phi_b \quad (4.5)$$

$$z_a = z_b + P_T \cos\theta_b \quad (4.6)$$

In Figure 4.2 the coordinates of the first and second collisions are represented to illustrate how the electron's direction of motion might change during its collisions with  $N_2$ . So far emphasis has been only on

the Cartesian coordinates. Now, calculate the azimuthal angle  $\phi_a$  and the polar angle  $\theta_a$  of the electron after a collision.

## 2. Second and Third Random Numbers, $R_2$ and $R_3$

In actuality the type of collision must be specified before the scattering can be calculated. It is assumed, however, that the type of collision is already known (see subsection IV.C.4). The second,  $R_2$ , and third,  $R_3$ , random numbers are not chosen if the collision is an excitation event and  $E$  is greater than 100 eV. They are chosen for all other collisions.

The  $R_2$  is used to calculate the azimuthal scattering angle,  $\phi'$ , of the electron from its direction of motion. The premise is that the azimuthal scattering is isotropic; therefore,

$$\phi' = R_2 2\pi \quad (4.7)$$

(Note that the  $\phi'$  angle is the only angle not represented in Figure 4.2. Inclusion of  $\phi'$  adds too much complication to an already cluttered figure.)

The third random number,  $R_3$ , is employed to calculate the polar scattering angle  $\theta'$  of the electron from its direction of motion. (The angle  $\theta'$  is represented twice in Figure 4.2: Once as the scattering due to the first collision and once as the scattering due to the second collision.)

For elastic collisions, Eq. (3.1), (3.12), (3.13), or (3.14) are used in determining  $\theta'$ . In all but one of these phase functions, an analytic expression can be used to determine  $\theta'$  from the random number,  $R_3$ . These analytic expressions are given below.

Using the screened Rutherford differential cross section form (see Eq. (3.1)), it follows that

$$\theta' = \cos^{-1} \left[ 1 + 2n - \frac{2n(1+n)}{1+n-R_3} \right] \quad (4.8)$$

For model 1 (see Eq. (3.12))

$$\theta' = \cos^{-1} \left[ \frac{-1}{R_3[(2+a)^{-1} - a^{-1}] + a^{-1}} + 1 + a \right] \quad (4.9)$$

and for model 2 (see Eq. (3.13))

$$\theta' = \cos^{-1} \left[ \frac{-B \pm \sqrt{B^2 - 4AC}}{2A} \right] \quad (4.10)$$

with

$$A = R_3 + \frac{f}{a[(2+a)^{-1} - a^{-1}]} - \frac{(1-f)}{(2+c)[(2+c)^{-1} - c^{-1}]}$$

$$B = -A(a-c) + \frac{f}{[(2+a)^{-1} - a^{-1}]} + \frac{(1-f)}{[(2+c)^{-1} - c^{-1}]}$$

and

$$C = -A(1+a)(1+c) + \frac{f(1+c)}{[(2+a)^{-1} - a^{-1}]} - \frac{(1-f)(1+a)}{[(2+c)^{-1} - c^{-1}]}$$

Model 3 (Eq. (3.14)) is not so easy to write in such a convenient form. The equation for primary scattering after an ionization event (Eq. (3.17)) is, also, not easily inverted.

For these two differential cross sections, the following approach is taken. The angular range from 0° to 180° is divided up into angular intervals. A certain probability for scattering at angles less than the end of each angle interval is calculated from the differential cross

section form. The angle  $\theta'$  is then found through the correct placement of  $R_3$  into an angular segment whose beginning and ending point scattering probabilities bracket  $R_3$ .

For this work twenty-four angular segments were chosen. Their end-points are given in Table 4.2. With twenty-four angular intervals, the results from the Monte Carlo calculation came out to be the same as with the use of forty angular intervals. If sixteen or even twenty segments were used, the MC computation gave results that were 5% to 10% different.

The  $\phi'$  and  $\theta'$  are not the scattering angles from the original coordinate system, but represent the azimuthal and polar scattering of the scattered electron from the direction of travel of the incident electron. In order to calculate  $\phi_a$  and  $\theta_a$ , the azimuthal and polar angles representing the motion of the electron after the collision, some spherical trigonometry must be used. The following relations hold in this transposition:

$$\begin{aligned} \cos\phi_a = & [\cos\theta_b \cos\phi_b \sin\theta' \cos\phi' \\ & - \sin\phi_b \sin\theta' \sin\phi' + \sin\theta_b \cos\phi_b \cos\theta']/\sin\theta_a \end{aligned} \quad (4.11)$$

$$\begin{aligned} \sin\phi_a = & [\cos\theta_b \sin\phi_b \sin\theta' \cos\phi' \\ & + \cos\phi_b \sin\theta' \sin\phi' + \sin\theta_b \sin\phi_b \cos\theta']/\sin\theta_a \end{aligned} \quad (4.12)$$

$$\phi'_a = \cos^{-1} (\cos\phi_a) \quad (4.13)$$

$$\cos\theta_a = \cos\theta_b \cos\theta' - \sin\theta_b \sin\theta' \cos\phi' \quad (4.14)$$

$$\sin\theta_a = \sqrt{1 - \cos^2\theta_a} \quad (4.15)$$

Table 4.2 Twenty-four angle intervals are given here that were used in the Monte Carlo calculation. First column lists the index of the segment and the second and third columns give the beginning and end points for each segment with units of radians (degrees).

Index	Beginning		End	
1	0.00	(0.00)	0.01	(0.57)
2	0.01	(0.57)	0.05	(2.87)
3	0.05	(2.87)	0.11	(6.30)
4	0.11	(6.30)	0.20	(11.46)
5	0.20	(11.46)	0.40	(22.92)
6	0.40	(22.92)	0.60	(34.38)
7	0.60	(34.38)	0.80	(45.84)
8	0.80	(45.84)	0.90	(51.57)
9	0.90	(51.57)	1.00	(57.30)
10	1.00	(57.30)	1.10	(63.03)
11	1.10	(63.03)	1.20	(68.75)
12	1.20	(68.75)	1.30	(74.48)
13	1.30	(74.48)	1.40	(80.21)
14	1.40	(80.21)	1.50	(85.94)
15	1.50	(85.94)	1.60	(91.67)
16	1.60	(91.67)	1.80	(103.13)
17	1.80	(103.13)	2.00	(114.59)
18	2.00	(114.59)	2.20	(126.05)
19	2.20	(126.05)	2.40	(137.51)
20	2.40	(137.51)	2.60	(148.97)
21	2.60	(148.97)	2.80	(160.43)
22	2.80	(160.43)	3.00	(171.89)
23	3.00	(171.89)	3.07	(175.90)
24	3.07	(175.90)	3.14	(180.00)

and

$$\theta_a = \cos^{-1}(\cos\theta_a) \quad (4.16)$$

Now the azimuthal angle  $\phi_a$  and the polar angle  $\theta_a$  have been established for the collision with respect to the fixed coordinate system. These angles are also represented in Figure 4.2. The two angular coordinates  $\phi_b$  and  $\theta_b$  of the electron before traveling to the next collision are then set as  $\phi_b = \phi_a$  and  $\theta_b = \theta_a$ .

### 3. Fourth Random Number, $R_4$

A fourth random number,  $R_4$ , is required if a secondary is produced and if that secondary has an energy above the cutoff energy,  $E_c$ . This  $R_4$  is chosen to determine the polar angle,  $\theta'$ , of scattering of the secondary. Again, an analytic formula can be employed to define  $\theta'$ . This equation was derived from Eq. (3.18) and is written as

$$\begin{aligned} \theta' = \cos^{-1} \left[ \frac{C}{\sqrt{B}} \tan \left[ R_4 \left\{ \tan^{-1} \left( \frac{-\sqrt{B}(1 + \cos\theta_0)}{C} \right) \right. \right. \right. \\ \left. \left. \left. - \tan^{-1} \left( \frac{\sqrt{B}(1 - \cos\theta_0)}{C} \right) \right\} \right] \right. \\ \left. + \tan^{-1} \left( \frac{\sqrt{B}(1 - \cos\theta_0)}{C} \right) \right] + \cos\theta_0 \end{aligned} \quad (4.17)$$

The  $\phi'$  for the secondary is found with the use of Eq. (4.7) and  $\theta_a$  and  $\phi_a$  result from the use of Eqs. (4.11) through (4.16).

### 4. Fifth Random Number, $R_5$

The fifth random number,  $R_5$ , determines the type of collision that occurs. Here, the type may be either elastic or inelastic. If the

type is inelastic then the individual excitation or ionization event is found as well.

There are cross sections for thirty-four states of  $N_2$  employing the papers of Jackman, Garvey, and Green (1977) and Porter, Jackman, and Green (1976). Using all these states in the MC calculation would greatly increase the cost. It was therefore decided to reduce these thirty-four states to nine states. Two allowed states, the  $b^1\pi_u$  and the  $b^1\Sigma_u^+$ , and the six ionization states were kept the same as given in the papers. For the ninth state, all the Rydberg and forbidden states were combined.

Above 200 eV, the forbidden states are contributing only a minuscule amount to the total cross section. Since the other states have roughly the same  $\ln E/E$  fall-off at high energies, it is assumed that the probabilities for excitation to any of these states will be constant. These probabilities were simply found from the ratio of the cross section of the state in question to the total inelastic cross section at the electron energy of 5 KeV.

In Table 4.3 these states, their probabilities, and thresholds are presented. The probability,  $p_c$ , of the composite state is simply

$$p_c = \sum_{i=1}^m p_i \quad (4.18)$$

where  $m$  = the total number of Rydberg and forbidden states and  $p_i$  is the probability for excitation of the  $i$ th Rydberg or forbidden state. The average threshold,  $w_c$ , for exciting the composite state is found easily with the following equation

$$w_c = \frac{\sum_{i=1}^m p_i w_i}{\sum_{i=1}^m p_i} \quad (4.19)$$

Table 4.3  $N_2$  inelastic states, their probabilities,  $p$ , and thresholds,  $W$ , taken for electron energies above 200 eV are presented below.

State	$p$	$W$ (eV)
$N_2$ $b^1\pi_u$	0.092	12.80
$N_2$ $b^1\Sigma_u^+$	0.042	14.00
$N_2$ Composite	0.233	15.40
$N_2^+$ $X^2\Sigma_g^+$	0.289	15.58
$N_2^+$ $A^2\pi_u$	0.127	16.73
$N_2^+$ $B^2\Sigma_u^+$	0.066	18.75
$N_2^+$ $D^2\pi_g$	0.044	22.00
$N_2^+$ $C^2\Sigma_u^+$	0.044	23.60
$N_2^+$ 40 eV	0.063	40.00

with  $W_j$  being the threshold of the Rydberg or forbidden state.

Below 200 eV, the probabilities for excitation to the various inelastic states are changing quite rapidly. The parameters for the eight individual states are taken from Jackman et al. (1977b) and Porter et al. (1976). The composite state's properties are found in the same manner that they were above. In these lower energy regimes the probability and energy loss are changing fairly rapidly, thus Table 4.4 illustrates these probabilities and threshold values at several energies.

With the background on the inelastic cross sections and their subsequent probabilities, consider now the collision type. The  $R_5$  random number determines the type of collision that occurs in the following manner: If

$$R_5 \leq \frac{\sigma_{TE}(E)}{\sigma_T(E)} \quad \text{for all electron energies} \quad (4.20)$$

where  $\sigma_{TE}(E)$  is the total elastic cross section, then the collision is elastic. If

$$\frac{\sigma_{TE}(E)}{\sigma_T(E)} < R_5 \leq \frac{p_1 \sigma_{TI}(E) + \sigma_{TE}(E)}{\sigma_T(E)} \quad \text{and } E > 200 \text{ eV} \quad (4.21)$$

where  $\sigma_{TI}(E)$  is the total inelastic cross section and  $p_1$  is the probability for exciting the first inelastic state (in Table 4.2 the first state is the  $b^1\pi_u$  thus  $p_1 = 0.092$ ), then the inelastic collision results in the excitation of the first state.

A relation follows from Eq. (4.21) that holds true for  $j = 2$  to 9 such that: If

Table 4.4 N<sub>2</sub> inelastic composite state with its characteristic probability, p, and average energy loss, W, given for several energies between 2 and 200 eV.

E (eV)	p	W (eV)
2	1.000	0.57
3	1.000	1.03
4	1.000	0.922
5	1.000	0.835
6	1.000	0.772
7	1.000	0.728
8	1.000	0.696
9	1.000	7.00
10	1.000	7.21
12	1.000	8.25
14	1.000	8.91
16	0.971	9.12
18	0.866	9.34
20	0.745	9.68
30	0.426	11.70
40	0.344	12.80
50	0.296	13.30
60	0.271	13.70
70	0.255	13.90
100	0.229	14.30
150	0.214	14.60
200	0.234	14.80

$$\frac{\sum_{i=1}^{j-1} p_i \sigma_{TI}(E) + \sigma_{TE}(E)}{\sigma_T(E)} < R_5 \leq \frac{\sum_{i=1}^j p_i \sigma_{TI}(E) + \sigma_{TE}(E)}{\sigma_T(E)} \quad \text{and } E > 200 \text{ eV} \quad (4.22)$$

then the inelastic collision results in the excitation of the  $j$ th state. Thus the  $R_5$  random number for an electron of energy  $E > 200$  eV will determine which type of collision occurred when satisfying Eq. (4.20), (4.21), or (4.22).

For energies below 200 eV, the following relations must be considered: If

$$\frac{\sigma_{TE}(E)}{\sigma_T(E)} < R_5 \leq \frac{\sigma_1(E) + \sigma_{TE}(E)}{\sigma_T(E)} \quad \text{and } E \leq 200 \text{ eV} \quad (4.23)$$

where  $\sigma_1(E)$  is the cross section for exciting the first inelastic state, then the inelastic collision results in the excitation of this state.

A relation similar to Eq. (4.22) can now be established for  $j = 2$  to 8 such that: If

$$\frac{\sum_{i=1}^{j-1} \sigma_i(E) + \sigma_{TE}(E)}{\sigma_T(E)} < R_5 \leq \frac{\sum_{i=1}^j \sigma_i(E) + \sigma_{TE}(E)}{\sigma_T(E)} \quad \text{and } E \leq 200 \text{ eV} \quad (4.24)$$

then the  $j$ th inelastic state is excited. If

$$R_5 \geq \frac{\sum_{i=1}^8 \sigma_i(E) + \sigma_{TE}(E)}{\sigma_T(E)} \quad \text{and } E \leq 200 \text{ eV} \quad (4.25)$$

then the excitation of the composite state is assumed and the energy loss,  $W_c$ , in this case is found through a linear interpolation with the use of the values given in Table 4.3.

### 5. Sixth Random Number, $R_6$

The sixth random number,  $R_6$ , is computed only if the collision type is an ionization event. This  $R_6$  determines the energy lost by the primary in creating a secondary of energy,  $T_s$ . Using the  $S(E,T)$  from Eq. (3.19) the following relationship is established:

$$R_6 = \frac{\int_0^{T_s} S(E,T) dT}{\sigma_{ION}(E)} \quad (4.26)$$

Integrating the numerator in Eq. (4.26) and using Eq. (3.21) to solve for  $T_s$ , Eq. (4.27) is derived.

$$T_s = \Gamma(E) \left[ \tan \left\{ R_6 \tan^{-1} \left[ (T_M - T_0(E)) / \Gamma(E) \right] \right. \right. \\ \left. \left. + (R_6 - 1) \tan^{-1} [T_0(E) / \Gamma(E)] \right\} \right] + T_0(E) \quad (4.27)$$

The energy loss,  $W$ , is then found by the relation:

$$W = I_k + T_s \quad (4.28)$$

where  $I_k$  is the ionization threshold for the  $k$ th ionization state.

### 6. Multiple Elastic Scattering Distribution Used Below 30 eV

The MC calculation can be used to degrade an electron down to practically any energy. Even below the lowest threshold for excitation to any vibrational level, the electron will still lose energy via elastic collisions with molecules of nitrogen as well as other electrons. This energy loss to other electrons is fairly low unless a substantial fraction of the gas has been ionized (see Cravens, Victor, and Dalgarno,

1975). In this study the fraction of ionization is assumed to be negligible; therefore, this loss is ignored.

Unless there is a very large amount of money available for computer time, an electron can not be followed to its thermal energy with any practicality. This implies that a multiple elastic scattering distribution (hereafter referred to as MESD) must be used below some given energy. In this work the MESD will be used below 30 eV.

Bethe, Rose, and Smith (1938) used the Fokker-Planck differential equation, neglecting energy loss, to consider the penetration of electrons through thick plates. This, however, leads to a Gaussian solution in the small-angle approximation so that the tail of the angular distribution was omitted. The large-angle multiple scattering has been studied by Goudsmit and Saunderson (1940) [hereafter referred to as GS] who used a series of Legendre polynomials to determine the resultant angle of scattering.

Lewis (1950) studied the integro-differential diffusion equation of the multiple scattering problem in an infinite, homogeneous medium, without the usual small-angle approximation. He obtained the GS solution for the scattering angle and also derived certain moments for the longitudinal and transverse distributions.

Berger (1963) applied a MESD for condensed case history MC calculations. His application of the MESD is at the energies above 200 eV and probably is not accurate for electrons with energies less than about 100 eV. Furthermore, Berger's (1963) work contains approximations that are only good for the sharply forward peaked cross sections of higher energy electrons.

In this work a different problem exists. The MC calculation is used to degrade electrons in a collision by collision manner all the way down to 30 eV. At this energy, the elastic collisions are occurring with twice the frequency of the inelastic events, and at energies below 30 eV the number of elastic collisions between inelastic events may be up to several hundred or thousand. Keeping track of all these elastic collisions would be very costly.

Kutcher and Green (1976) [hereafter referred to as KG] studied the radial, longitudinal, and polar angle distributions for elastic scattering by  $H_2$  in the energy range from 2 to 50 eV. An approach similar to KG's could be applied to  $N_2$ . Since such a project would require a substantial amount of time and computer money, the possibility of adapting the KG results was first considered.

With this in mind, consider the differences between  $N_2$  and  $H_2$ . First of all, there are some dissimilarities between the differential cross sections. There is more backscatter observed experimentally in  $N_2$  at all energies. Secondly, the total inelastic and elastic cross sections are different. The second difference is no real problem because the MESDs are given in terms of the mean free path lengths (hereafter referred to as MFPs). The first dissimilarity does pose a minor problem which is solved in a simplistic way below.

Above 5 or 6 MFPs the polar angle is approximately random. At most energies below 30 eV, the number of MFPs between inelastic collisions is above 5 or 6. Since the distribution found in KG is not easily inverted, a reasonable assumption is that the polar angle is oriented randomly.

Knowledge of the radial distribution is not crucial for our purposes. The most interesting radial distribution output from this MC calculation is that of the 3914 Å emission. Electrons below 30 eV make little contribution to this profile because the cross section for excitation to this  $N_2^+ B^2\Sigma_u^+$  state is fairly low (see Figure 5.1). Thus knowledge of the radial distribution of these electrons multiply scattered is not extremely important.

An approximation, however, is employed in most MC computations to calculate a fairly reasonable radial distance. The average radial distance, as observed from the calculations in KG, for most energies and at the longer path lengths is approximately one-sixth of the total path lengths, thus

$$\rho_{ave} = s/6 \quad (4.29)$$

The most important spatial displacement is the longitudinal distance  $z$ . In order to calculate  $z$ , the total path length  $s$  must be known. This length  $s$  is calculated from the random number,  $R_1$ , the total elastic cross section,  $\sigma_{TE}(E)$ , and the total inelastic cross section,  $\sigma_{TI}(E)$ , by using

$$s = - \frac{\sigma_{TE}(E)}{\sigma_{TI}(E)} \ln (R_1) \quad (4.30)$$

The ratio  $\sigma_{TE}(E)/\sigma_{TI}(E)$  is simply a fairly accurate approximation of the number of elastic collisions occurring per inelastic collision. The value  $-\ln(R_1)$  [see Eq. (4.2)] is the path length (in units of MFPS) traveled by the electron between collisions. Thus knowing the number of elastic collisions occurring and the path length traveled between collisions allows one to write Eq. (4.30) as the expression for the

total path length  $s$  (in units of MFPs) traveled between inelastic collisions.

In KG an equation which can be easily inverted to calculate the  $z$  distance (in units of MFPs) from some random number,  $R_2$ , and path length  $s$ , is written

$$z = \ln \frac{\left\{ \frac{[R_2^{-1/\nu} - 1]}{[F(0)^{-1/\nu} - 1]} \right\}}{-u} \quad (4.31)$$

where

$$\nu(s) = 1 - \exp[-(s/s_\nu)^D]$$

$$F(0) = K\{1 - \exp[-(s/s_f)^{0.75}]\}$$

and

$$u(s) = (H + s^I)/s^J$$

where  $K = 0.425$ .

Since there is more backscatter during  $N_2$  elastic collisions (because of its differential backscatter contribution), it seems reasonable that the parameters for Eq. (4.31), which are useful for  $N_2$ , are different than those derived in KG. One approach to this dilemma might be to correlate the elastic differential cross section (hereafter called EDCS) from  $N_2$  at some energy  $E'$  with the EDCS from  $H_2$  at some energy  $E$ . This would work if the  $H_2$  EDCSs showed more backscatter than the  $N_2$  EDCSs; however, the opposite is observed experimentally. Thus the  $N_2$  EDCSs from some  $E'$  (around 6-7 eV) values correlate with the  $H_2$  EDCSs at  $E$  values less than 2 eV (where the Kutcher and Green, 1976, MESD is not defined).

Another straightforward and simplistic approach is to do the following. Calculate the approximate backscatter at three energies, the two endpoints and the middle (2 eV, 15 eV, and 30 eV), from the KG H<sub>2</sub> EDCS form and the experimental data on N<sub>2</sub> EDCSs (given in Sawada, Ganas, and Green, 1974). At these energies the backscatter with the KG H<sub>2</sub> EDCS form is less than that of the N<sub>2</sub> EDCS by the following values: 2 eV ~ 5%, 15 eV ~ 10%, and 30 eV ~ 10%. An average of these three values is about 8%. Since the major influences of the backscatter in Eq. (4.31) is the value of K, this parameter is the only one that is changed from the KG formulation. It is, therefore, increased by ~8% so that in these MC calculations  $K = 0.46$ . The other parameters in Eq. (4.31) are listed in Table 4.5.

Actually it appears that the value of K makes little difference in the MC computational results. Two MC calculations at an incident electron energy of 100 eV with  $K = 0.46$  and with  $K = 0.425$  were undertaken (all other parameters and inputs were the same). The yield spectra (described in Chapters II and VII) changes substantially only at fairly large longitudinal distances (where the distances are about 1.5 times the range). At these large distances there are relatively few electrons anyway, thus there is little effect on the major aspects of the spatial electron energy deposition process.

The Cartesian coordinates  $x_a$ ,  $y_a$ , and  $z_a$  are found from the coordinates  $x_b$ ,  $y_b$ , and  $z_b$  in the following manner. After  $z$  is calculated in units of MFPs with the use of Eq. (4.31), it can then be written in units of cm or km by multiplying by the MFP,  $\lambda$  (calculated from Eq. (4.1)), thus  $z_a = z_b + z\lambda$ .

Table 4.5 Parameters from Kutcher and Green (1976) for several energy intervals used in Eq. (4.28).

Energy Interval (eV)	H	I	J	D	$s_v$	$s_F$
2-5	12.	1.37	1.71	1.75	5.05	8.5
5-10	9.6	1.32	1.67	2.50	4.25	8.5
10-20	15.5	1.28	1.67	2.31	6.29	10.3
20-30	23.5	1.24	1.69	1.98	9.65	13.6

As established earlier, the polar angle  $\theta_a$  and azimuthal angle  $\phi_a$ , representing the motion of the electron after the collision, can be chosen in a random way from the two random numbers,  $R_3$  and  $R_4$ , using

$$\begin{aligned}\theta_a &= \pi R_3 \\ \phi_a &= 2\pi R_4\end{aligned}\tag{4.32}$$

A reasonable approximation of  $x_a$  and  $y_a$  can then be made using Eqs. (4.29) and (4.32) such that

$$x_a = x_t + \rho_{ave} \lambda \cos\phi_a$$

and

$$y_a = y_t + \rho_{ave} \lambda \sin\phi_a$$

In the MESD the fifth random number,  $R_5$ , is used to determine the inelastic collision type. A method similar to that illustrated in subsection IV.C.4 is employed, the only difference is the fact that the collision is only inelastic.

### 7. Value of the Cutoff Energy, 2 eV

The  $E_c$  used in this work has been set at 2 eV because the lowest threshold for excitation to an inelastic state is 1.85 eV. With this cutoff energy the yield spectra can be defined down to 2 eV at all longitudinal distances. Subsequently, a reasonable calculation of the excitation to any  $N_2$  state may be made.

#### D. Statistical Error in the Monte Carlo Calculation

The statistical error inherent in the MC computation can be derived by considering the following. Since the MC calculation is a probabilistic method of degrading an electron in energy, the multinomial distribution can be used to find the statistical standard deviation for each bin considered. This discussion of the statistical error employed the work of Eadie, Dryard, James, Roos, and Sadoulet (1971).

The probability of getting an excitation of a certain state  $j$  in bin  $k$  is  $p_{jk}$ . The  $p_{jk}$  is normalized such that

$$\sum_{k=1}^m \sum_{j=1}^n p_{jk} = 1 \quad (4.33)$$

In this MC study the multinomial distribution is an array of histograms containing  $N$  events distributed in  $n$  states and  $m$  bins with  $r_{jk}$  events in state  $j$  and bin  $k$ . The  $r_{jk}$  values are normalized such that

$$\sum_{k=1}^m \sum_{j=1}^n r_{jk} = N \quad (4.34)$$

Thus, the  $r_{jk}$  observations can be considered somewhat conditional on the fixed observational value of  $N$ . The variance of the calculation is represented as

$$V(r_{jk}) = N p_{jk} (1 - p_{jk}) \quad (4.35)$$

In this work the  $m \times n$  variables  $r_{jk}$  can all be correlated. For the specific example of electron deposition represented in Figure 5.2,  $p_{jk} \ll 1$ . This is true because there are total almost  $5 \times 10^5$  collisions (i.e.,  $N = 5 \times 10^5$ ) to consider in this degradation scheme and

at maximum  $r_{jk} \approx 4000$ . Using this information, Eq. (4.35) can then be approximated by

$$V(r_{jk}) \sim N p_{jk} \sim r_{jk} \quad (4.36)$$

and the statistical standard deviation of the number of  $N_2^+ B^2\Sigma_u^+$  events in a bin becomes

$$\sigma_{jk} \sim \sqrt{r_{jk}} \quad (4.37)$$

Equation (4.37) holds true for the specific example represented in Figure 5.2 and it also holds true for all the intensity plots, energy loss plots, and yield spectra that were studied in this work. Thus, in order to obtain the approximate standard deviation for any MC generated number, the square root of this value is its standard deviation. The error bars found in the rest of this paper are determined in this manner.

Now that the MC calculational technique has been outlined, this method will be used in the next three chapters to deal with the spatial and energetic aspects of electron energy degradation.

## CHAPTER V

### MONTE CARLO INTENSITY PLOTS AND COMPARISON WITH EXPERIMENT

Incident electrons with energies between 0.1 and 5.0 KeV are degraded in  $N_2$  using the MC method described in Chapter IV with the cross sections given in Chapter III. The intensity plots of the 3914 Å emission are described in this chapter.

Emission intensity plots of the 3914 Å radiation from the  $N_2^+ B^2\Sigma_u^+$  state are used in describing the range (found by extrapolating the linear portion of the longitudinal 3914 Å intensity plot to the abscissa) for incident electrons. Section V.A describes the excitation of the  $N_2^+ B^2\Sigma_u^+$  state. In section V.B the range of the electrons is defined more completely. Previous experimental and theoretical work on the 3914 Å emission of  $N_2^+$  is given in section V.C. The range results from the MC calculation are then discussed in section V.D. Finally, section V.E describes the intensity plots resulting when plotted as functions of the radial direction.

#### A. Excitation of the $N_2^+ B^2\Sigma_u^+$ State

The main concern of this chapter will be the intensity plots showing the emission of the 0-0 first negative band ( $B^2\Sigma_u^+$  state) of  $N_2^+$  at 3914 Å. Experimentally (see Rapp and Englander-Golden, 1965; McConkey, Woolsey, and Burns, 1967; and Borst and Zipf, 1969), it has been shown that the number of photons at 3914 Å produced for each ionization of  $N_2$  is

independent of the energy of the exciting electron for energies from 30 eV at least up to 3 KeV.

In Figure 5.1 the  $N_2$  total ionization cross section and cross section for ionization and excitation to the  $B \ ^2\Sigma_u^+$  state of  $N_2^+$  are presented. The curves are approximately parallel thus even if the absolute values for the two cross sections are slightly in error, the shapes of the intensity plots that result from this MC calculation should be fairly accurate.

The total ionization curve lies nicely in the middle of an array of experiments (namely, Opal, Beaty, and Peterson, 1972; Tate and Smith, 1932; Rapp and Englander-Golden, 1965; and Schram, de Heer, Wiel, and Kistenaker, 1965) but the  $B \ ^2\Sigma_u^+$  cross section values may be high when compared to experiments (see Holland, 1967; and McConkey, Woolsey, and Burns, 1967).

The threshold for excitation to this  $B \ ^2\Sigma_u^+$  state is 18.75 eV, thus any electron above that energy can excite and ionize a ground state  $N_2$  molecule up to this level. The cross section for excitation and ionization to the  $B \ ^2\Sigma_u^+$  state is not large when compared with the total inelastic cross section. In fact, the probability for exciting this state is only 0.066 for electron energies above 200 eV. The accuracy of the MC calculation is dependent on the number of excitations in each bin (see section IV.D). In order to enhance the precision of the MC results, excitations of the  $X \ ^2\Sigma_g^+$  and  $A \ ^2\Pi_u$  states of  $N_2^+$  are added to the  $B \ ^2\Sigma_u^+$  excitations. The ionization cross sections for these two states are found to be proportional to the  $B \ ^2\Sigma_u^+$  state for electron energies above 30 eV.

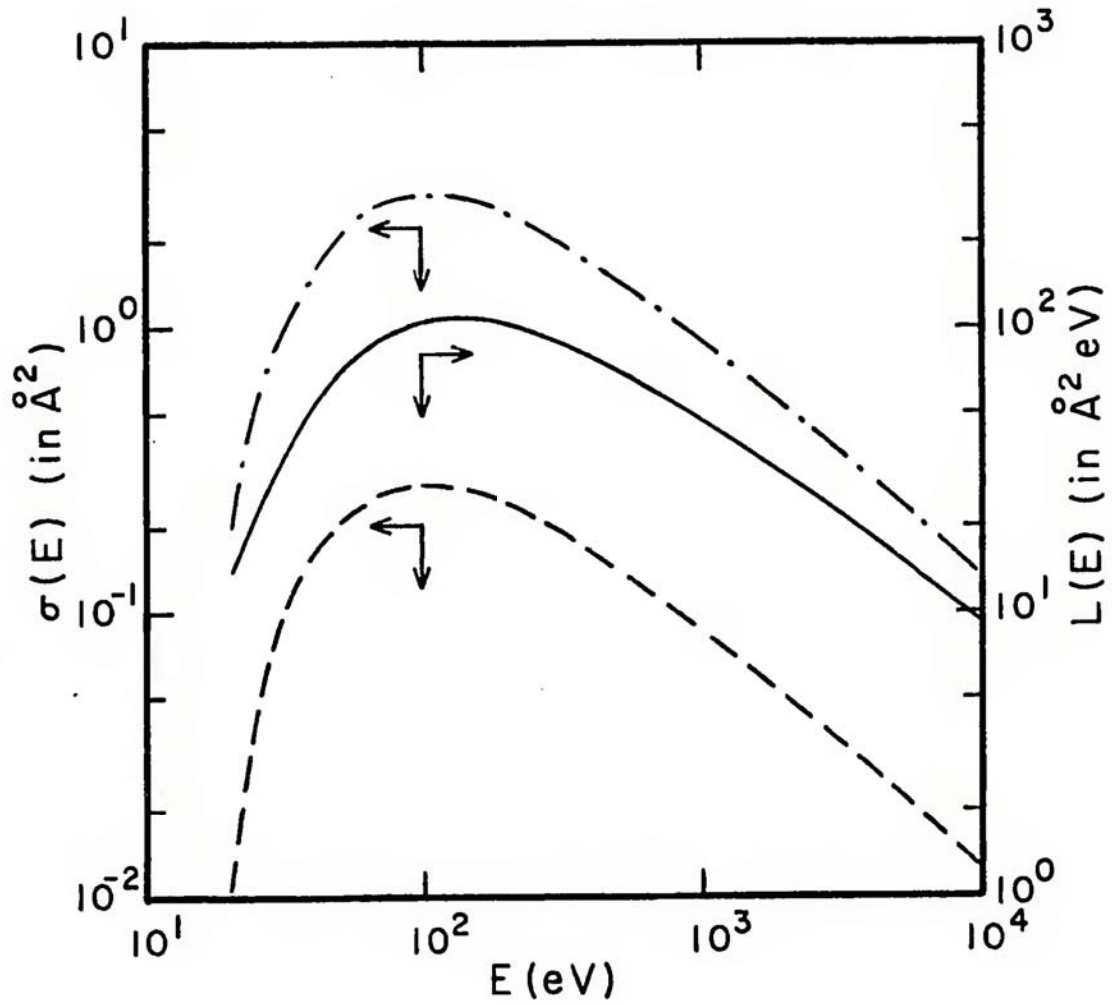


Figure 5.1 Total loss function  $L(E)$  from  $\text{N}_2$ , denoted by the solid line; total ionization cross sections for  $\text{N}_2$ , denoted by the dash-dot line; and the  $\text{N}_2 \text{ B } ^2\Sigma_u^+$  cross section, denoted by the dashed line, are given as functions of energy,  $E$ .

Previous workers (Barrett and Hays, 1976; Cohn and Caledonia, 1970; and Grün, 1957) have used the 3914 Å emission as a measure of the energy deposited. In these works it is assumed that since the 3914 Å radiation is proportional to the number of ionizations in a given volume and if the number of ionizations is proportional to the energy deposited in that volume, then the 3914 Å intensity is proportional to the energy deposited in that volume. These experimenters, therefore, measured the 3914 Å radiation at several energies, extrapolated their intensity plots to find a range (to be described in section V.B), and derived an empirical expression for the range that could be used to find the energy loss function.

This idea of using the 3914 Å emission to derive the energy loss scheme is useful for energies above 2 KeV. In Figure 5.1, compare the loss function,  $L(E)$ , used in this work and the  $N_2^+ B^2 \Sigma_u^+$  state cross section.

The two curves are not parallel below 2 KeV. This implies that the energy loss function can not be derived directly from the range results at incident energies below 2 KeV. The energy loss plots from this MC study are given in section VII.A and more will be discussed in that section about them.

### B. Range of Electrons

The concept of the mean range must be defined next. For each monoenergetic primary electron impinging into a gas, a range can be calculated. In general (at least above 100 eV), the higher the electron energy the further the electron will penetrate into the medium. If an electron is incident along the z-axis, the excitations of the  $N_2^+ B^2 \Sigma_u^+$

state can be graphed in an intensity plot with the z-axis as the abscissa.

In Figure 5.2, the intensity plot from 5000 incident 1 KeV electrons is graphed (the model used in this MC calculation should only be taken as an illustrative example) in histogram form. Bins along the z-axis are taken to be 0.5 cm in width for these incident electrons. The linear portion of the curve may be extrapolated, as illustrated by the dashed line, to define a mean range of the beam.

All the intensity plots are normalized in this paper so that the beam starts out at  $z = 0$  cm along the z-axis. The intensity in Figure 5.2 seen at negative values of  $z$  is brought about by backscattered electrons. The error bars given near the peak of the histogram are found simply from a method described in section IV.D.

From Figure 5.2, the range is seen to be 16 cm for these 1 KeV electrons. Range values,  $R_g$ , in units of  $\text{gm/cm}^2$  are written

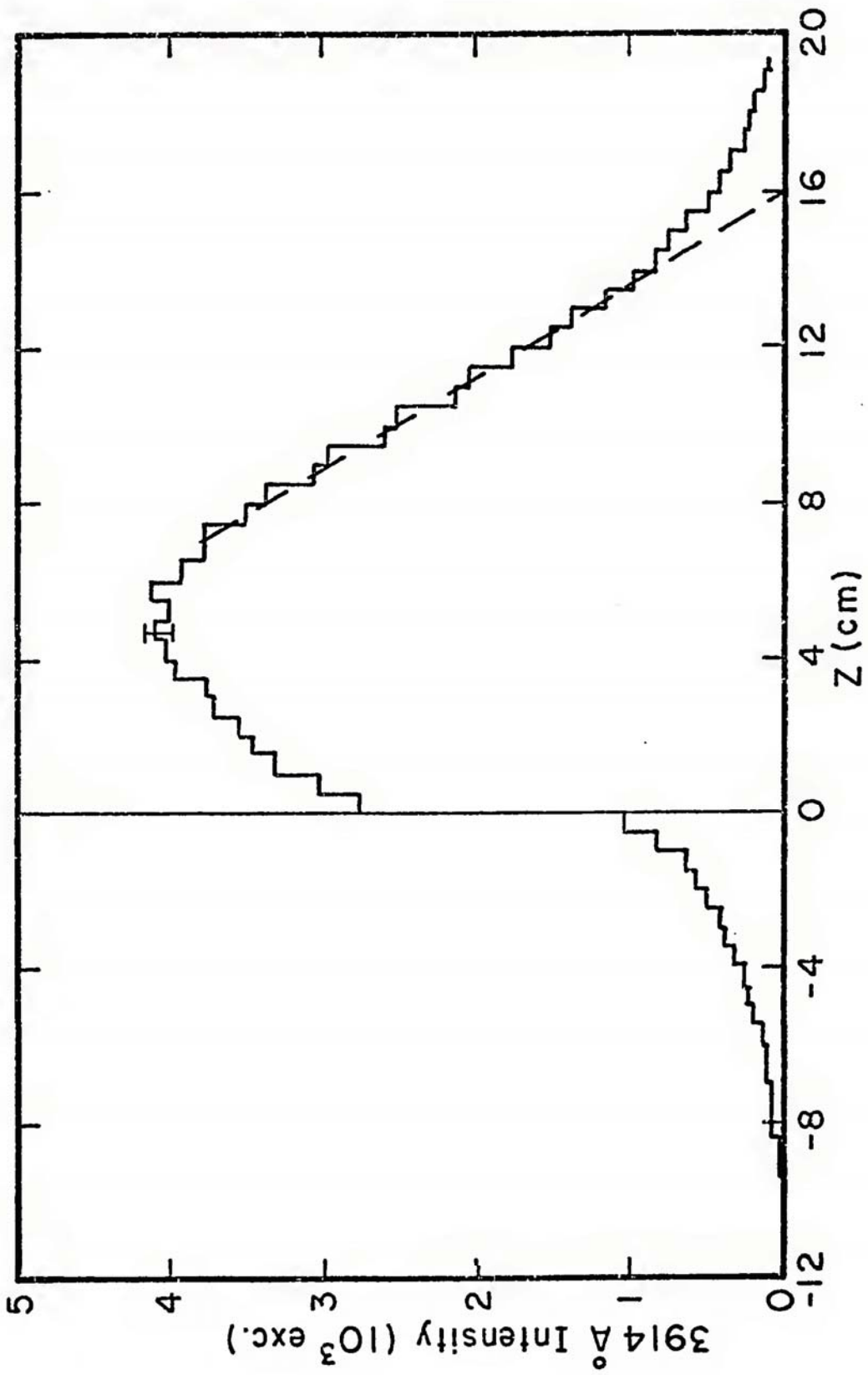
$$R_g = R_c \rho \quad (5.1)$$

where  $R_c$  is the range in cm,  $\rho = n M_{N_2}$  (in  $\text{gm/cm}^3$ ),  $n$  is the number density of  $N_2$  molecules (in  $\#/\text{cm}^3$ ), and  $M_{N_2}$  is the weight (in gms) of an  $N_2$  molecule. In this case,  $n = 8.2 \times 10^{15}$  molecules of  $N_2/\text{cm}^3$ ,  $M_{N_2} = 4.651 \times 10^{-23}$  gm/ $N_2$  molecule, and  $R_c = 16$  cm; therefore,  $R_g = 6.06 \times 10^{-6}$   $\text{gm/cm}^2$ .

### C. Previous Experimental and Theoretical Work on the 3914 Å Emission of $N_2$

Grün (1957) measured for air the total luminosity of the 3914 Å radiation in planes perpendicular to the axis of the electron beam with

Figure 5.2 The intensity of 3914 Å radiation is given as a function of  $z$  for 5000 electrons with incident energies of 1 KeV. The range, found by extrapolating the linear portion of the histogram (illustrated by the dashed line) to the abscissa, is 16 cm. The  $I$  indicates the standard error involved in the MC calculation.



an initial energy of 5 to 54 KeV. Cohn and Caledonia (1970) measured intensity profiles of electron beams with incident energies from 2 to 5 KeV impacting into  $N_2$ . Barrett and Hays (1976) then extended the incident electron range down to 300 eV by measuring the radiation profiles of  $3914 \text{ \AA}$  resulting from electron beams with energies from 0.3 to 5.0 KeV impinging on  $N_2$ .

Spencer (1959) used the Spencer and Fano (1954) method of spatial energy deposition and found good agreement between his energy loss plots and the  $3914 \text{ \AA}$  intensity plots of Grün (1957). The Berger, Seltzer, and Maeda (1974) [BSM] MC calculation provided energy loss plots down to 2 KeV. These plots are also in fairly good agreement with the experiments mentioned above.

Comparisons will be made in this paper between the available experimental electron energy loss data and the MC calculations done here. Since this MC calculation follows the incident electrons, as well as its secondaries and tertiaries down to 2 eV, this MC computation is one of the most detailed ever employed for electron impact energy degradation. It is, therefore, of interest to compare the results from this study with experimental results for incident electrons with energies from 300 eV up to 5 KeV.

#### D. Range Results and Longitudinal Intensity Plots from the Monte Carlo Calculation

Range data at several incident electron energies are calculated with the use of the screened Rutherford and the model 3 differential elastic cross sections. The screened Rutherford model is used because it is the most widely used form for elastic scattering in theoretical

studies and, also, because BSM were quite successful in using this form down to incident energies of 2 KeV. Model 3 was used because of its very close agreement with experimental differential cross section data in the range from 30 eV up to 1 KeV.

Table 5.1 presents the range data (for perpendicularly incident electrons) from three different experiments, the theoretical calculation by BSM, and two sets of theoretical computations from this study. The values in parentheses from BH (Barrett and Hays, 1976), CC (Cohn and Caledonia, 1970), and G (Grün, 1957) are simply calculated from the empirical formulae given in these works.

For the rest of this chapter, the results of this work will be compared with those of BH. This is the most recent experimental study and is probably the most reliable experimental work. They also use the same incident electron energy regime as that employed in this work. In Table 5.1 it is apparent that the BH values have the largest ranges of the experimental studies.

The two separate MC calculations in this study seem to bracket the BH results at all energies. The model 3 ranges are consistently larger than those of BH. These results are 10% higher at 5 KeV and about 19% higher at 0.3 KeV. The screened Rutherford ranges, on the other hand, are about 9% lower at 5 KeV and about 10% lower at 0.3 KeV.

If it can be assumed that the BH results are indeed the most reliable data, then the following conclusion can be made: The screened Rutherford phase function scatters the electron too much while the model 3 phase function provides too little scattering. This conclusion is made assuming that the total cross sections described in Chapter III are fairly accurate.

Table 5.1 Range data (in  $10^{-6}$  gm/cm<sup>2</sup>) at several energies, E (in KeV), are given below. The second column M3 (model 3), third column SR (screened Rutherford), fourth column BH (Barrett and Hays, 1976), fifth column CC (Cohn and Caledonia, 1970), sixth column G (Grün, 1957), and seventh column BSM (Berger, Seltzer, and Maeda, 1974) range values are presented.

E (KeV)	M3	SR	BH	CC	G	BSM
0.1	0.37	0.34	(0.53)	(0.07)	(0.08)	--
0.3	1.25	0.95	1.06	(0.51)	(0.56)	--
1.0	6.45	5.57	5.72	(4.17)	(4.57)	--
2.0	18.6	16.8	17.7	14.0	(15.4)	15.2
5.0	91.5	75.9	83.0	69.7	76.4	71.9

In this work model 3 is the result of a careful investigation of the detailed molecular nitrogen cross sections. Therefore no attempt will be made here to change the cross sections compiled in Chapter III. Model 3 will be used in most of the MC calculations in the rest of this chapter and also in Chapter VII (BSM have, however, chosen  $\eta_c$ , used in the screened Rutherford cross section, to be a constant value whose value was selected so as to obtain the best agreement between their MC calculation and the experimental results of G and CC).

In Table 5.1 the importance of the elastic phase functions is clearly illustrated. Up to a 25% change in the range is observed when comparing the screened Rutherford with the model 3 phase functions. More elaboration on the effects of various phase functions on the energy deposition process will be given in Chapter VI.

Figures 5.3 and 5.4 give intensity plots for the 3914 Å radiation resulting from 2 KeV and 0.3 KeV incident electrons, respectively. The experimental work of BH and the calculations using model 3 and the screened Rutherford are presented in these figures. The shapes appear to be somewhat similar; however, the BH results at both energies predict a range that is between the two theoretical calculations.

#### E. Intensity Plots in the Radial Direction

Most attention, so far in this study, has been concentrated on the intensity plots in the longitudinal direction. There is experimental data available on the intensity of the 3914 Å radiation as a function of  $\rho$  (the axis perpendicular to  $z$ ). Experimentally, G, CC, and BH all present data of this type.

Figure 5.3 An intensity plot for electrons of energy 2 KeV is presented as a function of the longitudinal direction. The x's represent relative experimental values from Barrett and Hays (1976) and the histograms present the data from model 3 (heavy line) and the screened Rutherford (light line). The straight solid and the straight dashed lines represent extrapolations to find the range for the model 3 and the screened Rutherford elastic differential cross sections, respectively.

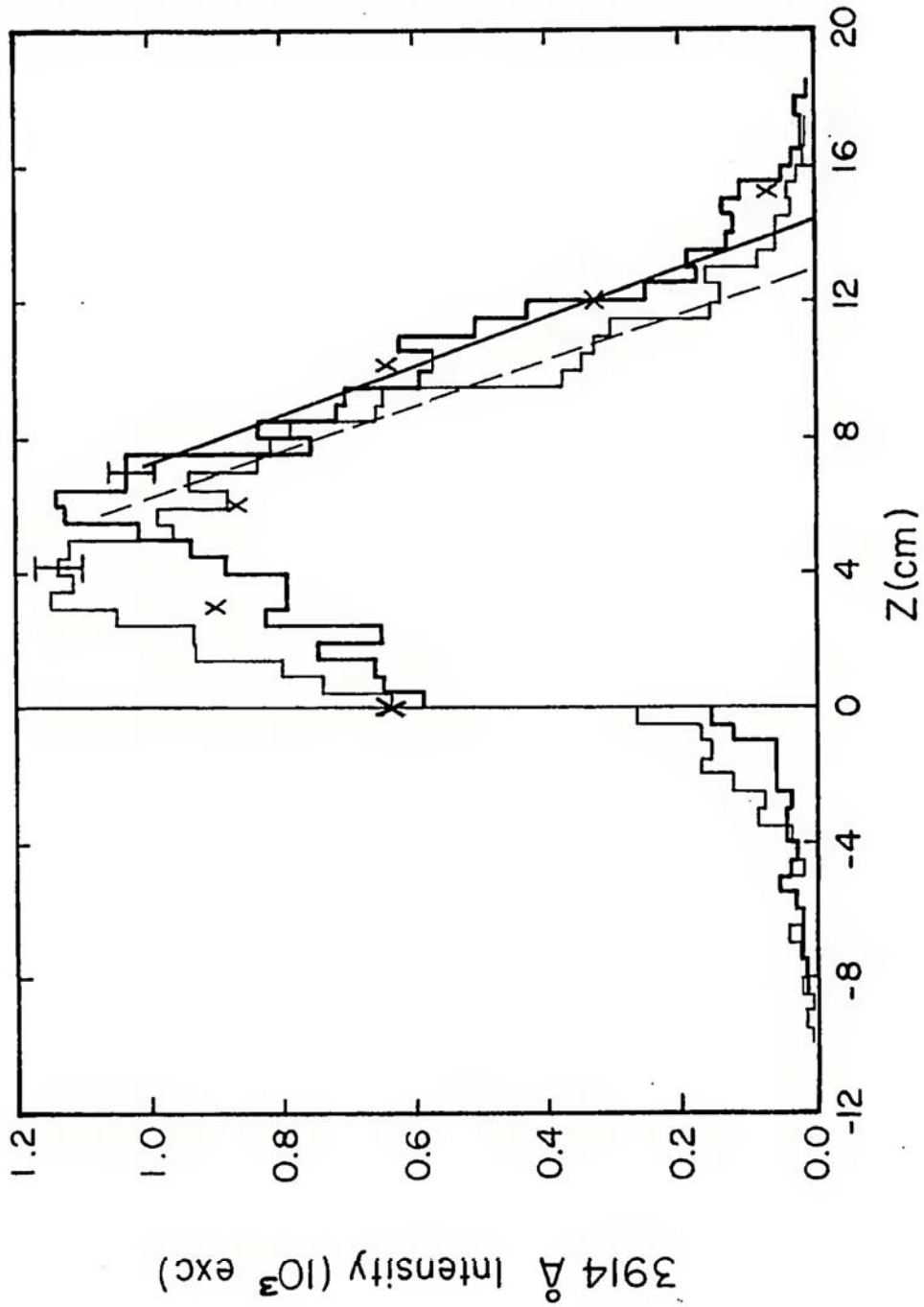
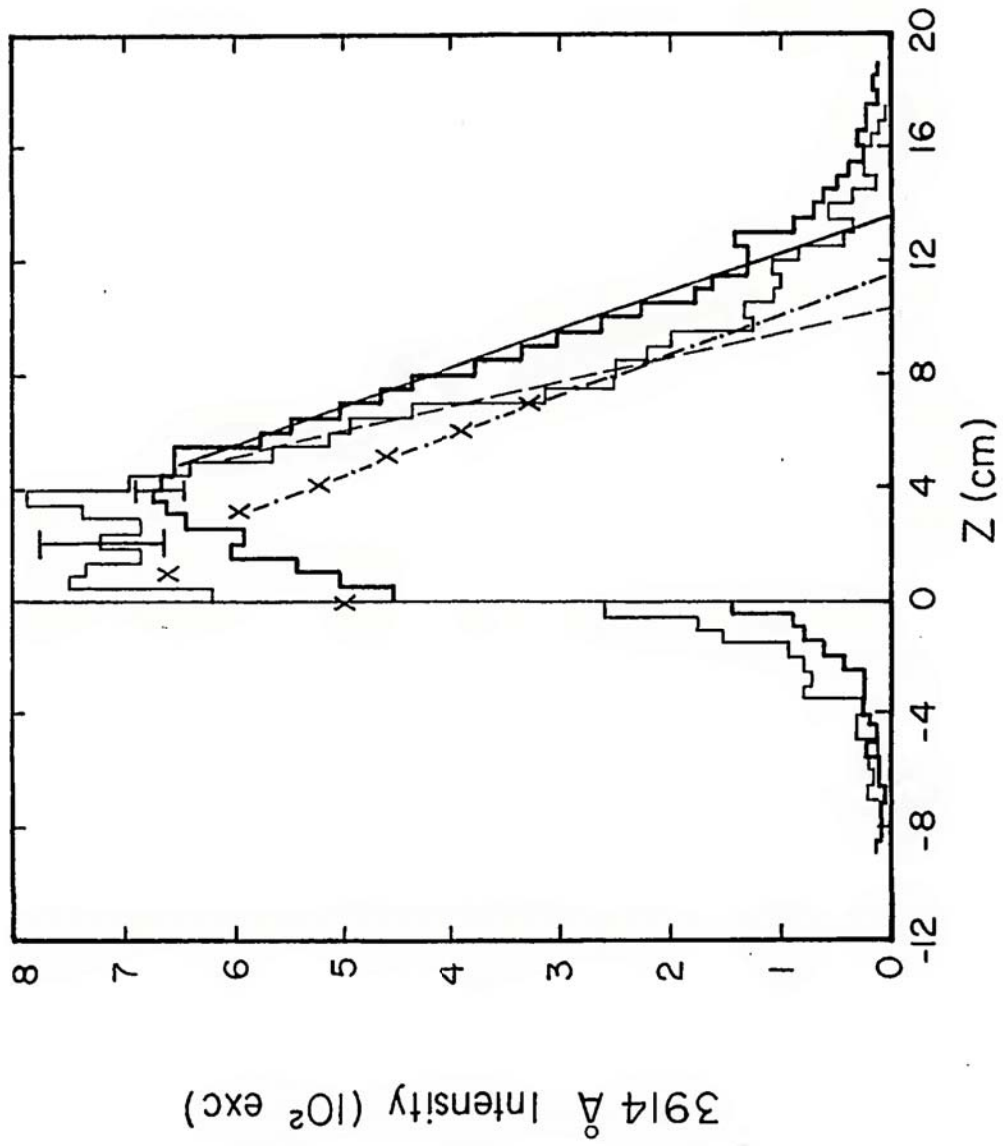


Figure 5.4 An intensity plot for electrons of energy 0.3 KeV is presented as a function of the longitudinal direction. The x's represent relative experimental values from Barrett and Hays (1976) and the histogram presents the data from model 3 (heavy line) and the screened Rutherford (light line). The straight lines extrapolated to the z-axis are all measures of the range. The solid line indicates the model 3 range; the dashed line indicates the screened Rutherford range; and the dash-dot line indicates the Barrett and Hays (1976) range.



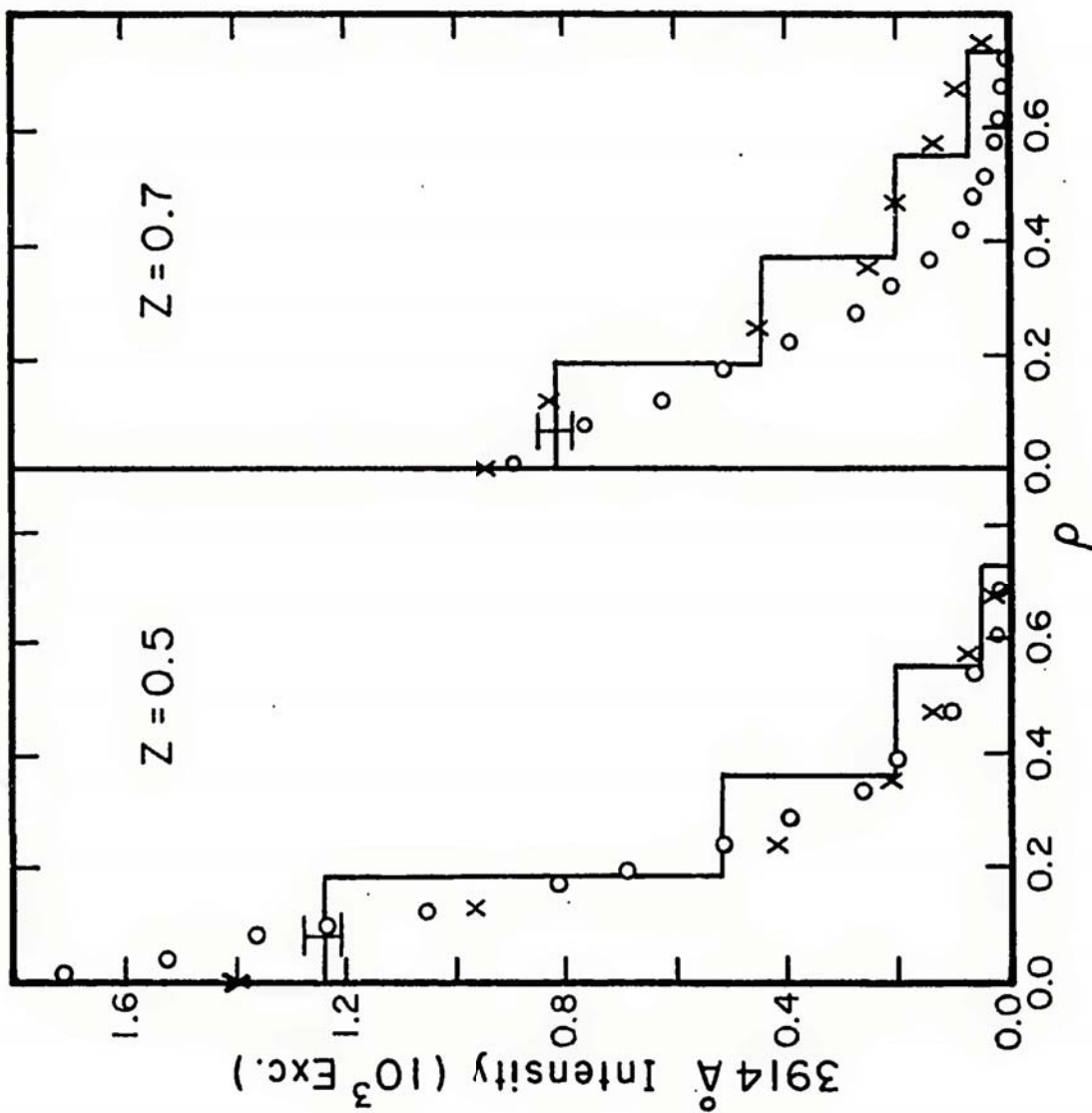
This study uses the experimental data of BH as a comparison with the results of this study. The next three graphs, Figures 5.5, 5.6, and 5.7, portray sample results for incident electrons with energies 5.0, 1.0, and 0.3 KeV, respectively. The  $z$  and  $\rho$  values given in these three figures are in units of fractions of the total range.

Fairly good agreement between the MC calculation (using model 3 cross sections) and the experimental work of BH and Barrett (1975) is observed at all three incident energies. The largest differences between the two sets of data are noted at 0.3 and 1.0 KeV.

For the 1.0 KeV case, the MC calculation tends to predict more intensity at the lower values of  $\rho$  for  $z$  values of 0.3 and 0.4. A similar result is apparent for the  $z$  values of 0.36, 0.48, and 0.60 for an energy of 0.3 KeV. At a  $z$  value of 0.12, however, the experimental data tend to predict more intensity at all values of  $\rho$ .

Two conclusions can be drawn from these comparisons, if it is assumed that the experimental data of BH and Barrett (1975) are correct. First, the cross section for excitation to the  $N_2^+ B^2\Sigma_u^+$  may be underestimated in the energy regime between 0.3 and 1.0 KeV. Raising this cross section in this energy regime could bring about an increase in the intensity observed early in the electron's degradation process with a subsequent decrease in intensity later in the electron's degradation process. Second, more scattering from the elastic collisions would help to reduce the total intensity at low  $\rho$  values and raise it at the higher  $\rho$  values. The screened Rutherford differential cross section has more scattering than model 3. Use of this set of cross sections in the MC calculation did result in a little better agreement at 1.0 KeV, but only about the same type of agreement at 0.3 KeV.

Figure 5.5 Intensity plots for electrons with incident energy 5.0 KeV are presented at two  $z$  values as functions of  $\rho$ . The solid line histogram indicates the results using model 3. The x's denote the experimental data of BH and the o's denote the theoretical work of BSM.



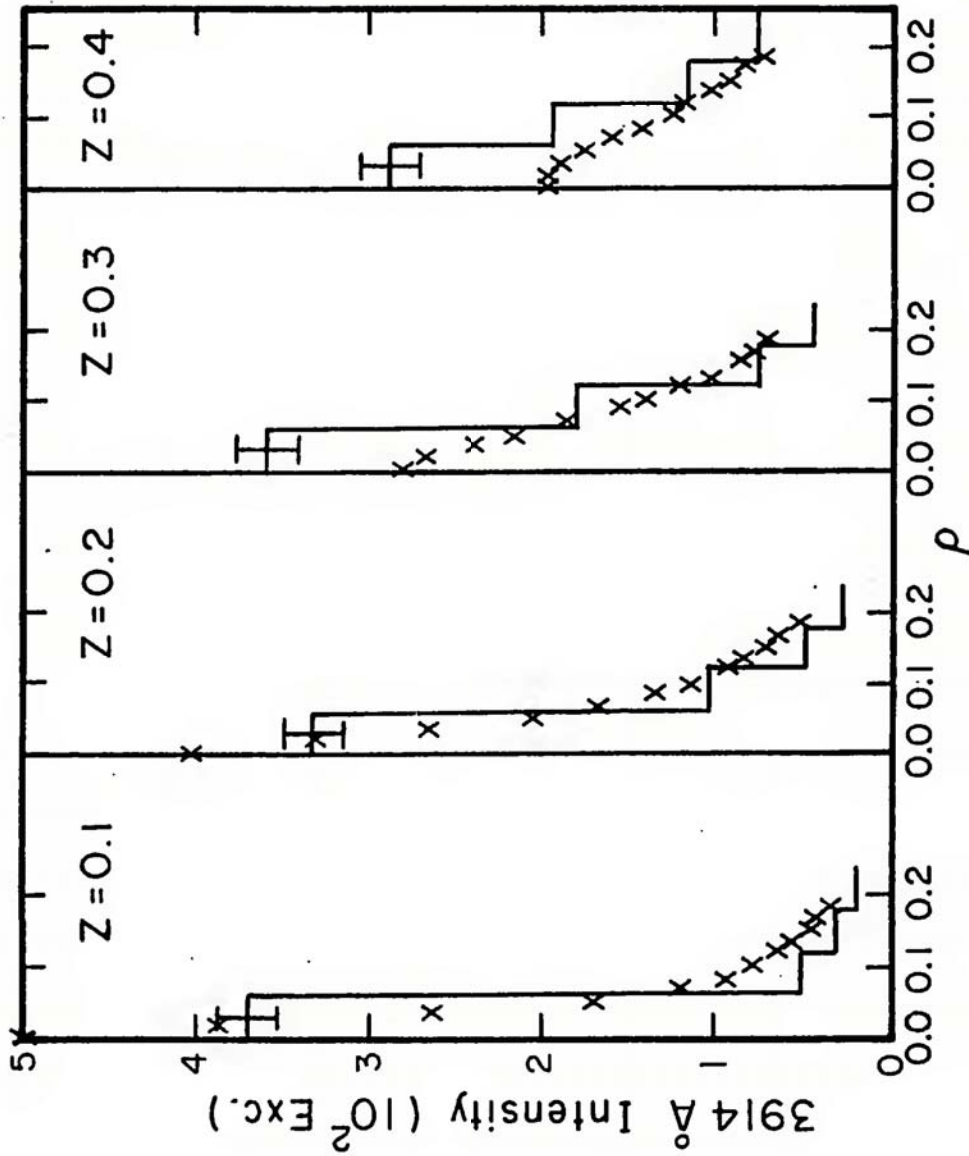


Figure 5.6 Intensity plots for electrons with incident energy 1.0 keV are presented at four  $z$  values as functions of  $\rho$ . The solid line histogram indicates the results using model 3. The x's denote the experimental data of Barrett (1975).

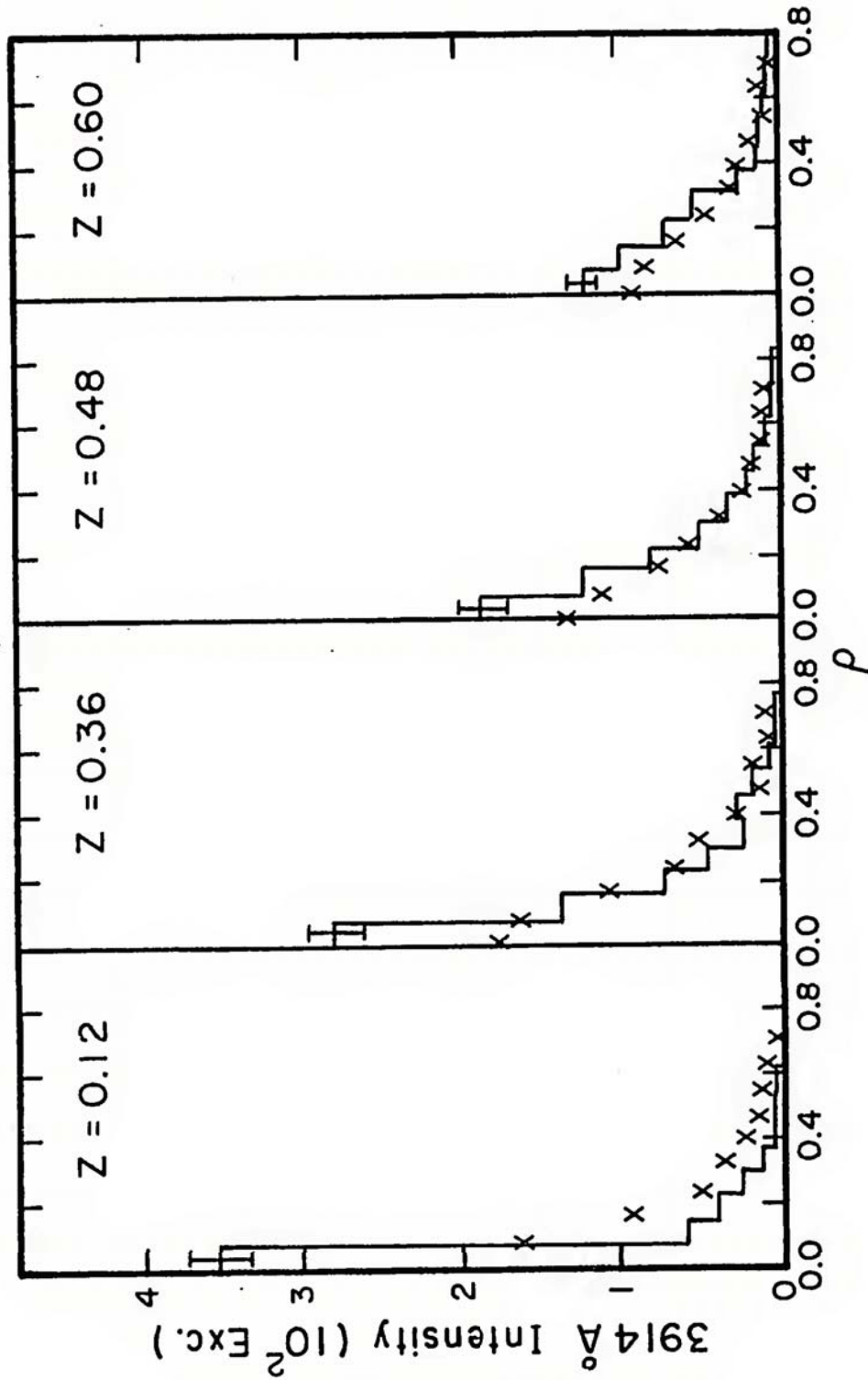


Figure 5.7 Intensity plots for electrons with incident energy 0.3 KeV are presented at four  $z$  values as functions of  $\rho$ . The solid line histogram indicates the results using model 3. The x's denote the experimental data of BH.

At 5.0 KeV a comparison is made between the theoretical calculations from this work and those of BSM. The results from this work appear to agree much better with the BH data than does the BSM work. In BSM, they follow only the primary and secondaries down to 200 eV. Since this work follows the primary, secondaries, and tertiaries down to 2 eV, it seems straightforward that the agreement should be better in this work.

---

## CHAPTER VI

### SENSITIVITY STUDY OF THE SPATIAL ELECTRON ENERGY DEGRADATION

In section V.D the ranges from two separate models of the elastic differential cross section have been compared. A sensitivity study of the influence of other differential cross sections on the electron energy deposition is the subject of this chapter. The effects of the ionization differential cross sections on the intensity distribution are considered in section VI.A. Section VI.B then discusses the influence of the inelastic differential cross sections on the intensity distribution.

In sections VI.C and VI.D, several different elastic phase functions are compared. (The elastic collisions cause more scattering than the inelastic collisions at any electron energy.) Section VI.C includes a calculation with no energy loss, while section VI.D discusses the influence of several variations of the model 1 phase function on the electron energy deposition.

As illustrated in sections VI.A through VI.D, the scattering phase functions are quite important in determining the electron energy deposition intensity or collision profiles. The total elastic cross sections are also of some significance in determining the intensity profiles and will be discussed in section VI.E.

### A. Effects of Ionization Differential Cross Sections on the Intensity Distributions

The primary and secondary differential ionization forms represented in Eqs. (3.18) and (3.19) are convenient for calculating the scatter of the electrons during an ionization event. Here, the influence of these forms on the intensity plots will be considered.

Other MC calculations have computed the scattering of the electrons during an ionization event. Brinkmann and Trajmar (1970) calculated the primary scattering angle from experimental energy loss differential cross section data. They then employed an empirical simplification of the coincidence data obtained by Ehrhardt, Schulz, Tekaas, and Willmann (1969), in which half of the secondary electrons were presumed to scatter at four times the primary scattering angle and the other half at  $\pi$  radians plus four times the primary scattering angle.

In another MC approach, Berger, Seltzer, and Maeda (1970, 1974) used the Moller cross section for the scattering of secondary electrons as a result of an ionization collision. The angular deflection  $\theta$  is given such that

$$\sin^2 \theta = \frac{4\epsilon}{\tau(1 - 2\epsilon) + \tau + 4} \quad (6.1)$$

where  $\epsilon$  is the energy transfer in units of  $E$ , and  $\tau$  is the kinetic energy in units of the rest mass.

At the maximum incident energy of 5000 eV used in this work,  $\tau \approx 0.01$ . Using this value of  $\tau$  for primary scattering, in which  $\epsilon < 0.5$ , all scatterings are between  $0^\circ$  and  $45^\circ$ . The secondary scattering turns out to be between  $45^\circ$  and  $90^\circ$ , since  $0.5 \leq \epsilon < 1.0$ . This means that

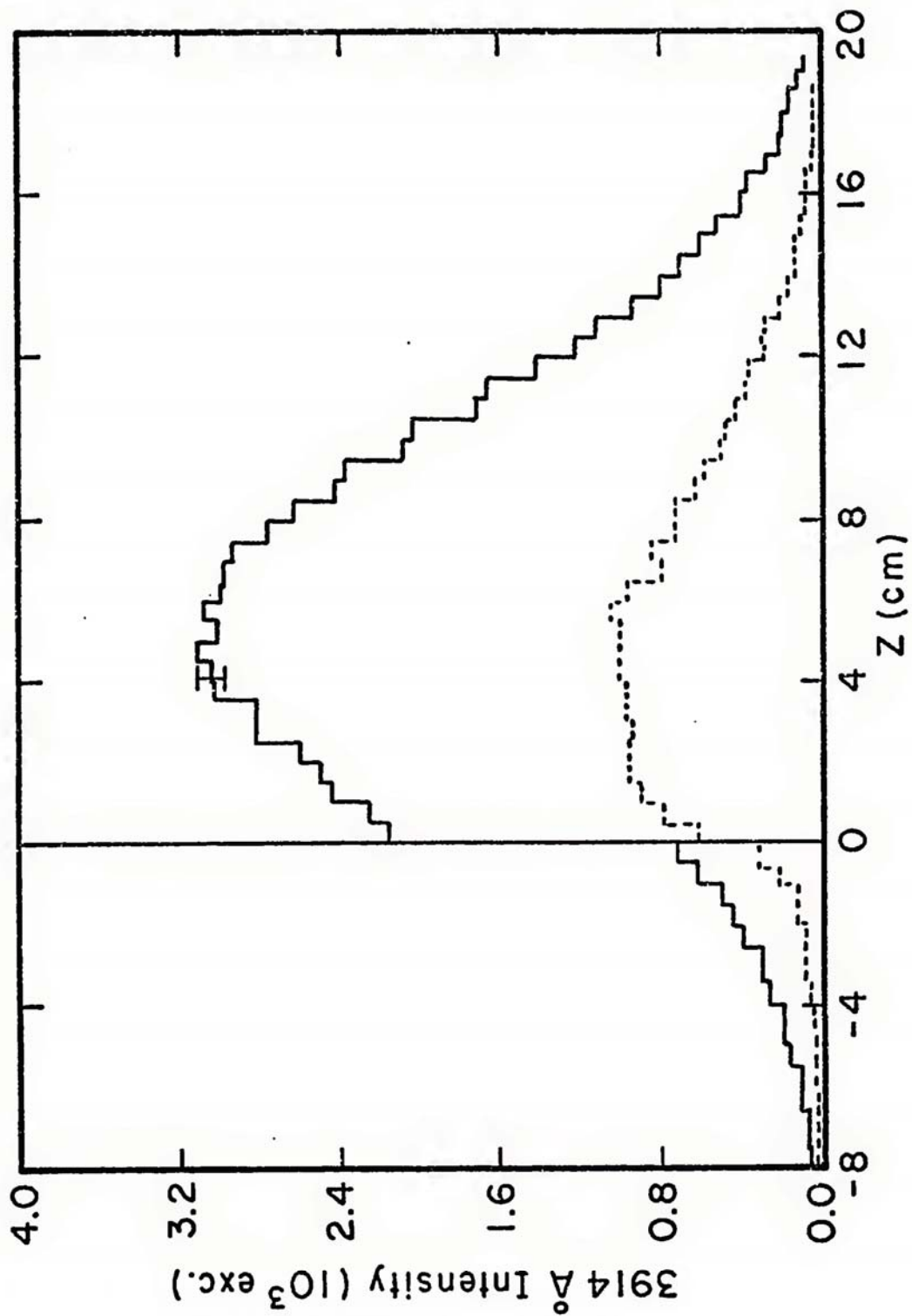
most deflections of the primary electron are at small angles while most deflections of the secondary electrons are clustered near  $90^\circ$ .

Strickland, Book, Coffey, and Fedder (1976) used a variety of different secondary doubly differential ionization cross sections. Their solutions to the equation of transfer show little dependence on the functional form being used. Thus it is valid to ask if different primary or secondary ionization differential cross sections will have any influence on the intensity plots resulting from a MC calculation.

The primary electron is scattered the least. Therefore, for comparison, it is assumed that no scattering of the primary electron was incurred during the ionization event. The results of this comparison, using the  $3914 \text{ \AA}$  intensity plots for incident electron energies of 2000 and 300 eV, were not too surprising: There was virtually no observed difference in the two intensity plots. This simply means that the scattering of the primary during an ionization event is minuscule compared to the much larger scatterings inherent in the elastic collisions. For most of the calculations following this comparison, it was assumed that no scattering of the primary electron occurred in an ionization event. This resulted in a factor of eight savings in the computer time and cost.

In Figure 6.1, the effect of the primaries and secondaries on the total  $3914 \text{ \AA}$  radiation is clearly seen at the incident energy of 1 KeV. The major contribution of the secondaries is early in the history of the incident electron, when it has sufficient energy to create high energy secondaries capable of producing the  $3914 \text{ \AA}$  emission. Also, the contribution by the primaries is a more sharply peaked curve than that of the secondaries. The backscatter contribution from the secondaries is

Figure 6.1 An intensity plot for electrons of energy 1 keV is presented as a function of  $z$ . The solid line represents the primary or incident electron's contribution to the 3914 Å emission while the dashed line illustrates the contribution from the secondary electrons.



seen to be fairly high. Secondaries are at lower energies; therefore, more of them are backscattered.

In considering the secondaries, it is of interest to discover any difference in the intensity plots that may be due to the use of a different secondary scattering distribution. Consequently, a comparison was made between Eq. (3.18) and an isotropic secondary scattering function. The difference in the two resulting intensity plots was so small that they were the same within their standard deviation error bars. This result, although surprising at first glance, did not seem as surprising under careful inspection.

Consideration of Table 5.1 gives the answer. A 5 KeV electron has a range of  $91.5 \times 10^{-6} \text{ gm/cm}^2$  while a 0.3 KeV electron has a range of  $1.25 \times 10^{-6} \text{ gm/cm}^2$ . Most of the secondaries contributing to the 3914 Å emission that are produced by an incident electron of energy 5 KeV have energies of only a few hundred eV or less. These electrons do not travel far, relative to the total range of the incident particle. Therefore their characteristic 3914 Å intensity profiles do not alter the total 3914 Å profile noticeably.

A 0.3 KeV electron traveling in  $\text{N}_2$  at a density of  $2 \times 10^{15}$  molecules/cm<sup>3</sup> (which corresponds to a height in the atmosphere of roughly 70 km) has range of about 12 cm. At 150 km (where the density is about  $5 \times 10^{10}$  molecules/cm<sup>3</sup>) this same electron will have a range of about 5 km. The secondary doubly differential ionization cross sections may thus have an influence on the energy deposition in applications to the upper atmosphere. As mentioned earlier, however, Strickland et al. (1976) do not observe such an effect. Inclusion of Eq. (3.19) only

increases the MC computation by 2-3%. Therefore it was left in all the calculations.

### B. Influence of Inelastic Differential Cross Sections on the Intensity Distributions

Model 3 includes scattering from inelastic excitation collisions. Because of the very highly forward peaked nature of most optically allowed excitations, inelastic excitation scattering is only used below 100 eV and then only in an ad hoc manner. Below 100 eV, scattering due to inelastic excitation collisions is assumed to be the same as that due to elastic collisions (see section III.B).

The main purpose of this section is to determine whether this ad hoc excitation collision scattering makes a significant difference in the spatial energy deposition. When a MC calculation is run assuming no excitation scattering at any energy, no difference is detectable in the 3914 Å intensity plots at energies above 300 eV.

For electrons of energies 300 and 100 eV, a difference is detected. The range (in units of  $10^{-6}$  gm/cm<sup>2</sup>) changes from 1.25 to 1.34 for an electron energy of 300 eV and from 0.365 to 0.391 for an electron energy of 100 eV. This means that the extra scattering due to the inelastic excitation events reduces the range by about 7% at these two energies.

### C. Comparison of Different Elastic Phase Functions on the Electron-N<sub>2</sub> Collision Profile

The large influence of the phase functions on the spatial energy deposition has been pointed out in section V.D and will be further discussed in section VI.D. These phase functions all have some type of

energy dependence. Another way to approach a sensitivity study of the elastic phase functions is the following: 1) Fix the number of collisions allowed in the MC calculations at some set number, say 25000; 2) allow only elastic collisions; and 3) assume that there can be no energy loss during a collision (the electron energy remains fixed at 300 eV).

Employing all the above assumptions, the scattering problem is very similar to the photon scattering process. The aspects of this section may, therefore, be of interest both to researchers in photon scattering as well as electron scattering.

One of the simplest ways to represent elastic scattering phase functions is with model 1 [Eq. (3.12):  $P_{M3}(\theta, E) \propto \{1 - \cos\theta + a(E)\}^{-2}$ ]. This scattering form, as noted earlier, is very similar to the screened Rutherford cross section. Figure 6.2 illustrates five trial phase functions, designated as A1 through A5, whose properties are indicated in Table 6.1.

These five phase function trials were then run in a MC computation using the three restrictions given above. The collision plots for three of these trials are given in Figure 6.3. The input number density in all cases was  $4 \times 10^{15}$  molecules/cm<sup>3</sup> and electrons entered the N<sub>2</sub> gas until the total number of collisions was 25000.

From Figure 6.3 several observations can be made. Generally, the number of backscatter collisions decreased as the forward peaking of the differential cross section increased. The number of collisions occurring close to the origin of the perpendicularly incident electrons also decreased, while the number of collisions at distances forward from the origin increased.

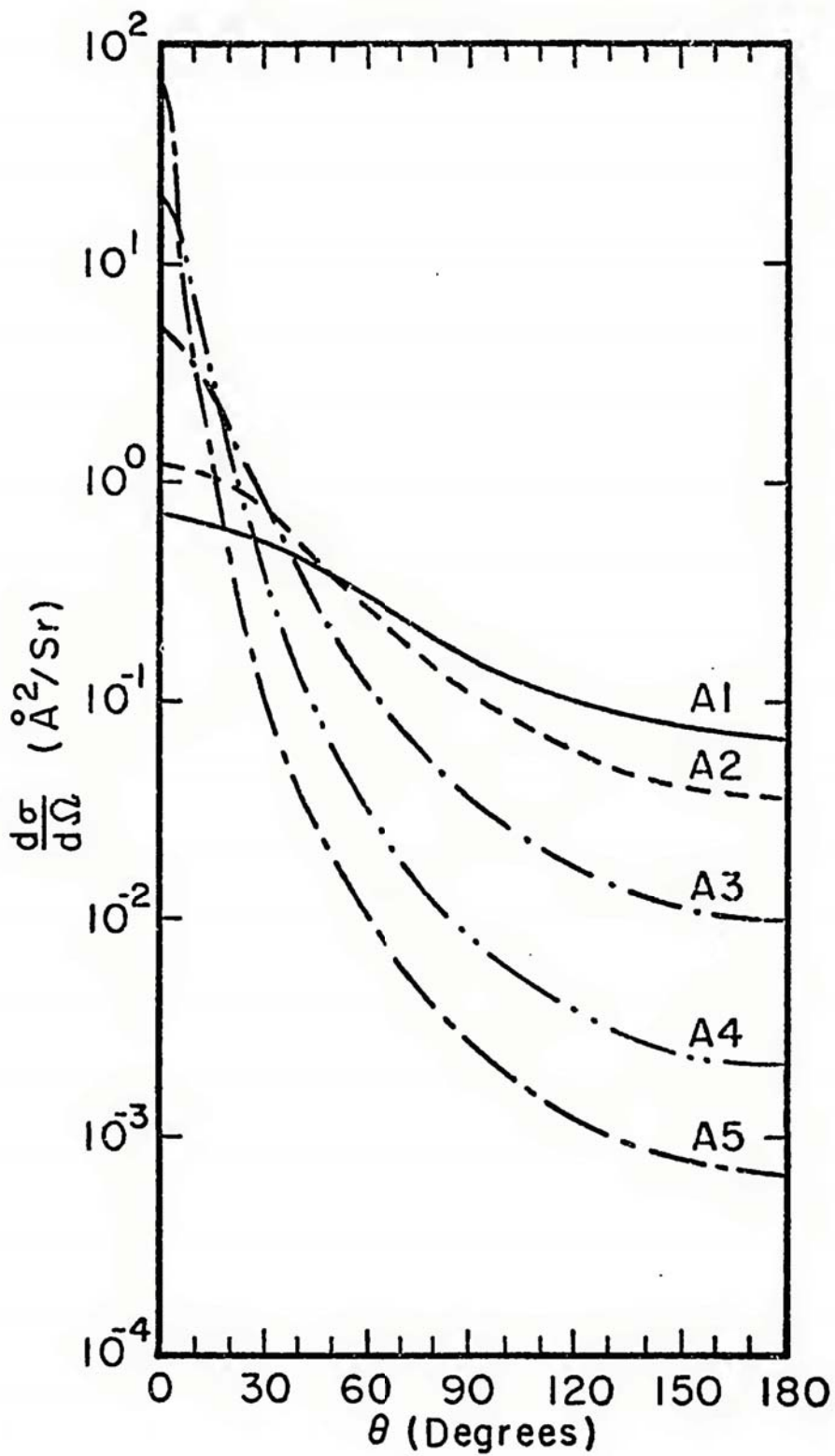


Figure 6.2 Differential cross section graph for model 1 trials: A1, A2, A3, A4, and A5.

Table 6.1 Model 1 parameter values (column labeled "a") and phase function properties for various trials. The phase function fall-off (column labeled PFFO) is indicated in the number of orders of magnitude difference between the differential cross section at  $0^\circ$  and its value at  $180^\circ$ . The average angle of scattering (column labeled AAS) is found using Eq. (6.3).

Trial	a	PFFO	AAS
A1	0.9	1.0	$64.5^\circ$
A2	0.4	1.5	$52.2^\circ$
A3	0.095	2.5	$31.6^\circ$
A4	0.02	4.0	$16.3^\circ$
A5	0.0065	5.0	$9.7^\circ$

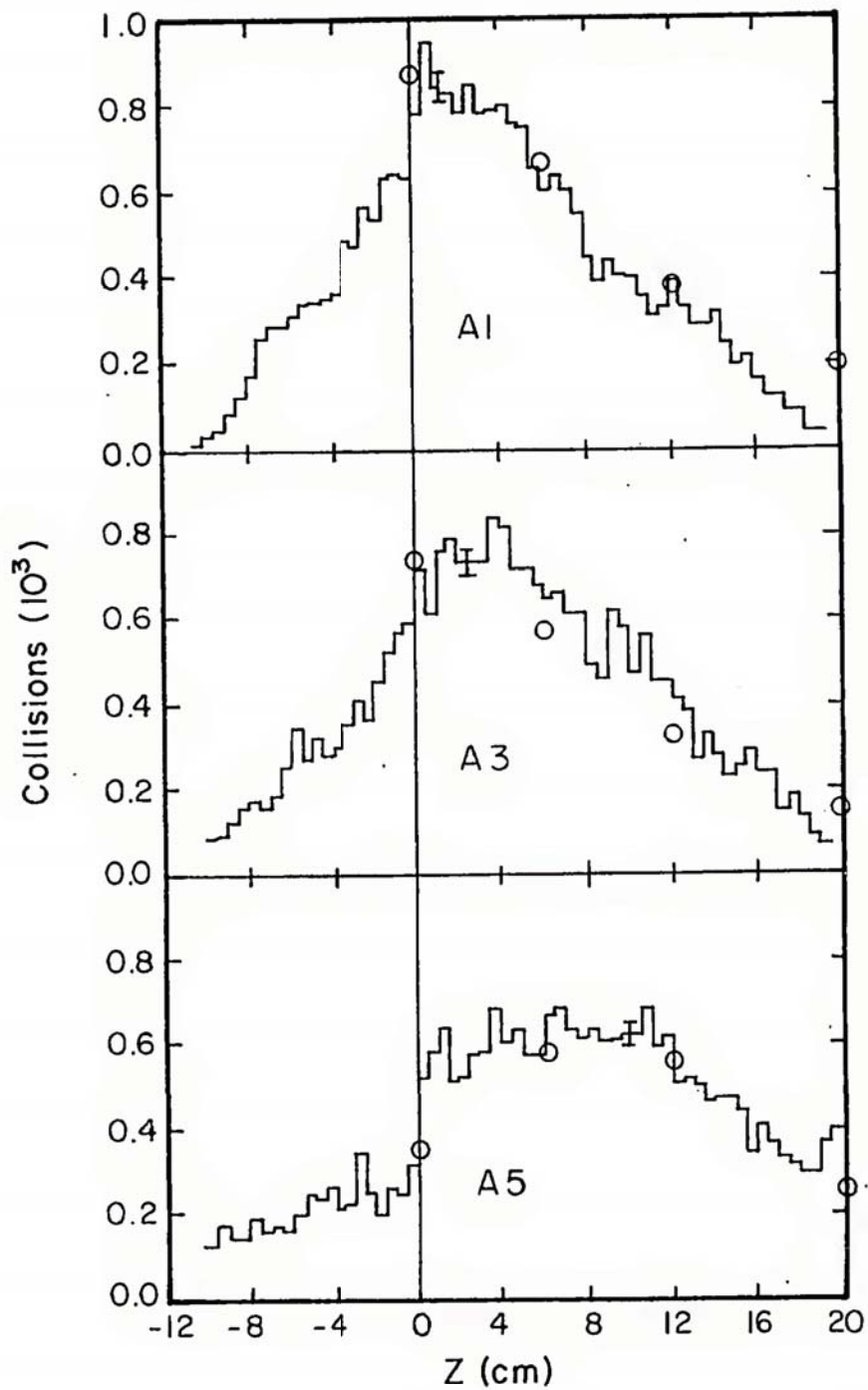


Figure 6.3 Collision plots for MC trials A1, A3, and A5. The histograms represent the MC data while the o's represent the fit using Eq. (6.2).

The shape of the collision profile at positive longitudinal distances appears to have a distribution which is dependent on the "a" parameter. This functional form for the distribution of collisions  $D(z)$  can be represented simply as

$$D(z) = \frac{1}{\alpha(z - z_0)^2 + \beta} \quad (6.2)$$

where

$$\alpha = -0.148 \ln\left(\frac{a}{766}\right)$$

$$\beta = -0.09 \ln\left(\frac{a}{3.2 \times 10^5}\right)$$

and

$$z_0 = 0.056/a$$

The o's in Figure 6.3 represent a visual fit to these data. Equation (6.2) does a reasonable job of indicating the gross features of the collision profile. The features illustrated with this form are the height of the peak, the width of the distribution, and the location of the peak.

The location of the peak is observed to be inversely proportional to the value of the screening parameter  $a$ . The values of  $\alpha$  and  $\beta$  are directly proportional to the natural logarithm of the screening parameter  $a$ , thereby causing the peak of the collision profile to decrease in value as "a" decreases.

Model 2 [Eq. (3.13):  $P_{M2}(\theta, E) \propto \frac{-f}{(1 - \cos\theta + a)^2} - \frac{(1 - f)}{(1 + \cos\theta + c)^2}$ ] can also be used in a MC computation of a similar nature. Figure 6.4 indicates the differential cross sections (trials B1, B2, and B3) used in this comparison and Table 6.2 lists the properties of these trials.

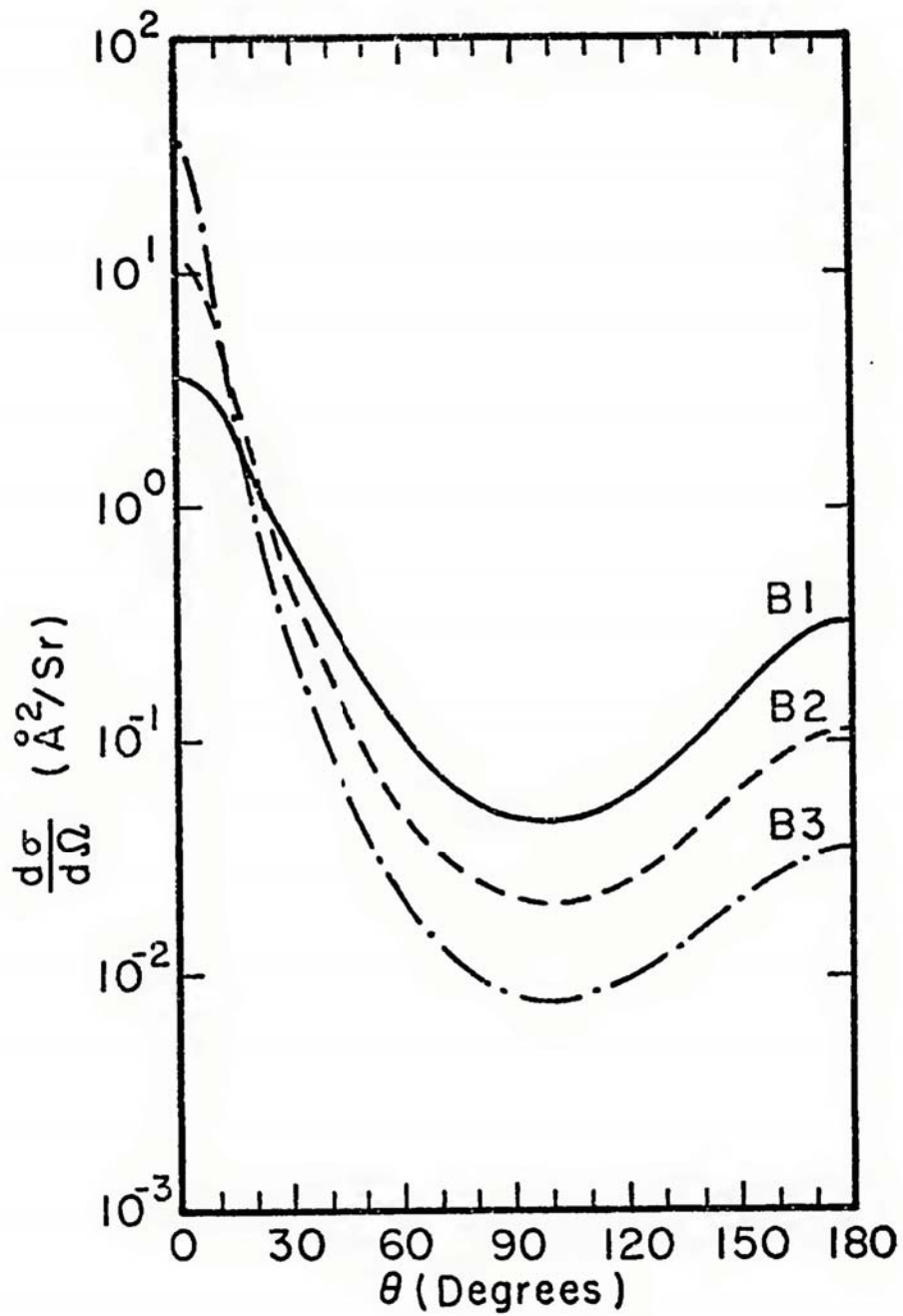


Figure 6.4 Differential cross section graph for model 2 (which contains a forward and a backward scattering contribution) trials: B1, B2, and B3.

Table 6.2 Model 2 parameter values (columns "a," "c," and "f") and phase function properties for various trials. The PFFO and AAS columns are described in Table 6.1.

Trial	a	c	f	PFFO	AAS
B1	0.1	0.3	0.8	1.0	52.3°
B2	0.033	0.38	0.92	2.0	29.0°
B3	0.012	0.46	0.97	3.0	16.3°

The results of these MC calculations are illustrated in Figure 6.5. There is no sharp discontinuity at the origin. The peak of the distribution moves along the z-axis as the forward scattering increases. The reason for this continuity in the collision distribution arises from the backscatter peak.

The average scattering angle is given by

$$\theta_{\text{ave}} = \int_0^{2\pi} \int_0^{\pi} \epsilon P(\theta) \sin\theta d\theta d\phi \quad (6.3)$$

where  $P(\theta)$  is the phase function. The average scattering angle is nearly the same in trials A2 and B1; A3 and B2; and A4 and B3 (compare Tables 6.1 and 6.2). This means that the shape of the backward scattering part of the phase function is also very important in determining the spatial energy deposition of an electron.

#### D. Influence of Different Elastic Phase Functions on the Intensity Profiles

A sensitivity study involving several different, but constant, phase functions was the subject of section VI.C. The elastic scattering phase function of electrons changes with energy. Generalizing the influence of the energy dependent phase function is the subject of this section.

Section V.D includes a comparison of the screened Rutherford and the model 3 phase functions and their influence on the range values. It was learned that in the electron energy regime of interest, 2 eV to 5000 eV, the screened Rutherford causes more scattering than the model 3 phase function. The screened Rutherford range values, therefore, tend to be lower than the model 3 range values (see Table 5.1).

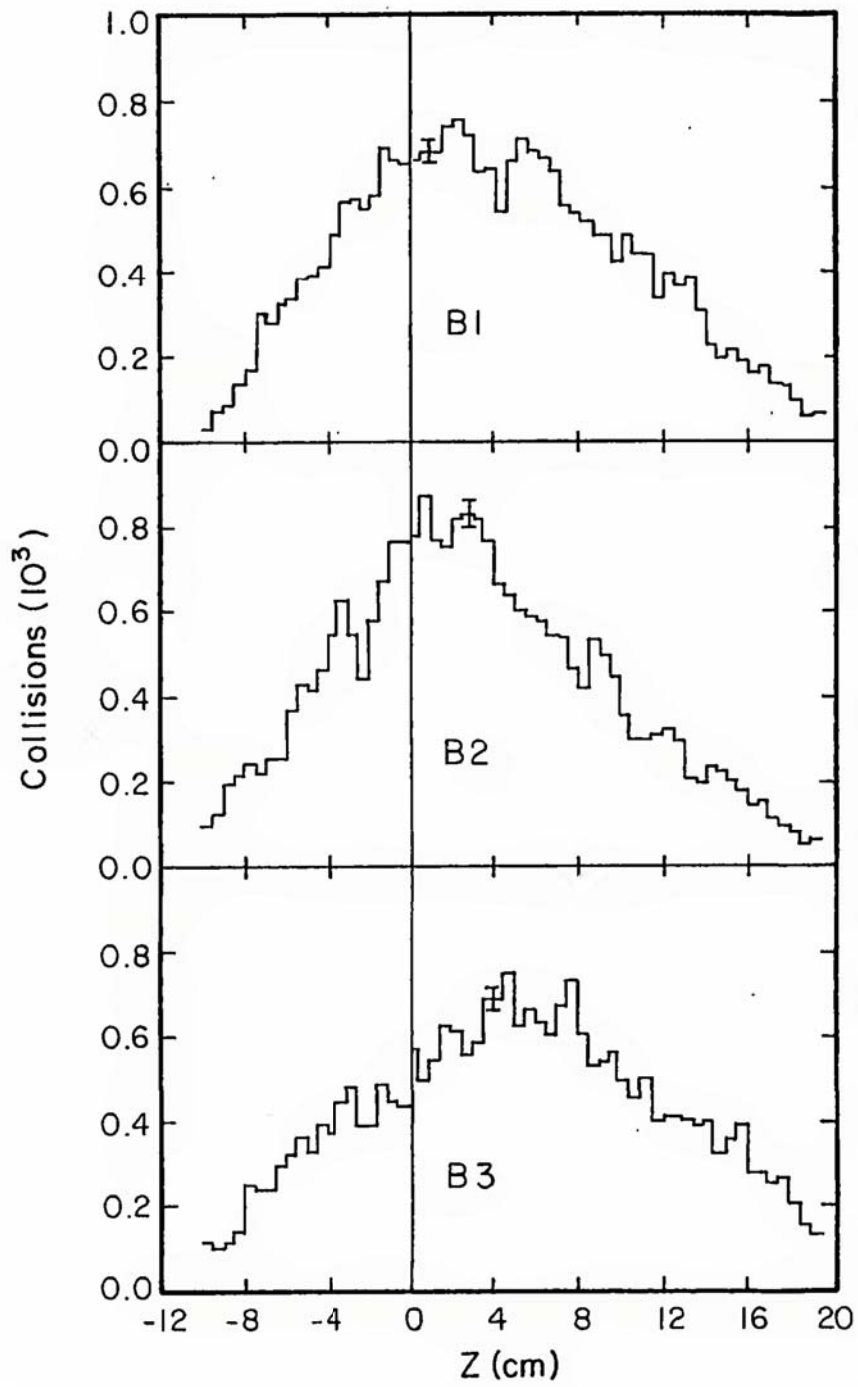


Figure 6.5 Collision plots for MC trials B1, B2, and B3. The histograms represent the MC data.

The screened Rutherford and model 3 phase functions have somewhat different forms. Thus it is difficult to compare them in ways other than the way they were compared in section V.D.

A more convenient phase function form to use for comparison is that of model 1. Model 1 depends on the one screening parameter,  $a$ , which can be written as a function of the energy such that  $a(E) = a_1(E/1 \text{ eV})^{a_2}$ . When  $a_1 = 32$  and  $a_2 = -1$ , this form simulates the screened Rutherford phase function and  $a(E)$  in this case is represented in Figure 6.6 by the solid line (trial C1).

Four other representations of the parameter  $a(E)$  are given in Figure 6.6. These five trials represent attempts to characterize the influence of this screening parameter on the energy deposition process. All five trials (C1, C2, C3, C4, and C5) used 1000 perpendicularly incident electrons with energies of 1 KeV and the trials and their parameters are given in Table. 6.3.

Trials C2 and C3 were attempts to detect the influence of the starting screening parameter  $a(1000 \text{ eV})$  on the energy deposition. For trial C2  $a(1000 \text{ eV})$  [from Table 6.3] is a factor of ten lower than  $a(1000 \text{ eV})$  for trial C1. For trial C3  $a(1000 \text{ eV})$  [from Table 6.3] is a factor of ten higher than the  $a(1000 \text{ eV})$  for trial C1. However, for trials C1, C2, and C3 the  $a(30 \text{ eV})$  values are the same.

The range and fraction of incident energy backscattered obtained from trials C1, C2, and C3 (and also trials C4 and C5) are given in Table 6.4. The range from trial C1 is 38% lower than the range from trial C2 and 38% higher than the range from trial C3. The symmetry of these results is remarkable and probably fortuitous.

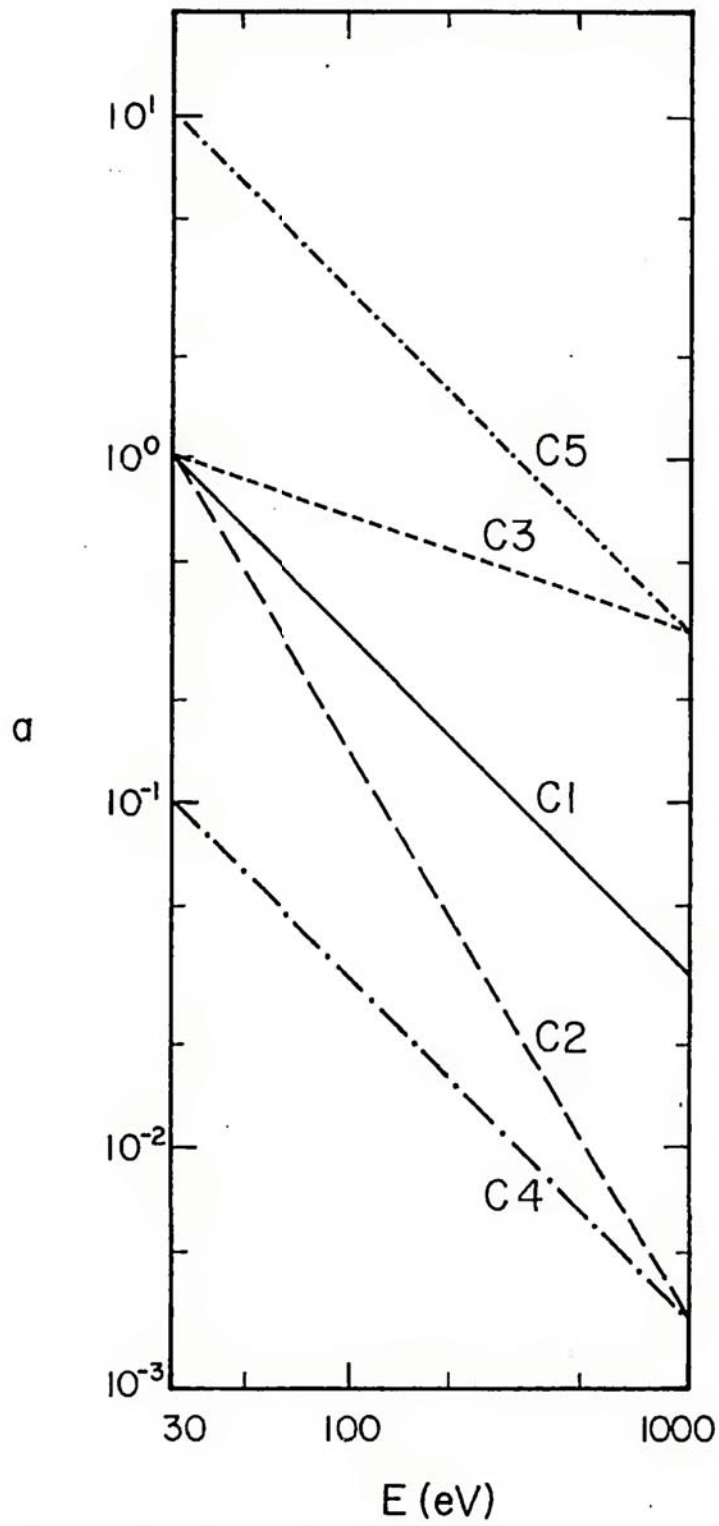


Figure 6.6 Five trials (C1, C2, C3, C4, and C5) of  $a(E)$  for use in model 1.

Table 6.3 Parameters  $a_1$ ,  $a_2$ ,  $a(1000 \text{ eV})$ , and  $a(30 \text{ eV})$  for trials C1, C2, C3, C4, and C5.

Trial	$a_1$	$a_2$	$a(1000 \text{ eV})$	$a(30 \text{ eV})$
C1	32	-1.0	0.032	1.07
C2	303	-1.66	0.0032	1.07
C3	3.44	-0.344	0.32	1.07
C4	3.2	-1.0	0.0032	0.107
C5	320	-1.0	0.32	10.7

Table 6.4 Range,  $R_g$  (in  $10^{-6}$  gm/cm<sup>2</sup>), and fraction of energy back-scattered,  $F_B$ , are given for trials C1, C2, C3, C4, and C5.

Trial	$R_g$	$F_B$
C1	5.57	0.078
C2	7.70	0.012
C3	3.43	0.236
C4	8.16	0.009
C5	3.32	0.211

Using only these three trials it is found that essentially

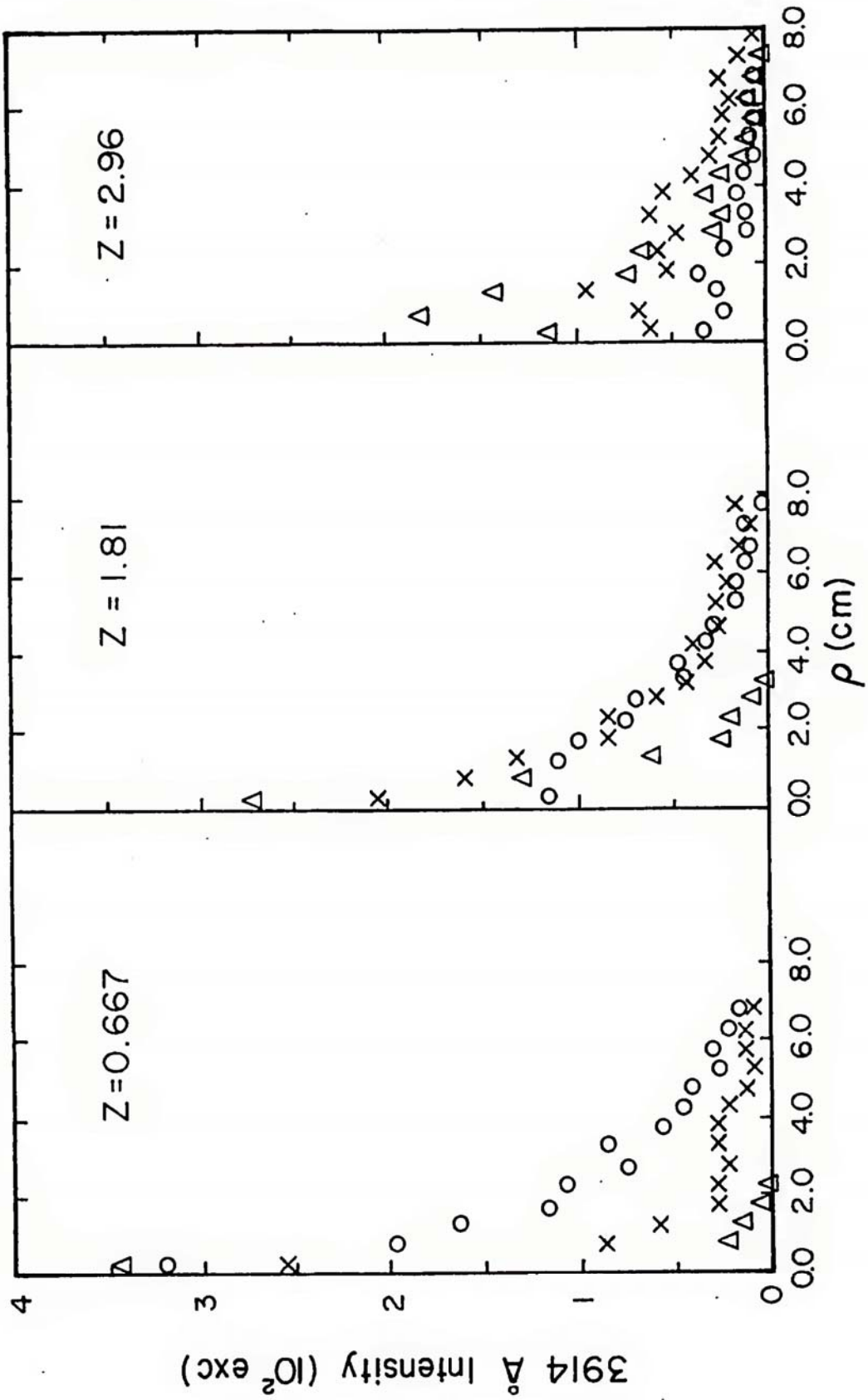
$$R_g(F_c) \approx R_{g0} \left( 1.0 + \frac{1}{\ln(F_c)} \right) \quad (6.4)$$

where  $R_g(F_c)$  is the range of the electrons using the screening parameter  $a(1000 \text{ eV}) = F_c a_0(1000 \text{ eV})$ . The  $F_c$  is some factor (in the case of trial C2,  $F_c = 0.1$ ) and  $R_{g0}$  is the range of the electron using the screening parameter  $a_0(1000 \text{ eV})$ . Again (see Eqs. (6.2) and (6.4)) there appears to be a logarithmic type dependence on the screening parameter. In section VII.C shapes of the collision profiles were found to be proportional to  $\ln(a)$ . Here, the range appears to be approximately proportional to  $\ln(a)$  for the three cases studied.

Next, use two more new trials, C4 and C5. The energy dependence of "a" in C1, C4, and C5 is the same and is illustrated in Figure 6.6. As seen from Table 6.4, the screening parameter for the incident energy has the most influence on the spatial energy deposition. The energy dependence of "a" influences the energy deposition such that if the parameter, a, is lower throughout the entire energy regime for a given trial than the "a" used in another trial (for example, C4 compared with C2), then the electrons will penetrate further during the course of that trial (the C4 range is greater than the C2 range).

The radial distribution of the 3914 Å intensity profile is another quantity of interest. Figure 6.7 illustrates this radial distribution for trials C1, C2, and C3 at three set distances into the medium. The sharpest forward peaked phase function (hereafter the last four words can be called FPPF) trial, C2, has an intensity distribution clustered close to the z-axis throughout the x regime. The least FPPF trial, C3, has

Figure 6.7 At three longitudinal distances (given in  $10^{-6}$  gm/cm<sup>2</sup>), the intensity distribution is given as a function of  $\rho$  for the three trials C1, x; C2,  $\Delta$ ; and C3, o.



its intensity distribution spread out the most from the z-axis throughout the z regime.

In Figure 6.8, a cut is taken through each intensity profile at the distance  $z = 0.3$  (units are fraction of range). This type of distribution continues for all the longitudinal distances throughout the range. The 3914 Å intensity profile of the sharpest FPPF, C2, again hugs the z-axis, whereas the profile of the least FPPF, C3, again shows the greatest spread from the z-axis.

#### E. Effects of the Total Elastic Cross Section on the Electron Energy Degradation

As illustrated in the previous sections of this chapter, the spatial electron energy degradation is governed mainly by the elastic differential cross section. Consider the effects of the total elastic cross section on the electron energy degradation.

The total elastic cross section given by Eq. (3.9) is used in practically all the MC calculations of this study. This analytic form agrees quite well with experiment.

Berger, Seltzer, and Maeda (1970, 1974) used the integrated Rutherford cross section for their total elastic cross section. This cross section is somewhat different from the experimental data and is plotted in Figure 3.2.

If a MC calculation is made with this lower elastic cross section, it is expected that the 1 KeV electrons will penetrate further into the medium. Figure 6.9 illustrates the results of this calculation where the screened Rutherford phase function was used.

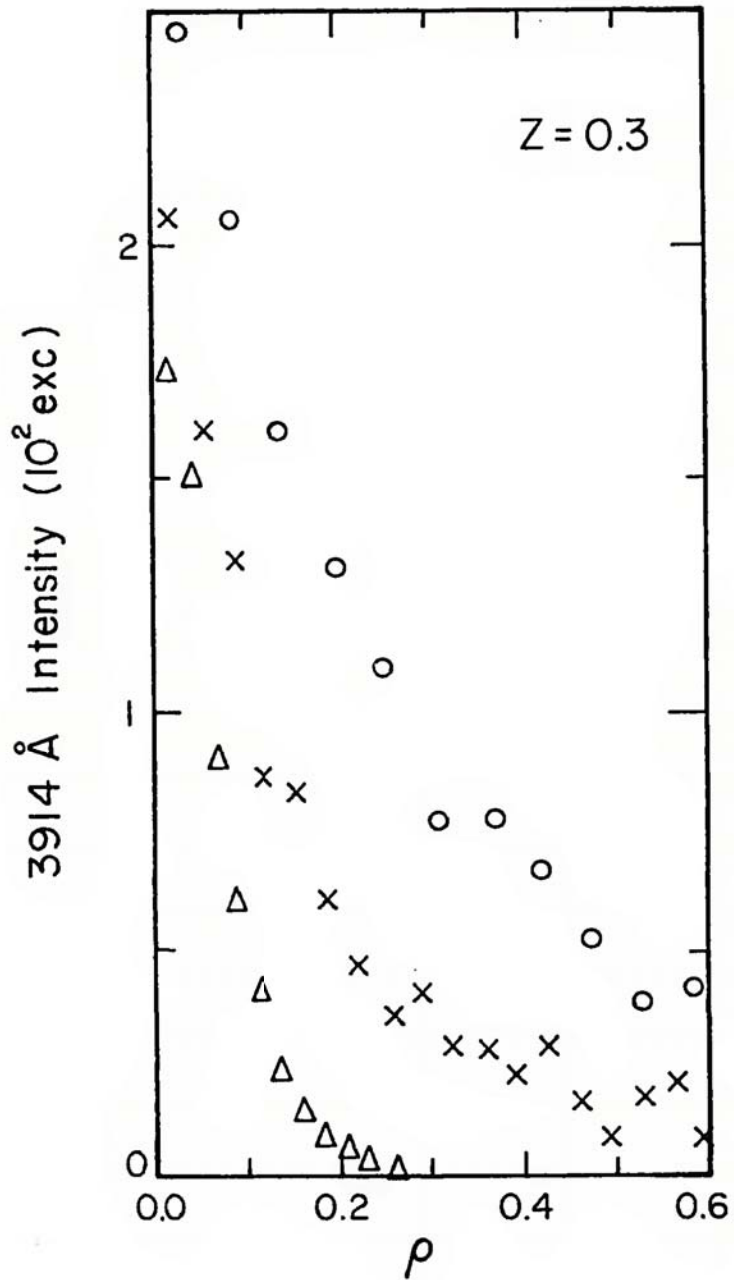


Figure 6.8 At the cut  $z = 0.3$ , the 3914 Å intensity distribution is given as a function of  $\rho$  for the three trials C1, x; C2,  $\Delta$ ; and C3, o.

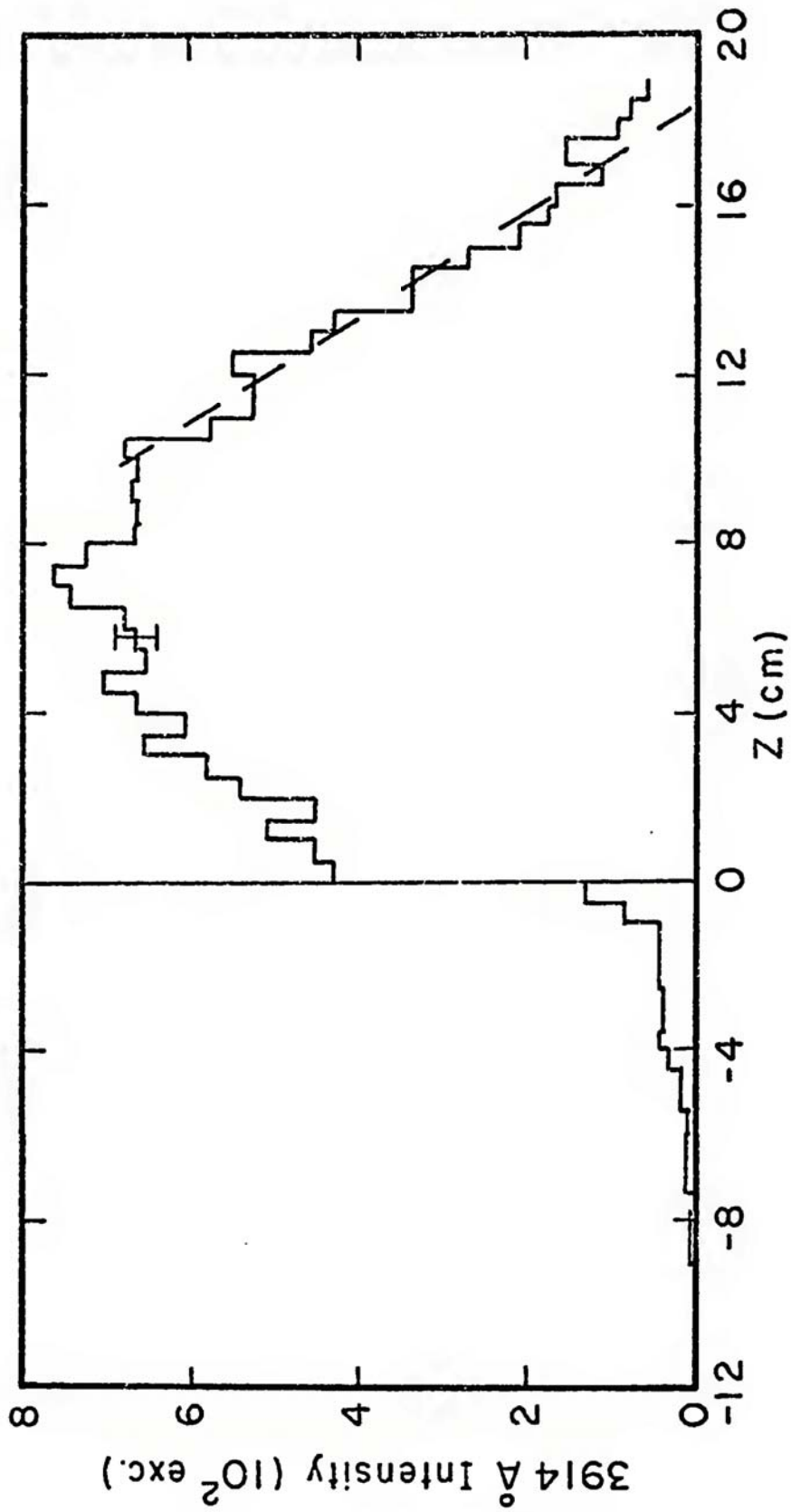


Figure 6.9 An intensity plot for electrons of energy 1 KeV is presented as a function of z. The differential and total screened Rutherford elastic cross section are used in this calculation. The range, found from the dashed line is 18.3 cm or  $6.98 \times 10^{-6}$  gm/cm<sup>2</sup>.

The range is observed to be  $6.98 \times 10^{-6} \text{ gm/cm}^2$  as compared with  $5.57 \times 10^{-6} \text{ gm/cm}^2$  using the cross sections given by Eq. (3.9) (hereafter called MSR). The shape of the intensity profile of the 3914 Å emission is also different. The maximum of the profile is less peaked than that given by MSR.

Banks, Chappell, and Nagy (1974) used cross section values which are shown in Figure 3.2. These cross section points are somewhat different than the cross sections from MSR in the range from 100 to 500 eV. This indicates that electrons degraded with these cross sections have a range less than that of MSR.

This section completes the sensitivity study. The next chapter discusses the MC calculation, the important yield spectra, and the general energy loss scheme.

CHAPTER VII  
MONTE CARLO ENERGY LOSS PLOTS AND YIELD SPECTRA

In this chapter two other very important energy degradation outputs are discussed. The rate of energy loss as the electron impinges into the medium is a very important quantity. This concept, the fraction of energy backscattered, and the correlation between the range and the loss function are discussed in section VII.A.

The most important output from the MC calculation is the spatial yield spectrum. In section VII.B, this yield spectrum is calculated at several energies and at several positions in the gas. Both the three variable spatial yield spectrum  $U(E,z,E_0)$  and the four variable spatial yield spectrum  $U(E,\rho,z,E_0)$  are considered in this section. Because the yield or number of excitations to any  $N_2$  state is calculated quite easily from the spatial yield spectrum, an attempt is made to represent it analytically.

A. Energy Loss of Electrons in  $N_2$

The rate of energy loss by electrons in a medium is a useful quantity. For higher energy electrons (above 2 KeV), the degradation of these electrons could be accomplished with the use of the loss function,  $L(E)$ , and the continuous slowing down approximation (discussed in Chapter II).

This is one important reason why the range values of the electrons are under investigation. Assuming a continuous slowing down of the electron, the range  $R(E_0)$  for an electron of incident energy  $E_0$  may be defined as

$$R(E_0) = \int_{E_0}^0 \frac{dE}{dE/dx} \quad (7.1)$$

(employing Eq. (2.2)). Since  $nL(E) = -\frac{dE}{dx}$  (as noted in Chapter II), then

$$R(E_0) = \frac{1}{n} \int_0^{E_0} \frac{dE}{L(E)} \quad (7.2)$$

In the Born-Bethe approximation  $L(E)$  is proportional to  $\ln E/E$ . At the higher energies,  $\ln E/E$  can approximately be written as  $E^{-.75}$  (see Green and Peterson, 1968). Using this approximation in Eq. (7.2), the range is

$$R(E_0) = C E_0^{1.75} \quad (7.3)$$

where  $C$  is a constant.

Grün (1957) and Cohn and Caledonia (1970) have shown that such an expression is correct for electron energies from 2 to 54 KeV. Barrett and Hays (1976), on the other hand, extended this energy range down to 0.3 KeV and derived a slightly more complicated empirical formula for the electron energies from 0.3 to 5 KeV.

Much of the significance of the range is built on the idea that all the energy of the electrons is lost between  $z = 0.0$  and  $z = 1.0$  where  $z =$  the fraction of the range traveled. Such an approximation is quite good above 2 KeV; however, at energies below 1 KeV this is not such a good approximation.

In Figure 7.1 an energy remaining plot is given for three separate calculations with 1 KeV incident electrons. At  $z = 0.0$ , which is the point of incidence for the 1 KeV electrons, all calculations assume that no energy has been lost. Thus the amount of "energy left" is simply 1 KeV.

Stolarski (1968) integrated the universal energy loss curve derived from Grün's (1957) data to obtain the mean energy. Barrett and Hays (1976) used their empirical range formula to calculate the mean range and, subsequently, the energy remaining in the incident electron at various distances into the medium. In the MC calculation of this study only the energy lost for positive  $z$  values was employed to find the energy remaining.

The Stolarski (1968) values are closest to the MC calculation values. The major differences between Stolarski's results and this MC computation are due to three factors: First, some energy is lost by backscatter electrons to negative  $z$  values; second, some energy is lost by electrons which penetrate to  $z$  values greater than 1.0 (straggling electrons); and third, the universal energy loss curve may not be as accurate as a MC computation.

Graphing the energy loss data in Figure 7.1 is really not very informative. Figure 7.2 illustrates a more lucid way of representing the energy loss data. In Figure 7.2, the fraction of the primary energy lost is plotted as a function of  $z$  for four energies (0.1, 0.3, 1.0, and 5.0 KeV). As the incident electron's energy is reduced, the relative backscatter is increased. The most backscatter (21%) and the most energy lost in straggling (6%) is observed for the 0.1 KeV electrons.

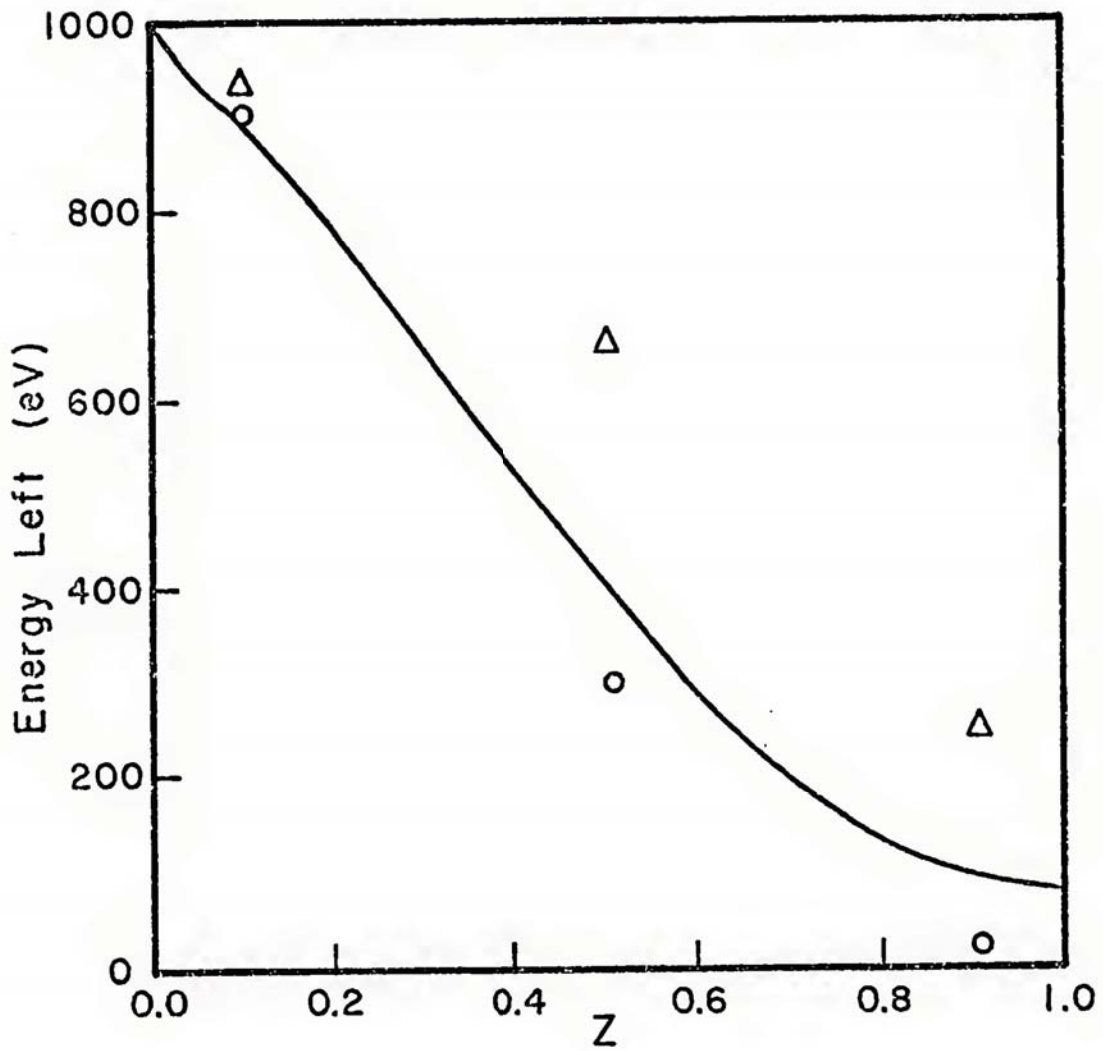


Figure 7.1 Energy remaining plot for electrons with energies incident at 1 KeV. The  $\Delta$ 's give the calculation of Barrett and Hays (1976), the o's give the values from Stolarski (1968), and the solid line gives the average energy left at various z values from this MC work.

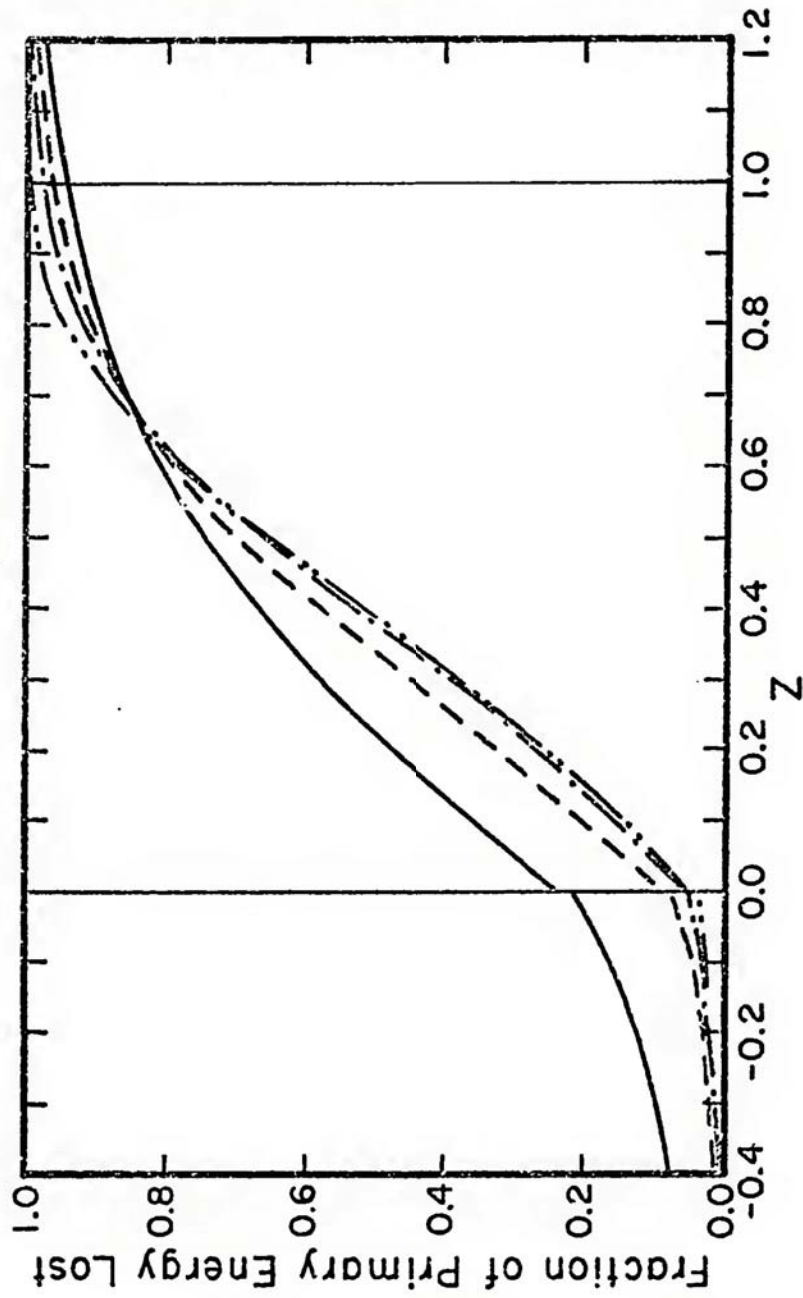


Figure 7.2 Energy loss plot for four incident electron energies: 100 eV, solid line; 300 eV, dashed line; 1000 eV, dash-dot line; and 5000 eV, dash-dot-dot line.

The fraction of energy backscattered is also of interest. The backscattering of electrons from the ionosphere has been observed in rocket experiments by McDiarmid, Rose, and Budzinski (1961) and in the Injun III satellite experiments of O'Brien (1964). Berger, Seltzer, and Maeda (1974) [BSM] have calculated backscattering coefficients for mono-energetic electrons incident on a semi-infinite air medium at energies from  $10^4$  KeV down to 2 KeV.

One quantity calculated by BSM is  $R_E$ , the energy albedo (computed by summing the energy backscattered). Since the incident energy range used in this work overlaps the incident energy range used by BSM from 2 to 5 KeV, a comparison of the  $R_E$ 's from both calculations is of interest.

Table 7.1 presents the results from the model 3 (hereafter called M3) and the screened Rutherford (hereafter called SR) phase functions and the work of BSM. The M3 energy albedos are lower than those energy albedos resulting from the SR and the BSM calculations (at least where there are values available) down to the energy of 0.1 KeV. At this energy the M3 phase function reveals a fairly substantial backscatter with approximately one-fifth of the incident energy lost in backscatter.

Although little consideration is given to the backscattered electrons in this study, there is much information that can be derived from studying these backscattered particles in detail. This detailed spatial MC technique would be an appropriate method of studying these backscattered particles.

#### B. Spatial Yield Spectra for Electrons Impinging on $N_2$

The yield spectrum for an electron energy degradation process contains all the information necessary for computing excitations from that

Table 7.1 Energy albedos presented at five energies  $E_0$  with the use of the model 3 (column labeled M3) and the screened Rutherford (column labeled SR) phase functions and the work of BSM.

$E_0$ (KeV)	M3	SR	BSM
0.1	0.210	0.188	--
0.3	0.072	0.105	--
1.0	0.051	0.078	--
2.0	0.041	0.068	0.062
5.0	0.039	0.045	0.052

calculation. Green, Jackman, and Garvey (1977) [hereafter called GJG] have discussed the use of the yield spectrum  $U(E, E_0)$ , which was described in Chapter II of this work. This yield spectrum can be used to calculate the yield of any state by means of the equation

$$J_j(E_0) = \int_{W_j}^{E_0} U(E, E_0) p_j(E) dE \quad (7.4)$$

where  $p_j(E) = \sigma_j(E)/\sigma_{TI}(E)$  is the probability for excitation of the  $j$ th state with excitation energy  $W_j$ .

In these MC calculations information about the yield spectrum can be attained at any longitudinal and radial distance. The three variable yield spectrum  $U(E, z, E_0)$ , which is a function of the longitudinal distance  $z$ , as well as the incident electron energy  $E_0$  and the energy  $E$ , is considered in subsection VII.B.1. The four variable yield spectrum  $U(E, \rho, z, E_0)$ , which is also a function of the radial distance  $\rho$ , is then considered in subsection VII.B.2.

### 1. Three Variable Spatial Yield Spectra

The three variable spatial yield spectrum  $U(E, z, E_0)$  is found in the following manner. A MC calculation takes place for a certain incident energy  $E_0$  which places all the collisions with their characteristics on a magnetic tape. The longitudinal- or  $z$ -axis is divided up into several equal intervals of  $\Delta z_{Int}$  gm/cm<sup>2</sup> each and the energy regime from 2 eV up to the incident energy  $E_0$  is divided up into several intervals of  $\Delta E_{Int}$  eV each (not all intervals being equivalent in energy).

If the spatial yield spectrum  $U(E_E, z_E, E_0)$  for a certain energy value  $E_E$  and longitudinal distance  $z_E$  is desired, then the two-dimensional

rectangle with longitudinal endpoint coordinates  $z_E - \Delta z_{Int}/2$  and  $z_E + \Delta z_{Int}/2$  and energy width endpoint coordinates  $E_E - \Delta E_{Int}/2$  and  $E_E + \Delta E_{Int}/2$  is established. If the longitudinal distance to any inelastic collision (elastic collisions are excluded because of the real lack of interest in their spatial properties and also because they are not well defined at electron energies below 30 eV),  $z_c$ , is between  $z_E - \Delta z_{Int}/2$  and  $z_E + \Delta z_{Int}/2$  and the energy of the electron before the collision,  $E_{bc}$ , is between  $E_E - \Delta E_{Int}/2$  and  $E_E + \Delta E_{Int}/2$  then the number of electrons in that rectangle,  $N(E_E, z_E)$ , is incremented by one. This process continues until all the collisions are accounted for.

The spatial yield spectrum [in  $\#/eV/(gm/cm^2)$ ] is then written as

$$U(E_E, z_E, E_0) = \frac{N(E_E, z_E)}{\Delta E_{Int} \Delta z_{Int}} \quad (7.5)$$

(This spatial yield spectrum is also normalized to one electron.) This process then continues for each two-dimensional rectangle across the entire plane of interest. As an example, the  $U(E, z, E_0)$  for three longitudinal distances is given in Figure 7.3 for the incident energy of 1 KeV.

This  $U(E, z, E_0)$  [as observed in Figure 7.3], although more complex than the  $U(E, E_0)$  of GJG, has some nice general characteristics that continue throughout the entire incident energy range (from 0.1 KeV up to 5 KeV). It is, therefore, reasonable to continue the philosophy of analytic representation (see Green and Barth, 1965; Green and Dutta, 1967; Stolarski and Green, 1967; and GJG). The analytic properties of  $U(E, z, E_0)$  will permit researchers to infer important spatially derived properties of  $N_2$  with a degree of accuracy which should suffice for many atmospheric applications.

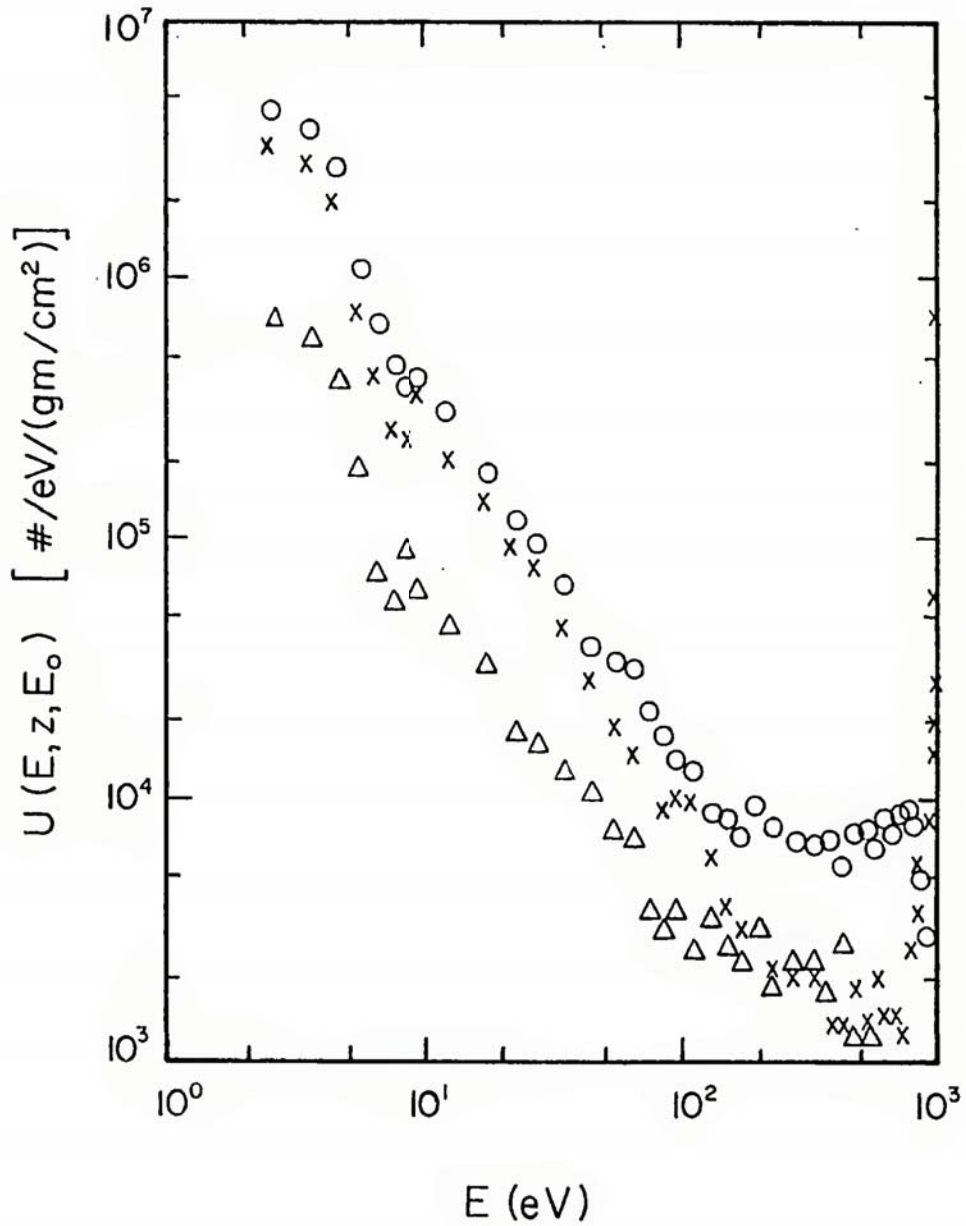


Figure 7.3 Three variable spatial yield spectrum for an incident energy of 1 KeV given at three longitudinal distances (in fractions of the range):  $z = 0.0739$  represented by x,  $z = 0.429$  represented by o, and  $z = 0.96$  represented by Δ.

It should be noted that at the small longitudinal distances a fairly large "source" term persists at energies  $E = E_0$ . In the interval from about 4 eV to about 10 eV there is a noticeable dip in the yield spectra. In this range (see Figure 3.6), the total inelastic cross sections show a very large dip, thus many of the electrons in this range do not interact inelastically with the  $N_2$  gas in the region of interest.

For the purposes of many applications it is useful to represent the yield spectra by

$$U(E, z, E_0) = U_a(E, z, E_0) \theta(E_0 - E - E_\theta) + \delta(E_0 - E) D(z, E_0) \quad (7.6)$$

(following the notation of GJG), where  $\theta$  is the Heaviside function with  $E_\theta$ , the minimum threshold of the states considered, and  $\delta(E_0 - E)$  is the Dirac delta function which allows for the contribution of the source itself. The  $U_a(E, z, E_0)$  is represented approximately by

$$U_a(E, z, E_0) = A(z, E_0) + B_1(z, E_0)[E_R]^{B_2} + C_1(z, E_0)[E_R]^{C_2} \quad (7.7)$$

and

$$A(z, E_0) = \frac{a_1(E_0)}{[z_R - a_2(E_0)]^2 + a_3(E_0)}$$

$$B_1(z, E_0) = \frac{b_{11}(z, E_0)}{[z_R - b_{12}(E_0)]^2 + b_{13}}$$

$$C_1(z, E_0) = \frac{c_{11}(z, E_0)}{e^{z_R/c_{12}} + 1}$$

$$D(z, E_0) = \frac{d_1(E_0)}{e^{z_R/d_2} + 1}$$

$$a_1(E_0) = a_{11} \xi_0^{a_{12}}$$

$$a_2(E_0) = a_{21} \left(1 - \frac{a_{22}}{\xi_0}\right)$$

$$a_3(E_0) = a_{31} + \frac{a_{32}}{\xi_0}$$

$$b_{11}(z, E_0) = \frac{b_{111} \xi_0^{b_{112}} \left[1 + \frac{(1 - \xi_0)}{b_{113}}\right]}{[\exp\{(z_R - f_1(E_0))/f_2(E_0)\} + 1]}$$

$$b_{12}(E_0) = b_{121} \left(1 - \frac{b_{122}}{\xi_0}\right)$$

$$c_{11}(z, E_0) = c_{111} \xi_0^{c_{112}} / [\exp\{(z_R - f_1(E_0))/f_2(E_0)\} + 1]$$

$$d_1(E_0) = d_{11} \xi_0^{d_{12}}$$

$$f_1(E_0) = f_{11} \left(1 + \frac{f_{12}}{\xi_0}\right)$$

$$f_2(E_0) = f_{21} \xi_0^{f_{22}}$$

$$R_g(E_0) = r_1 + r_2 \xi_0^{r_3} = \text{Range of an electron of primary energy } E_0$$

where the parameters and their values are all given in Table 7.2. Also,  $\xi_0 = E_0/1000$ ,  $E_R = E/E_0$ , and  $z_R = z/R_g(E_0)$ .

Table 7.2 Parameters and their values are given below which are to be used in Eq. (7.7) for the molecular nitrogen spatial yield spectrum.

Parameter	Value	Parameter	Value
$a_{11}$	587	$d_{11}$	$0.6 \times 10^5$
$a_{12}$	-1.63	$d_{12}$	-1.68
$a_{21}$	0.4	$d_2$	0.2
$a_{22}$	0.075	$f_{11}$	0.9
$a_{31}$	0.1	$f_{12}$	0.044
$a_{32}$	0.019	$f_{21}$	0.104
$b_{111}$	81	$f_{22}$	-0.39
$b_{112}$	-1.8	$g_{11}$	0.85
$b_{113}$	8.0	$g_{12}$	0.07
$b_{121}$	0.4	$g_2$	0.2
$b_{122}$	0.05	$r_1$	$2.27 \times 10^{-7} \text{ gm/cm}^2$
$b_{13}$	0.2	$r_2$	$6.22 \times 10^{-6} \text{ gm/cm}^2$
$B_2$	-1.52	$r_3$	1.67
$c_{111}$	$1.30 \times 10^4$		
$c_{112}$	-1.5		
$c_{12}$	0.15		
$c_2$	10		

The yield of any state is then found from

$$J_j(z, E_0) = \int_{z - \frac{\Delta z}{2}}^{z + \frac{\Delta z}{2}} \int_{W_j}^{E_{ui}} U(E, z, E_0) dE dz \quad (7.8)$$

where

$$E_{ui} = \frac{E_0}{[e^{\{z_R - g_1(E_0)\}} / g_2 + 1]}$$

and

$$g_1(E_0) = \frac{g_{11}}{(1 + \frac{g_{12}}{\epsilon_0})}$$

The upper limit of integration in Eq. (7.8) is not  $E_0$  but is  $E_{ui}$ . As the electrons penetrate further and further into the medium, they lose more and more of the high energy particles. The energy  $E_{ui}$  is thus a cutoff energy which must be invoked.

Equation (7.6) represents the yield spectra data fairly well in this regime of incident electron energies. The fit can be seen in Figure 7.4 for five incident energies at five longitudinal values.

A comparison is given in Table 7.3 between the yield using Eq. (7.8) and the yield using the MC calculation for several incident energies and longitudinal values for the yield of the 3914 Å emission. The two calculations are in fair agreement throughout the entire range considered. It should be noted, however, that Eq. (7.8) is not accurate at longitudinal values in the backscatter direction.

Maeda and Aikin (1968) attempted to apply an analytic degradation spectrum to problems of the atmosphere. They calculated the number of oxygen atoms resulting from the dissociation of  $O_2$  from auroral events.

Figure 7.4 The three variable spatial yield spectrum  $U(E,z,E_0)$  is plotted as function of  $E_R$ . The MC calculations are represented by symbols for each  $z$  (in fractions of the range) and  $E_0$  (in KeV):  $\circ$ ,  $z = 0.126$ ,  $E_0 = 0.1$ ;  $\Delta$ ,  $z = 0.316$ ,  $E_0 = 0.3$ ;  $\times$ ,  $z = 0.606$ ,  $E_0 = 1.0$ ;  $\nabla$ ,  $z = 0.928$ ,  $E_0 = 2.0$ ; and  $\square$ ,  $z = 1.052$ ,  $E_0 = 5.0$ . The analytic fit using Eq. (7.6) is represented by the solid line with the source term contribution represented by  $\otimes$ .

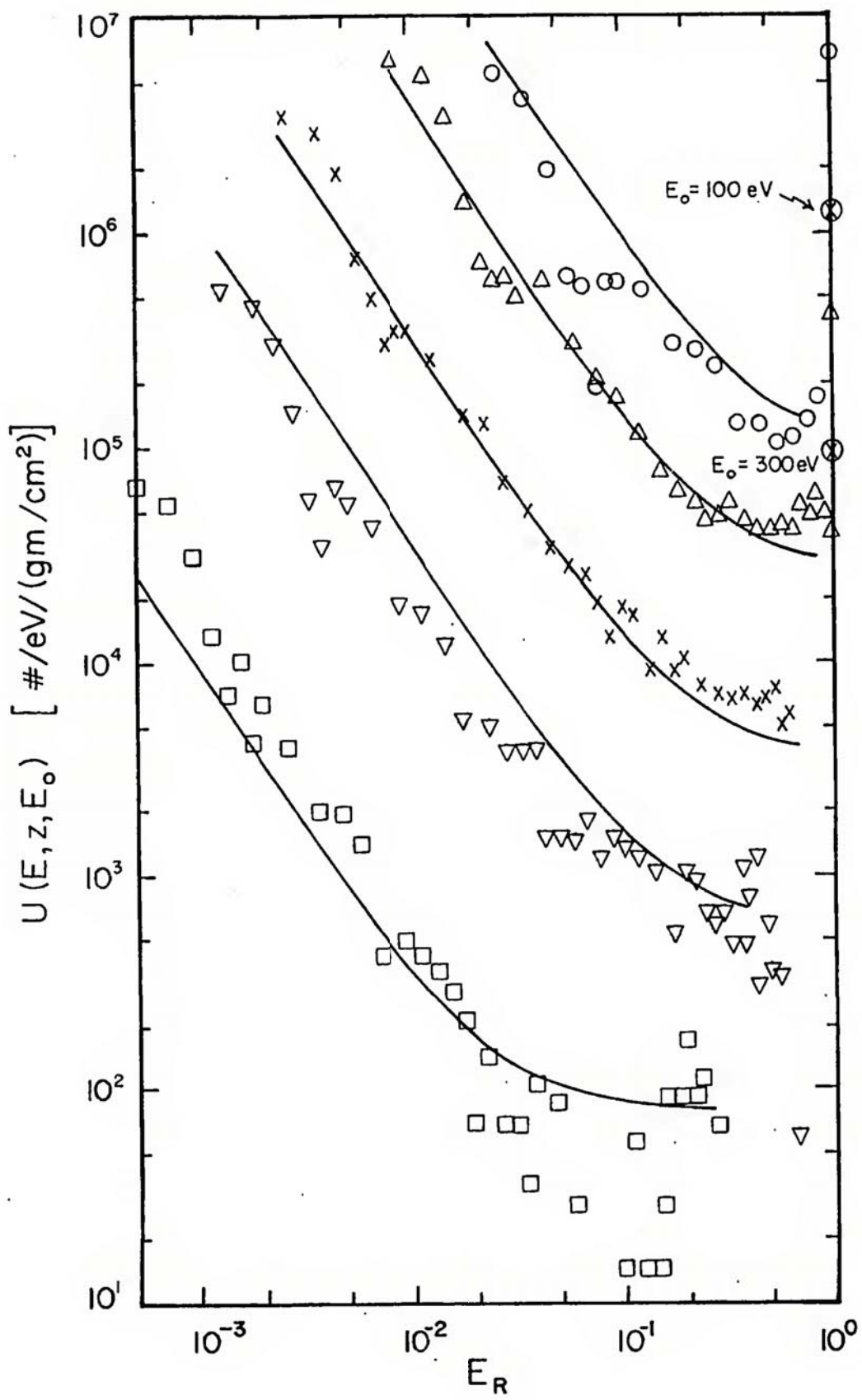


Table 7.3 Comparison between the yield of the 3914 Å emission [#/(.5 cm)] from the MC calculation [column labeled MC] and with the use of Eq. (7.6) in Eq. (7.8) [column labeled AF] for several incident energies [column labeled  $E_0$  (in KeV)] and longitudinal distances [column labeled  $z$  (in fractions of the range)].

$E_0$	$z$	MC	AF
0.1	0.01	280	287
0.1	0.2	240	272
0.1	0.5	155	168
0.1	0.8	70.0	82.3
0.1	1.0	35.2	49.7
0.3	0.01	452	406
0.3	0.2	626	523
0.3	0.5	490	429
0.3	0.8	174	177
0.3	1.0	74.2	73.2
1.0	0.01	550	556
1.0	0.2	740	797
1.0	0.4	860	908
1.0	0.7	500	456
1.0	1.0	100	91.9
2.0	0.01	600	578
2.0	0.2	780	841
2.0	0.4	1050	995
2.0	0.7	600	517
2.0	1.0	130	85.5
5.0	0.01	1300	1323
5.0	0.2	1760	1927
5.0	0.4	2100	2337
5.0	0.7	1380	1214
5.0	1.0	200	160

This yield of 0 atoms was then used to predict the variation of polar mesospheric oxygen and ozone during auroral events.

Shemansky, Donahue, and Zipf (1972), however, showed that Maeda's spectra are deficient in low-energy degraded primary electrons. This conclusion was also supported by BSM.

The spatial yield spectrum calculated with the use of this MC approach should be quite accurate statistically from 2 eV up to the incident energy  $E_0$ . There may be some errors inherent in the assumptions and approximations used in these MC calculations however. The analytic spatial yield spectrum given by Eq. (7.6) does represent fairly well the actual spatial yield spectrum. Thus the analytic spatial yield spectrum can be applied to some of the problems in aeronomy involving impinging electrons into the atmosphere.

Consider now the use of Eq. (7.6) with an incident electron energy flux of  $\phi(E_0)$  [in units of  $\#/cm^2/sec/eV$ ]. A yield  $J_j[z, \phi(E_0)]$  in units of  $\#/cm^3/sec$  can be calculated using

$$J_j[z, \phi(E_0)] = \int_{W_j}^{\infty} \int_{W_j}^{E_{uj}} \phi(E_0) U(E, z, E_0) \rho(z) dE dE_0 \quad (7.9)$$

where  $\rho(z)$  is the density (in  $gm/cm^3$ ) of the air at altitude  $z$ . Equation (7.9) is not applied by the author to any given flux  $\phi(E_0)$  in this work. Future studies can make use of Eq. (7.9) in applications to aurorae and their effects on the atmosphere.

The spatial yield spectrum for  $N_2$  can be used fairly accurately for problems dealing with the atmosphere in spite of the fact that the atmosphere is not entirely molecular nitrogen. In Green, Jackman, and Garvey (1977) the two variable yield spectrum  $U(E, E_0)$  was observed to be

quite similar in all the gases considered. Thus it is expected that the spatial yield spectrum  $U(E,z,E_0)$  will also be similar for electron energy degradation into the other atmospheric gases.

## 2. Four Variable Spatial Yield Spectra

The last subsection (VII.B.1) was only concerned with the spatial yield spectra in the longitudinal direction. This subsection deals with the four variable spatial yield spectra  $U(E,\rho,z,E_0)$  which is also a function of the radial direction  $\rho$ .

The MC calculation appropriately accounts for the coordinate  $\rho$  down to the energy of 30 eV, below which the multiple elastic scattering distribution is used. In subsection IV.C.6 an approximation was made which assumed that  $\rho$  was about one-sixth of the total path length. A better approximation would be to simply assume that the  $\rho$  distribution for  $N_2$  is similar to that of  $H_2$ .

With this assumption and inverting Eq. (8) from Kutcher and Green (1976), the expression for  $\rho$  is

$$\rho = [-\ln(1 - R)/\delta]^{1/\gamma} \quad (7.10)$$

where

$$\delta = \frac{(22 + (\frac{s}{0.3})^{1/2})}{(s + 0.3)^{1.5}}$$

$$\gamma = 2[1 - \exp(-\frac{s}{4})]$$

and  $R$  = a random number. The parameters are found by averaging those parameters in Table I of Kutcher and Green (1976).

Use of Eq. (7.10) in the MC computations resulted in the spatial yield spectra  $U(E,\rho,z,E_0)$  which is fairly accurate down to 2 eV.

The  $U(E, \rho, z, E_0)$  was computed in a manner similar to the way that  $U(E, z, E_0)$  was computed. In subsection VII.B.1 a rectangle  $\Delta E_{Int}$  by  $\Delta z_{Int}$  was taken as the area of interest. Here, a volume  $\Delta z_{Int}$  by  $\Delta E_{Int}$  by  $\Delta P_{Area}$  is used. The  $\Delta P_{Area}$  is in units of area  $[(gm/cm^2)^2]$  and is defined as

$$P_{Area} = \pi \left[ \left( \rho + \frac{\Delta \rho_{Int}}{2} \right)^2 - \left( \rho - \frac{\Delta \rho_{Int}}{2} \right)^2 \right]$$

where  $\rho$  is the mid-point of the area of interest and  $\Delta \rho_{Int}$  is the radial interval of interest.

If the spatial yield spectrum  $U(E_E, \rho_E, z_E, E_0)$  at a certain energy value  $E_E$ , longitudinal distance  $z_E$ , and radial distance  $\rho_E$  for an electron of incident energy  $E_0$  is desired, then the volume with energy width endpoint coordinates  $E_E - (\Delta E_{Int}/2)$  and  $E_E + (\Delta E_{Int}/2)$ , longitudinal endpoint coordinates  $z_E - (\Delta z_{Int}/2)$  and  $z_E + (\Delta z_{Int}/2)$ , and radial endpoint coordinates  $\rho_E - (\Delta \rho_{Int}/2)$  and  $\rho_E + (\Delta \rho_{Int}/2)$  is established. If the longitudinal distance,  $z_C$ , is between  $z_E - (\Delta z_{Int}/2)$  and  $z_E + (\Delta z_{Int}/2)$  the radial distance,  $\rho_C$ , is between  $\rho_E - (\Delta \rho_{Int}/2)$  and  $\rho_E + (\Delta \rho_{Int}/2)$ , and the energy before the collision,  $E_{bc}$ , is between  $E_E - (\Delta E_{Int}/2)$  and  $E_E + (\Delta E_{Int}/2)$ , for an inelastic collision; then the number of electrons in that volume,  $N(E_E, \rho_E, z_E)$  is incremented by one.

The spatial yield spectrum [in  $\#/eV/(gm/cm^2)^3$ ] is then written as

$$U(E_E, \rho_E, z_E, E_0) = \frac{N(E_E, \rho_E, z_E)}{\Delta E_{Int} \Delta P_{Area} \Delta z_{Int}} \quad (7.11)$$

This process then continues for each small volume across the entire volume of interest. Again, it should be recognized that this yield spectrum is normalized to one electron.

The four variable spatial yield spectrum is presented in Figure 7.5 (a, b, c, and d) for an incident electron energy of 1 KeV. It is given at four radial distances at each longitudinal cut (all in units of fractions of the range). The  $U(E, \rho, z, E_0)$  from other incident electron energies are not presented here but show a similar type of behavior.

The shape of  $U(E, \rho, z, E_0)$  is observed to be quite similar to  $U(E, z, E_0)$  [see Figure 7.3] and, indeed even to  $U(E, E_0)$  [see Green, Jackman, and Garvey, 1977, Figure 1e]. The lower energy power fall-off is  $\propto E_R^{-1.52}$  in all three yield spectra. All three spectra also exhibit a constant component in the middle energies with the source term feature at the incident energy ( $E_R = 1.0$ ).

The four variable and three variable spatial yield spectra illustrate an increasing tendency at higher values of energy ( $E_R \approx 0.9 \rightarrow 1.0$ ) and at the lower values of  $z$  and  $\rho$ . This feature is not as prominent in the non-spatial yield spectrum  $U(E, E_0)$ , which is calculated by integrating over the spatial component of the spatial yield spectra. In the integration process the higher energy spectra increase is averaged out by the equally important higher energy spectra decrease exhibited at the higher values of  $z$  and  $\rho$ .

Knowledge of  $U(E, \rho, z, E_0)$  implies more detailed information about the entire spatial degradation process. Once the  $U(E, \rho, z, E_0)$  is known then the number of excitations  $J_j(\rho_{1 \rightarrow 2}, z)$  of the  $j$ th state can be found. This  $J_j(\rho_{1 \rightarrow 2}, z)$  is a result of an incident electron flux  $\phi(E_0)$  and is the number of excitations at altitude  $z$  in the ring between  $\rho_1$  and  $\rho_2$ . Thus

$$J_j(\rho_{1 \rightarrow 2}, z) = \pi(\rho_2^2 - \rho_1^2) \int_{W_j}^{\infty} \int_{W_j}^{E_0} \phi(E_0) U(E, \rho, z, E_0) \rho(z) dE dE_0 \quad (7.12)$$

Figure 7.5 (a, b, c, and d) Four variable spatial yield spectra for an incident electron energy of 1 KeV given at four longitudinal distances:  $z = 0.061$  (Figure 7.5a),  $z = 0.305$  (Figure 7.5b),  $z = 0.549$  (Figure 7.5c), and  $z = 0.793$  (Figure 7.5d). At each longitudinal cut the yield spectrum is given at four radial distances:  $\rho = 0.061$ ,  $\circ$ ;  $\rho = 0.305$ ,  $\bullet$ ;  $\rho = 0.549$ ,  $\blacksquare$ ; and  $\rho = 0.793$ ,  $\blacktriangle$ .

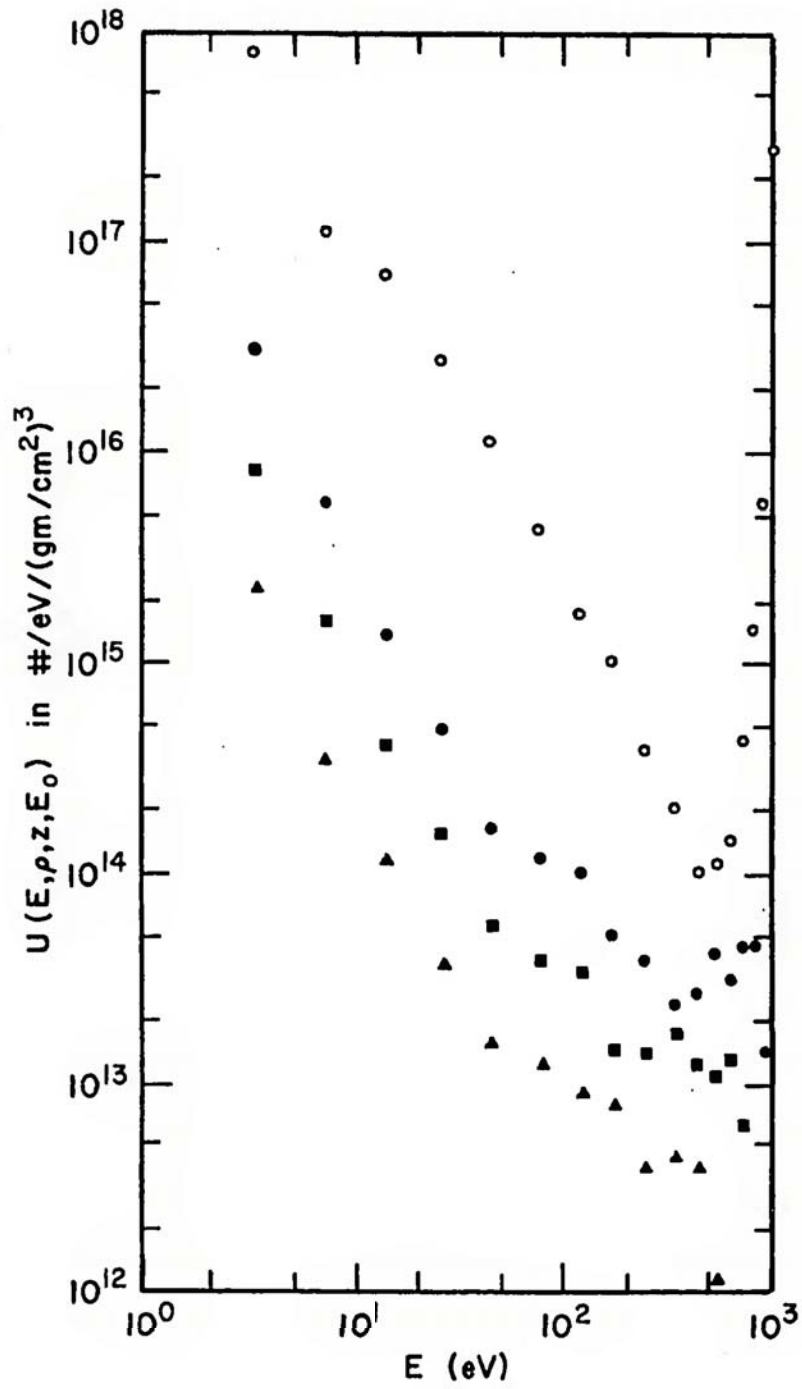


Figure 7.5a

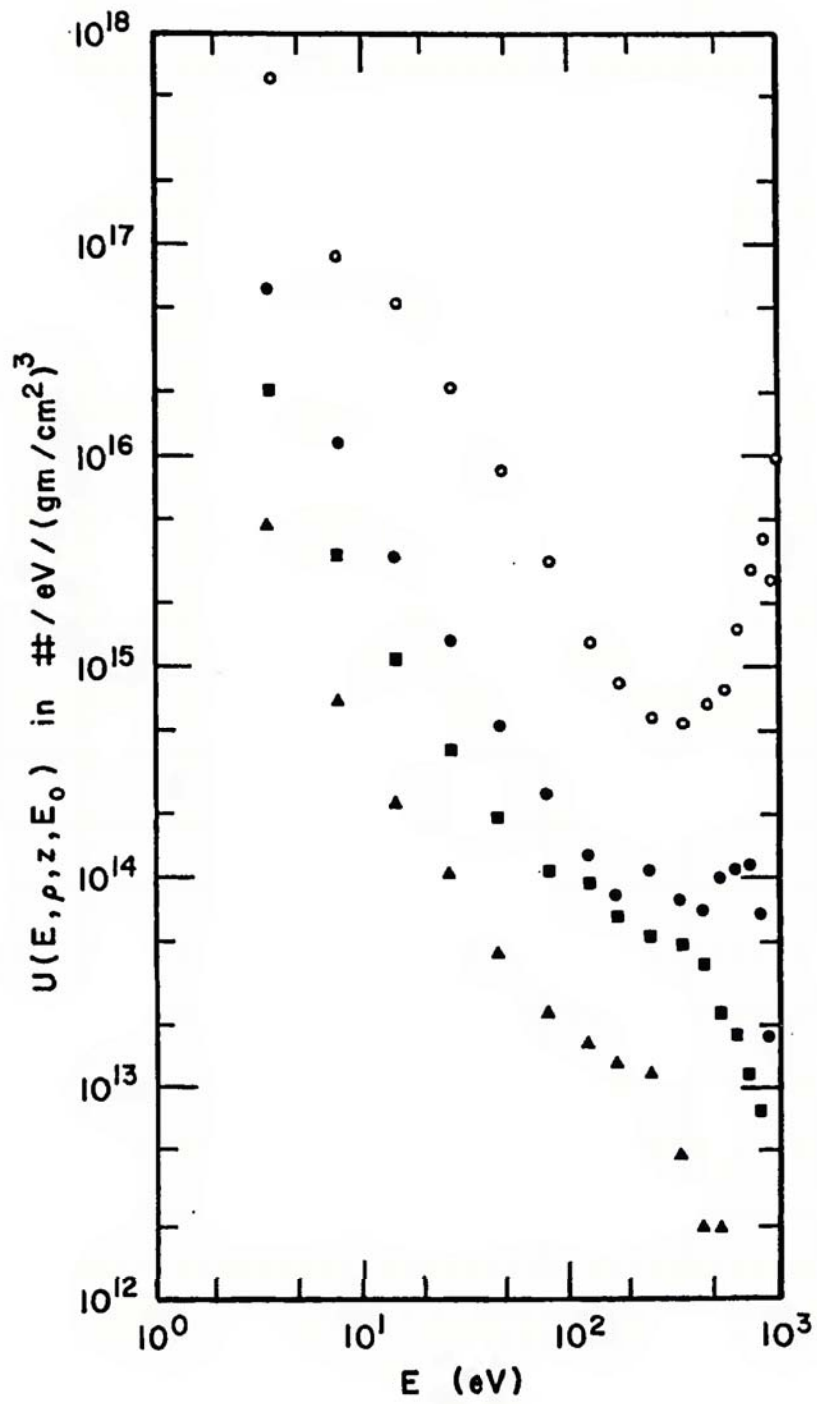


Figure 7.5b

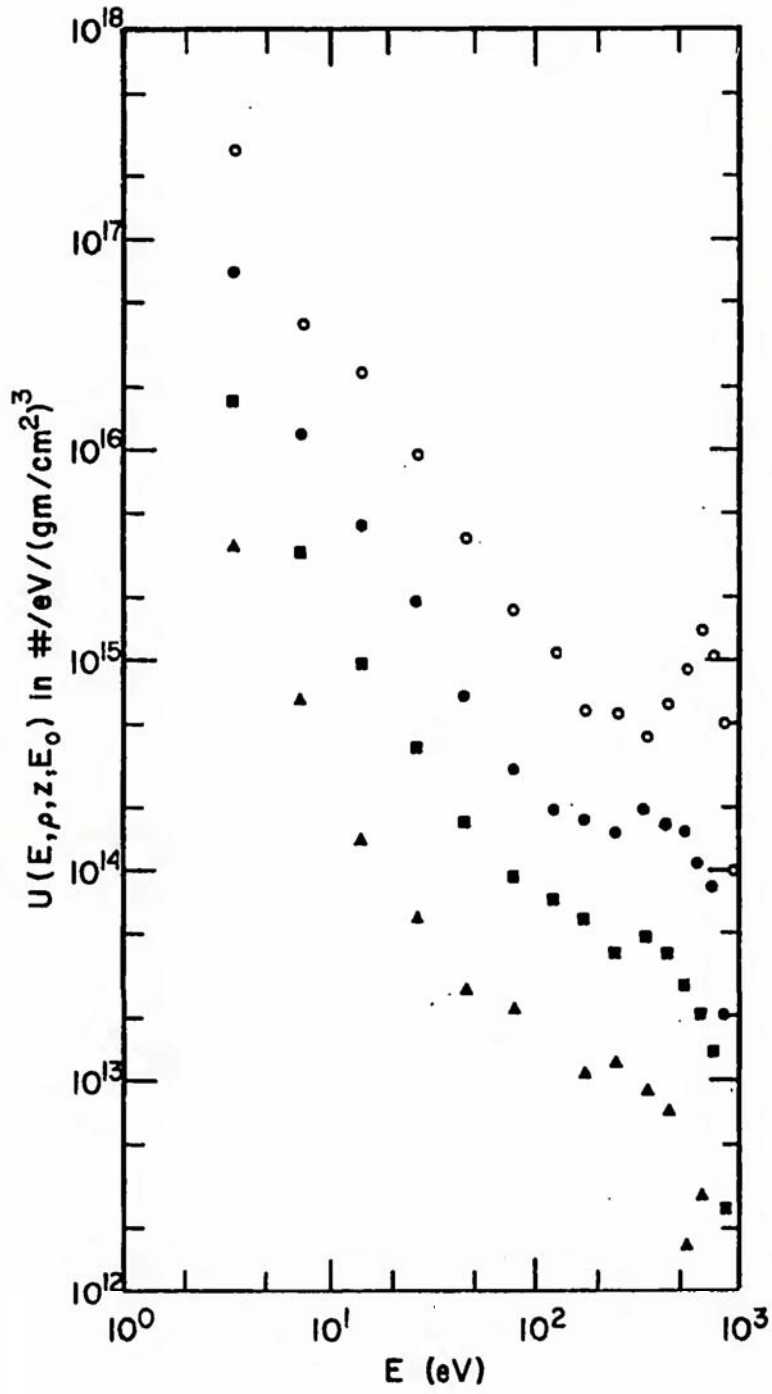


Figure 7.5c

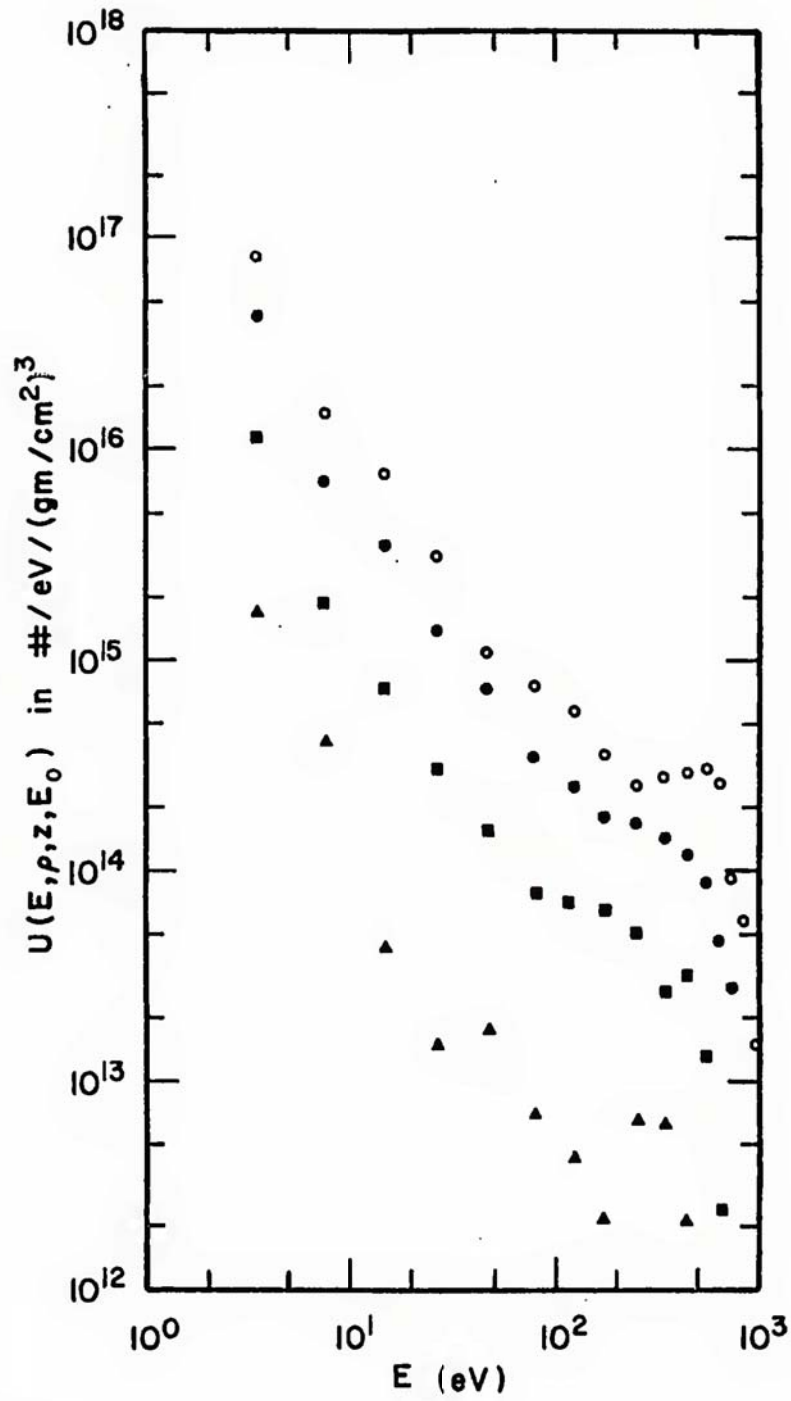


Figure 7.5d

No analytic expression has been derived for  $U(E, \rho, z, E_0)$ ; however, it does have systematics that tend to point toward some type of representation which would be useful for atmospheric scientists.

This concludes the discussion about the results from the MC calculation. The most important output from the MC computations is the spatial yield spectra because many of the other results given in Chapters V, VI, and VII can be derived easily from this spatial quantity.

## CHAPTER VIII

### CONCLUSIONS

There are several different theoretical approaches now being employed to study the auroral electron energy deposition problem. Researchers using these methods have concentrated for the most part on the details of the computation and on the input atmospheric parameters.

One of the concerns of this work was the cross sections, both differential and total, and their impact on the spatial and energetic aspects of the electron energy deposition. This research has shown that the input cross sections have a very large influence on the resulting electron energy deposition.

Perpendicularly incident electrons with energies from 0.1 through 5.0 KeV were degraded in molecular nitrogen using a Monte Carlo spatial energy deposition technique. This degradation method followed each electron, its secondaries, and its tertiaries in a collision by collision manner down to 30 eV. Below 30 eV, a multiple elastic scattering distribution was used to describe the energy deposition process down to the cutoff energy of 2 eV.

This Monte Carlo calculation employed new phenomenological differential elastic and doubly differential ionization cross sections which agree quite well with experimental data. Other cross sections previously developed for  $N_2$  were also used in these computations.

To the author's knowledge, this was the first theoretical calculation resulting in three dimensional intensity profiles for incident electron energies below 2 KeV which could easily be compared to experimental work. The  $N_2^+ B^2\Sigma_u^+$  intensity profiles and range values for incident energies from 0.3 to 5.0 KeV showed reasonable agreement with experimental electron energy degradation work in both the longitudinal and the radial direction.

A sensitivity study was included in this work which characterized the influence of 1) the differential ionization cross sections, 2) the differential inelastic cross sections, 3) the different shaped elastic phase functions, and 4) the total elastic cross sections on the energy deposition process. In particular, it was shown that: 1) Differential ionization cross sections have very little influence on the degradation process; 2) inelastic scattering appeared to be somewhat important for incident electrons with energies below 0.3 KeV; 3) the shape of the electron collision profiles and the range from the 3914 Å intensity profiles were functions of the screening parameter of the model 1 elastic scattering phase function; and 4) the total elastic cross section had a significant influence on the electron's spatial degradation process.

The resultant energy loss plots are used to help determine the energy albedo of the incident electrons and also the rate at which energy is lost in the medium. The spatial yield spectrum is easily employed to find the excitation profiles for any  $N_2$  state at any position in the medium. For this reason the three variable spatial yield spectrum  $U(E,z,E_0)$  is analytically characterized. The four variable spatial yield spectrum  $U(E,\rho,z,E_0)$  is even more complex than  $U(E,z,E_0)$ ; nevertheless the systematics of this quantity are described qualitatively.

This work compiled a reasonably comprehensive and realistic cross section set for  $N_2$  in the energy range from 2 to 5000 eV. The influence of various differential and total cross sections on the spatial and energetic aspects of the electron energy deposition problem was also characterized. Finally, this study presented a spatial yield spectrum along with an analysis and analytic fit of some of its most important properties.

APPENDIX A  
MONTE CARLO PROGRAM

The Monte Carlo program which is a modified version of a program used in Brinkmann and Trajmar (1970) is listed in this appendix. This program (written in Fortran IV) degrades electrons in the range from 2 to 5000 eV in a spatial manner. Each collision with its characteristics are placed on a magnetic tape.



```

106      WRITE(6,106)NPIN,NOP,NPHF
          FORMAT(/,,' THE NUMBER OF PRIMARY SEGMENTS=',I5,
          * /,,' THE NUMBER OF PRIMARIES IN EACH SEGMENT=',I5,/,
          * , INDEX FOR PHASE FUNCTION=',I5,/)
          READ(5,105) ISEED,ILAST,ISTOP,NX,NSEC
          ISEED IS THE INITIAL RANDOM NUMBER STARTER
          ILAST = 0 IN ALL CASES
          IF ISTOP=1 THEN WE HAVE ANOTHER RUN TO MAKE
          IF ISTOP=0 THEN THIS IS THE ONLY RUN
          NX IS THE NUMBER OF ANGLES USED IN FINDING THE SCATTERING
          ANGLE IF NO ANALYTIC EXPRESSION CAN BE USED.
          NSEC IS THE NUMBER OF LOWER ENERGY BIN ENDS.
          NSEC IS USEFUL ONLY IF A LOCAL ENERGY DEGRADATION SCHEME IS
          EMPLOYED BELOW SOME ENERGY AND IF PRELIMINARY OUTPJT IS DESIRED.
105      FORMAT(8I10)
          READ(5,550)EMIN,TMIN,EMSD,EINEL
          EM IN IS THE ENERGY TO WHICH THE PRIMARY ELECTRON IS DEGRADED BEFORE
          LOCAL DEGRADATION IS USED
          TMIN IS THE ENERGY TO WHICH THE SECONDARY AND TERTIARY ELECTRONS ARE
          DEGRADED.
          BELOW EMSD USE THE MULTIPLE SCATTERING DISTRIBUTION.
          EINEL IS THE HIGHEST ENERGY AT WHICH ELECTRONS ARE ALLOWED TO
          SCATTER INELASTICALLY.
          FORMAT(8E10,3)
550      WRITE(6,620)ISEED,ILAST,ISTOP,EMIN,TMIN,EMSD,EINEL
620      FORMAT(' ISEED=',I10,/, ' ILAST=',I10,/, ' ISTOP=',I5,/,
          * , EMIN=',1PE10.4, ' EV,/, ' TMIN=',1PE10.4, ' EV,/,
          A
MAIN0047
MAIN0048
MAIN0049
MAIN0050
MAIN0051
MAIN0052
MAIN0053
MAIN0054
MAIN0055
MAIN0056
MAIN0057
MAIN0058
MAIN0059
MAIN0060
MAIN0061
MAIN0062
MAIN0063
MAIN0064
MAIN0065
MAIN0066
MAIN0067
MAIN0068
MAIN0069
MAIN0070
MAIN0071
MAIN0072
MAIN0073

```

14 JULY 1978 NERDC --- CARD LIST UTILITY

```

B * EMSD=.1PE10.4. EV./, EINEL=.1PE10.4. EV',//)
  NA=NX-1
  WRITE(6,250)NX
  250 FORMAT(////.3X,'THE DISTRIBUTION FUNCTION IS EVALUATED AT ',I5,
  A,' ANGLES BETWEEN ZERO AND PI',////)
  WRITE(6,622)
622 FORMAT(' INDEX OF ANGLE',5X,'ANGLE VALUE IN RADIANS',//)
  C THET(I) ARE THE ANGULAR BIN ENDS USEFUL IN CALCULATING THE ANGLE
  C OF SCATTER,
  DO 3 I=1,NX
  WRITE(6,624) I,THET(I)
624 FORMAT(18,14X,1PE10.4)
  3 CONTINUE
  C NAR IS THE NUMBER OF ALTITUDE INTERVALS
  C ZALT(I) ARE THE ARRAY OF Z VALUES.
  C THIS ARRAY IS MAINLY USEFUL IF PRELIMINARY OUTPUT IS DESIRED.
  C ZALT(1) AND ZALT(NAR) ARE THE LIMITS ON THE Z DIMENSION
  C OF THE BOX FOR DEGRADATION.
  C IF AN ELECTRON REACHES OUTSIDE THE DIMENSIONS (IN Z) OF THE BOX,
  C THEN THE ELECTRON HAS ESCAPED.
131 FORMAT(8E10.0)
  WRITE(6,632)
632 *//, I,INDEX OF ALTITUDE RANGE',5X,'ALTITUDE IN KILOMETERS',
  *//)
  DO 10 J=1,NAR
  WRITE(6,634) J,ZALT(J)
634 FORMAT(18,21X,1PE12.4)
  10 CONTINUE
  C WIS(I) ARE THE LOWER ELECTRON ENERGY BIN ENDS.
  NTOP=NSEC-1
  READ(5,131)(WIS(I), I=1,NSEC)
  C EXC5(I) ARE THE NUMBER OF EXCITATIONS OF THE 3914A EMISSION STATE
  C RESULTING FROM THE LOCAL DEGRADATION OF THE SECONDARIES IN THAT BIN.
  C THIS ARRAY IS USEFUL ONLY IF PRELIMINARY OUTPUT IS DESIRED.
640 *//, I,BOUNDARIES OF BINS FOR SECONDARIES IN EV',
  *//, NO. OF 3914A EMISSIONS EXCITED',//)
  DO 20 I=1,NTOP
  IPI=I+1
  WRITE(6,645)WIS(I),WIS(IPI),EXC5(I)
645 FORMAT(1PE12.3,5X,1PE12.3,14X,1PE12.3)

```

```

MAIN0074
MAIN0075
MAIN0076
MAIN0077
MAIN0078
MAIN0079
MAIN0080
MAIN0081
MAIN0082
MAIN0083
MAIN0084
MAIN0085
MAIN0086
MAIN0087
MAIN0088
MAIN0089
MAIN0090
MAIN0091
MAIN0092
MAIN0093
MAIN0094
MAIN0095
MAIN0096
MAIN0097
MAIN0098
MAIN0099
MAIN0100
MAIN0101
MAIN0102
MAIN0103
MAIN0104
MAIN0105
MAIN0106
MAIN0107
MAIN0108
MAIN0109
MAIN0110
MAIN0111
MAIN0112
MAIN0113
MAIN0114
MAIN0115
MAIN0116
MAIN0117
MAIN0118

```

```

20      CONTINUE
C      READ(5,120) NPRIM,COSI,EIN,H,ZSTART
C      NPRIM IS THE NUMBER OF PRIMARIES
C      COSI IS THE COSINE OF THE INITIAL ELECTRON
C      EIN IS THE ENERGY OF THE PRIMARY ELECTRON
C      H IS THE MAGNETIC FIELD
C      ZSTART IS THE ALTITUDE AT WHICH THE PRIMARY ELECTRON IMPINGES
120     FORMAT(10,F10.5,3E10.0)
C      WRITE(6,210) NPRIM,COSI,EIN,H,ZSTART
210     FORMAT(/,/,1THE BATCH OF PARTICLES=,15,/
A      /,9X,THE NUMBER OF PARTICLES=,15,/
B9X,COSINE OF THE INITIAL POLAR ANGLE=,F6.3,
C      /,9X,INCIDENT ENERGY=,F12.3,2X,EV,
D      /,9X,MAGNETIC FIELD=,F12.3,2X,GAUSS,
E      /,9X,INITIAL ALTITUDE=,1PE12.3,2X,KILOMETERS, )
C
C      CALL DATA SUBROUTINE TO READ IN THE REST OF THE DATA
C      CALL DATA
C      NARI=NAR+1
C      NUMG=NUMST+NUMGAS
C
C      CALL SUBROUTINE MC WHICH DEGRADES ALL THE PRIMARIES
C      CALL MC
C      IF(ISTOP.EQ.0)GO TO 2
C      GO TO 1

```

MAIN0119  
 MAIN0120  
 MAIN0121  
 MAIN0122  
 MAIN0123  
 MAIN0124  
 MAIN0125  
 MAIN0126  
 MAIN0127  
 MAIN0128  
 MAIN0129  
 MAIN0130  
 MAIN0131  
 MAIN0132  
 MAIN0133  
 MAIN0134  
 MAIN0135  
 MAIN0136  
 MAIN0137  
 MAIN0138  
 MAIN0139  
 MAIN0140  
 MAIN0141  
 MAIN0142  
 MAIN0143  
 MAIN0144  
 MAIN0145

NERDC --- CARD LIST UTILITY

14 JULY 1978

2 CONTINUE  
STOP  
END

MAIN0146  
MAIN0147  
MAIN0148

#

14 JULY 1978 NERDC --- CARD LIST UTILITY

```

SUBROUTINE COLTYP
  SUBROUTINE COLTYP *****
  THIS SUBROUTINE IS ACCESSED THROUGH MC AND MESD.
  THIS SUBROUTINE COMPUTES THE TYPE OF COLLISION THAT OCCURS.
  SOME OF THIS SUBROUTINE IS SET UP TO TAKE MORE THAN ONE GAS.
  COMMON ALPE(6),BETE(6),CE(6),FE(6),WE(6),ALFA(15),BEFA(15),
  1 CFA(15),FFA(15),WFA(15),WF(15),FACI(15),NFA,NAR,SA(3,80),
  2 ZALT(80),ENR(30),PCFA(3,30),WCFA(3,30),NENR,FDG(3),PSE(3),
  3 PION(3),AT(3),A(6,3),B(5,3),G(5,3),UH(10),UI(10),UJ(10),
  4 UD(10),USNU(10),USF(10),UEIN(11),IUTP,IUTMI,DG(3),NSG(3),NIG(3),
  5 NUMGAS,NUMST,WIS(50),NSEC,MUNIT,ISEED,ISTOP,ILAST,EIN,NPRIM,COSI,
  6 H,EMIN,ZSTART,TMIN,THRESH(3),AK(2,3),AJ(3,3),GAVA(2,3),
  7 TD(3,3),FAC(6),AGE(6),AIE(6),BOE(6),BIE(6),COE(5),DOE(6),
  8 DIE(6),PROB(40),W(40),NIE(40),A21(3),A22(3),A31(3),A32(3),
  9 A33(3),B11(3),B12(3),B13(3),C1(3),C21(3),C22(3),C31(3),
  A C32(3),D1(3),D2(3),F1(3),F2(3),THRI(16),AKI(2,15),AJI(3,16),
  B GAMAI(2,16),TOI(3,16),SIGT(6),THET(40),NX,CSIE(20),EIT(20),
  C IEILS,IEILMI,P,R,ZDIS,NPIN,NOP,COSPA,RT,F(40),R1,R2,R3,R4,
  D R5,XV,YV,ZV,XVN,YVN,ZVN,PA,PHI,EV,WLOSS,NSTAT,NSCS,NPHF,
  E IRI,IR2,NG,EVPRI,RAN,EMSD,EINEL,EXC5(50),COSPAN,T,FOVAL

E=EV
EV IS THE ENERGY FROM THE MAIN PROGRAM
DGT=0.0
DO 30 I=1,NUMGAS
  DGT=DGT+DG(I)
  CALCULATE DGT, THE TOTAL DENSITY OF THE GASES.
DO 20 I=1,NUMGAS
  FDG(I)=DGT(I)/DGT
  CALCULATE FDG(I), THE FRACTION OF THE TOTAL MODEL ATMOSPHERE THAT
  IS THE ITH SPECIE.
  SIGEE=0.0
  K=0
  DO 1 I=1,NUMGAS
  DO 1 J=1,2
  K=K+1
  SIGEE=SIGEE+SIGT(K)*FDG(I)
  CALCULATE SIGEE, THE TOTAL CROSS SECTION.
  PSE(1)=SIGT(2)/SIGEE
  P=PSE(1)
  IF(R,LT,P) GO TO 403
  GO TO 404
  NSTAT=NUMST+1
  GO TO 4

```

COLTYP01  
COLTYP02  
COLTYP03  
COLTYP04  
COLTYP05  
COLTYP06  
COLTYP07  
COLTYP08  
COLTYP09  
COLTYP10  
COLTYP11  
COLTYP12  
COLTYP13  
COLTYP14  
COLTYP15  
COLTYP16  
COLTYP17  
COLTYP18  
COLTYP19  
COLTYP20  
COLTYP21  
COLTYP22  
COLTYP23  
COLTYP24  
COLTYP25  
COLTYP26  
COLTYP27  
COLTYP28  
COLTYP29  
COLTYP30  
COLTYP31  
COLTYP32  
COLTYP33  
COLTYP34  
COLTYP35  
COLTYP36  
COLTYP37  
COLTYP38  
COLTYP39  
COLTYP40  
COLTYP41  
COLTYP42  
COLTYP43  
COLTYP44  
COLTYP45

```

404      IF (NUMGAS .EQ. 1) GO TO 6
        J=2
        C   COME TO THIS SECTION WHEN THERE ARE MORE THAN ONE GASES.
        ITOP=2*NUMGAS
        DO 2 I=4,ITOP,2
          PSE(J)=SIGT(I)/SIGEE
          P=P+PSE(J)
          IF (R .LT. P) GO TO 5
          J=J+1
          CONTINUE
          GO TO 6
        2   NSCS=2
        C   ELASTIC COLLISIONS ARE SENT TO STATEMENT 4.
        GO TO 7
        4   NSCS=J
        5   NSTAT=NUMST+J
        7   RETURN
        6   NSCS=-1
           RAN=R
           C   RAN AND R ARE THE RANDOM NUMBERS.
           IF (E .LT. 200.) CALL CTB200
           C   GO TO SUBROUTINE CTB200 FOR ENERGIES LESS THAN 200 EV.
           IF (E .LT. 200.) GO TO 12
           NSTAT=1
           JL=1
           DO 11 I=1,NUMGAS
             NSCS=NSCS+2
COLTYP46
COLTYP47
COLTYP48
COLTYP49
COLTYP50
COLTYP51
COLTYP52
COLTYP53
COLTYP54
COLTYP55
COLTYP56
COLTYP57
COLTYP58
COLTYP59
COLTYP60
COLTYP61
COLTYP62
COLTYP63
COLTYP64
COLTYP65
COLTYP66
COLTYP67
COLTYP68
COLTYP69
COLTYP70
COLTYP71
COLTYP72

```



14 JULY 1978 NERDC --- CARD LIST UTILITY

```

SUBROUTINE CRSEC
SUBROUTINE CRSEC ***
THIS SUBROUTINE IS ACCESSED THROUGH MC AND ZVAL.
THIS SUBROUTINE CALCULATES THE TOTAL ELASTIC AND TOTAL INELASTIC
CROSS SECTIONS.
COMMON ALPE(6), BETE(6), CE(6), FE(6), WE(6), ALFA(15), BEFA(15),
1 CFA(15), FFA(15), WFA(15), WFI(15), FACI(15), NFA(15), NAR, SA(3,80),
2 ZALT(80), ENR(30), PCFA(3,30), WCFA(3,30), NENR, FDG(3), PSE(3),
3 PION(3), AT(3), A(6,3), B(5,3), G(5,3), UH(10), UI(10), UJ(10),
4 UD(10), USNU(10), USF(10), UEIN(11), IUTP, IUTM, DG(3), NSG(3), NIG(3),
5 NUMGAS, NUMST, WIS(50), NSEC, MUNIT, ISEED, ISTOP, ILAST, EIN, NPRI, M, COSI,
6 H, EMIN, ZSTART, TMIN, THRESH(3), AK(2,3), AJ(3,3), GAMA(2,3),
7 TO(3,3), FAC(6), AOE(6), AIE(6), BOE(6), BIE(6), COE(5), DOE(6),
8 DIE(6), PROB(40), W(40), NIE(40), A21(3), A22(3), A31(3), A32(3),
9 A33(3), B11(3), B12(3), B13(3), C1(3), C21(3), C22(3), C31(3),
A C32(3), D1(3), D2(3), F1(3), F2(3), THRI(16), AKI(2,16), AJI(3,16),
B GAMA1(2,16), TOI(3,16), SIGT(6), THET(40), NX, CSIE(20), EIT(20),
C IEILS, IEILMI, P, K, ZDIS, NPIN, NUP, COSPA, RT, F(40), R1, R2, R3, R4,
D R5, XV, YV, ZV, XVN, YVN, ZVN, PA, PHI, EV, WLDSS, NSTAT, NSCS, NPHF,
E IRI, IR2, NG, EVPRI, RAN, EMSD, EINEL, EXCS(50), COSPAN, T, FOVAL

E=EV
IF(E .LT. EIT(1))GO TO 1
Q0=651.3
ST1=(1.-(WE(1)/E)**ALPE(1))**BETE(1)
ST2=ALOG(4.*E*CE(1)/WE(1)+EXP(1.))
SIGT(1)=Q0*FE(1)*ST1*ST2/E/WE(1)
SIGT(1) IS THE TOTAL INELASTIC CROSS SECTION.
GO TO 4
DO 2 K=1, IEILMI
KPI=K+1
IF(E .LE. EIT(K) .AND. E .GE. EIT(KPI))GO TO 3
CONTINUE
SIGT(1)=CSIE(K)+(E-EIT(K))*(CSIE(KPI)-CSIE(K))/(EIT(KPI)-EIT(K))
CONTINUE
T1=E*(.23)/1.95E-03/(475.+E*(1.23))
T2=1.6E+03/((E-15.5)*(E-15.5)+590.5)
T3=2.17/((E-2.47)*(E-2.47)+0.296)
SIGT(2)=2.5*(T1+T2+T3)
SIGT(2) IS THE TOTAL ELASTIC CROSS SECTION.
RETURN
END

```

CRSEC001  
CRSEC002  
CRSEC003  
CRSEC004  
CRSEC005  
CRSEC006  
CRSEC007  
CRSEC008  
CRSEC009  
CRSEC010  
CRSEC011  
CRSEC012  
CRSEC013  
CRSEC014  
CRSEC015  
CRSEC016  
CRSEC017  
CRSEC018  
CRSEC019  
CRSEC020  
CRSEC021  
CRSEC022  
CRSEC023  
CRSEC024  
CRSEC025  
CRSEC026  
CRSEC027  
CRSEC028  
CRSEC029  
CRSEC030  
CRSEC031  
CRSEC032  
CRSEC033  
CRSEC034  
CRSEC035  
CRSEC036  
CRSEC037  
CRSEC038  
CRSEC039  
CRSEC040  
CRSEC041  
CRSEC042  
CRSEC043

14 JULY 1978 NERDC --- CARD LIST UTILITY

```

C SUBROUTINE CTB200
C SUBROUTINE CTB200 ***
C THIS SUBROUTINE IS ACCESSED THROUGH COLTYP.
C THIS SUBROUTINE CALCULATES THE TYPE OF COLLISION IF THE ENERGY E IS
C LESS THAN 200 EV.
  COMMON ALPE(6),BETE(6),CE(6),FE(6),WE(6),ALFA(15),BEFA(15),
  1 CFA(15),FFA(15),WFA(15),WFI(15),FACI(15),NFA,NAR,SA(3,80),
  2 ZALT(80),ENR(30),PCFA(3,30),WCFA(3,30),NENR,FDG(3),PSE(3),
  3 PION(3),AT(3),A(6,3),B(5,3),G(5,3),UH(10),UI(10),UJ(10),
  4 UD(10),USNU(10),USF(10),UEIN(11),IUTP,IUTM,DG(3),NSG(3),NIG(3),
  5 NUMGAS,NUMST,WIS(50),NSEC,MUNIT,ISEED,ISTOP,ILAST,EIN,NPRIM,COSI,
  6 H,EMIN,ZSTART,TMIN,THRESH(3),AK(2,3),AJ(3,3),GAMA(2,3),
  7 TO(3,3),FAC(6),AOE(6),AIE(6),BOE(6),BIE(6),COE(6),DOE(6),
  8 DIE(6),PROB(40),W(40),NIE(40),A21(3),A22(3),A31(3),A32(3),
  9 A33(3),B11(3),B12(3),B13(3),C1(3),C21(3),C22(3),C31(3),
  A C32(3),D1(3),D2(3),F1(3),F2(3),F3(3),THRI(16),AKI(2,16),AJI(3,16),
  B GAMA(2,16),TOI(3,16),SIGT(6),THET(40),NX,CSIE(20),EIT(20),
  C IEILS,IEILM,P,R,ZDIS,NPIN,NOP,CO SPA,RT,F(40),RI,R2,R3,R4,
  D R5,XV,YV,ZV,XVN,YVN,ZVN,PA,PHI,EV,WLOSS,NSTAT,NSCS,NPHF,
  E IRI,IR2,NG,EVPRI,RAN,EMSD,EINEL,EXC5(50),COSPAN,T,FOVAL

E=EV
IF(E .LT. 12.8)KADD=8
IF(E .LT. 12.8)GO TO 30
12.8 EV IS THE LOWEST THRESHOLD OF THE EIGHT N2 STATES WHICH ARE
ACCOUNTED FOR INDIVIDUALLY.
00=651.3
K=0
DO 3 I=1,NUMGAS
N=2*I-1
JTOP=NSG(I)-1-NIG(I)
DO 3 J=1,JTOP
K=K+1
IF(E .LT. WF(K))GO TO 3
ST1=(1.-(WF(K)/E))*ALFA(K)**BEFA(K)
ST2=(WF(K)/E)*CFA(K)/WF(K) *E
ST2=ALOG(4.*E*CFA(K)/WF(K) +EXP(1.))
IF(NIE(K) .EQ. 1) ST2=STF2
SIGFA=GO*FFA(K)*ST1*ST2/E/WF(K)
P=(SIGFA/SIGT(N))*FDG(I)*(1.-PSE(I))+P
IF(P .GT. RAN) GO TO 12
INDIVIDUAL ALLOWED STATE PROBABILITIES ARE CALCULATED.
CONTINUE
KID=0

```

```

CTB200001
CTB200002
CTB200003
CTB200004
CTB200005
CTB200006
CTB200007
CTB200008
CTB200009
CTB200010
CTB200011
CTB200012
CTB200013
CTB200014
CTB200015
CTB200016
CTB200017
CTB200018
CTB200019
CTB200020
CTB200021
CTB200022
CTB200023
CTB200024
CTB200025
CTB200026
CTB200027
CTB200028
CTB200029
CTB200030
CTB200031
CTB200032
CTB200033
CTB200034
CTB200035
CTB200036
CTB200037
CTB200038
CTB200039
CTB200040
CTB200041
CTB200042
CTB200043
CTB200044
CTB200045

```

CTB20046  
 CTB20047  
 CTB20048  
 CTB20049  
 CTB20050  
 CTB20051  
 CTB20052  
 CTB20053  
 CTB20054  
 CTB20055  
 CTB20056  
 CTB20057  
 CTB20058  
 CTB20059  
 CTB20060  
 CTB20061  
 CTB20062  
 CTB20063  
 CTB20064  
 CTB20065  
 CTB20066  
 CTB20067  
 CTB20068  
 CTB20069  
 CTB20070  
 CTB20071  
 CTB20072

```

DO 4 I=1, NUMGAS
N=2*I-1
JTOP=NIG(I)
DO 4 J=1, JTOP
KIO=KIO+1
IF(E .LT. THRI(KIO))GO TO 4
TSET=TOI(1,KIO)-TOI(2,KIO)/(E+TOI(3,KIO))
GSET=GAMAI(1,KIO)*E/(E+GAMAI(2,KIO))
TM=(E-THRI(KIO))/2
ASET=(AKI(1,KIO)/(E+AKI(2,KIO)))*ALOG(E/AJI(1,KIO)+AJI(2,KIO))+
1 AJI(3,KIO)/E)
SIGI=ASET*GSET*(ATAN((TM-TSET)/GSET)+ATAN(TSET/GSET))
P=SIGI/SIGT(N)*FOG(I)*(1.-PSE(I))+P
IF(P .GE. RAN) GO TO 13
CONTINUE
KADD=K+KIO
J=0
DO 6 I=1, NENR
J=J+1
IF(E .LT. ENR(I)) GO TO 20
CONTINUE
JM1=J-1
DO 5 I=1, NUMGAS
N=2*I-1
NSTAT=KADD+I
EMEN=E-ENR(JM1)

```

C INDIVIDUAL IONIZATION STATE PROBABILITIES ARE CALCULATED.

4

30

6

20

14 JULY 1978 NERDC --- CARD LIST UTILITY

CTB200073  
 CTB200074  
 CTB200075  
 CTB200076  
 CTB200077  
 CTB200078  
 CTB200079  
 CTB200080  
 CTB200081  
 CTB200082  
 CTB200083  
 CTB200084  
 CTB200085  
 CTB200086

```

ENME=ENR(J)-E
ENMEN=ENR(J)-ENR(JM1)
WLOSS = (WCFA(I,J)*EMEN+ WCFA(I,JM1)*ENME)/ENMEN
ENERGY LOSS FOR THE COMBINED STATE IS CALCULATED.
CONTINUE
GO TO 15
WLOSS=WFA(K)
NSTAT=K
GO TO 15
WLOSS=THRI(KIO)
NSTAT=K+KIO
NSCS=N
RETURN
END

```

C 5  
 12  
 13  
 15

14 JULY 1978 NERDC --- CARD LIST UTILITY

```

SUBROUTINE DATA **
THIS SUBROUTINE IS ACCESSED THROUGH THE MAIN PROGRAM,
ALL THE REST OF THE DATA IS READ IN HERE INCLUDING THE CROSS SECTION
PARAMETERS AND ALSO ALL THE OTHER PARAMETERS NEEDED.
COMMON ALPE(6),BETE(6),CE(6),FE(6),WE(6),ALFA(15),REFA(15),
1 CFA(15),FFA(15),WFA(15),WFI(15),FACI(15),NFA,NAR,SA(3,80),
2 ZALT(80),ENR(30),PCFA(3,30),WCF(3,30),NENR,FDG(3),PSE(3),
3 PION(3),AT(3),A(6,3),B(5,3),G(5,3),UH(10),UI(10),UJ(10),
4 UD(10),USNU(10),USEF(10),UEIN(11),IUTP,IUTM,DG(3),NSG(3),NIG(3),
5 NUMGAS,NUMST,WIS(50),NSEC,MUNIT,ISEED,ISTOP,ILAST,EIN,NPRIM,COSI,
6 H,EMIN,ZSTART,TMIN,THRESH(3),AK(2,3),AJ(3,3),GAMA(2,3),
7 TO(3,3),FAC(6),AOE(6),AIE(6),BOE(6),BIE(6),COE(6),DOE(6),
8 DIE(6),PROB(40),W(40),NIE(40),A21(3),A22(3),A31(3),A32(3),
9 A33(3),B11(3),B12(3),B13(3),C1(3),C21(3),C22(3),C31(3),
A C32(3),D1(3),D2(3),F1(3),F2(3),THRI(16),AKI(2,16),AJI(3,16),
B GAMAI(2,16),TOI(3,16),SIGT(6),THET(40),NX,CSIE(20),EIT(20),
C IEILS,IEILMI,P,R,ZDIS,NPIN,NOP,COSPA,RT,F(40),R1,R2,R3,R4,
D R5,XV,YV,ZV,XVN,YVN,ZVN,PA,PHI,EV,WLDSS,NSTAT,NSCS,NPHF,
E IR1,IR2,NG,EVPR1,RAN,EMSD,EINEL,EXC5(50),COSPAN,T,FOVAL
DATA0001
DATA0002
DATA0003
DATA0004
DATA0005
DATA0006
DATA0007
DATA0008
DATA0009
DATA0010
DATA0011
DATA0012
DATA0013
DATA0014
DATA0015
DATA0016
DATA0017
DATA0018
DATA0019
DATA0020
DATA0021
DATA0022
DATA0023
DATA0024
DATA0025
DATA0026
DATA0027
DATA0028
DATA0029
DATA0030
DATA0031
DATA0032
DATA0033
DATA0034
DATA0035
DATA0036
DATA0037
DATA0038
DATA0039
DATA0040
DATA0041
DATA0042
DATA0043
DATA0044
DATA0045

C SUBROUTINE DATA **
C THIS SUBROUTINE IS ACCESSED THROUGH THE MAIN PROGRAM,
C ALL THE REST OF THE DATA IS READ IN HERE INCLUDING THE CROSS SECTION
C PARAMETERS AND ALSO ALL THE OTHER PARAMETERS NEEDED.
C COMMON ALPE(6),BETE(6),CE(6),FE(6),WE(6),ALFA(15),REFA(15),
1 CFA(15),FFA(15),WFA(15),WFI(15),FACI(15),NFA,NAR,SA(3,80),
2 ZALT(80),ENR(30),PCFA(3,30),WCF(3,30),NENR,FDG(3),PSE(3),
3 PION(3),AT(3),A(6,3),B(5,3),G(5,3),UH(10),UI(10),UJ(10),
4 UD(10),USNU(10),USEF(10),UEIN(11),IUTP,IUTM,DG(3),NSG(3),NIG(3),
5 NUMGAS,NUMST,WIS(50),NSEC,MUNIT,ISEED,ISTOP,ILAST,EIN,NPRIM,COSI,
6 H,EMIN,ZSTART,TMIN,THRESH(3),AK(2,3),AJ(3,3),GAMA(2,3),
7 TO(3,3),FAC(6),AOE(6),AIE(6),BOE(6),BIE(6),COE(6),DOE(6),
8 DIE(6),PROB(40),W(40),NIE(40),A21(3),A22(3),A31(3),A32(3),
9 A33(3),B11(3),B12(3),B13(3),C1(3),C21(3),C22(3),C31(3),
A C32(3),D1(3),D2(3),F1(3),F2(3),THRI(16),AKI(2,16),AJI(3,16),
B GAMAI(2,16),TOI(3,16),SIGT(6),THET(40),NX,CSIE(20),EIT(20),
C IEILS,IEILMI,P,R,ZDIS,NPIN,NOP,COSPA,RT,F(40),R1,R2,R3,R4,
D R5,XV,YV,ZV,XVN,YVN,ZVN,PA,PHI,EV,WLDSS,NSTAT,NSCS,NPHF,
E IR1,IR2,NG,EVPR1,RAN,EMSD,EINEL,EXC5(50),COSPAN,T,FOVAL

C READ(5,500) NUMGAS,NUMST,(NSG(I),I=1,NUMGAS),(NIG(I),I=1,NUMGAS)
C NUMGAS IS THE NUMBER OF GASES.
C NUMST IS THE TOTAL NUMBER OF STATES.
C NSG(I) ARE THE NUMBER OF STATES IN THE ITH GAS.
C NIG(I) ARE THE NUMBER OF IONIZATION STATES IN THE ITH GAS.
500 FORMAT(8I5)
691 WRITE(6,691) NUMGAS,NUMST
FORMAT(//, ' THE NUMBER OF GASES= ',I5,/,/,
1 , ' THE TOTAL NUMBER OF STATES= ',I5,/)
695 WRITE(6,695)
FORMAT(//, ' STATES',3X,'ND, ION STATES',3X,'GAS NUMBER',/)
DO 22 I=1,NUMGAS
WRITE(6,693) NSG(I),NIG(I),I
693 FORMAT(16,7X,I6,10X,I6)
22 CONTINUE
601 WRITE(6,601)
FORMAT(//, ' TOTAL INELASTIC CROSS SECTION PARAMETERS ARE GIVEN
1 HERE',//,6X,'GAS',15X,'ALPHA',3X,'BETA',5X,'C',7X,'F',7X,'W',/)
NUP=2*NUMGAS
DO 1 I=1,NUMGAS
READ(5,502) G1,G2,G3,G4,G5,ALPE(I),BETE(I),CE(I),FE(I),WE(I)
C READ IN THE TOTAL INELASTIC PARAMETERS.
502 FORMAT(5A4,7E8,0)

```

```

605 WRITE(6,605)G1,G2,G3,G4,G5,ALPE(I),BETE(I),CE(I),FE(I),WE(I)
1  FORMAT(1X,SA4,9F8.3)
CONTINUE
609 WRITE(6,609)
1  FORMAT(//),, THE P(E,T) PARAMETERS FOLLOW',/,6X,'GAS',14X,
1  'THRESH',6X,'K',5X,'KB',7X,'J',6X,'JB',6X,'JC',7X,'GAMMAS',
1  2X,'GAMMAB',6X,'TS',5X,'TA',7X,'TB',/
DO 3 I=1,NUMGAS
1  READ(5,502) G1,G2,G3,G4,G5,THRESH(I),(AK(K,I),K=1,2),
1  (AJ(J,I),J=1,3)
1  READ(5,504) (GAMA(K,I),K=1,3)
C  READ IN THE P(E,T) PARAMETERS. THESE ARE USED TO FIND THE SECONDARY
C  ELECTRON ENERGY AFTER AN IONIZATION EVENT.
504 FORMAT(20X,SE8.0)
1  WRITE(6,611) G1,G2,G3,G4,G5,THRESH(I),(AK(K,I),K=1,2),
1  (AJ(J,I),J=1,3),(GAMA(K,I),K=1,2),(TO(K,I),K=1,3)
611 FORMATT(1X,SA4,F8.3,1X,5F8.3,2X,2F8.3,F10.3,F8.1,F8.3)
3  CONTINUE
613 WRITE(6,613)
1  FORMAT(//),, THE DOUBLY DIFFERENTIAL IONIZATION CROSS SECTION PAR
1  AMETERS ARE READ IN NOW',/,6X,'GAS',14X,'I/B1',7X,'AT/B2',
1  7X,'A1/B3',5X,'A2/B4',6X,'A3/B5',6X,'A4/G1',6X,'A5/G2',7X,
1  'A6/G3',7X,'/G4',8X,'/G5',/
DO 4 I=1,NUMGAS
1  READ(5,562) G1,G2,G3,G4,G5,PION(I),AT(I),(A(K,I),K=1,4)
C  READ IN THE DOUBLY DIFFERENTIAL IONIZATION CROSS SECTION PARAMETERS
C  FOR THE PRIMARY SCATTERING.

```

```

DATA0046
DATA0047
DATA0048
DATA0049
DATA0050
DATA0051
DATA0052
DATA0053
DATA0054
DATA0055
DATA0056
DATA0057
DATA0058
DATA0059
DATA0060
DATA0061
DATA0062
DATA0063
DATA0064
DATA0065
DATA0066
DATA0067
DATA0068
DATA0069
DATA0070
DATA0071
DATA0072

```

NERDC --- CARD LIST UTILITY

14 JULY 1978

```

C THIS SCATTERING IS NO LONGER INCLUDED IN THE MONTE CARLO
C CALCULATION.
C THE SUBROUTINE DFDW AND THE FUNCTION DCS ARE INCLUDED AT THE
C END OF THIS LISTING AND CAN BE MODIFIED A LITTLE TO BE PUT INTO
C THE MONTE CARLO COMPUTATION.
562 FORMAT(SA4,SE10,0,E10,2)
    READ(5,522) (A(K,I),K=5,6)
    WRITE(6,615) G1,G2,G3,G4,G5,PION(I),AT(I),(A(K,I),K=1,6)
    FORMAT(1X,5A4,2X,F6,2,3X,1PE10,3,2X,F8,2,3X,F7,3,3X,1PE10,3,1X,
615 1 1PE10,3,3X,F8,2,1X,F8,2)
    READ(5,506) (B(K,I),K=1,5),(G(K,I),K=1,5)
    FORMAT(10E8,0)
    WRITE(6,617) (B(K,I),K=1,5),(G(K,I),K=1,5)
617 1 2X,F8,3,3X,F8,3,2X,1PE10,3,2X,F8,3,3X,1PE10,3
4 CONTINUE
    WRITE(6,643)
643 * FORMAT(//,' THE DOUBLY DIFFERENTIAL SECONDARY IONIZATION
* CRDSS SECTIONS ARE READ IN, //,6X,'GAS',14X,'F1/C1',6X,'F2/C2',
* 4X,'A2/C22',3X,'A22/C31',3X,'A31/C32',3X,'A32/D1',4X,'A33/D2',
* 4X,'B11',8X,'B12',8X,'B13',//)
    DO 15 I=1,NUMGAS
    READ(5,562)G1,G2,G3,G4,G5,F1(I),F2(I),B11(I),B12(I),B13(I)
    READ(5,564)C1(I),C21(I),C22(I),C31(I),C32(I),D1(I),D2(I)
C READ IN THE DOUBLY DIFFERENTIAL SECONDARY SCATTERING PARAMETERS.
C READ IN THE STATES AND THEIR THRESHOLDS.
564 * FORMAT(8E10,0)
    READ(5,564)A21(I),A22(I),A31(I),A32(I),A33(I)
    WRITE(6,645)G1,G2,G3,G4,G5,F1(I),F2(I),A21(I),A22(I),
* A31(I),A32(I),A33(I),B11(I),B12(I),B13(I)
    FORMAT(1X,5A4,7(F8,3,2X),F8,3,2X,F10,0,2X,F8,3)
645 WRITE(6,647)C1(I),C21(I),C22(I),C31(I),C32(I),D1(I),D2(I)
647 * FORMAT(21X,7(F8,3,2X))
15 CONTINUE
    WRITE(6,619)
619 * FORMAT(/,1THE STATES WITH THEIR PROBABILITIES AND THRESHOLDS ARE
1 NOW READ IN, //,5X,STATE',16X,'PROBABILITY',5X,'THRESHOLD',3X,
1 ,IONEXC NO.',3X,'INDEX NUMBER',/)
    DO 5 I=1,NUMST
    READ(5,540) G1,G2,G3,G4,G5,PROB(I),W(I),NIE(I)
C READ IN THE PROBABILITIES AND THRESHOLDS FOR THE STATES ABOVE 200 EV
540 * FORMAT(SA4,2E8,0,15)
    WRITE(6,621) G1,G2,G3,G4,G5,PROB(I),W(I),NIE(I),I
621 * FORMAT(1X,5A4,5X,F10,5,6X,F8,3,4X,15,9X,15)
5 CONTINUE
DATA0073
DATA0074
DATA0075
DATA0076
DATA0077
DATA0078
DATA0079
DATA0080
DATA0081
DATA0082
DATA0083
DATA0084
DATA0085
DATA0086
DATA0087
DATA0088
DATA0089
DATA0090
DATA0091
DATA0092
DATA0093
DATA0094
DATA0095
DATA0096
DATA0097
DATA0098
DATA0099
DATA0100
DATA0101
DATA0102
DATA0103
DATA0104
DATA0105
DATA0106
DATA0107
DATA0108
DATA0109
DATA0110
DATA0111
DATA0112
DATA0113
DATA0114
DATA0115
DATA0116
DATA0117

```

```

623 NUMG=NUMST+1
      NIE(NUMG)=4
      WRITE(6,623)
      FORMAT(//), THE STATES WITH THEIR CROSS SECTION PARAMETERS ARE
1 READ IN, (//)
625 WRITE(6,625)
      FORMAT(6X, STATE, 15X, W, 7X, ALPHA, 4X, BETA, 6X,
1 WBAR, 7X, C OR O, 10X, F, 9X, FACI, /)
      K=0
      DO 7 I=1, NUMGAS
        JTOP=NSG(I)-1-NIG(I)
      DO 7 J=1, JTOP
        K=K+1
      READ(5,524) G1, G2, G3, G4, G5, WF(K), WFA(K), FACI(K), ALFA(K),
        BEFA(K), CFA(K), FFA(K)
1 READ IN THE PARAMETERS USED FOR THE INDIVIDUAL CROSS SECTIONS BELOW
      C 200 EV.
      S24 FORMAT(5A4, 6E6.0, E8.0)
        WF(K)=ABS(WF(K))
        WRITE(6,627) G1, G2, G3, G4, G5, WF(K), ALFA(K), BEFA(K), WFA(K).
1 CFA(K), FFA(K), FACI(K)
        FORMAT(1X, 5A4, 3F9.3, F10.3, F11.3, F15.6, 2F10.3)
      CONTINUE
      NFA=K
      JL=1
629 WRITE(6,629)
      FORMAT(//), THE S(E,T) PARAMETERS FOLLOW, //, 6X, ION, STATES, 7X, DATA0118
      DATA0119
      DATA0120
      DATA0121
      DATA0122
      DATA0123
      DATA0124
      DATA0125
      DATA0126
      DATA0127
      DATA0128
      DATA0129
      DATA0130
      DATA0131
      DATA0132
      DATA0133
      DATA0134
      DATA0135
      DATA0136
      DATA0137
      DATA0138
      DATA0139
      DATA0140
      DATA0141
      DATA0142
      DATA0143
      DATA0144

```

NERDC --- CARD LIST UTILITY

14 JULY 1978

```

1  'THRI',6X,'KI',6X,'KBI',5X,'JI',5X,'JBI',5X,'JCI',6X,'GAMSI',3X, DATA0145
1  'GAMBI',7X,'TSI',4X,'TAI',5X,'TBI',/ DATA0146
   DO 10 I=1,NUMGAS DATA0147
   JU=NIG(I) DATA0148
   DO 9 J=JL,JU DATA0149
   READ(5,502) G1,G2,G3,G4,G5,THRI(J),(AKI(K,J),K=1,2),(AJI(K,J), DATA0150
   K=1,3) DATA0151
1  READ(5,504)(GAMAI(K,J),K=1,2),(TOI(K,J),K=1,3) DATA0152
C  READ IN THE S(E,T) PARAMETERS FOR THE INDIVIDUAL IONIZATION CROSS DATA0153
C  SECTIONS. DATA0154
1  WRITE(6,611) G1,G2,G3,G4,G5,THRI(J),(AKI(K,J),K=1,2),(AJI(K,J), DATA0155
   K=1,3),(GAMAI(K,J),K=1,2),(TOI(K,J),K=1,3) DATA0156
9  CONTINUE DATA0157
   JL=JU+1 DATA0158
10  CONTINUE DATA0159
   READ(5,500) NENR DATA0160
   READ(5,522) (ENR(I),I=1,NENR) DATA0161
   DO 8 I=1,NUMGAS DATA0162
   READ(5,522) (PCFA(I,J),J=1,NENR) DATA0163
   READ(5,522) (WCFA(I,J),J=1,NENR) DATA0164
C  READ IN THE COMPOSITE STATE PARAMETERS OR ITS PROBABILITY AND DATA0165
C  THRESHOLD VALUES FOR ENERGIES LESS THAN 200 EV. DATA0166
8  CONTINUE DATA0167
   WRITE(6,633) DATA0168
   FORMAT(///,' THE COMPOSITE LEFT-OVER STATES ARE NOW READ IN',//, DATA0169
1  4X,'ENERGY',6X,'PROBABILITY',5X,'AVE,ENERGY LOSS',3X, DATA0170
1  'GAS INDEX',/) DATA0171
   DO 11 I=1,NUMGAS DATA0172
   DO 11 J=1,NENR DATA0173
   WRITE(6,635) ENR(J),PCFA(I,J),WCFA(I,J),I DATA0174
   FORMAT(3G15.7,3X,I7) DATA0175
11  CONTINUE DATA0176
   FORMAT(8E10.0) DATA0177
   READ(5,500) IEILS DATA0178
   IEILM1=IEILS-1 DATA0179
   DO 24 I=1,NUMGAS DATA0180
   READ(5,522) (EIT(J),J=1,IEILS) DATA0181
   READ(5,522) (CSIE(J),J=1,IEILS) DATA0182
C  READ IN THE TOTAL INELASTIC CROSS SECTION AT ENERGIES BELOW 30 EV. DATA0183
24  CONTINUE DATA0184
   WRITE(6,671) DATA0185
   FORMAT(///,' THE TOTAL INELASTIC CROSS SECTION IS READ IN FOR DATA0186
671  *ENERGIES BELOW 30 EV. THE UNITS ARE 10**(-16) CM**2',//, DATA0187
   * 4X,'ENERGY',6X,'CROSS SECTION',/) DATA0188
   DO 26 I=1,NUMGAS DATA0189

```

```

673 DO 26 J=1,IEILS
26 WRITE(6,673)EIT(J),CSIE(J)
FORMAT(2G15.7)
CONTINUE
572 READ(5,572)IUTP,FOVAL
FORMAT(15,4E10.0)
IUTM1=IUTP-1
READ(5,522)(UEIN(I),I=1,IUTP)
READ(5,522)(UH(I),I=1,IUTM1)
READ(5,522)(UI(I),I=1,IUTM1)
READ(5,522)(UJ(I),I=1,IUTM1)
READ(5,522)(UD(I),I=1,IUTM1)
READ(5,522)(USNU(I),I=1,IUTM1)
READ(5,522)(USF(I),I=1,IUTM1)
C READ IN THE MULTIPLE ELASTIC SCATTERING PARAMETERS FOR THE LONGITU-
C DINAL DISTRIBUTION.
WRITE(6,651)
651 FORMAT(1P)PARAMETERS FOR THE LONGITUDINAL OR Z CHARACTERIZATION OF
*THE ELECTRONS WITH ENERGIES BELOW 30 EV ARE NOW PRESENTED,/,
*4X, *E MIN, *4X, *E MAX, *6X, *H, *RX, *I, *RX, *J, *RX, *D, *5X, *S SUB NJ, .
*2X, *S SUB F, *3X, *FOVAL,/,)
DO 30 I=1,IUTM1
IPI=I+1
WRITE(6,653)UEIN(I),UEIN(IPI),UH(I),UI(I),UJ(I),UD(I),USNU(I),
*USF(I),FOVAL
653 FORMAT(9F9.2)
30 CONTINUE
DATA0190
DATA0191
DATA0192
DATA0193
DATA0194
DATA0195
DATA0196
DATA0197
DATA0198
DATA0199
DATA0200
DATA0201
DATA0202
DATA0203
DATA0204
DATA0205
DATA0206
DATA0207
DATA0208
DATA0209
DATA0210
DATA0211
DATA0212
DATA0213
DATA0214
DATA0215
DATA0216

```

NERDC --- CARD LIST UTILITY

14 JULY 1978

```

C      DO 6 I=1,NUMGAS
C      READ(5,522)SA(1,1)
C      READ IN THE MODEL ATMOSPHERE.
C      RIGHT NOW THIS IS SET UP FOR ONLY ONE DENSITY AND ONLY ONE GAS BUT
C      IT CAN BE EASILY MODIFIED.
C      CONTINUE
6      WRITE(6,637)
637    FORMAT(//,/, ' THE STANDARD ATMOSPHERE IS NOW PRINTED',
1      , ' WITH DENSITIES IN 1/CM*3, //,3X,
1      , ' ALTITUDE, 10X, GAS 1, 10X, GAS 2, 10X, GAS 3, /)
639    WRITE(6,639)ZALT(1),SA(1,1)
        FORMAT(4G15.7)
        RETURN
        END
DATA0217
DATA0218
DATA0219
DATA0220
DATA0221
DATA0222
DATA0223
DATA0224
DATA0225
DATA0226
DATA0227
DATA0228
DATA0229
DATA0230

```

14 JULY 1978 NERDC --- CARD LIST UTILITY

```

C SUBROUTINE MC
C SUBROUTINE MC **
C THIS IS THE MAJOR SUBROUTINE
C THIS SUBROUTINE IS ACCESSED THROUGH THE MAIN PROGRAM.
C IN THIS SUBROUTINE THE ELECTRON IS DEGRADED IN ENERGY IN A COLLISION
C BY COLLISION MANNER DOWN TO THE CUTOFF ENERGY EMIN.
C THE FOLLOWING SUBROUTINES ARE CALLED FROM THIS SUBROUTINE:
C 1)RANDU
C 2)ZVAL
C 3)PHF
C 4)PHFEL
C 5)PETI
C 6)SDIFM
C 7)CRSEC
C 8)COLTYP
C 9)MESD
C COMMON ALPE(6),BETE(6),CE(6),FF(6),WF(6),ALFA(15),RFFA(15),
1 CFA(15),FFA(15),WFA(15),WFA(15),FACI(15),NFA,NAR,SA(3,80),
2 ZALT(80),ENR(30),PCFA(3,30),WCFA(3,30),NENR,FDG(3),PSE(3),
3 PION(3),AT(3),A(6,3),R(5,3),G(5,3),UH(10),UI(10),UJ(10),
4 UD(10),USNU(10),USF(10),UEIN(11),IUTP,IUTM1,DG(3),NSG(3),NIG(3),
5 NUMGAS,NUMST,WIS(50),NSEC,MUNIT,ISEED,ILAST,EIN,NPRIM,COSI,
6 H,EMIN,ZSTART,TMIN,THRESH(3),AK(2,3),AJ(3,3),GAMA(2,3),
7 TO(3,3),FAC(6),AOE(6),AIE(6),BOE(6),BIE(6),COE(6),DOE(6),
8 DIE(6),PROB(40),W(40),NIE(40),A21(3),A22(3),A31(3),A32(3),
9 A33(3),B11(3),B12(3),B13(3),C1(3),C21(3),C22(3),C31(3),
A C32(3),D1(3),D2(3),F1(3),F2(3),THRI(16),AKI(2,16),AJI(3,16),
B GAMAI(2,16),TOI(3,16),SIGT(6),THET(40),NX,CSIE(20),EIT(20),
C IEILS,IEILM1,P,R,ZDIS,NPIN,NOP,COSPA,RT,F(40),R1,R2,R3,R4,
D R5,XV,YV,ZV,XVN,YVN,ZVN,PA,PHI,EV,WLOSS,NSTAT,NSCS,NPHF,
E IRI,IR2,NG,EVPRI,RAN,EMSD,EINEL,EXC5(50),COSPAN,T,FOVAL
C
C WRITE(6,9002)
C FORMAT('I')
C HEADING FOR ELECTRON COUNT CAN BE PUT HERE
C INITIALIZE SOME INTEGERS
C NA=NX-1
C IRI=ISEED
C NI2=0
C NSPA=0
C NG200=0
C IEL=0
C M=9

```

```

MC000001
MC000002
MC000003
MC000004
MC000005
MC000006
MC000007
MC000008
MC000009
MC000010
MC000011
MC000012
MC000013
MC000014
MC000015
MC000016
MC000017
MC000018
MC000019
MC000020
MC000021
MC000022
MC000023
MC000024
MC000025
MC000026
MC000027
MC000028
MC000029
MC000030
MC000031
MC000032
MC000033
MC000034
MC000035
MC000036
MC000037
MC000038
MC000039
MC000040
MC000041
MC000042
MC000043
MC000044
MC000045

```

```

C C M IS THE UNIT NUMBER FOR THE TAPE.
C C DO 8 M1=1,NPIN
C C NPIN = 1 IN OUR CASE, IT CAN BE VARIED HOWEVER TO ALLOW FOR DIFFER-
C C ENT GROUPS OF ELECTRONS TO BE DEGRADED,
C C N=0
C C N KEEPS TRACK OF THE NUMBER OF COLLISIONS
C C DO 18 IPRI=1,NOP
C C NOP= THE NUMBER OF PRIMARIES
C C IEL=IEL+1
C C IEL KEEPS TRACK OF THE NUMBER OF PRIMARY ELECTRONS THAT HAVE
C C ALREADY BEEN DEGRADED.
C C WRITE OUT IEL IF DESIRED
C C
C C STARTING PARAMETERS
C C ZV=ZSTART
C C XV=0.0
C C YV=0.0
C C COSPA=COSI
C C PHI=0.0
C C PA=ARCOS(COSI)
C C S=0.
C C EV=EIN
C C IF(EV .LE. EMIN)GO TO 27
C C EMIN IS THE CUTOFF ENERGY.
C C IESCP=0

```

```

MC000046
MC000047
MC000048
MC000049
MC000050
MC000051
MC000052
MC000053
MC000054
MC000055
MC000056
MC000057
MC000058
MC000059
MC000060
MC000061
MC000062
MC000063
MC000064
MC000065
MC000066
MC000067
MC000068
MC000069
MC000070
MC000071
MC000072

```

14 JULY 1978 NERDC --- CARD LIST UTILITY

MC000073  
 MC000074  
 MC000075  
 MC000076  
 MC000077  
 MC000078  
 MC000079  
 MC000080  
 MC000081  
 MC000082  
 MC000083  
 MC000084  
 MC000085  
 MC000086  
 MC000087  
 MC000088  
 MC000089  
 MC000090  
 MC000091  
 MC000092  
 MC000093  
 MC000094  
 MC000095  
 MC000096  
 MC000097  
 MC000098  
 MC000099  
 MC000100  
 MC000101  
 MC000102  
 MC000103  
 MC000104  
 MC000105  
 MC000106  
 MC000107  
 MC000108  
 MC000109  
 MC000110  
 MC000111  
 MC000112  
 MC000113  
 MC000114  
 MC000115  
 MC000116  
 MC000117

```

T=0.0
C THIS T=0.0 IS INITIALIZED HERE SO THAT THE STATEMENT
C IF(T.LT.TMIN)GO TO 27 CAN WORK, OTHERWISE THE T WOULD BE
C GREATER THAN TMIN FOR MORE CASES THAN DESIRED
C WRITE(M)N12
C WRITE(M)N12
C ARGC=1.-COSPA*COSPA
C IF(ARGC.LT.0.0E0)GO TO 8989
C SINPA=SQRT(ARGC)
C GO TO 8980
C SINPA=0.0E0
C CONTINUE
C SINPHI=SIN(PHI)
C COSPHI=COS(PHI)

C IF(VEV.GE.EMSD)GO TO 7139
C WE GO HERE WHEN THE ELECTRON ENERGY IS LESS THAN EMSD
C CALL RANDU
C IR1=IR2
C R1=R
C CALL RANDU
C IR1=IR2
C R2=R
C CALL RANDU
C IR1=IR2
C R3=R
C CALL RANDU
C IR1=IR2
C R4=R
C CALL RANDU
C IR1=IR2
C R5=R
C CALL MESD
C GO TO 2213
C CONTINUE

7139
C
C CALCULATE PATHLENGTH RT HERE
C CALL RANDU
C IR1=IR2
C CALL ZVAL
C ZVN IS CALCULATED IN ZVAL.

```





MC000190  
 MC000191  
 MC000192  
 MC000193  
 MC000194  
 MC000195  
 MC000196  
 MC000197  
 MC000198  
 MC000199  
 MC000200  
 MC000201  
 MC000202  
 MC000203  
 MC000204  
 MC000205  
 MC000206  
 MC000207  
 MC000208  
 MC000209  
 MC000210  
 MC000211  
 MC000212  
 MC000213  
 MC000214  
 MC000215  
 MC000216

```

771 GO TO 761
761 CALL PHFEL
      SINPAN=SQRT(1.-COSPAN*COSPAN)
      COSPLF=COSPA*COSPAN-SINPA*SINPAN*COSA ZA
      IF(COSPLF.GT.0.999) COSPLF=0.999
      IF(COSPLF.LT.-0.999) COSPLF=-0.999
      ARGC=1.-COSPLF*COSPLF
      IF(ARGC.LT.0.0E0)GO TO 8979
      SINPLF=SQRT(ARGC)
      GO TO 8970
      SINPLF=1.0E-6
      CONTINUE
      PLF=ARCOS(COSPLF)
      IF(COSPLF.LE.0.99) GO TO 20
      ALF=0.0
      GO TO 21
      COSALF=(COSPA*COSPHI*SINPAN*COSA ZA-SINPHI*SINPAN*SINA ZA+
20 1 SINPA*COSPHI*COSPAN)/SINPLF
      1 SINALF=(COSPA*SINPHI*SINPAN*COSA ZA+COSPHI*SINPAN*SINA ZA
      +SINPA*SINPHI*COSPAN)/SINPLF
      IF(COSALF.LT.-0.999)COSALF=-0.999
      IF(COSALF.GT.0.999)COSALF=0.999
      ALF=ARCOS(COSALF)
      IF(SINALF.LT.0.0) ALF=6.283185-ALF
      21 CONTINUE
      COSPA=COSPLF
      PHI=ALF

```

14 JULY 1978 NERDC --- CARD LIST UTILITY

```

2213 PA=PLF
      CONTINUE
      IF(NCHE .EQ. NSCS)WLOSS=EV*(1.-COSPA)*7.776E-5
C   COMPUTE ENERGY LOSS DURING AN ELASTIC COLLISION.
      WRITE(M)NSTAT,WLOSS
C   WRITE(M)NSTAT,WLOSS
      IF(NIE(NSTAT) .EQ. 2)WRITE(M)T
C   WRITE(M)T
      EVN=EV-WLOSS
      IF(NIE(NSTAT) .EQ. 2) EVN=EVN-T
      ZV=ZVN
      XV=XVN
      YV=YVN
C   WRITE(M)XV,YV,ZV,EVN,PA,PHI,NG200,EV
      WRITE(M)XV,YV,ZV,EVN,PA,PHI,NG200,EV
      N=N+1
      EV=EVN
      IF(ZV .GT. ZALT(1)) GO TO 801
      IF(ZV .LT. ZALT(NAR))GO TO 801
      IF(NG200.EQ.2)GO TO 27
      IF(NG200.EQ.1)GO TO 31
C   IF NG200=0 THEN THERE IS A PRIMARY COLLISION
C   IF NG200=1 THEN THERE IS A SECONDARY COLLISION
C   IF NG200=2 THEN THERE IS A TERTIARY COLLISION
      IF(T .LT. TMIN) GO TO 27
C   TMIN IS THE CUTOFF FOR THE SECONDARIES
C   IF T IS GREATER THAN TMIN THEN WE DEGRADE IT OTHERWISE WE DO NOT.
      NG200=1
C
C   SAVE THE PRIMARY PARAMETERS
      EVSAV=EV
      EV=T
      CPSAV=COSPA
      PASAV=PA
      PHISV=PHI
      XVSV=XV
      YVSV=YV
      ZVSV=ZV
C
C   CALCULATE THE SECONDARY ELECTRON SCATTERING
      CALL RANDU
      IR1=IR2
      CALL SDIFM

```

```

MC000217
MC000218
MC000219
MC000220
MC000221
MC000222
MC000223
MC000224
MC000225
MC000226
MC000227
MC000228
MC000229
MC000230
MC000231
MC000232
MC000233
MC000234
MC000235
MC000236
MC000237
MC000238
MC000239
MC000240
MC000241
MC000242
MC000243
MC000244
MC000245
MC000246
MC000247
MC000248
MC000249
MC000250
MC000251
MC000252
MC000253
MC000254
MC000255
MC000256
MC000257
MC000258
MC000259
MC000260
MC000261

```

MC000262  
MC000263  
MC000264  
MC000265  
MC000266  
MC000267  
MC000268  
MC000269  
MC000270  
MC000271  
MC000272  
MC000273  
MC000274  
MC000275  
MC000276  
MC000277  
MC000278  
MC000279  
MC000280  
MC000281  
MC000282  
MC000283  
MC000284  
MC000285  
MC000286  
MC000287  
MC000288

```

COSPLF=COSPA*COSPAN-SINPA*SINPAN*COSAZA
IF(COSPLF.GT.0.999)COSPLF=0.999
IF(COSPLF.LT.-0.999)COSPLF=-0.999
ARGC=1.-COSPLF*COSPLF
IF(ARGC.LT.0.0E0)GO TO 6979
SINPLF=SQRT(ARGC)
GO TO 6970
6979 SINPLF=1.0E-6
6970 CONTINUE
PLF=ARCOS(COSPLF)
IF(COSPLF.LE.0.99)GO TO 60
ALF=0.0
GO TO 61
60 COSALF=(COSPA*COSPAN*SINPA*SINPAN*COSAZA-SINPHI*SINPAN*SINAZA+
1 SINPA*COSPAN*COSPAN)/SINPLF
1 SINALF=(COSPA*SINPHI*SINPAN*COSAZA+COSPAN*SINPAN*SINAZA
+SINPA*SINPHI*COSPAN)/SINPLF
IF(COSALF.LT.-0.999)COSALF=-0.999
IF(COSALF.GT.0.999)COSALF=0.999
ALF=ARCOS(COSALF)
IF(SINALF.LT.0.0)ALF=6.283185-ALF
61 CONTINUE
COSPAN=COSPLF
PHI=ALF
PA=PLF
GO TO 27
C

```

14 JULY 1978 NERDC --- CARD LIST UTILITY

```

C
C
31 IF(T *LT. TMIN)GO TO 27
C TMIN IS CUTOFF OF THE TERTIARIES
C NG200=2
C SAVE THE SECONDARY PARAMETERS
  EVSAVS=EV
  EV=T
  CPSAVS=COSPA
  PASAVS=PA
  PHISVS=PHI
  XVSVS=XV
  YVSVS=YV
  ZVSVS=ZV
C CALCULATE THE TERTIARY ELECTRON SCATTERING
  CALL RANDU
  IR1=IR2
  CALL SDIFM
  COSPLF=COSPA*COSPA*COSPAN-SINPA*SINPAN*COSAZA
  IF(COSPLF *GT. 0.999) COSPLF=0.999
  IF(COSPLF *LT. -0.999) COSPLF=-0.999
  ARGC=1.-COSPLF*COSPLF
  IF(ARGC *LT. 0.0E0)GO TO 5979
  SINPLF=SQRT(ARGC)
  GO TO 5970
  SINPLF=1.0E-6
  CONTINUE
5979 PLF=ARCCOS(COSPLF)
5970 IF(COSPLF *LE. 0.99) GO TO 70
  ALF=0.0
  GO TO 71
  COSALF=(COSPA*COSPHI*SINPAN*COSAZA-SINPHI*SINPAN*SINAZA+
1 SINPA*COSPHI*COSPAN)/SINPLF
1 SINALF=(COSPA*SINPHI*SINPAN*COSAZA+COSPHI*SINPAN*SINAZA
  +SINPA*SINPHI*COSPAN)/SINPLF
  IF(COSALF *LT. -0.999)COSALF=-0.999
  IF(COSALF *GT. 0.999)COSALF=0.999
  ALF=ARCCOS(COSALF)
  IF(SINALF *LT. 0.0) ALF=6.283185-ALF
71 CONTINUE
  COSPA=COSPLF
  PHI=ALF
  PA=PLF
C
C

```

```

MC000289
MC000290
MC000291
MC000292
MC000293
MC000294
MC000295
MC000296
MC000297
MC000298
MC000299
MC000300
MC000301
MC000302
MC000303
MC000304
MC000305
MC000306
MC000307
MC000308
MC000309
MC000310
MC000311
MC000312
MC000313
MC000314
MC000315
MC000316
MC000317
MC000318
MC000319
MC000320
MC000321
MC000322
MC000323
MC000324
MC000325
MC000326
MC000327
MC000328
MC000329
MC000330
MC000331
MC000332
MC000333

```

MC000334  
 MC000335  
 MC000336  
 MC000337  
 MC000338  
 MC000339  
 MC000340  
 MC000341  
 MC000342  
 MC000343  
 MC000344  
 MC000345  
 MC000346  
 MC000347  
 MC000348  
 MC000349  
 MC000350  
 MC000351  
 MC000352  
 MC000353  
 MC000354  
 MC000355  
 MC000356  
 MC000357  
 MC000358  
 MC000359  
 MC000360

```

C 27      IF(EV .GT. EMIN)GO TO 16
          IF(NG200 .EQ. 0)GO TO 29
          EVD=EV
          ZVD=ZV
C
C
C 39      IF(NG200.EQ.1)GO TO 33
          NOW DEGRADE THE SECONDARY
          EV=EVSAYS
          COSPA=CPSAVS
          PA=PASAVS
          PHI=PHISVS
          XV=XVSVS
          YV=YVSVS
          ZV=ZVSVS
          NG200=1
          IF(IESCP .EQ. 1)GO TO 16
          NI2=1
          WRITE(M)NI2
          WRITE(M)EVD,ZVD
          N=N+1
          NI2=0
          GO TO 16
C
C

```

14 JULY 1978 NERDC --- CARD LIST UTILITY

```

C 33 IF(NG200 .EQ. 0)GO TO 29
C C
C C NOW DEGRADE THE PRIMARY
EV=EVSAV
COSPA=CPSAV
PA=PA SAV
PHI=PHISV
XV=XVSV
YV=YVSV
ZV=ZVSV
IF(IESCP .EQ. 1)GO TO 37
N12=1
WRITE(M)N12
WRITE(M)N12
C IF N12=1 THEN THE PRIMARY OR SECONDARY HAS SLIPPED BELOW EMIN AND
C NEEDS TO BE ACCOUNTED FOR
C IF N12=0 THEN THE PRIMARY OR SECONDARY BEING DEGRADED IS ABOVE EMIN
C WRITE(M)EVD,ZVD
WRITE(M)EVD,ZVD
N=N+1
N12=0
IF(NG200 .EQ. 0)GO TO 18
37 NG200=0
GO TO 16
C C
C C THE PRIMARY OR SECONDARY HAS ESCAPED IF WE REACH HERE
801 WRITE(6,650) ZV,EV
650 FORMAT(,' THE ELECTRON HAS ESCAPED AT ALTITUDE=',1PE12.3,
1 4X,' WITH AN ENERGY=',1PE14.6)
C IESCP=1
IF(NG200 .NE. 0)GO TO 39
18 CONTINUE
655 WRITE(6,655)N
8 FORMAT(,' THE TOTAL NUMBER OF COLLISIONS FOR ALL ELECTRONS=',I12)
8 CONTINUE
483 WRITE(6,483)IR1,IR2
RETURN
END
MC000361
MC000362
MC000363
MC000364
MC000365
MC000366
MC000367
MC000368
MC000369
MC000370
MC000371
MC000372
MC000373
MC000374
MC000375
MC000376
MC000377
MC000378
MC000379
MC000380
MC000381
MC000382
MC000383
MC000384
MC000385
MC000386
MC000387
MC000388
MC000389
MC000390
MC000391
MC000392
MC000393
MC000394
MC000395
MC000396
MC000397
MC000398
MC000399
MC000400
MC000401
MC000402
MC000403

```

14 JULY 1978 NERDC --- CARD LIST UTILITY

MESD00001  
MESD00002  
MESD00003  
MESD00004  
MESD00005  
MESD00006  
MESD00007  
MESD00008  
MESD00009  
MESD00010  
MESD00011  
MESD00012  
MESD00013  
MESD00014  
MESD00015  
MESD00016  
MESD00017  
MESD00018  
MESD00019  
MESD00020  
MESD00021  
MESD00022  
MESD00023  
MESD00024  
MESD00025  
MESD00026  
MESD00027  
MESD00028  
MESD00029  
MESD00030  
MESD00031  
MESD00032  
MESD00033  
MESD00034  
MESD00035  
MESD00036  
MESD00037  
MESD00038  
MESD00039  
MESD00040  
MESD00041  
MESD00042  
MESD00043  
MESD00044  
MESD00045

```

SUBROUTINE MESD
  SUBROUTINE MESD ***
  THIS SUBROUTINE IS ACCESSED THROUGH MC.
  THIS SUBROUTINE CALCULATES THE COORDINATES RESULTING FROM THE
  MULTIPLE ELASTIC SCATTERING OF AN ELECTRON BETWEEN INELASTIC
  COLLISIONS.
  THE FOLLOWING SUBROUTINE IS CALLED HERE:
  1)COLTYP
  COMMON ALPE(6),BETE(6),CE(6),FE(6),WE(6),ALFA(15),BEFA(15),
  1 CFA(15),FFA(15),WFA(15),WFI(15),FACI(15),NFA,NAR,SA(3,80),
  2 ZALT(80),ENR(30),PCFA(3,30),WCFA(3,30),NENR,FDG(3),PSE(3),
  3 PION(3),AT(3),A(6,3),B(5,3),G(5,3),UH(10),UI(10),UJ(10),
  4 UD(10),USNU(10),USF(10),UEIN(11),IUTP,IUTM1,DG(3),NSG(3),NIG(3),
  5 NUMGAS,NUMST,WIS(50),NSEC,MUNIT,I SEED,I LAST,EIN,NPRI M,COSI,
  6 H,EMIN,ZSTART,TMIN,THRESH(3),AK(2,3),AJ(3,3),GAMA(2,3),
  7 TD(3,3),FAC(6),AOE(6),AIE(6),BOE(6),BIE(6),COE(6),DOE(6),
  8 DIE(6),PROB(40),W(40),NIE(40),A21(3),A22(3),A31(3),A32(3),
  9 A33(3),B11(3),B12(3),B13(3),C1(3),C21(3),C22(3),C31(3),
  A C32(3),D1(3),D2(3),F1(3),F2(3),THRI(16),AKI(2,16),AJI(3,16),
  B GAMAI(2,16),TOI(3,16),SIGT(6),THET(40),NX,CSIE(20),EIT(20),
  C IEILS,IEILM1,P,R,ZDIS,NPIN,NOP,COSPA,RT,F(40),R1,R2,R3,R4,
  D R5,XV,YV,ZV,XVN,YVN,ZVN,PA,PHI,EV,WLOSS,NSTAT,NSCS,NPHF,
  E IRI,IR2,NG,EVPRI,RAN,EMSD,EINEL,EXCS(50),COSPAN,T,FOVAL
  CALL CRSEC
  RT=SIGT(2)/SIGT(1)
  PL=ALOG(R1)*RT
  PL IS THE PATH LENGTH IN MEAN FREE PATH LENGTHS
  J=0
  DO 1 I=1,IUTM1
  J=J+1
  IPI=I+1
  IF(EV.GE. UEIN(I),AND, EV.LE. UEIN(IPI))GO TO 2
  CONTINUE
  UMU=(UH(J)+PL**UI(J))/PL**UJ(J)
  FO=FOVAL
  IF(PL.LT. 500.0)FO=FOVAL*(1.-EXP(-(PL/USF(J))*0.75))
  UNU=1.
  CH3=(PL/USNU(J))*UD(J)
  IF(CH3.LT. 1.0E-5)GO TO 3
  IF(PL.LT. 25.0)UNU=1.-EXP(-(PL/USNU(J))*UD(J))
  GO TO 4
  UNU=1.0E-5
  UNUIN=1./UNU
  CH1=UNUIN*ALOG(R2)
  CH2=UNUIN*ALOG(F0)

```

MESD00046  
 MESD00047  
 MESD00048  
 MESD00049  
 MESD00050  
 MESD00051  
 MESD00052  
 MESD00053  
 MESD00054  
 MESD00055  
 MESD00056  
 MESD00057  
 MESD00058  
 MESD00059  
 MESD00060  
 MESD00061  
 MESD00062  
 MESD00063  
 MESD00064  
 MESD00065  
 MESD00066  
 MESD00067  
 MESD00068  
 MESD00069  
 MESD00070  
 MESD00071  
 MESD00072

```

ANUM=-1.0
ADEN=-1.0
IF(CH1.GT.-55.0)ANUM=R2**UNUIN-1.0
IF(CH2.GT.-55.0)ADEN=F0**UNUIN-1.0
Z=-ALOG(ANUM/ADEN)/UMU
C Z IS IN MEAN FREE PATHS
SIGEE=SIGT(1)+SIGT(2)
FMFP=1./SIGEE/SA(1,1)/1.E-16
C FMFP IS IN CM.
ZADD=Z*FMFP*1.E-5
C ZADD IS IN KM.
ZVN=ZV+ZADD
C CALCULATE THE Z COORDINATE
PA=3.141592*R4
PHI=6.283185*R5
GAM=2.0
IF(PL.LT.400.)GAM=2.0*(1.-EXP(-PL/4.))
DEL=(22.+SQRT(PL/0.3))/(PL+0.3)**1.5
RHO=0.0
IF(GAM.GT.0.2)RHO=(-ALOG(1.-R4)/DEL)**(1./GAM)
XADD=COS(PHI)*RHO*FMFP*1.E-5
YADD=SIN(PHI)*RHO*FMFP*1.E-5
XVN=XV+XADD
YVN=YV+YADD
C CALCULATE THE X AND Y COORDINATES.
P=0.0
PSE(1)=0.0

```



14 JULY 1978 NERDC --- CARD LIST UTILITY

```

C SUBROUTINE PETI
C SUBROUTINE IS ACCESSED THROUGH MC.
C THIS SUBROUTINE CALCULATES THE ENERGY OF THE SECONDARY ELECTRON
C AFTER AN IONIZATION EVENT.
1 CFA(15),FFA(15),WFA(15),WFI(15),FACI(15),NFA,NAR,SA(3,80),
2 ZALT(80),ENR(30),PCFA(3,30),WCFA(3,30),NENR,FDG(3),PSE(3),
3 PION(3),AT(3),A(6,3),B(5,3),G(5,3),UH(10),UI(10),UJ(10),
4 UQ(10),USNU(10),USF(10),UEIN(11),IUTP,IUTMI,DG(3),NSG(3),NIG(3),
5 NUMGAS,NUMST,WIS(50),NSEC,MUNIT,I SEED,I STOP,I LAST,EIN,NPRIM,COSI,
6 H,EMIN,ZSTART,TMIN,THRESH(3),AK(2,3),AJ(3,3),GAVA(2,3),
7 TQ(3,3),FAC(6),AOE(6),AIE(6),BOE(6),BIE(6),COE(6),DOE(6),
8 DIE(6),PROB(40),W(40),NIE(40),A21(3),A22(3),A31(3),A32(3),
9 A33(3),B11(3),B12(3),B13(3),C1(3),C21(3),C22(3),C31(3),
A C32(3),D1(3),D2(3),F1(3),F2(3),THRI(16),AKI(2,15),AJI(3,16),
B GAMAI(2,16),TDI(3,16),SIGT(6),THET(40),NX,CSIE(20),FIT(20),
C IEILS,IEILM1,P,R,ZDIS,NPIN,NOP,CDSPA,RT,F(40),R1,R2,R3,R4,
D RS,XV,YV,ZV,XVN,YVN,ZVN,PA,PHI,EV,WLOSS,NSTAT,NSCS,NPHF,
E I R1,IR2,NG,EVPRI,RAN,EMSD,EINEL,EXC5(50),COSPAN,T,FOVAL

C
E=EV
RN=R
N=NG
TSET=TO(1,N)-TO(2,N)/(E+TO(3,N))
GSET=GAMA(1,N)*E/(E+GAMA(2,N))
TM=(E-THRESH(N))/2,
TN1P=ATAN2((TM-TSET),GSET)
TN2P=ATAN2(TSET,GSET)
TN1=TAN(RN*TN1P+(RN-1.)*TN2P)
T=GSET*TN1 + TSET
C T IS THE KINETIC ENERGY OF THE SECONDARY ELECTRON.
RETURN
END
PETI0001
PETI0002
PETI0003
PETI0004
PETI0005
PETI0006
PETI0007
PETI0008
PETI0009
PETI0010
PETI0011
PETI0012
PETI0013
PETI0014
PETI0015
PETI0016
PETI0017
PETI0018
PETI0019
PETI0020
PETI0021
PETI0022
PETI0023
PETI0024
PETI0025
PETI0026
PETI0027
PETI0028
PETI0029
PETI0030
PETI0031
PETI0032
PETI0033
PETI0034
PETI0035

```

14 JULY 1978 NERDC --- CARD LIST UTILITY

```

SUBROUTINE PHF PHF ***
THIS SUBROUTINE IS ACCESSED THROUGH MC.
THIS SUBROUTINE HELPS CALCULATE THE POLAR ANGLE OF SCATTERING
AS A RESULT OF AN ELASTIC COLLISION.
ANY PHASE FUNCTION FORM MAY BE PLACED HERE.
RIGHT NOW MODEL 3 IS EXPRESSED HERE.
THIS SUBROUTINE IS MAINLY FOR PHASE FUNCTIONS WHICH ARE NOT
EASILY INTEGRATED AND SOLVED FOR THE POLAR ANGLE OF SCATTERING.
COMMON ALPE(6),BETE(6),CE(6),FE(6),WE(6),ALFA(15),BEFA(15),
1 CFA(15),FFA(15),WFA(15),WFA(15),FACI(15),NFA,NAR,SA(3,80),
2 ZALT(80),ENR(30),PCFA(3,30),WCFA(3,30),NENR,FDG(3),PSE(3),
3 PION(3),AT(3),A(6,3),B(5,3),G(5,3),UH(10),UI(10),UJ(10),
4 UD(10),USNU(10),USF(10),UEIN(11),IUTP,IUTMI,DG(3),NSG(3),NIG(3),
5 NUMGAS,NUMST,WIS(50),NSEC,MUNIT,I SEED,I STOP,I LAST,EIN,NPRIM,COSI,
6 H,EMIN,ZSTART,TMIN,THRESH(3),AK(2,3),AJ(3,3),GAMA(2,3),
7 TO(3,3),FAC(6),AOE(6),AIE(6),BOE(6),BIE(6),CJE(6),DOE(6),
8 DIE(6),PROB(40),W(40),NIE(40),A21(3),A22(3),A31(3),A32(3),
9 A33(3),B11(3),B12(3),B13(3),C1(3),C21(3),C22(3),C31(3),
A A32(3),D1(3),D2(3),F1(3),F2(3),THRI(16),AKI(2,16),AJI(3,16),
B GAMA I(2,16),TOI(3,16),SIGT(6),THET(40),NX,CSIE(20),EIT(20),
C IEILS,IEILM,P,R,ZDIS,NPIN,NOP,COSPA,RT,F(40),R1,R2,R3,R4,
D RE5,XV,YV,ZV,XVN,YVN,ZVN,PA,PHI,EV,WLDSS,NSTAT,NSCS,NPHF,
E I R1, I R2, N G, E V P R I, R A N, E M S D, E I N E L, E X C 5 ( 5 0 ), C O S P A N, T, F O V A L

```

PHF00001  
PHF00002  
PHF00003  
PHF00004  
PHF00005  
PHF00006  
PHF00007  
PHF00008  
PHF00009  
PHF00010  
PHF00011  
PHF00012  
PHF00013  
PHF00014  
PHF00015  
PHF00016  
PHF00017  
PHF00018  
PHF00019  
PHF00020  
PHF00021  
PHF00022  
PHF00023  
PHF00024  
PHF00025  
PHF00026  
PHF00027  
PHF00028  
PHF00029  
PHF00030  
PHF00031  
PHF00032  
PHF00033  
PHF00034  
PHF00035  
PHF00036  
PHF00037  
PHF00038  
PHF00039  
PHF00040  
PHF00041  
PHF00042  
PHF00043  
PHF00044  
PHF00045

```

E=EV
FT=(E/10.)**(.5)
FM=FT/(FT+.87)
C=1.27*(1.-(12./E))*+.27)
O2=0.43*E*(-0.29)
QT=(E/100.)**(.84)
Q1=OT/(OT+1.92)
AA=0.11
FC=1.-O1
FCP=0. JE0
IF(E .LT. 200.)FC=FC*FM
IF(E .LT. 200.)FCP=1.-O1-FC
FF1=FC/(1.+(2.+AA)-1./AA)
FF2=FCP/(1.+(2.+C)-1./C)
AL=1./AA
CL=1./(C+2.)
NXM1=NX-1
DO 1 I=2,NXM1
TU=COS(THET(I))

```

PHF00046  
PHF00047  
PHF00048  
PHF00049  
PHF00050  
PHF00051  
PHF00052  
PHF00053  
PHF00054  
PHF00055  
PHF00056  
PHF00057  
PHF00058

```
1 AU=1./(1.+AA-TU)
  CU=1./(1.+C+TU)
  RLU=1.-EXP(-THET(I)/Q2)*(SIN(THET(I))/Q2+COS(THET(I)))
  F3=Q1/(1.+EXP(-3.*1416/Q2))
  F3R=F3*RLU
  F(I)=FF1*(AU-AL)-FF2*(CU-CL)+F3R
  CONTINUE
  F(I)=0.0
  F(NX)=1.0
  C THE ARRAY F(I) OF PROBABILITIES FOR SCATTERING IN CERTAIN ANGULAR
  C REGIMES HAS BEEN SET,
  RETURN
  END
```



14 JULY 1978 NERDC --- CARD LIST UTILITY

```

C C SUBROUTINE RANDU ***
C C THIS SUBROUTINE IS ACCESSED THROUGH MC.
C C THIS SUBROUTINE CALCULATES THE RANDOM NUMBERS WHOSE VALUES ARE
C C BETWEEN 0.0 AND 1.0.
C C RANDOM NUMBER GENERATOR (SEE IBM 360 SSP DESCRIPTION)
C C COMMON ALPE(6),BETE(6),CE(6),FE(6),WE(6),ALFA(15),BEFA(15),
1 CFA(15),FFA(15),WFA(15),WF(15),FAC(15),NFA,NAR,SA(3,80),
2 ZALT(80),ENR(30),PCFA(3,30),WCFA(3,30),NENR,FDG(3),PSE(3),
3 PIDN(3),AT(3),A(6,3),B(5,3),G(5,3),UH(10),UI(10),UJ(10),
4 UD(10),USNU(10),USE(10),UEIN(11),IUTP,IUTM,DG(3),NSG(3),NIG(3),
5 NUMGAS,NUMST,WIS(50),NSEC,MUNIT,ISEED,ISTOP,ILAST,EIN,NPRIM,COSI,
6 H,EMIN,ZSTART,TMIN,THRESH(3),AK(2,3),AJ(3,3),GAMA(2,3),
7 TO(3,3),FAC(6),AOE(6),ALE(6),BOE(6),BIE(6),COE(6),DOE(6),
8 DIE(6),PROB(40),W(40),NIE(40),A21(3),A22(3),A31(3),A32(3),
9 A33(3),B11(3),B12(3),B13(3),C1(3),C21(3),C22(3),C31(3),
A C32(3),D1(3),D2(3),F1(3),F2(3),THRI(16),AKI(2,16),AJI(3,16),
B GAMAI(2,16),TOI(3,16),SIGT(6),THET(40),NX,CSIE(20),EIT(20),
C IEILS,IEILM1,P,R,ZDIS,NPIN,NOP,CO SPA,RT,F(40),R1,R2,R3,R4,
D R5,XV,YV,ZV,XVN,YVN,ZVN,PA,PHI,EV,WLOSS,NSTAT,NSCS,NPHF,
E IR1,IR2,NG,EVPRI,RAN,EMSD,EINEL,EXC5(50),COSPAN,T,FOVAL

C C YFL AND R ARE THE RANDOM NUMBERS.
C C IX=IR1
C C IY=IX#65539
C C IF(IY) 5,6,6
5 IY=IY+2147483647+1
6 YFL=IY
YFL=YFL*.4656613E-9
IR2=IY
R=YFL
RETURN
END

```

```

RANDU001
RANDU002
RANDU003
RANDU004
RANDU005
RANDU006
RANDU007
RANDU008
RANDU009
RANDU010
RANDU011
RANDU012
RANDU013
RANDU014
RANDU015
RANDU016
RANDU017
RANDU018
RANDU019
RANDU020
RANDU021
RANDU022
RANDU023
RANDU024
RANDU025
RANDU026
RANDU027
RANDU028
RANDU029
RANDU030
RANDU031
RANDU032
RANDU033

```

14 JULY 1978 NERDC --- CARD LIST UTILITY

```

SUBROUTINE SDIFM ***
THIS SUBROUTINE IS ACCESSED THROUGH MC.
THIS SUBROUTINE CALCULATES THE POLAR ANGLE OF SCATTERING OF THE
SECONDARY ELECTRON.
  1 CFA(15),FFA(15),WFA(15),WF(15),FACI(15),NFA,NAR,SA(3,80),
  2 ZALT(80),ENR(30),PCFA(3,30),WCFA(3,30),NENR,FDG(3),PSE(3),
  3 PION(3),AT(3),A(6,3),B(5,3),G(5,3),UH(10),UI(10),UJ(10),
  4 UD(10),USNU(10),USF(10),UEIN(11),IUTP,IUTM,DG(3),NSG(3),NIG(3),
  5 NUMGAS,NUMST,WIS(50),NSEC,MUNIT,I SEED,I STOP,I LAST,EIN,NPRIM,COSI,
  6 H,EMIN,ZSTART,TMIN,THRESH(3),AK(2,3),AJ(3,3),GAMA(2,3),
  7 TO(3,3),FAC(6),AOE(6),AIE(6),BOE(6),BIE(6),COE(6),DOE(6),
  8 DIE(6),PROB(40),W(40),NIE(40),A21(3),A22(3),A31(3),A32(3),
  9 A33(3),B11(3),B12(3),B13(3),C1(3),C21(3),C22(3),C31(3),
  A C32(3),D1(3),D2(3),F1(3),F2(3),THRI(16),AKI(2,16),AJI(3,16),
  B GAMA1(2,16),TDI(3,16),SIGT(6),THET(40),NX,CSIE(20),EIT(20),
  C I EILS,I EILM1,P,R,ZDIS,NPIN,NDP,CUSPA,RT,F(40),R1,R2,R3,R4,
  D R5,XV,YV,ZV,XVN,YVN,ZVN,PA,PHI,EV,WLOSS,NSTAT,NSCS,NPHF,
  E I R1,IR2,NG,EVPRI,RAN,EMSD,EINEL,EXCS(50),COSPAN,T,FOVAL

E=EVPRI
D=D1(NG)/(T+D2(NG))
D IS THE C(T) IN THE SEC. DIF. FORM.
BB=B11(NG)+(E/B12(NG))*B13(NG)
B IS THE B(E) IN THE SEC. DIF. FORM.
C2=C21(NG)+C22(NG)*E
C2 IS THE THETA SUBSCRIPT A (E)
C3=C31(NG)+C32(NG)*E
C3 IS THE THETA SUBSCRIPT B (E)
SQB=SQRT(BB)
TH0=C1(NG)+C2/(T+C3)
CST=COS(TH0)
FTN=SQB*(-1.-CST)
STN=SQB*(1.-CST)
TMNM=ATAN2(FTN,D)-ATAN2(STN,D)
SLI=ATAN2(STN,D)
RATAN=R*TMNM+SLI
TM1=D*ATAN(RATAN)/SQB
COSPAN=TM1+CST
PAN IS THE POLAR SCATTERING ANGLE.
PAN=ARCOS(COSPAN)
IF(PAN.GT.3.1416)PAN=PI-3.1416
RETURN

```

```

SDIFM001
SDIFM002
SDIFM003
SDIFM004
SDIFM005
SDIFM006
SDIFM007
SDIFM008
SDIFM009
SDIFM010
SDIFM011
SDIFM012
SDIFM013
SDIFM014
SDIFM015
SDIFM016
SDIFM017
SDIFM018
SDIFM019
SDIFM020
SDIFM021
SDIFM022
SDIFM023
SDIFM024
SDIFM025
SDIFM026
SDIFM027
SDIFM028
SDIFM029
SDIFM030
SDIFM031
SDIFM032
SDIFM033
SDIFM034
SDIFM035
SDIFM036
SDIFM037
SDIFM038
SDIFM039
SDIFM040
SDIFM041
SDIFM042
SDIFM043
SDIFM044
SDIFM045

```

SDIFM046

END

14 JULY 1978 NERDC --- CARD LIST UTILITY

```

SUBROUTINE ZVAL
  SUBROUTINE IS ACCESSED THROUGH MC.
  THIS SUBROUTINE CALCULATES THE PATH LENGTH TO THE COLLISION AND
  THE LONGITUDINAL DISTANCE TO THE COLLISION.
  THE FOLLOWING SUBROUTINE IS CALLED HERE:
  1) CRSEC
     COMMON ALPE(6),BETE(6),CE(6),FE(6),WE(6),ALFA(15),BEFA(15),
     CFA(15),FFA(15),WFA(15),WF(15),FACI(15),NFA,NAR,SA(3,80),
     ZALT(80),ENR(30),PCFA(3,30),WCFA(3,30),NENR,FDG(3),PSE(3),
     3 PION(3),AT(3),A(6,3),B(5,3),G(5,3),UH(10),UI(10),UJ(10),
     UD(10),USNU(10),USF(10),UEIN(11),IUTP,IUTM,DG(3),NSG(3),NIG(3),
     5 NUMGAS,NUMST,WIS(50),NSEC,MUNIT,ISEED,ISTOP,ILAST,EIN,NPRIM,COSI,
     H,EMIN,ZSTART,TMIN,THRESH(3),AK(2,3),AJ(3,3),GAMA(2,3),
     7 TO(3,3),FAC(6),AOE(6),ALE(6),BOE(6),BIE(6),COE(6),DOE(6),
     8 DIE(6),PROB(40),W(40),NIE(40),A21(3),A22(3),A31(3),A32(3),
     9 A33(3),B11(3),B12(3),B13(3),C1(3),C21(3),C22(3),C31(3),
     A C32(3),D1(3),D2(3),F1(3),F2(3),THRI(10),AKI(2,16),AJI(3,16),
     B GAMAI(2,16),TOI(3,16),SIGT(6),THET(40),NX,CSIE(20),EIT(20),
     C IEILS,IEILM1,P,R,ZDIS,NPIN,NOP,COSPA,RT,F(40),R1,R2,R3,R4,
     D R5,XV,YV,ZV,XVN,YVN,ZVN,PA,PHI,EV,WLOSS,NSTAT,NSCS,NPHF,
     E IRI,IR2,NG,EVPRI,RAN,EMSD,EINEL,EXC5(50),COSPAN,T,FOVAL

R=1.-R
AC=ABS(COSPA)
STUN=1.E-16
FRAC=0.0
ZCHE=ZV
ZADD=ZCHE*1.E-5
ZCHE=ZCHE-ZADD
J=1
IF(PA.GT.1.5708) J=NAR
ZDIS=0.0
DG(1)=SA(1,1)
CALL CRSEC
DO 45 IDS=1,NUMGAS
  JU=2*IDS
  JL=JU-1
  SUM=0.0
  DO 45 JDS=JL,JU
    SUM=SUM + DG(IDS)*SIGT(JDS)*STUN
  CONTINUE
  RMFP=1./SUM
  RMFP IS THE MEAN FREE PATH OF THE ELECTRON IN THE MODEL ATMOSPHERE.

```

- ZVAL0001
- ZVAL0002
- ZVAL0003
- ZVAL0004
- ZVAL0005
- ZVAL0006
- ZVAL0007
- ZVAL0008
- ZVAL0009
- ZVAL0010
- ZVAL0011
- ZVAL0012
- ZVAL0013
- ZVAL0014
- ZVAL0015
- ZVAL0016
- ZVAL0017
- ZVAL0018
- ZVAL0019
- ZVAL0020
- ZVAL0021
- ZVAL0022
- ZVAL0023
- ZVAL0024
- ZVAL0025
- ZVAL0026
- ZVAL0027
- ZVAL0028
- ZVAL0029
- ZVAL0030
- ZVAL0031
- ZVAL0032
- ZVAL0033
- ZVAL0034
- ZVAL0035
- ZVAL0036
- ZVAL0037
- ZVAL0038
- ZVAL0039
- ZVAL0040
- ZVAL0041
- ZVAL0042
- ZVAL0043
- ZVAL0044
- ZVAL0045

45

ZVAL0046  
ZVAL0047  
ZVAL0048  
ZVAL0049  
ZVAL0050  
ZVAL0051  
ZVAL0052  
ZVAL0053  
ZVAL0054  
ZVAL0055  
ZVAL0056  
ZVAL0057

```
RMFP=RMFP*1.E-5  
RV=-ALOG(R)*RMFP  
RT=RV  
C RV AND RT ARE THE PATH LENGTHS TO THE COLLISION.  
RVCOS=RV*AC  
IF(PA.GT.1.5708) GO TO 7  
ZVN=ZV-RVCOS  
C ZVN IS THE NEW Z COORDINATE OF THE ELECTRON.  
RETURN  
ZVN=ZV+RVCOS  
7 RETURN  
END
```

14 JULY 1978 NERDC --- CARD LIST UTILITY

```

C SUBROUTINE DFDW(W,E,F,NSCS)
C SUBROUTINE DFDW ***
C THIS SUBROUTINE CAN BE USED TO HELP CALCULATE THE POLAR SCATTERING
C ANGLE OF THE PRIMARY ELECTRON IN AN IONIZATION EVENT.
C THIS SUBROUTINE IS NOT ACCESSED BY MC AND IS INCLUDED ONLY
C BECAUSE IT CAN BE EASILY ADAPTED TO BE ACCESSED BY MC.
C THIS SUBROUTINE CALLS THE FOLLOWING FUNCTION:
C 1)DCS
  NG=NSCS*2 - 1
  SUM2=0.0
  NA=NX-1
  IF(NX-1)44,33,11
  11 DO 22 I=2,NX
    SUM1=SUM2
    XL=THET(I-1)
    XU=THET(I)
    AA=.5*(XU+XL)
    BB=XU-XL
    CC=.4305682*BB
    Z=AA+CC
    G1=DCS(E,W,NG,Z)
    Z=AA-CC
    G2=DCS(E,W,NG,Z)
    Y=.1739274*(G1+G2)
    CC=.1699905*BB
    Z=AA+CC
    G1=DCS(E,W,NG,Z)
    Z=AA-CC
    G2=DCS(E,W,NG,Z)
    Y=BB*(Y+.3260726*(G1+G2))
    SUM2=SUM2+Y
  22 F(I-1)=SUM1
  33 F(NX)=SUM2
  44 CONTINUE
  DO 4 J=1,NX
    F(J)=F(J)/F(NX)
  CONTINUE
  F(1)=0.0
  F(NX)=1.0
C THE ARRAY F(I) OF SCATTERING PROBABILITIES WITHIN CERTAIN
C ANGULAR BINS IS ESTABLISHED.
  RETURN
  END

```

DFDW0001  
DFDW0002  
DFDW0003  
DFDW0004  
DFDW0005  
DFDW0006  
DFDW0007  
DFDW0008  
DFDW0009  
DFDW0010  
DFDW0011  
DFDW0012  
DFDW0013  
DFDW0014  
DFDW0015  
DFDW0016  
DFDW0017  
DFDW0018  
DFDW0019  
DFDW0020  
DFDW0021  
DFDW0022  
DFDW0023  
DFDW0024  
DFDW0025  
DFDW0026  
DFDW0027  
DFDW0028  
DFDW0029  
DFDW0030  
DFDW0031  
DFDW0032  
DFDW0033  
DFDW0034  
DFDW0035  
DFDW0036  
DFDW0037  
DFDW0038  
DFDW0039  
DFDW0040  
DFDW0041  
DFDW0042  
DFDW0043

NERDC --- CARD LIST UTILITY

14 JULY 1978

```

C      FUNCTION DCS(E,W,NG,Z)
C      FUNCTION DCS ***
C      THIS FUNCTION IS ACCESSED BY DFDW.
C      THIS FUNCTION AIDS IN THE CALCULATION OF THE PLAR ANGLE OF
C      SCATTERING OF THE PRIMARY ELECTRON IN AN IONIZATION EVENT.
C      THIS FUNCTION CALCULATES THE DIFFERENTIAL CROSS SECTION DCS.
C      THIS FUNCTION MUST BE CHANGED SOME TO BE USEFUL FOR IMPLEMENT
C      WITH THE MONTE CARLO PROGRAM.
      RE=13.6
      A0=.5292E-8
      PI=PION(NG)
      WP=W/PI
      ARG=WP-1.0E0
      IF(ARG .LT. 0.0E0)GO TO 20
      T=W-PI
      ALPH2=SQRT(ARG)
      GO TO 21
      ALPH2=0.0E0
      T=1.0E-8
      CONTINUE
      AT1=(T+0.1)**A(3,NG)/(T**A(2,NG) + A(1,NG)**A(2,NG))
      AT2=A(4,NG)/(A(5,NG)**A(6,NG) + T**A(6,NG))
      AT3=AT(NG)*(AT1+AT2)
      BETA1=B(1,NG)*(T+0.1)**B(4,NG)/(T**B(3,NG) + B(2,NG)**B(3,NG))
      GAM=G(1,NG)*(T+0.1)**G(4,NG)/(T**G(3,NG) + G(2,NG)**G(3,NG))
      BETA1=BETA1+B(5,NG)
      GAM=GAM+G(5,NG)
      X=2.0*E*(1.0-COS(Z))*SQRT(1.0-W/E)-W/2.0/E)/RE
      FN1=ATS*GAM**3*WP*(X+WP/3.0)
      FD1=((X-BETA1*WP)**2+4.0*GAM*X)**3
      FN2=EXP(-1.0)
      IF(ALPH2 .GT. 1.0E-6)FN2=EXP(-2.0*ATAN2(ALPH2,2.0)/ALPH2)
      FD2=1.0
      IF(ALPH2 .GT. .1)FD2=1.0-EXP(-6.2832/ALPH2)
      FOX=FN1*FN2/FD1/FD2
      DEN=4.0*A0*A0*SQRT(1.0-W/E)/W/X
      DCS=DEN*FOX*1.0E+16*SIN(Z)
C      DCS IS THE DIFFERENTIAL CROSS SECTION FOR AN ELECTRON OF ENERGY
C      LOSING ENERGY W WITH A SCATTERING OF Z (POLAR ANGLE).
      RETURN
      END

```

```

DCS00001
DCS00002
DCS00003
DCS00004
DCS00005
DCS00006
DCS00007
DCS00008
DCS00009
DCS00010
DCS00011
DCS00012
DCS00013
DCS00014
DCS00015
DCS00016
DCS00017
DCS00018
DCS00019
DCS00020
DCS00021
DCS00022
DCS00023
DCS00024
DCS00025
DCS00026
DCS00027
DCS00028
DCS00029
DCS00030
DCS00031
DCS00032
DCS00033
DCS00034
DCS00035
DCS00036
DCS00037
DCS00038
DCS00039
DCS00040
DCS00041

```

APPENDIX B  
GETDAT PROGRAM

The Getdat program is listed in this appendix. This program was written entirely by the author. This program (written in Fortran IV) collects the collision data from the magnetic tape and coalesces and systematizes it.



NERDC --- CARD LIST UTILITY

14 JULY 1978

```

C          SUBROUTINE RDCARD
C          SUBROUTINE IS ACCESSED BY THE MAIN PROGRAM.
C          THIS PROGRAM READS IN THE DATA FROM THE CARDS AND SETS UP ALL
C          THE NECESSARY INFORMATION.
C          COMMON ALAB(20),ANEI(5,20,100),ALT(20),EAVE(3),EIP(100),
1         EXC5(50),JES(50),JIS(50),JZE(3,50,80),JSEC(50,80),KREX(10,40,40),
2         NIE(40),NZX(20),NOFE(3,80),NCRO(10),RHO(40),SA(3,80),SIG(100),
3         TOTE(3,80),TNI(3,80),TNS(3,80),TN10(3,80),WIE(50),WIS(50),
4         YSPEC(100),ZNUM(10),ZALT(80),NUMGAS,NARI,NVR,NUMST,NUMG,NRM,
5         NSEC,NSPZ,NEIP,NEXC,NTOP,NAR,NSPEC,NRHO,NAVEE,NPRIM,EIN,
6         ZVAL,EMIN,DENGS,M,NSPUN,NSPR,ANER(1,10,20,100),RYS(10),NSPRO
C          READ IN THE NECESSARY DATA CARDS
C          M=9
C          M IS THE LOGICAL UNIT NUMBER FOR THE TAPE.
7         READ(5,2248)(ALAB(I),I=1,20)
C          FIRST CARD IS THE TITLE CARD.
2248      FORMAT(20A4)
2249      WRITE(6,2249)(ALAB(I),I=1,20)
          FORMAT(1,20A4,/)
          READ(5,2244)NAVEE,NRHO,NVR,NPM,NSPEC,NSPUN,NSPRO
C          IF NAVEE=1 THEN WE WANT TO CALCULATE THE AVERAGE ENERGY OF THE
C          PRIMARY AT A GIVEN DISTANCE
C          IF NRHO=1 THEN WE WANT TO CALCULATE THE DISTRIBUTION OF THE
C          EXCITATIONS AS A FUNCTION OF RHO FOR A GIVEN NVR NO. OF Z VALUES.
C          NVR IS THE NO. OF Z VALUES AT WHICH YOU WANT THE DISTRIBUTION
C          NRM IS THE NUMBER OF RHO VALUES IN THE MATRIX IN WHICH THE
C          EXCITATIONS WILL BE INPUT
C          IF NSPEC=1 THEN WE WANT TO GET OUT THE SPECTRUM OF ELECTRONS
C          IF NSPUN = 1 THEN WE WANT TO PUNCH OUT THE YIELD SPECTRUM OF THE
C          ELECTRONS.
C          IF NSPRO = 1 THEN WE WANT THE YIELD SPECTRUM AS A FUNCTION OF RHO
C          IF(NVR.EQ.0)NVR=1
C          NVR=1 FOR DEFAULT
          WRITE(6,710) NAVEE,NRHO,NVR,NRM,NSPEC,NSPUN,NSPRO
710      FORMAT(1,NAVEE=,15/,NRHO=,15/,NVR=,15/,NRM=,15/,
          * , NSPEC=,15/,NSPUN=,15/,NSPRO=,15,/)
          READ(5,2246)NEXC,NPRIM,NAR,NSEC,NUMST,NUMGAS,NEIP,NSPZ,NSPR
          FORMAT(10,14I5)
2246      NEXC IS THE TOTAL NUMBER OF COLLISIONS
C          NPRIM IS THE NUMBER OF PRIMARY ELECTRONS
C          NAR IS THE NUMBER OF ALTITUDE INTERVALS
C          NSEC IS THE NUMBER OF LOWER ELECTRON ENERGY BIN ENDS.
RDCARD01
RDCARD02
RDCARD03
RDCARD04
RDCARD05
RDCARD06
RDCARD07
RDCARD08
RDCARD09
RDCARD10
RDCARD11
RDCARD12
RDCARD13
RDCARD14
RDCARD15
RDCARD16
RDCARD17
RDCARD18
RDCARD19
RDCARD20
RDCARD21
RDCARD22
RDCARD23
RDCARD24
RDCARD25
RDCARD26
RDCARD27
RDCARD28
RDCARD29
RDCARD30
RDCARD31
RDCARD32
RDCARD33
RDCARD34
RDCARD35
RDCARD36
RDCARD37
RDCARD38
RDCARD39
RDCARD40
RDCARD41
RDCARD42
RDCARD43
RDCARD44
RDCARD45

```



NERDC --- CARD LIST UTILITY

14 JULY 1978

```

C   READ(5,2255)(ALT(I),I=1,NSPZ)
C   ALT(I) ARE THE Z VALUES AT WHICH THE YIELD SPECTRUM IS CALCULATED.
C   READ(5,2255)(RYS(I),I=1,NSPR)
C   RYS(I) ARE THE RHO VALUES AT WHICH THE YIELD SPECTRUM IS CALCULATED.
C   READ(5,2255)(EIP(I),I=1,NEIP)
C   EIP(I) ARE THE ENERGY VALUES AT WHICH THE YIELD SPECTRUM IS CALCULATED.
C   NEIP=NEIP-1
C   WRITE(6,3499)
C   FORMAT( , INDEX, 5X, 'ALT. IN KM.', //)
3499 * , INDEX, 5X, 'ALT. IN KM.', //,
C   DO 3497 I=1,NSPZ
C   WRITE(6,3504)NZX(I),ALT(I)
C   CONTINUE
3497 WRITE(6,3599)
C   FORMAT( , RHO (IN KM. ), //)
3599 * , RHO (IN KM. ), //,
C   DO 3597 I=1,NSPR
C   WRITE(6,3604)RYS(I)
C   FORMAT(1PE11.3)
C   CONTINUE
3597 WRITE(6,3515)
C   FORMAT(//, , SPECTRA INDEX, 8X, 'ENERGY INTERVAL ENDS', //)
C   DO 4515 I=2,NEIP
C   IM1=I-1
C   WRITE(6,3517)IM1,EIP(IM1),EIP(I)
C   FORMAT(17,12X,1PE11.3,3X,1PE11.3)
C   CONTINUE
C   CONTINUE
C   NARI=NARI+1
C   NUMG=NUMST+NUMGAS
C   NTQP=NSEC-1
C   IF(NRHO .NE. 1) GO TO 1141
C   READ(5,2244)(NCRO(J),J=1,NVR)
C   NCRO(J) ARE THE INDEX VALUES OF THE Z DISTANCES AT WHICH A RHO
C   INTENSITY PLOT IS DESIRED.
C   READ(5,2255)(ZNUM(J),J=1,NVR)
C   ZNUM(J) ARE THE Z VALUES AT WHICH A RHO INTENSITY PLOT IS DESIRED.
C   WRITE(6,3503)
C   FORMAT(//, , ALTITUDES WHERE RHO EXC. WILL BE CALCULATED', //)
C   * , INDEX, 5X, 'ALT. IN KM.', //)
C   DO 4503 J=1,NVR
C   WRITE(6,3504)NCRO(J),ZNUM(J)
C   FORMAT(15,5X,1PE11.3)
3504 READ(5,2255)(RHO(I),I=1,NRM)
RDCARD73
RDCARD74
RDCARD75
RDCARD76
RDCARD77
RDCARD78
RDCARD79
RDCARD80
RDCARD81
RDCARD82
RDCARD83
RDCARD84
RDCARD85
RDCARD86
RDCARD87
RDCARD88
RDCARD89
RDCARD90
RDCARD91
RDCARD92
RDCARD93
RDCARD94
RDCARD95
RDCARD96
RDCARD97
RDCARD98
RDCARD99
RDCARD100
RDCARD101
RDCARD102
RDCARD103
RDCARD104
RDCARD105
RDCARD106
RDCARD107
RDCARD108
RDCARD109
RDCARD110
RDCARD111
RDCARD112
RDCARD113
RDCARD114
RDCARD115
RDCARD116
RDCARD117

```

```

C RHD(I) ARE THE RHD VALUES AT WHICH THE RHO INTENSITY PLOT IS
C CALCULATED,
WRITE(6,3505)
3505 FORMAT(//,,,' RHO INTERVAL',10X,'RHO BIN ENDS',/)
DO 4505 I=2,NRM
IM1=I-1
4505 WRITE(6,3506)IM1,RHO(IM1),RHO(I)
3506 FORMAT(15,11X,1PE11.3,5X,1PE11.3)
1141 CONTINUE
C READ(5,2255)(ZALT(I),I=1,NAR)
C ZALT(I) ARE THE Z INTERVALS INTO WHICH THE LONGITUDINAL REGIME
C IS DIVIDED.
C ZALT(1) AND ZALT(NAR) MUST CORRESPOND TO THE Z BOUNDS SET IN THE
C MONTE CARLO PROGRAM.
C THE OTHER VALUES IN BETWEEN ARE VARIABLE.
3507 WRITE(6,3507)
FORMAT(,'1ALT',INDEX',8X',ALT',ENDS',/)
DO 4507 I=1,NAR
4507 WRITE(6,3508)I,ZALT(I)
3508 FORMAT(18,9X,1PE11.3)
C
C
C WIS(I) AND EXC5(I) ARE MAINLY USEFUL WHEN LOCAL ENERGY DEGRADA-
C TION IS USED BELOW EMIN.
C READ(5,2255)(WIS(I),I=1,NSEC)
C WIS(I) ARE THE ENERGY BIN ENDS FOR THE LOW ENERGY ELECTRONS.
C READ(5,2255)(EXC5(I),I=1,NTOP)
RDCAR118
RDCAR119
RDCAR120
RDCAR121
RDCAR122
RDCAR123
RDCAR124
RDCAR125
RDCAR126
RDCAR127
RDCAR128
RDCAR129
RDCAR130
RDCAR131
RDCAR132
RDCAR133
RDCAR134
RDCAR135
RDCAR136
RDCAR137
RDCAR138
RDCAR139
RDCAR140
RDCAR141
RDCAR142
RDCAR143
RDCAR144

```

14 JULY 1978 NERDC --- CARD -1ST UTILITY

```

C   EXC5(I) ARE THE NUMBER OF EXCITATIONS THAT CAUSE THE 3914 A
C   EMISSION THAT ARE EXCITED BY EACH ELECTRON IN THESE LOWER ENERGY
C   BINS.
2255  FORMAT(8E10.0)
      WRITE(6,3509)
3509  FORMAT(1EXC, OF 3914A BY SECONDARIES,5X,ENERGY BIN ENDS,./)
      DO 4509 I=1,NTOP
        IPI=I+1
4509  WRITE(6,3510)EXC5(I),WIS(I),WIS(IPI)
3510  FORMAT(G15.7,G15.7,5X,G15.7)
      READ(5,2266)(NIE(I),I=1,NUMG)
C   NIE(I) INDICES INDICATE WHICH STATES ARE IONIZATION AND WHICH
C   ARE ELASTIC.
2266  FORMAT(16I5)
      WRITE(6,3511)
3511  FFORMAT(///, STATE NO.,5X,NIE VALUE,./)
      DO 4511 I=1,NUMG
4511  WRITE(6,3512)I,NIE(I)
3512  FORMAT(17,112)
      RETURN
      END
RDCAR145
RDCAR146
RDCAR147
RDCAR148
RDCAR149
RDCAR150
RDCAR151
RDCAR152
RDCAR153
RDCAR154
RDCAR155
RDCAR156
RDCAR157
RDCAR158
RDCAR159
RDCAR160
RDCAR161
RDCAR162
RDCAR163
RDCAR164
RDCAR165

```

14 JULY 1978 NERDC --- CARD LIST UTILITY

```

C      SUBROUTINE MATIN ***
C      SUBROUTINE IS ACCESSED BY THE MAIN PROGRAM.
C      THIS SUBROUTINE INITIALIZES ALL THE MATRICES.
      COMMON ALAB(20),ANEI(5,20,100),ALT(20),EAVE(3),EIP(100),
1     EXC5(50),JES(50),JIS(50),JZE(3,50,80),JSEC(50,80),KREX(10,40,40),
2     NIE(40),NZX(20),NOFE(3,80),NCRO(10),RHO(40),SA(3,80),SIG(100),
3     TOTE(3,80),TNI(3,80),TNS(3,80),TNI0(3,80),WIE(50),WIS(50),
4     YSPEC(100),ZNUM(10),ZALT(80),NUMGAS,NAR1,NVR,NUVST,NUMG,NRM,
5     NSEC,NSPZ,NEIP,NEXC,NTOP,NAR,NSPEC,NRHO,NAVEE,NPRIM,EIN,
6     ZVAL,EMIN,DENGS,M,NSPUN,NSPR,ANER(1,10,20,100),RYS(10),NSPRO
      MATIN001
      MATIN002
      MATIN003
      MATIN004
      MATIN005
      MATIN006
      MATIN007
      MATIN008
      MATIN009
      MATIN010
      MATIN011
      MATIN012
      MATIN013
      MATIN014
      MATIN015
      MATIN016
      MATIN017
      MATIN018
      MATIN019
      MATIN020
      MATIN021
      MATIN022
      MATIN023
      MATIN024
      MATIN025
      MATIN026
      MATIN027
      MATIN028
      MATIN029
      MATIN030
      MATIN031
      MATIN032
      MATIN033
      MATIN034
      MATIN035
      MATIN036
      MATIN037
      MATIN038
      MATIN039
      MATIN040
      MATIN041
      MATIN042
      MATIN043
      MATIN044

```

INITIALIZE THE MATRICES

```

      DO 26 K=1,3
      DO 26 I=1,NARI
      TOTE(K,I)=0.0E0
      NOFE(K,I)=0
      TNI0(K,I)=0.0E0
      TNS(K,I)=0.0E0
      DO 139 I=1,NVR
      DO 139 J=1,NUMG
      DO 139 K=1,NRM
      KREX(I,J,K)=0
      DO 140 K=1,3
      DO 140 I=1,NUMG
      DO 140 J=1,NARI
      JZE(K,I,J)=0
      DO 142 I=1,NSEC
      DO 142 J=1,NARI
      JSEC(I,J)=0
      DO 143 J=1,NSEC
      JIS(J)=0
      DO 144 J=1,NUMG
      WIE(J)=0.0E0
      JES(J)=0
      DO 145 K=1,1
      DO 145 I=1,NSPZ
      DO 145 J=1,NEIP
      ANEI(K,I,J)=0.0E0
      DO 145 L=1,NSPR
      ANER(K,L,I,J)=0.0E0
      RETURN
      END

```

```

C      26
C      139
C      140
C      142
C      143
C      144
C      145

```



```

1131 IF(NAVEE .EQ. 1)GO TO 6611
      GO TO 30
      CONTINUE
      READ(M),WL
      ELOSS=ELOSS+WL
      N=NUMBER OF THE STATE
      WL=ENERGY LOSS OF THE PRIMARY ELECTRON IN EXCITING STATE N
      WIE(N)=WL
      JES(N)=JES(N)+1
      IF(NIE(N) .EQ. 2) GO TO 3
      GO TO 20
      READ(M) WL
      I1=NSEC
4466 WE PUT THE SECONDARY AND TERTIARY HERE INITIALLY. IF THE ELECTRON'S
      ENERGY IS ABOVE THE TMIN THEN THE ELECTRON STAYS HERE.
      READ(M)X,Y,Z,E,PA,PHI,NG200,EBEF
      X= THE X COORDINATE
      Y= THE Y COORDINATE
      Z= THE Z COORDINATE
      E= THE ENERGY OF THE PRIMARY OR SECONDARY AT THIS POINT IN ITS
      DEGRADATION.
      PA = THE POLAR ANGLE OF THE ELECTRON.
      PHI = THE AZIMUTHAL ANGLE
      IF NG200=0 THEN WE HAVE A PRIMARY HERE
      IF NG200=1 THEN WE HAVE A SECONDARY HERE.
      IF NG200=2 THEN WE HAVE A TERTIARY HERE
      EBEF IS THE ENERGY OF THE ELECTRON BEFORE THE COLLISION.
      RDTAPE46
      RDTAPE47
      RDTAPE48
      RDTAPE49
      RDTAPE50
      RDTAPE51
      RDTAPE52
      RDTAPE53
      RDTAPE54
      RDTAPE55
      RDTAPE56
      RDTAPE57
      RDTAPE58
      SRDTAPE59
      RDTAPE60
      RDTAPE61
      RDTAPE62
      RDTAPE63
      RDTAPE64
      RDTAPE65
      RDTAPE66
      RDTAPE67
      RDTAPE68
      RDTAPE69
      RDTAPE70
      RDTAPE71
      RDTAPE72

```

14 JULY 1978 NERDC --- CARD LIST UTILITY

```

IF(NIE(N) .NE. 2)GO TO 5577
IF(NG200 .EQ. 2)GO TO 5588
IF(WL .GT. WIS(NSEC))GO TO 5577
5588 ELOSS=ELOSS+WL
5577 IF(Z .GT. ZALT(1) ,OR. Z .LT. ZALT(NAR))ELOSS=ELOSS+E
C
C
C
IF(ELOSS .LT. 0.4)GO TO 1143
C DO NOT COUNT ELASTIC COLLISIONS IN YIELD SPECTRA
C SOMETIMES ELOSS MAY BE GREATER THAN 0.4 AND STILL BE AN ELASTIC COL.
C THE ELOSS IS GREATER ONLY IN THE CASE WHERE THE ELECTRON HAS AN
C ELASTIC COLLISION OUTSIDE THE BOX AND ESCAPES.
IF(NSPEC .NE. 1)GO TO 1143
DO 2203 IL=1,NSPZ
INIE=IL
N1=NZX(IL)
N1M1=N1-1
IF(Z .GT. ZALT(N1) ,AND. Z .LT. ZALT(N1M1))GO TO 2204
2203 CONTINUE
GO TO 1143
2204 DO 69 IM=2,NEIP
IMM1=IM-1
IF(EBEF .GT. EIP(IMM1) ,AND. EBEF .LT. EIP(IM))JNIE=IMM1
69 CONTINUE
ANEI(1,INIE,JNIE)=ANEI(1,INIE,JNIE)+1.0
IF(NSPRO .NE. 1)GO TO 1143
RHOV=SQRT(X*X+Y*Y)
DO 2205 IN=2,NSPR
IN1=IN-1
IF(RHOV .GT. RYS(IN1) ,AND. RHOV .LT. RYS(IN)) GO TO 2207
2205 CONTINUE
GO TO 1143
2207 AREA=3.14159*(RYS(IN)*RYS(IN)-RYS(IN1)*RYS(IN1))*CONST
ANER(1,IN1,INIE,JNIE)=ANER(1,IN1,INIE,JNIE)+1.0/AREA
1143 CONTINUE
C
C
C
IF(NRHO .EQ. 1)GO TO 151
IF(NAVEE .EQ. 1)GO TO 6611
6622 IF(NIE(N) .NE. 2)GO TO 702
DO 63 I1=1,NTOP
I1P1=I1+1
IF(WL .GT. WIS(I1) ,AND, WL .LT. WIS(I1P1))I1=I1

```

```

RDTAPE73
RDTAPE74
RDTAPE75
RDTAPE76
RDTAPE77
RDTAPE78
RDTAPE79
RDTAPE80
RDTAPE81
RDTAPE82
RDTAPE83
RDTAPE84
RDTAPE85
RDTAPE86
RDTAPE87
RDTAPE88
RDTAPE89
RDTAPE90
RDTAPE91
RDTAPE92
RDTAPE93
RDTAPE94
RDTAPE95
RDTAPE96
RDTAPE97
RDTAPE98
RDTAPE99
RDTAP100
RDTAP101
RDTAP102
RDTAP103
RDTAP104
RDTAP105
RDTAP106
RDTAP107
RDTAP108
RDTAP109
RDTAP110
RDTAP111
RDTAP112
RDTAP113
RDTAP114
RDTAP115
RDTAP116
RDTAP117

```

```

63      CONTINUE
      IF(Z .GT. ZALT(1))JSEC(II,1)=JSEC(II,1)+1
      IF(Z .LT. ZALT(NAR))JSEC(II,NAR1)=JSEC(II,NAR1)+1
      DO 64 I2=2,NAR
      I2M1=I2-1
      IF(Z .GT. ZALT(I2) ,AND. Z .LT. ZALT(I2M1))JSEC(II,I2)=
* JSEC(II,I2)+1
      CONTINUE
      JIS(II)=JIS(II)+1
702     CONTINUE
      IF(EBEF .LT. WIS(NSEC))GO TO 30
      IF(Z .GT. ZALT(1))JZE(3,N,1)=JZE(3,N,1)+1
      IF(Z .LT. ZALT(NAR)) JZE(3,N,NAR)=JZE(3,N,NAR)+1
      DO 31 IA=2,NAR
      IAM1=IA-1
      IASET=IA
      IF(Z .GT. ZALT(IA) ,AND. Z .LT. ZALT(IAM1))GO TO 555
      CONTINUE
31      GO TO 30
      DO 560 KA=1,3
      JZE(KA,N,IASET)=JZE(KA,N,IASET)+1
555     IF(NG200 .EQ. 1)JZE(1,N,IASET)=-1
560     IF(NG200 .EQ. 0)JZE(2,N,IASET)=JZE(2,N,IASET)-1
      GO TO 30
C
C
C      THIS PART OF THE PROGRAM CALCULATES THE DISTRIBUTION OF EXCITATIONS
      RDTAPI118
      RDTAPI119
      RDTAPI120
      RDTAPI121
      RDTAPI122
      RDTAPI123
      RDTAPI124
      RDTAPI125
      RDTAPI126
      RDTAPI127
      RDTAPI128
      RDTAPI129
      RDTAPI130
      RDTAPI131
      RDTAPI132
      RDTAPI133
      RDTAPI134
      RDTAPI135
      RDTAPI136
      RDTAPI137
      RDTAPI138
      RDTAPI139
      RDTAPI140
      RDTAPI141
      RDTAPI142
      RDTAPI143
      RDTAPI144

```

14 JULY 1978 NERDC --- CARD LIST UTILITY

```

C AT A GIVEN ALTITUDE AS A FUNCTION OF RHO.
151 DO 6149 IZV=1,NVR
    IC=IZV
    NC=NCRO(IZV)
    NCRM1=NCRO(IZV)-1
    IF(Z.GT.ZALT(NC),AND,Z.LT.ZALT(NCRM1))GO TO 155
    CONTINUE
6149 GO TO 1161
155 RHOV=ABS(X)
    DO 159 I3=2,NRM
    I3M1=I3-1
    IF(RHOV.LT.RHO(I3).AND,RHOV.GT.RHD(I3M1))
    * KREX(IC,N,I3)=KREX(IC,N,I3)+1
    CONTINUE
    GO TO 1161
C
C THIS PART OF THE PROGRAM CALCULATES THE AVERAGE ENERGY AT A GIVEN
C ALTITUDE.
6611 CONTINUE
    IF(Z.LT.ZALT(1))GO TO 6767
    NOFE(1,1)=NOFE(1,1)+1
    TOTE(1,1)=TOTE(1,1)+ELOSS
    IF(PA.LE.1.57)NOFE(2,1)=NOFE(2,1)+1
    IF(PA.LE.1.57)TOTE(2,1)=TOTE(2,1)+ELOSS
    IF(PA.GT.1.57)NOFE(3,1)=NOFE(3,1)+1
    IF(PA.GT.1.57)TOTE(3,1)=TOTE(3,1)+ELOSS
    GO TO 6769
6767 IF(Z.GT.ZALT(NAR))GO TO 6768
    NOFE(1,NAR1)=NOFE(1,NAR1)+1
    TOTE(1,NAR1)=TOTE(1,NAR1)+ELOSS
    IF(PA.LE.1.57)NOFE(2,NAR1)=NOFE(2,NAR1)+1
    IF(PA.LE.1.57)TOTE(2,NAR1)=TOTE(2,NAR1)+ELOSS
    IF(PA.GT.1.57)NOFE(3,1)=NOFE(3,1)+1
    IF(PA.GT.1.57)TOTE(3,1)=TOTE(3,1)+ELOSS
    GO TO 6769
6768 DO 13 I4=2,NAR
    I4M1=I4-1
    IF(Z.GT.ZALT(I4),AND,Z.LT.ZALT(I4M1))NI Z=1
    IF(NI Z.EQ.1)NOFE(1,I4)=NOFE(1,I4)+1
    IF(NI Z.EQ.1)TOTE(1,I4)=TOTE(1,I4)+ELOSS
    IF(NI Z.EQ.1)AND,PA.LE.1.57)NOFE(2,I4)=NOFE(2,I4)+1
    IF(NI Z.EQ.1)AND,PA.LE.1.57)TOTE(2,I4)=TOTE(2,I4)+ELOSS
    IF(NI Z.EQ.1)AND,PA.GT.1.57)NOFE(3,I4)=NOFE(3,I4)+1
    IF(NI Z.EQ.1)AND,PA.GT.1.57)TOTE(3,I4)=TOTE(3,I4)+ELOSS
RDTAP145
RDTAP146
RDTAP147
RDTAP148
RDTAP149
RDTAP150
RDTAP151
RDTAP152
RDTAP153
RDTAP154
RDTAP155
RDTAP156
RDTAP157
RDTAP158
RDTAP159
RDTAP160
RDTAP161
RDTAP162
RDTAP163
RDTAP164
RDTAP165
RDTAP166
RDTAP167
RDTAP168
RDTAP169
RDTAP170
RDTAP171
RDTAP172
RDTAP173
RDTAP174
RDTAP175
RDTAP176
RDTAP177
RDTAP178
RDTAP179
RDTAP180
RDTAP181
RDTAP182
RDTAP183
RDTAP184
RDTAP185
RDTAP186
RDTAP187
RDTAP188
RDTAP189

```

RDTAPI190  
RDTAPI191  
RDTAPI192  
RDTAPI193  
RDTAPI194  
RDTAPI195  
RDTAPI196  
RDTAPI197  
RDTAPI198  
RDTAPI199  
RDTAP200

13 N1Z=0  
6769 CONTINUE  
IF(NCNE .EQ. 1)GO TO 30  
30 GO TO 6622  
333 CONTINUE  
334 CONTINUE  
WRITE(6,334) ISAV  
FORMAT(' ISAV=', I9)  
RETURN  
END

NERDC --- CARD LIST UTILITY

14 JULY 1978

```

C SUBROUTINE WRTDAT
C SUBROUTINE WRITES OUT THE MATRICES THAT HAVE BEEN FILLED
C THIS SUBROUTINE WRITES OUT THE DEGRADATION PROCESS.
C WITH INFORMATION ABOUT THE MAIN PROGRAM.
C THIS SUBROUTINE IS ACCESSED BY THE MAIN PROGRAM.
1 EXC5(50),ANEI(5,20,100),ALT(20),EAVE(3),EIP(100),
2 NIE(40),NZX(20),NOFE(3,80),NCRD(10),RHO(40),SA(3,80),SIG(100),
3 TOTE(3,80),TNI(3,80),TNS(3,80),TN10(3,80),WIE(50),WIS(50),
4 YSPEC(100),ZNUM(10),ZALT(80),NUMGAS,NARI,NVR,NJMST,NUMG,NRM,
5 NSEC,NSPZ,NEIP,NEXC,NTOP,NAR,NSPEC,NRHD,NAVEE,NPRIM,EIN,
6 ZVAL,EMIN,DENGS,M,NSPUN,NSPR,ANER(1,10,20,100),RYS(10),NSPRO
C
C WRITE OUT ALL THE STATISTICS YOU NEED HERE
DO 1 K=1,3
DO 1 I=1,NARI
DO 1 J=1,NUMG
C WE HAVE SUPPLEMENTED THE 3914A EMISSION WITH 3RD AND 4TH STATES
IF(J.EQ.3)GO TO 6655
IF(J.EQ.4)GO TO 6655
IF(J.EQ.5)GO TO 6655
GO TO 767
6655 TN5(K,I)=TN5(K,I)+JZE(K,J,I)
757 IF(J.NE.10)GO TO 1
TN10(K,I)=TN10(K,I)+JZE(K,J,I)
1 CONTINUE
DO 4 K=2,3
DO 4 I=1,NARI
DO 4 J=1,NTOP
4 TN5(K,I)=TN5(K,I)+ JSEC(J,I)*EXC5(J)
CONTINUE
DO 46 K=1,3
IF(K.EQ.1)WRITE(6,780)
IF(K.EQ.2)WRITE(6,781)
IF(K.EQ.3)WRITE(6,782)
780 FORMAT('PRIMARY COLLISIONS',/)
781 FORMAT('SECONDARY COLLISIONS',/)
782 FORMAT('PRIMARY PLUS SECONDARY COLLISIONS',/)
WRITE(6,755)
755 * FORMAT('ALT. INTERVAL',8X,'ALT. VALUE',9X,'3914A EXC.',8X,
'ELASTIC EXC.',/)
DO 46 I=2,NAR
IM1=I-1
ZMV=(ZALT(I)+ZALT(IM1))/2.

```

WRTDAT01  
WRTDAT02  
WRTDAT03  
WRTDAT04  
WRTDAT05  
WRTDAT06  
WRTDAT07  
WRTDAT08  
WRTDAT09  
WRTDAT10  
WRTDAT11  
WRTDAT12  
WRTDAT13  
WRTDAT14  
WRTDAT15  
WRTDAT16  
WRTDAT17  
WRTDAT18  
WRTDAT19  
WRTDAT20  
WRTDAT21  
WRTDAT22  
WRTDAT23  
WRTDAT24  
WRTDAT25  
WRTDAT26  
WRTDAT27  
WRTDAT28  
WRTDAT29  
WRTDAT30  
WRTDAT31  
WRTDAT32  
WRTDAT33  
WRTDAT34  
WRTDAT35  
WRTDAT36  
WRTDAT37  
WRTDAT38  
WRTDAT39  
WRTDAT40  
WRTDAT41  
WRTDAT42  
WRTDAT43  
WRTDAT44  
WRTDAT45

```

32 ZMV=ZVAL-ZMV
46 WRITE(6,32) I,ZMV,TNS(K,I),TN10(K,I)
C FORMAT(110.11X,1PE12.4,6X.G15.7,4X.G15.7)
C CONTINUE
C
C WRITE OUT THE YIELD SPECTRA INFORMATION
IF(NSPEC.NE.1)GO TO 1144
ZDEL=(ZALT(1)-ZALT(2))*1.E+05*DENG*S*4.651E-23
DO 790 I=1,NSPZ
  NI=NZX(I)
  NI1=NI-1
  ZMV=(ZALT(NI)+ZALT(NI1))/2.
  ZMV=(ZVAL-ZMV)*1.E+05
  ZRNG=ZMV*DENG*S*4.651E-23
C ZRNG IS THE PATH LENGTH IN GM/CM**2
C THERE ARE 4.651E-23 GM/MOLECULE
  WRITE(6,791)ZMV,ZRNG
791 FORMAT(1AT AN ALTITUDE=,1PE11.3, CM, WITH A VALUE OF.,
1 1PE11.3, GM/CM**2,/, WE HAVE THE FOLLOWING ELECTRON SPECTRA.,
2 4X, YIELD SPECTRA = U(E) IN #/EV/(GM/CM**2),,/,
3 , MID-ENERGY, 8X, U(E),/)
  NF IP1=NEIP-1
  DO 795 J=2,NEIP
    JM1=J-1
    EMID=(EIP(JM1)+EIP(J))/2.
  
```

```

WRIDAT46
WRIDAT47
WRIDAT48
WRIDAT49
WRIDAT50
WRIDAT51
WRIDAT52
WRIDAT53
WRIDAT54
WRIDAT55
WRIDAT56
WRIDAT57
WRIDAT58
WRIDAT59
WRIDAT60
WRIDAT61
WRIDAT62
WRIDAT63
WRIDAT64
WRIDAT65
WRIDAT66
WRIDAT67
WRIDAT68
WRIDAT69
WRIDAT70
WRIDAT71
WRIDAT72

```

14 JULY 1978 NERDC --- CARD LIST UTILITY

```

C      EDEL=EIP(J)-EIP(JM1)
C      THIS IS FOR THE LONGITUDINAL YIELD SPECTRA.
C      YSPEC(JM1)=ANEI(1,I,JM1)/EDEL/NPRIM/ZDEL
C      NORMALIZE THE YIELD SPECTRA TO ONE ELECTRON
C      YSPEC(JM1) IS IN UNITS OF #/EV/(GM/CM**2).
C      ANEI(1,I,JM1) HAS THE EXTRA DIMENSION OF THE MATRIX IN CASE A
C      DEGRADATION SPECTRA OR SOME OTHER FLUX IS DESIRED.
C      IF(J.EQ.NEIP) YSPEC(JM1)=YSPEC(JM1)*EDEL
C      THIS EXPRESSION TAKES CARE OF THOSE ELECTRONS IN THE SOURCE TERM,
793    WRITE(6,793)EMID,YSPEC(JM1)
      FORMAT(1PE11.3,5X,1PE11.3)
      IF(YSPEC(JM1).LT.1.E-30)GO TO 795
      IF(NSPUN.EQ.1)WRITE(7,850)EMID,ZRNG,EIN,YSPEC(JM1)
850    FORMAT(2X,4E12.5)
795    CONTINUE
      IF(NSPRO.NE.1)GO TO 790
      DO 803 IR=2,NSPR
      IR1=IR-1
      RMID=(RYS(IR)+RYS(IR1))/2.*1.E+5
      WRITE(6,800)ZMV,RMID
      FORMAT(1AT A Z VALUE=,1PE11.3, CM.,
      * 2X, AND AT A RHO VALUE=,1PE11.3, CM, WE HAVE THE FOLLOWING ,
      * //, ELECTRON SPECTRA, YIELD SPECTRA = U(E) IN #/EV/(GM/CM**2)**3,
      * //, MID-ENERGY, 8X, U(E), //)
      DO 803 JR=2,NEIP
      JRM1=JR-1
      EMID=(EIP(JRM1)+EIP(JR))/2.
      EDEL=EIP(JR)-EIP(JRM1)
C      THIS IS FOR THE RADIAL YIELD SPECTRA.
C      YSRHO=ANER(1,IR1,I,JRM1)/EDEL/NPRIM/ZDEL
C      YSRHO HAS THE DIMENSIONS OF #/EV/(GM/CM**2)**3.
C      IF(JR.EQ.NEIP)YSRHO=YSRHO*EDEL
C      THIS EXPRESSION TAKES CARE OF THE SOURCE TERM.
803    WRITE(6,793)EMID,YSRHO
790    CONTINUE
1144  CONTINUE
C
C
C      WRITE OUT A QUICK AND DIRTY ENERGY CONSERVATION COMPARISON,
C      THIS IS NOT ACCURATE FOR REASONS GIVEN BELOW.
C      ESI=NPRIM*EIN
C      ESI IS THE INCIDENT ENERGY.
      ESF=0.0E0

```

WRD DAT 73  
WRD DAT 74  
WRD DAT 75  
WRD DAT 76  
WRD DAT 77  
WRD DAT 78  
WRD DAT 79  
WRD DAT 80  
WRD DAT 81  
WRD DAT 82  
WRD DAT 83  
WRD DAT 84  
WRD DAT 85  
WRD DAT 86  
WRD DAT 87  
WRD DAT 88  
WRD DAT 89  
WRD DAT 90  
WRD DAT 91  
WRD DAT 92  
WRD DAT 93  
WRD DAT 94  
WRD DAT 95  
WRD DAT 96  
WRD DAT 97  
WRD DAT 98  
WRD DAT 99  
WRD DAT 100  
WRD DAT 101  
WRD DAT 102  
WRD DAT 103  
WRD DAT 104  
WRD DAT 105  
WRD DAT 106  
WRD DAT 107  
WRD DAT 108  
WRD DAT 109  
WRD DAT 110  
WRD DAT 111  
WRD DAT 112  
WRD DAT 113  
WRD DAT 114  
WRD DAT 115  
WRD DAT 116  
WRD DAT 117



NERDC --- CARD LIST UTILITY

14 JULY 1978

```

730 DD 160 I=1,NVR
      ZMV=(ZVAL-ZNUM(I))*1.E+05
      WRITE(6,730)ZMV,NCRO(I)
      FORMAT(1A7,Z VALUE OF,1PE11.3,CM, AND NCRO=,15,/,
      * WE HAVE THE FOLLOWING EXCITATION DISTRIBUTION,///,
      * RHO VALUE,6X,3914A EXC,8X,ELASTIC EXC,/,/)
      DO 160 J=2,NRM
        JM1=J-1
        RMV=(RHO(J)+RHO(JM1))/2.0
        K345=KREX(I,3,J)+KREX(I,4,J)+KREX(I,5,J)
        WRITE(6,705)RMV,K345,KREX(I,10,J)
        FORMAT(2X,1PE10.4,2X,19.9X,110)
        CONTINUE
      C
      C
      C
3311 WR ITE OUT THE ENERGY LOST INFORMATION,
      IF(NAVEE.NE.1) GO TO 6633
      DO 4477 I=1,3
        EAVE(I)=0.0D0
        WRITE(6,712)
        FORMAT(1THE AVE. ENERGY LOST IN EACH Z VALUE IS PRINTED OUT NOW',
        * //,ALT. INTERVAL,8X,ALT. VALUE,4X,MEAN ENERGY(ALL),
        * 5X,MEAN ENERGY(PAKPI/2),5X,MEAN ENERGY(PA>PI/2),/)
      DO 15 I=1,NARI
        IF(I.EQ.1)GO TO 2965
        IF(I.EQ. NARI)GO TO 2966
        IM1=I-1
        ZMV=(ZALT(I)+ZALT(IM1))/2.0
        ZMV=ZVAL-ZMV
        GO TO 2967
      ZMV=ZVAL-ZALT(1)
      GO TO 2967
2966 ZMV=ZVAL-ZALT(NAR)
2967 DO 2961 J=1,3
      EAVE(J)=EAVE(J)+TOTE(J,I)
      CONTINUE
      EV1=EAVE(1)/NPRIM
      EV2=EAVE(2)/NPRIM
      EV3=EAVE(3)/NPRIM
      WRITE(6,714)I,ZMV,EV1,EV2,EV3
      FORMAT(10,10X,1PE12.4,7X,G15.7,6X,G15.7,10X,G15.7)
      CONTINUE
      CONTINUE
      RETURN
714 15
      6633
      WR TDA145
      WR TDA146
      WR TDA147
      WR TDA148
      WR TDA149
      WR TDA150
      WR TDA151
      WR TDA152
      WR TDA153
      WR TDA154
      WR TDA155
      WR TDA156
      WR TDA157
      WR TDA158
      WR TDA159
      WR TDA160
      WR TDA161
      WR TDA162
      WR TDA163
      WR TDA164
      WR TDA165
      WR TDA166
      WR TDA167
      WR TDA168
      WR TDA169
      WR TDA170
      WR TDA171
      WR TDA172
      WR TDA173
      WR TDA174
      WR TDA175
      WR TDA176
      WR TDA177
      WR TDA178
      WR TDA179
      WR TDA180
      WR TDA181
      WR TDA182
      WR TDA183
      WR TDA184
      WR TDA185
      WR TDA186
      WR TDA187
      WR TDA188
      WR TDA189

```

WRTDA190

END

## REFERENCES

- Banks, P.M., C.R. Chappell, and A.F. Nagy, A new model for the interaction of auroral electrons with the atmospheres: Spectral degradation, backscatter, optical emission, and ionization, J. Geophys. Res., 79, 1459, 1974.
- Barrett, J.L., Energy loss of electrons in nitrogen, Ph.D. thesis, University of Michigan, Ann Arbor, Michigan, 1975.
- Barrett, J.L., and P.B. Hays, Spatial distribution of energy deposited in nitrogen by electrons, J. Chem. Phys., 64, 743, 1976.
- Berger, M.J., Monte Carlo calculation of the penetration and diffusion of fast charged particles, Methods in Computational Physics, 1, 135, 1963.
- Berger, M.J., S.M. Seltzer, and K. Maeda, Energy deposition by auroral electrons in the atmosphere, J. Atmos. Terr. Phys., 32, 1015, 1970.
- Berger, M.J., S.M. Seltzer, and K. Maeda, Some new results on electron transport in the atmosphere, J. Atmos. Terr. Phys., 36, 591, 1974.
- Bethe, H., Zur theorie des durchgangs schneller korpuskularstrahler durch materie, Ann. Phys., 5, 325, 1930.
- Bethe, H.A., M.E. Rose, and L.P. Smith, The multiple scattering of electrons, Proc. Amer. Phil. Soc., 78, 573, 1938.
- Blaauw, H.J., F.J. de Heer, R.W. Wagenaar, and D.H. Barends, Total cross sections for electron scattering from N<sub>2</sub> and He, J. Phys. B: Atom. Molec. Phys., 10, L299, 1977.
- Bohr, N., On the theory of the decrease of velocity of moving electrified particles on passing through matter, Phil. Mag., 25, 10, 1913.
- Bohr, N., On the decrease of velocity of swiftly moving electrified particles in passing through matter, Phil. Mag., 30, 581, 1915.
- Borst, W.L. and E.C. Zipf, Cross section for electron impact excitation of the (0,0) first negative band of N<sub>2</sub><sup>+</sup> from threshold to 3 KeV, Phys. Rev. A, 1, 834, 1969.
- Brinkmann, R.T. and S. Trajmar, Electron impact excitation of N<sub>2</sub>, Ann. Geophys., 26, 201, 1970.

- Cartwright, D.C., A. Chutjian, S. Trajmar, and W. Williams, Electron impact excitation of the electronic states of  $N_2$ . I. Differential cross sections at incident energies from 10 to 50 eV, Phys. Rev. A, 16, 1013, 1977.
- Chutjian, A., D.C. Cartwright, and S. Trajmar, Electron impact excitation of the electronic states of  $N_2$ . III. Transitions in the 12.5-14.2 eV energy-loss region at incident energies of 40 and 60 eV, Phys. Rev. A, 16, 1052, 1977.
- Cicerone, R.J. and S.A. Bowhill, Photoelectron escape fluxes obtained by a Monte Carlo technique, Radio Sci., 5, 49, 1970.
- Cicerone, R.J. and S.A. Bowhill, Photoelectron fluxes in the ionosphere computed by a Monte Carlo method, J. Geophys. Res., 76, 8299, 1971.
- Cohn, A. and G. Caledonia, Spatial distribution of the fluorescent radiation emission caused by an electron beam, J. Appl. Phys., 41, 3767, 1970.
- Cravens, T.E., G.A. Victor, and A. Dalgarno, The absorption of energetic electrons by molecular hydrogen gas, Planet. Space Sci., 23, 1059, 1975.
- Dalgarno, A., 15. Range and energy loss, Atomic and Molecular Processes: 13, pp. 622-662, edited by D.R. Bates, Academic Press, New York, 1962.
- Dalgarno, A. and G. Lejeune, The absorption of electrons in atomic oxygen, Planet. Space Sci., 19, 1553, 1971.
- Douthat, D.A., Energy deposition by electrons and degradation spectra, Radiat. Res., 64, 141, 1975.
- DuBois, R.D. and M.E. Rudd, Absolute doubly differential cross sections for ejection of secondary electrons from gases by electron impact. II. 100-500-eV electrons on neon, argon, molecular hydrogen, and molecular nitrogen, Phys. Rev. A, 17, 843, 1978.
- Eadie, W.T., D. Dryard, F.E. James, M. Roos, and B. Sadoulet, Statistical Methods in Experimental Physics, pp. 44-47, North-Holland Publishing Company, Amsterdam, 1971.
- Ehrhardt, H., M. Schulz, T. Tekaas, and K. Willmann, Ionization of helium: Angular correlation of the scattered and ejected electrons, Phys. Rev. Lett., 22, 89, 1969.
- Fowler, R.H., Theory of motion of  $\alpha$ -particles through matter, Proc. Camb. Philos. Soc., 121, 521, 1922-23.
- Garvey, R.H., H.S. Porter, and A.E.S. Green, An analytic degradation spectrum for  $H_2$ , J. Appl. Phys., 48, 190, 1977.
- Goudsmit, S. and J.L. Saunderson, Multiple scattering of electrons, Phys. Rev., 57, 24, 1940.
- Green, A.E.S. and C.A. Barth, Calculations of ultraviolet molecular nitrogen emissions from the aurora, J. Geophys. Res., 70, 1083, 1965.

- Green, A.E.S. and C.A. Barth, Calculations of the photoelectron excitation of the dayglow, J. Geophys. Res., 72, 3975, 1967.
- Green, A.E.S. and S.K. Dutta, Semi-empirical cross sections for electron impacts, J. Geophys. Res., 72, 3933, 1967.
- Green, A.E.S., C.H. Jackman, and R.H. Garvey, Electron impact on atmospheric gases. 2. Yield spectra, J. Geophys. Res., 82, 5104, 1977.
- Green, A.E.S. and L.R. Peterson, Energy loss functions for electrons and protons in planetary gases, J. Geophys. Res., 73, 233, 1968.
- Green, A.E.S. and T. Sawada, Ionization cross sections and secondary electron distributions, J. Atmos. Terr. Phys., 34, 1719, 1972.
- Green, A.E.S. and P.J. Wyatt, Atomic and Space Physics, p. 170, Addison-Wesley Publishing Company, Inc., Reading, Mass., 1965.
- Grün, A.E., Lumineszenz-photometrische messungen der energieabsorption in strahlungsfeld von elektronenquellen eindimensionalor fall in luft, Z. Naturforschg., 12a, 89, 1957.
- Heaps, M.G. and A.E.S. Green, Monte Carlo approach to the spatial deposition of energy by electrons in molecular hydrogen, J. Appl. Phys., 45, 3183, 1974.
- Herrmann, D., K. Jost, and J. Kessler, Differential cross sections for elastic electron scattering. II. Charge cloud polarization in N<sub>2</sub>, J. Chem. Phys., 64, 1, 1976.
- Holland, R.F., Cross sections for electron excitation of the 3914-Å<sup>0</sup> (0,0) band of the N<sub>2</sub><sup>+</sup> first negative system, Tech. Rep. LA-3783, Los Alamos Scientific Laboratory of the University of California, Los Alamos, New Mexico, 1967.
- Inokuti, M., D.A. Douthat, and A.R.P. Rau, Degradation spectra and ionization yields of electrons in gases, Proceedings of the Fifth Symposium on Microdosimetry, pp. 977-1006, Varbania-Pallanza, Italy, Sept. 22-26, 1975.
- Irvine, W.M., Multiple scattering by large particles, Astrophys. J., 142, 1563, 1965.
- Jackman, C.H., R.H. Garvey, and A.E.S. Green, Yield spectra and the continuous-slowing-down approximation, J. Phys. B: Atom Molec. Phys., 10, 2873, 1977a.
- Jackman, C.H., R.H. Garvey, and A.E.S. Green, Electron impact on atmospheric gases. 1. Updated cross sections, J. Geophys. Res., 82, 5081, 1977b.
- Jasperse, J.R., Boltzmann-Fokker-Planck model for the electron distribution function in the earth's ionosphere, Planet. Space Sci., 24, 33, 1976.

- Jasperse, J.R., Electron distribution function and ion concentrations in the earth's lower ionosphere from Boltzmann-Fokker-Planck theory, Planet. Space Sci., 25, 743, 1977.
- Jung, K., E. Schubert, D.A.L. Paul, and H. Ehrhardt, Angular correlation of outgoing electrons following ionization of H<sub>2</sub> and N<sub>2</sub> by electron impact, J. Phys. B: Atom. Molec. Phys., 8, 1330, 1975.
- Jura, M., Models of the interstellar gas, Ph.D. thesis, Harvard Univ., Cambridge, Mass., 1971.
- Jusick, A.T., C.E. Watson, L.R. Peterson, and A.E.S. Green, Electron impact cross sections for atmospheric species. 1. Helium, J. Geophys. Res., 72, 3943, 1967.
- Kamiyami, H., The electron density distribution in the lower ionosphere produced through impact ionization by precipitating electrons and through photoionization by the associated bremsstrahlung x-rays, J. Geomag. and Geoelec., 19, 27, 1967.
- Kieffer, L.J., Low-energy electron-collision cross-section data, part III: Total scattering; differential elastic scattering, Atomic Data, 2, 293, 1971.
- Kutcher, G.J. and A.E.S. Green, Multiple elastic scattering of slow electrons: Parametric study for H<sub>2</sub>, J. Appl. Phys., 47, 2175, 1976.
- Lewis, H.W., Multiple scattering in an infinite medium, Phys. Rev., 78, 526, 1950.
- Maeda, K. and A.C. Aikin, Variations of polar mesospheric oxygen and ozone during auroral events, Planet. Space Sci., 16, 371, 1968.
- Mantas, G.P., Theory of photoelectron thermalization and transport in the ionosphere, Planet. Space Sci., 23, 337, 1975.
- McConkey, J.W., J.M. Woolsey, and D.J. Burns, Absolute cross section for electron impact excitation of 3914 Å N<sub>2</sub><sup>+</sup>, Planet. Space Sci., 15, 1332, 1967.
- McDiarmid, J.B., D.C. Rose, and E. Budzinski, Direct measurement of charged particles associated with auroral zone radio absorption, Can. J. Phys., 39, 1888, 1961.
- Moliere, G., Theory of scattering of fast charged particles. I. Single scattering in a screened Coulomb field, Z. Naturf., 2a, 133, 1947.
- Moliere, G., Theory of scattering of fast charged particles. II. Plural and multiple scattering, Z. Naturf., 3a, 78, 1948.
- Mott, N.F. and H.S.W. Massey, The Theory of Atomic Collisions, Clarendon Press, Third Edition, Oxford, England, 1965.

- Mumma, M.J. and E.C. Zipf, Dissociative excitation of vacuum-ultraviolet emission features by electron impact on molecular gases. II. N<sub>2</sub>, J. Chem. Phys., 55, 5582, 1971.
- O'Brien, D.J., High-latitude geophysical studies with satellite Injun 3. 3. Precipitation of electrons into the atmosphere, J. Geophys. Res., 69, 13, 1964.
- Opal, C.B., E.C. Beaty, and W.K. Peterson, Tables of secondary-electron-production cross sections, Atomic Data, 4, 209, 1972.
- Peterson, L.R., Discrete deposition of energy by electrons in gases, Phys. Rev., 187, 105, 1969.
- Polak, L.S., D.I. Slovetskii, and A.S. Sokolov, Dissociation of nitrogen molecules from excited electronic states. I. Predissociation efficiency, High Energy Chemistry, 6, 350, 1972.
- Porter, H.S. and A.E.S. Green, Comparison of Monte Carlo and continuous slowing-down approximation treatments of 1-KeV proton energy deposition in N<sub>2</sub>, J. Appl. Phys., 46, 5030, 1975.
- Porter, H.S., C.H. Jackman, and A.E.S. Green, Efficiencies for production of atomic nitrogen and oxygen by relativistic proton impact in air, J. Chem. Phys., 65, 154, 1976.
- Porter, H.S. and F.W. Jump, Jr., Analytic total and angular elastic electron impact cross sections for planetary atmospheres, Tech. Rep. CSC/TM-78/6017, prepared for Goddard Space Flight Center by Computer Sciences Corporation, Greenbelt, Maryland, 1978.
- Rapp, D. and P. Englander-Golden, Total cross sections for ionization and attachment in gases by electron impact. I. Positive ionization, J. Chem. Phys., 43, 1464, 1965.
- Rapp, D., P. Englander-Golden, and D. Briglia, Cross sections for dissociative ionization of molecules by electron impact, J. Chem. Phys., 42, 4081, 1965.
- Rees, M.H., A.I. Stewart, and J.C.G. Walker, Secondary electrons in aurora, Planet. Space Sci., 17, 1997, 1969.
- Riewe, F. and A.E.S. Green, Ultraviolet aureole around a source at a finite distance, to be published in Appl. Optics, 1978.
- Rohrlich, F. and B.C. Carlson, Positron-electron differences in energy loss and multiple scattering, Phys. Rev., 93, 38, 1954.
- Sawada, T., P.S. Ganas, and A.E.S. Green, Elastic scattering of electrons from N<sub>2</sub>, Phys. Rev. A, 9, 1130, 1974.
- Schram, B.L., F.J. de Heer, M.J. Van der Wiel, and J. Kistemaker, Ionization cross sections for electrons (0.6-20 KeV) in noble and diatomic gases, Physica, 31, 94, 1965.

- Shemansky, D.E., T.M. Donahue, and E.C. Zipf, Jr.,  $N_2$  positive and  $N_2^+$  band systems and the energy spectra of auroral electrons, Planet. Space Sci., 20, 905, 1972.
- Shyn, T.W., R.S. Stolarski, and G.R. Carignan, Angular distribution of electrons elastically scattered from  $N_2$ , Phys. Rev. A, 6, 1002, 1972.
- Silverman, S.M. and E.N. Lassetre, Generalized oscillator strengths and electronic collision cross sections for nitrogen at excitation energies above 10 eV, J. Chem. Phys., 42, 3420, 1965.
- Spencer, L.V., Energy dissipation by fast electrons, National Bureau of Stand. Monogr., 1, 1959.
- Spencer, L.V. and U. Fano, Energy spectrum resulting from electron slowing down, Phys. Rev., 93, 1172, 1954.
- Stolarski, R.S., Calculation of auroral emission rates and heating effects, Planet. Space Sci., 16, 1265, 1968.
- Stolarski, R.S., V.A. Dulock, Jr., C.E. Watson, and A.E.S. Green, Electron impact cross sections for atmospheric species. 2. Molecular nitrogen, J. Geophys. Res., 72, 3953, 1967.
- Stolarski, R.S. and A.E.S. Green, Calculations of auroral intensities from electron impact, J. Geophys. Res., 72, 3067, 1967.
- Strickland, D.J., D.L. Book, T.P. Coffey, and J.A. Fedder, Transport equation techniques for the deposition of auroral electrons, J. Geophys. Res., 81, 2755, 1976.
- Tate, J.T. and P.T. Smith, The efficiencies of ionization and ionization potentials of various gases under electron impact, Phys. Rev., 39, 270, 1932.
- Walt, M., W.M. MacDonald, and W.E. Francis, Penetration of auroral electrons into the atmosphere, Physics of the Magnetosphere, p. 534, edited by R.L. Carovillano, J.F. McClays, and H.R. Radoski, D. Reidel, Dordrecht, Netherlands, 1967.
- Watson, C.E., V.A. Dulock, Jr., R.S. Stolarski, and A.E.S. Green, Electron impact cross sections for atmospheric species. 3. Molecular oxygen, J. Geophys. Res., 72, 3961, 1967.
- Wedde, T., Scattering cross sections. A compilation of O,  $O_2$ , and  $N_2$  data between 1 and 1000 eV. I. Elastic scattering, Center for Research in Aeronomy, Tech. Rep. CRA 76-1, Utah State University, Logan, Utah, 1976.

Wedde, T. and T.G. Strand, Scattering cross sections for 40 eV to 1 KeV electrons colliding elastically with nitrogen and oxygen, J. Phys. B: Atom. Molec. Phys., 7, 1091, 1974.

Winters, H.F., Ionic adsorption and dissociation cross section for nitrogen, J. Chem. Phys., 44, 1472, 1966.

## BIOGRAPHICAL SKETCH

Charles Herbert Jackman was born on September 9, 1950, at David City, Nebraska. He graduated as salutatorian of his class from O'Neill Public High School of O'Neill, Nebraska, in May, 1968. In May, 1972, he received the degree of Bachelor of Science with highest distinction in physics and mathematics from Nebraska Wesleyan University in Lincoln, Nebraska. From September, 1972, until the present time he has pursued his work toward the degree of Doctor of Philosophy in the Department of Physics and Astronomy at the University of Florida. During this time he has held a graduate teaching and research assistantship.

His publications to date include:

- Green, A.E.S., R.H. Garvey, and C.H. Jackman, A Thomas-Fermi-like analytic independent particle model for atoms and ions, Int. J. Quantum Chem. Symp., 9, 43-50, 1975.
- Garvey, R.H., C.H. Jackman, and A.E.S. Green, Independent-particle-model potentials for atoms and ions with  $36 < Z \leq 54$  and a modified Thomas-Fermi atomic energy formula, Phys. Rev. A, 12, 1144-52, 1975.
- Porter, H.S., C.H. Jackman, and A.E.S. Green, Efficiencies for production of atomic nitrogen and oxygen by relativistic proton impact in air, J. Chem. Phys., 65, 154-67, 1976.
- Green, A.E.S., R.H. Garvey, and C.H. Jackman, Analytic yield spectra for electrons on  $H_2$ , Int. J. Quantum Chem. Symp., 11, 97-103, 1977.
- Jackman, C.H., R.H. Garvey, and A.E.S. Green, Yield spectra and the continuous-slowing-down approximation, J. Phys. B: Atom. Molec. Phys., 10, 2873-82, 1977.
- Jackman, C.H., R.H. Garvey, and A.E.S. Green, Electron impact on atmospheric gases, 1, Updated cross sections, J. Geophys. Res., 82, 5081-90, 1977.
- Green, A.E.S., C.H. Jackman, and R.H. Garvey, Electron impact on atmospheric gases, 2, Yield spectra, J. Geophys. Res., 82, 5104-11, 1977.

I certify that I have read this study and that in my opinion it conforms to acceptable standards of scholarly presentation and is fully adequate, in scope and quality, as a dissertation for the degree of Doctor of Philosophy.

*Alex E. S. Green*

---

Alex E.S. Green, Chairman  
Graduate Research Professor of Physics  
and Astronomy

I certify that I have read this study and that in my opinion it conforms to acceptable standards of scholarly presentation and is fully adequate, in scope and quality, as a dissertation for the degree of Doctor of Philosophy.

*Thomas L. Bailey*

---

Thomas L. Bailey  
Professor of Physics and Electrical  
Engineering

I certify that I have read this study and that in my opinion it conforms to acceptable standards of scholarly presentation and is fully adequate, in scope and quality, as a dissertation for the degree of Doctor of Philosophy.

*Stephen T. Gottesman*

---

Stephen T. Gottesman  
Associate Professor of Astronomy

I certify that I have read this study and that in my opinion it conforms to acceptable standards of scholarly presentation and is fully adequate, in scope and quality, as a dissertation for the degree of Doctor of Philosophy.

Lennart R. Peterson

Lennart R. Peterson  
Professor of Physics

I certify that I have read this study and that in my opinion it conforms to acceptable standards of scholarly presentation and is fully adequate, in scope and quality, as a dissertation for the degree of Doctor of Philosophy.

George R. Lebo

George R. Lebo  
Assistant Professor of Physics and  
Astronomy

This dissertation was submitted to the Graduate Faculty of the Department of Physics and Astronomy in the College of Arts and Sciences and to the Graduate Council, and was accepted as partial fulfillment of the requirements for the degree of Doctor of Philosophy.

August 1978

A. H. Sider

Dean, Graduate School

UNIVERSITY OF FLORIDA



3 1262 08667 026 1